POLYTECHNIQUE MONTRÉAL
affiliée à l'Université de Montréal

Fluidelastic Instability Study of a Rotated Square Array Subjected to Single and Two-phase Cross-flow

SAMEH DARWISH
Département de génie mécanique

Thèse présentée en vue de l'obtention du diplôme de *Philosophiæ Doctor*
Génie mécanique

Novembre 2022

© Sameh Darwish, 2022.

POLYTECHNIQUE MONTRÉAL
affiliée à l'Université de Montréal

Cette thèse intitulée :

Fluidelastic Instability Study of a Rotated Square Array Subjected to Single and Two-phase Cross-flow

présentée par **Sameh DARWISH**
en vue de l'obtention du diplôme de *Philosophiæ Doctor*
a été dûment acceptée par le jury d'examen constitué de :

Marcelo REGGIO, président
Njuki MUREITHI, membre et directeur de recherche
Cédric BÉGUIN, membre
Atef MOHANY, membre externe

DEDICATION

All praise and thanks are for Allah,
the One who, by His blessing and favor,
good works are accomplished...

ACKNOWLEDGEMENTS

It is my pleasure to express my deep thanks to my supervisor Prof. Njuki Mureithi for his support. His guidance and advice carried me through all the stages of this research work.

I would like to thank the team members at Polytechnique Montreal at the Fluid-Structure Interaction Laboratory (FSI) for their continues valuable support and technical assistance, Mr. Nour Aimène and Dr. Abdallah Hadji.

I would like also to express my gratitude towards my family; my parents Alsayed and Sahar, and my lovely sister Salma, for the encouragement which helped me in the completion of this thesis. Your support was what sustained me this far. Without your effort and sacrifices in the pursuit of my education It wouldn't have been possible to make this achievement.

I deeply appreciate and acknowledge Doosan Enerbility for funding this research work.

RÉSUMÉ

En 2012, en Californie, seulement après 11 mois de fonctionnement, un arrêt définitif non planifié des unités 2 et 3 de la centrale nucléaire de San Onofre (SONGS) a été effectué. Cet arrêt était le résultat d'une usure de tube et d'une fuite induites par des vibrations dans les générateurs de vapeur (GV) de remplacement. Les chocs inter-tubes étaient le résultat de violentes vibrations des tubes induites par l'instabilité fluidélastique (IFE) dans le plan découverte par la suite. L'instabilité fluidélastique est connue pour être une cause potentielle de défaillance des tubes dans les générateurs de vapeur. Cependant, il est historiquement connu que l'instabilité est plus susceptible de se produire dans la direction transverse à l'écoulement c'est à dire dans la direction hors du plan que dans le plan des tubes en U de GV. Des contre-mesures, appelées barres antivibratoires, sont désormais couramment installées dans les GV pour lutter contre l'instabilité hors du plan. L'instabilité dans le plan n'était pas connue pour être un problème pour les générateurs de vapeur. Avant 2012, l'instabilité dans le plan était connue pour se produire dans des expériences de laboratoire, mais n'a jamais été sérieusement considérée comme un risque pour le fonctionnement du générateur de vapeur. L'intérêt cette instabilité était plutôt limitée et peu de chercheurs se sont penchés sur ce phénomène. Cependant, l'incident de 2012 a montré que cette instabilité ne peut être ignorée et doit être prise en compte lors de la conception des GV. Dans le cadre d'une étude sur les instabilités fluidélastiques induites par les écoulements monophasiques et diphasiques, plusieurs géométries de faisceaux de tubes ont été étudiées, avec un accent particulier sur les dispositions triangulaires des faisceaux et les géométries régulières des faisceaux carrés. Ce sont les géométries les plus courantes dans l'industrie. Des études ont montré le caractère instable de ces faisceaux, où l'instabilité se retrouve principalement dans la direction transversale. En plus du problème de l'instabilité fluidélastique dans le plan lui-même, il est intéressant d'étudier le comportement de stabilité d'autre géométrie de faisceaux, plus particulièrement de celle du faisceau de géométrie 'carré tourné' (rotated square (RS) geometry). Il y a un regain d'intérêt pour l'étude du comportement de stabilité d'autres géométries de faisceau. Le faisceau RS est particulièrement intéressant. Cette géométrie de faisceau se retrouve dans certaines modèles de GV. Comparé à d'autres géométries, le faisceau RS a des propriétés dynamiques uniques. Par exemple, il s'avère généralement plus stable que les autres, en écoulement diphasique. En revanche, en écoulement monophasique, ce faisceau présente un comportement dynamique plus complexe. Le comportement prometteur (en termes de stabilité) du faisceau RS a motivé l'étude de la dynamique fluidélastique du faisceau dans ce travail. De plus, le besoin industriel fait partie des raisons de l'étude de

comportement de ce faisceau vu qu'il est actuellement utilisé dans des générateurs de vapeur.

Cette thèse présente une étude approfondie de la dynamique du faisceau RS soumis à un écoulement transversal monophasique et diphasique. L'objectif principal de cette étude est de comprendre le comportement des vibrations induites par l'écoulement (flow-induced vibration (FIV)) du faisceau RS pour différentes de conditions d'écoulement. La première partie de cette thèse étudie la réponse FIV du faisceau lorsqu'il est soumis à un écoulement d'eau. Dans cette étude, l'effet de la variation de la flexibilité du faisceau a été étudié, en effectuant des tests avec différents nombres de tubes flexibles. On a constaté que les tubes dans un écoulement d'eau vibraient de manière significative en raison des périodicités de l'écoulement, provoquant un verrouillage (lock-in) clair entre la fréquence naturelle du faisceau de tubes et la fréquence du délestage tourbillonnaire. Cette vibration violente est due à la formation de forts tourbillons dans les sillages des tubes. On a constaté que la plage de lock-in et l'intensité de la résonance sont plus élevées dans le faisceau RS par rapport à d'autres géométries (telles que la forme triangulaire tournée). Les nombres de Strouhal obtenus à partir des résultats expérimentaux sont cohérents avec ceux rapportés dans la littérature. Cependant, la présente étude a confirmé l'existence d'une troisième périodicité. Un test spécial a été réalisé en installant un brise-vortex dans le sillage du tube pour confirmer l'excitation du vortex dans le faisceau. Il a été démontré que le brise-tourbillon élimine les vibrations du tube. A' l'aide de simulations numériques, l'existence des deux principaux nombres de Strouhal trouvés dans les expériences a été confirmée numériquement, et ça par les structures du champ d'écoulement et l'analyse de fréquence correspondante. En outre, les simulations numériques ont aussi permis la reproduction du troisième nombre de Strouhal, qui est nettement inférieur.

Afin de déterminer la stabilité du faisceau en écoulement diphasique, des tests d'instabilité fluidélastique ont été réalisés dans la plage de 40 à 90% de taux de vide, suivis d'un essai spécial à un taux de vide très élevé de 97%. La flexibilité du faisceau a été ajustée dans l'une des deux directions : transversale ou dans le sens de l'écoulement. Les résultats de cette série d'expériences montrent que ce faisceau est généralement stable dans les deux sens. Cependant, le test à 97% de taux de vide a montré une légère augmentation des vibrations du tube pour un seul tube flexible au sein d'un faisceau rigide. On a constaté que les vibrations augmentent continûment à mesure que le nombre de degrés de liberté (tubes flexibles) dans le faisceau augmente. Cependant, les vibrations n'ont pas été maintenues à toutes des vitesses d'écoulement plus grandes. Contrairement au comportement d'instabilité fluidélastique "typique ou classique", le faisceau se stabilise à des vitesses d'écoulement élevées. Parmi les observations faites figure le taux d'amortissement de l'écoulement, qui augmente rapidement avec la vitesse d'écoulement. Il s'est avéré clairement que la stabilité du faisceau résultait d'un amortissement supplémentaire significatif dans l'écoulement diphasique. Le

changement de dynamique à forts taux de vide a rendu nécessaire l'étude des cas extrêmes de 100% de taux de vide ou d'écoulement d'air. Les essais d'écoulement d'air ont été réalisés dans une soufflerie pour différents arrangements de tubes flexibles. Les variations du nombre de tubes flexibles et de leurs positions ont été considérées pour élucider le seuil d'instabilité et les mécanismes qui le gouvernent. Les forces de couplage transversal entre les tubes adjacents de la matrice ont induit une instabilité fluidélastique dans le sens de l'écoulement. Les résultats ont indiqué que le mécanisme de contrôle de la rigidité est le mécanisme d'instabilité dominant dans le faisceau RS dans un flux d'air transversal et non le mécanisme d'amortissement négatif qui est produit dans le faisceau triangulaire rotatif.

Pour une compréhension approfondie du comportement dynamique du faisceau, les forces hydrodynamiques quasi-statiques ont été mesurées pour toutes les conditions d'écoulement dans les directions de portance et de traînée, chaque direction en soi. Ces forces sont les entrées essentielles au modèle quasi-statique, y compris les effets de synchronisation. Le coefficient de la force de portance par rapport au déplacement transversal du tube a été mesuré, aussi bien que le coefficient de la force de traînée par rapport au déplacement du tube dans le sens du courant. En outre, les dérivés de la force du fluide de couplage croisé ont également été mesurés en instrumentant les tubes entourant le tube central. La dérivée du coefficient de la force de portance s'avère positive pour l'écoulement de l'eau, et presque nulle pour l'écoulement diphasique. Le modèle quasi-stationnaire a prédit un comportement stable pour ce faisceau en écoulement diphasique avec un seul tube flexible, en confirmant l'absence de mécanisme d'instabilité à amortissement négatif dans le sens de l'écoulement et dans le sens transversal. L'instabilité en mode couplé de plusieurs tubes flexibles n'a pas été trouvée dans la plage pratique de vitesse d'écoulement dans les deux sens en écoulement diphasique et dans la plage de taux de vide de 40% à 90%. Dans un écoulement d'eau, le faisceau de tubes flexibles multiples est potentiellement instable. Cependant, l'instabilité a été dissimulée lors des tests de vibration par une résonance de basculement induite par le détachement de tourbillons au voisinage de la vitesse critique d'instabilité fluidélastique. Contrairement au scénario verrouillage classique, les tubes ne se sont jamais stabilisés après la désynchronisation des fréquences entre les tubes et les vortex. La réponse soutenue de grande amplitude au-delà du lock-in a été attribuée à l'instabilité fluidélastique, déclenchée à une vitesse d'écoulement qui se situe dans la plage de lock-in du détachement vortex. Une analyse quasi-stationnaire confirme que l'amortissement de l'écoulement diphasique augmente de manière monotone sur la majeure partie de taux de vide. Il est intéressant de noter que l'amortissement du fluide est invariant avec la vitesse d'écoulement à 97% de taux de vide. Cela explique en partie la condition "d'instabilité transversale apparente" qui a été constatée lors des essais de vibration avec un taux de vide de 97%. Dans le même temps, il est apparu clairement que les lim-

ites du modèle quasi-stationnaire ne permettaient pas d'expliquer complètement l'instabilité apparente. Il est devenu nécessaire d'utiliser un modèle transitoire plus sophistiqué. Une étude plus approfondie a donc été effectuée par des mesures de force instationnaire réalisées dans les mêmes conditions d'écoulement que les tests de stabilité. L'angle de phase entre le mouvement du tube et les forces du fluide a été extrait pour une large gamme de vitesses d'écoulement réduites. Ceci est réalisé en faisant varier à la fois la vitesse d'écoulement et la fréquence d'excitation dynamique du tube. On a observé que l'angle de phase à 97% de taux de vide augment d'abord à de faibles vitesses d'écoulement, puis diminue à des vitesses plus élevées. Cela conduit à une diminution initiale de l'amortissement et de l'instabilité induits par l'écoulement. L'amortissement augmente par la suite, et donc le tube se stabilise à des vitesses d'écoulement élevées. Ces résultats sont directement corrélés aux observations faites dans les tests dynamiques et expliquent "l'instabilité apparente" (telle que déjà mentionnée). En effet, les résultats obtenus ici confirment l'existence d'une instabilité appelée "instabilité à vitesse limitée", qui diffère de l'instabilité fluidélastique classique qui ne présente pas de restabilisation pour les vitesses d'écoulement élevées.

Les résultats de cette étude ont contribué à la compréhension de la stabilité du générateur de vapeur du réacteur APR1400. Comme le faisceau de tubes dans le générateur de vapeur est géométriquement hybride, une géométrie triangulaire tournée avec P/D=1,33 a été étudiée pour compléter le tableau de ce générateur de vapeur à géométrie hybride. Pour le faisceau triangulaire tourné, l'instabilité fluidélastique dans le sens de l'écoulement n'a pas été trouvée que pour le faisceau entièrement flexible. Alors même, le début de l'instabilité correspond à une constante de Connors élevée. Celui-ci indique que le faisceau est presque stable dans la direction du flux sur la plage des conditions de fonctionnement du GV.

Malgré la confirmation par expériences en laboratoire, de l'instabilité fluidélastique dans le plan et les défaillances du GV de SONGS, il n'existe toujours pas des directives formelles de conception de l'instabilité fluidélastique dans le plan proposé par l'industrie. Cette étude a contribué en proposant des directives de conception pour l'instabilité fluidélastique dans le plan des faisceaux de tubes des générateurs de vapeur. En plus des résultats de cette étude, les données mondiales sur l'IFE dans le plan rapportées dans la littérature ont été compilées et analysées. Les résultats ont montré que la limite de stabilité avec une constante de Connors K = 6,5 convient à l'instabilité fluidélastique dans le plan. Cette limite indique également que l'instabilité fluidélastique dans le plan est rare et peut être évitée avec des considérations de conception appropriées.

ABSTRACT

In 2012, in California, after only 11 months of operation, an unplanned permanent shut down of the San Onofre Nuclear Generating Station (SONGS) power plant Units 2 and 3 was effected. This shut down was the result of a vibration-induced tube wear and leakage within the replacement steam generators. Tube-to-tube impacting was the result of violent tube vibrations caused by what was later discovered to be in-plane fluidelastic instability (IPFEI). Fluidelastic instability has been known to be a potential course of tube failure in steam generators. The instability was, however, historically known to be most likely to occur in the direction transverse to the flow, or the out-of-plane (OOP) direction relative to the plane in the SG U-tubes. Counter-measures known as anti-vibration bars (AVBs) are now routinely installed in SG to counter out-of-plane instability. In-plane fluidelastic instability (IPFEI) was not known to be an issue for steam generators. Prior to 2012, IPFEI was known to occur in lab experiments but was never seriously considered a risk for operating steam generators and partly for this reason. Interest in in-plane fluidelastic instability has been quite limited, with only a few researchers work on the phenomenon. However, the 2012 incident showed that this instability cannot be ignored and must be considered in SG design. In research on fluidelastic instability induced by single and two-phase flows, several tube array geometries have been studied, with particular focus on the triangular array layout and the normal square array geometry. These are the geometries most commonly encountered in industry. The studies showed the unstable nature of these arrays, where the instability was found to be predominantly in the transverse direction. In addition to the problem of in-plane fluidelastic instability itself, there is renewed interest in the study of the stability behavior of other array geometries. Of particular interest is the rotated square array. This array geometry is found in a few SG designs. Compared to the other array geometries, this array has unique dynamic characteristics. For instance, the array has been found to be generally more stable than other arrays in two-phase flow. In single phase flow, however, the array presents dynamic behavior which is considerably more complex. The promising behaviour (from a stability viewpoint) of the rotated square array was a motivation to investigate the array fluidelastic dynamics in this work. In addition, there is an industrial need to investigate the rotated square array behaviour since it is presently used in currently operating steam generators.

This thesis presents an indepth study of the dynamics of the rotated square array subjected to single phase and two-phase cross-flow. The main objective of the current study is to understand the array flow-induced vibration (FIV) behaviour for a wide range of flow condi-

tions. In the first part of this thesis, the FIV response of the array when subjected to water flow is studied. In the study, the effect of varying array flexibility is investigated by testing with different numbers of flexible tubes. In water flow, the tubes were found to significantly vibrate due to flow periodicities that cause a clear lock-in between tube array natural frequency and the vortex shedding frequency. This violent vibration is due to the formation of strong flow vortices in the tube wakes. Compared to the other array geometries (e.g. the rotated triangle geometry), the lock-in range and intensity of resonance in this array were found to be considerably more significant. Vortex shedding Strouhal numbers obtained the experimental results and were found to match what was reported in the literature. However, the existence of a third periodicity was confirmed in the present work. A special test was conducted to unequivocally confirm the vortex excitation in the array by installing a vortex breaker in the tube wake. The vortex breaker was shown to eliminate the lock-in induced tube vibrations. With the use of Computational Fluid Dynamics (CFD) simulations to solve the Unsteady Reynolds Averaged Navier-Stokes (URANS) equations, the existence of the two main Strouhal numbers found in the experiments was numerically confirmed by the flow field structures and related frequency analysis. In addition, the significantly lower third Strouhal number could also be reproduced in the numerical simulations.

In order to determine the stability of the array in two-phase flow, fluidelastic instability tests were conducted in the range of 40%-90% void fraction, followed by a special test at a very high 97% void fraction. Array flexibility was set in one of two directions, in the transverse, or in the streamwise direction. The results of these set of experiments revealed the generally stable nature of this array in both the streamwise and transverse directions. However, the special test of 97% void fraction showed a moderate increase in tube vibrations for the case of a single flexible tube in an otherwise rigid array. The vibrations were found to continuously increase with the increase in the number of degrees-of-freedom (flexible tubes) in the array. The vibrations were, however, not sustained for all higher flow velocities. Unlike 'typical' fluidelastic instability behavior, the array was found to restabilize for high flow velocities. The observations made included the flow damping ratio that were seen to rapidly increase with the flow velocity. It became clear that the stable nature of the array resulted from a significant added damping in the two-phase flow. The change in dynamics at high void fractions made it necessary to investigate the extreme case of 100% void fraction or air flow. The air flow tests were performed in a wind tunnel for various flexible tube arrangements. A variation of the number of flexible tubes and tubes locations were considered to elucidate the instability threshold and the governing mechanisms. Cross-coupling forces between adjacent tubes in the array induced streamwise fluidelastic instability. The results revealed that the stiffness-controlled mechanism is the dominant instability mechanism in the rotated square

array in air cross-flow, rather than the negative-damping mechanism that is encountered in the rotated triangular array.

For an indepth understanding of the array dynamic behaviour, the quasi-static fluid forces were measured for all flow conditions in the lift and drag directions separately. These forces are the necessary inputs for a quasi-steady model including the time delay effect. The lift force coefficient with respect to tube transverse displacement was measured. Similarly, the drag force coefficient with respect to the tube streamwise displacement. In addition, the cross-coupling fluid force derivatives were also measured via instrumenting the tubes surrounding the central tube. The lift force coefficient derivative was found to be positive in water flow, and nearly vanishes in two-phase flow. The quasi-steady model predicted a stable behaviour for this array in two-phase flow when having a single flexible tube, confirming the finding of the absence of the negative-damping instability mechanism in the streamwise and transverse directions. Multiple flexible tubes coupled-mode instability was not found in the practical range of flow velocity in both directions in two-phase flow in the void fraction range 40% - 90%. In water flow, a multiple flexible tube array was found to be potentially unstable. The instability was, however, concealed in the vibration tests as a result by vortex-shedding induced lock-in resonance in the vicinity of the fluidelastic instability critical velocity. Unlike the classical lock-in scenario, tubes never stabilized after vortex-tube frequencies desynchronized. The sustained large amplitude response beyond lock-in was attributed to fluidelastic instability, triggered at a flow velocity which falls within the vortex-shedding lock-in range. The quasi-steady analysis confirmed the monotonic damping increase in two-phase flow for most void fractions. Interestingly, fluid damping was found to be invariant with flow velocity for 97% void fraction. This partially explained the condition of "apparent transverse instability" that was found at the 97% void fraction vibration tests. At the same time, it became clear that the limitations of the quasi-steady model made it impossible to fully explain the apparent instability. It became necessary to call upon the more sophisticated unsteady model. Further investigation was therefore done via unsteady force measurements which were conducted for the same flow conditions as the stability tests. The phase angle between the tube motion and the fluid forces was extracted for a wide range of reduced flow velocities. This is accomplished by varying both the flow velocity and the tube dynamic excitation frequency. The phase angle was seen in the 97% void fraction to initially increase at low reduced flow velocity, and then decrease at higher velocities. This translates into an initial decrease in the flow-induced damping thus leading to instability followed by an increase in damping and consequently tube restabilization for high flow velocities. This directly correlates with the observations made in the dynamics tests and this explains the ‘apparent instability’ described above. Indeed the results here confirm the existence of the instability

we term 'velocity limited' instability which, differs from the classical fluidelastic instability which shows no restabilization for high flow velocities.

The results of this study have contributed to the understanding of the stability of the APR1400 reactor steam generator. As the tube bundle in the steam generator is geometrically hybrid, a rotated triangular geometry with P/D=1.33 was studied to complete the picture for this hybrid geometry steam generator. For the rotated triangle array, streamwise fluidelastic instability was only found for the fully flexible array. Even then, the instability onset corresponded to a high Connors constant, indicating that the array is practically stable in the streamwise direction in the range of SG operating flow conditions.

Despite the confirmation of in-plane fluidelastic instability in lab experiments and the SONGS SG failures, there are still no formal in-plane FEI design guideline put forth by the industry. This study has contributed by proposing a design guideline for the in-plane fluidelastic instability of tube bundles of the steam generators. In addition to the findings of this study, world data on in-plane FEI reported in the literature was compiled and analyzed. The results showed that a stability boundary with a Connors constant K=6.5 is suitable for in-plane fluidelastic instability. This boundary also shows that in-plane fluidelastic instability should be rare and can be avoided with proper design considerations.

TABLE OF CONTENTS

DEDICATION iii

ACKNOWLEDGEMENTS iv

RÉSUMÉ v

ABSTRACT ix

TABLE OF CONTENTS xiii

LIST OF TABLES xvii

LIST OF FIGURES xviii

LIST OF SYMBOLS AND ACRONYMS xxvii

LIST OF APPENDICES xxix

CHAPTER 1 INTRODUCTION 1
1.1 Research Motivation and Objectives 5
1.2 Thesis Outline 7

CHAPTER 2 LITERATURE REVIEW 8
2.1 Tube Excitation Mechanisms 9
2.2 Vortex Shedding Excitation 10
2.3 Models of Vortex Induced Vibrations of Cylinders 12
2.3.1 Wake–oscillator models 13
2.3.2 Single-degree-of-freedom (SDOF) models 14
2.3.3 Force–decomposition models 15
2.4 Vibrations in Two-phase Flow 15
2.5 Damping Estimation 17
2.6 Added Mass 19
2.7 Fluidelastic Instability in Tube Bundles 20
2.7.1 Jet-switching model 21
2.7.2 Quasi-steady model 22
2.7.3 Analytical models 24

2.7.4 Nonlinear models . . . 25
2.8 FEI of Rotated Square Array ($\theta = 45^o$) . . . 25
2.9 FEI of Other Array Geometries . . . 29
2.9.1 Rotated triangular array ($\theta = 60^o$) . . . 29
2.9.2 Normal triangular array ($\theta = 30^o$) . . . 31
2.9.3 Normal square array ($\theta = 90^o$) . . . 31
2.10 Numerical Solutions of Fluidelastic Instability . . . 32
2.11 Concluding Remarks . . . 34

CHAPTER 3 ARTICLE 1: FLOW-INDUCED VIBRATIONS OF A ROTATED SQUARE TUBE ARRAY SUBJECTED TO SINGLE-PHASE CROSS-FLOW . . . 36
3.1 Introduction . . . 37
3.2 Experimental Apparatus . . . 40
3.3 Experimental Results . . . 43
3.3.1 Transverse FIV results . . . 43
3.3.2 Streamwise FIV results . . . 50
3.4 Investigation/Further Evidence of Excitation Mechanisms . . . 55
3.4.1 Effect of splitter plate on single flexible tube - transverse response . . . 55
3.4.2 Numerical results . . . 56
3.5 Conclusions . . . 63

CHAPTER 4 ARTICLE 2: EXPERIMENTAL INVESTIGATION OF FLUIDELASTIC INSTABILITY OF A ROTATED SQUARE ARRAY SUBJECTED TO TWO-PHASE AND AIR CROSS-FLOW . . . 65
4.1 Introduction . . . 66
4.2 Experimental Apparatus . . . 69
4.3 Array Dynamics in Two-phase Flow . . . 71
4.3.1 Transverse vibration response . . . 71
4.3.2 Streamwise vibration response . . . 76
4.4 Array Dynamics in Air Flow . . . 78
4.4.1 Streamwise direction dynamics . . . 79
4.4.2 Transverse direction dynamics . . . 83
4.4.3 Discussion . . . 85
4.5 Conclusions . . . 91

CHAPTER 5 ARTICLE 3: STABILITY BEHAVIOUR OF A ROTATED SQUARE TUBE ARRAY SUBJECTED TO TWO-PHASE CROSS-FLOW . . . 93

5.1 Introduction 94
5.2 Theoretical Formulation 96
5.2.1 Quasi-steady model formulation 97
5.2.2 Derivatives of fluid force coefficients 101
5.3 Experimental Apparatus 102
5.4 Experimental Results 105
5.4.1 Quasi-static force measurements 105
5.5 Fluidelastic Stability Analysis 115
5.5.1 Transverse direction stability behaviour 118
5.5.2 Streamwise direction stability behaviour 124
5.6 Conclusions 127

CHAPTER 6 UNSTEADY FORCE MEASUREMENTS & PROPOSED IPFEI DESIGN GUIDELINE 130
6.1 Unsteady Force Measurements 130

CHAPTER 7 GENERAL DISCUSSION 140
7.1 Flow-induced Dynamics of the Rotated Square Array 140
7.2 Practical Implications of Research Findings and Proposed IPFEI Design Guideline 142

CHAPTER 8 CONCLUSIONS 146
8.1 Research Contributions and Findings 146
8.2 Recommendations for Future Work 147
8.3 Publications 148
8.3.1 Journal articles 148
8.3.2 Conferences 148
8.3.3 Technical reports 148

REFERENCES 150

APPENDICES 163
A.1 Introduction 164
A.2 Tube Bundle Test Apparatus 166
A.3 Vibration Test Results 168
A.3.1 Single phase (water) flow results 169
A.3.2 Two-phase flow test results 176
A.4 Discussion 182

A.4.1 Damping measurements 182
A.4.2 Hydrodynamic mass 183
A.4.3 Stability map 185
A.5 Conclusion 189

LIST OF TABLES

Table 3.1	Central tubes numerical results	60
Table 5.1	Transverse fluid force derivatives.	103
Table 5.2	Streamwise fluid force derivatives.	103
Table A.1	Summary of FEI test results with instability constants	186

LIST OF FIGURES

Figure 1.1 Schematic drawing showing the internal structure of a steam generator (Source: www.unene.ca/essentialcandu) 2

Figure 1.2 Schematic drawing showing internal details of the APR1400 steam generator [1] 4

Figure 2.1 Basic cross-sectional tube array configurations: (a) normal triangle, (b) rotated triangle, (c) normal square, (d) rotated square 8

Figure 2.2 Common tube dynamic response in cross flow 10

Figure 2.3 Comparison between WIV, VIV response and downstream flexible cylinder in shear flow [2] 12

Figure 2.4 FRF fit method [3] 18

Figure 2.5 Fluidelastic stability threshold for tube bundles in heat exchangers [4] 20

Figure 2.6 Jet-flow model between two cylinders [5] 22

Figure 2.7 Lift coefficient transient variation: (a) in quasi-steady model, (b) in quasi-unsteady model [6] 23

Figure 2.8 The unit cell used in the model to describe the FEI mechanism [7] . . 24

Figure 2.9 Periodicity frequencies vs. flow velocity [8] 27

Figure 2.10 Streamwise and transverse response of single tube in rotated square array of P/D=1.7 in water cross flow [9]. 28

Figure 2.11 Number of flexible tubes in the array shows how this affects tubes dynamic behaviour: $\triangle$, one tube flexible; $*$, two tubes flexible; $\square$, one column flexible; $\times$, seven tubes flexible; and $\Diamond$, all tubes flexible [10]. 30

Figure 2.12 FIV regimes with and without splitter plate for single cylinder [11] . 34

Figure 3.1 Test loop showing: (a) loop components and (b) test section with tube bundle assembly 40

Figure 3.2 Schematic of the rotated square array tubes layout 41

Figure 3.3 Flexible tube design with its mounting 41

Figure 3.4 Sample of tube response and frequency spectrum in air 42

Figure 3.5 Vortex-induced vibrations of a transverse single flexible tube located in the 6th row 43

Figure 3.6 Response spectra of single flexible tube in the transverse direction - 6th row 44

Figure 3.7 Natural frequency of the tube and periodicity frequency in the transverse direction 45

Figure 3.8	Vortex-induced vibrations of a transverse single flexible tube located in the 4th row	46
Figure 3.9	Response spectra of single flexible tube in the transverse direction - 4th row	46
Figure 3.10	Natural frequency of the tube and periodicity frequency in the transverse direction	47
Figure 3.11	Dynamic behaviour of four flexible tubes in the transverse direction	48
Figure 3.12	Frequency spectra for the column configuration of : (a) tube 2, (b) tube 3	48
Figure 3.13	Flow periodicity frequencies and tubes natural frequencies; (a) tube 1, (b) tube 2, (c) tube 3, and (d) tube 4	49
Figure 3.14	Response frequencies vs. flow velocity, for the flexible tubes in a column, vibrating in the transverse direction	50
Figure 3.15	Fully flexible bundle behaviour in the transverse direction	50
Figure 3.16	Frequency analysis of tube 2 in the fully flexible array : (a) frequency spectra at low velocities, (b) tube natural frequency syncronization with shedding frequencies	51
Figure 3.17	Flexible tube dynamic response in different arrangements	51
Figure 3.18	Vortex-induced vibrations of a streamwise single flexible tube located in the 6th row	52
Figure 3.19	Response spectra of single flexible tube in the streamwise direction	53
Figure 3.20	Vortex-induced vibrations of a streamwise single flexible tube located in the 6th row	53
Figure 3.21	Dynamic behaviour of four flexible tubes in the streamwise direction	54
Figure 3.22	Flexible tube in a column located in the 6th row	54
Figure 3.23	Flow periodicity frequencies of tube 1. Only the smaller Strouhal number is found for the other tubes in the array	54
Figure 3.24	Response frequencies, of all flexible tubes in a column, in the streamwise direction vs. flow velocity	54
Figure 3.25	Fully flexible bundle behaviour in the streamwise direction	55
Figure 3.26	Frequency spectra of tube 2 in the fully flexible configuration	55
Figure 3.27	Flexible tube dynamic response in different arrangements in the streamwise directions	56
Figure 3.28	Splitter Plate downstream flexible tube to suppress vortex induced vibrations	56
Figure 3.29	Dynamic behaviour of single flexible tube followed by a splitter plate in transverse direction vs its behaviour without the splitter	57

Figure 3.30 Vibration spectra in the cross-flow direction of the single tube configuration using a plate splitter 57
Figure 3.31 Grid overview: (a) inflation layer around cylinders, (b) computational domain meshing, (c) grid independence study 58
Figure 3.32 Domain and boundary conditions of the CFD model 59
Figure 3.33 Flow vorticity field inside the array ($Re = 10702$, $V_p/fD = 2.1$) . . . 59
Figure 3.34 Time sample of tube 2 unsteady (a) lift coefficient and (b) drag coefficient 60
Figure 3.35 Fluid forces frequency spectra of the central tubes: (a & b) tube 1, (c & d) tube 2, (e & f) tube 3 61
Figure 3.36 Domain grid showing splitter plate placed between tube 2 and tube 3 62
Figure 3.37 Comparison of the lift coefficient signals for the same flow velocity . . 62
Figure 4.1 Tube array layout showing flow direction. 70
Figure 4.2 Test section showing tube bundle and flexible tube structure. 70
Figure 4.3 Transverse vibration response of a single flexible tube in water flow [12]: (a) non-dimensional tube rms tip vibrations, (b) frequency spectra at low flow velocities showing vortex shedding frequency, and (c) frequency spectra for the full range of flow velocity in log scale. 72
Figure 4.4 Single flexible tube vibrations in the transverse direction when surrounded with rigid tubes in mid void fractions (40-60%): (a) non-dimensional tube rms tip vibrations, (b) frequency spectra in 50% void fraction 73
Figure 4.5 Single flexible tube vibrations in the transverse direction when surrounded with rigid tubes in high void fractions (70-97%): (a) non-dimensional tube rms tip vibrations, (b) frequency spectra of 97% void fraction, and (c) damping ratio of 97% void fraction 74
Figure 4.6 Column of flexible tubes vibrations in the transverse direction for 80% void fraction: (a) tube rms vibrations, (b) frequency spectra. 75
Figure 4.7 Fully flexible array vibrations in the transverse direction in water flow [12]: (a) non-dimensional tube rms tip vibrations, (b) non-dimensional tube rms tip vibrations, (c) frequency spectra at low flow velocities showing vortex shedding frequency 76
Figure 4.8 Fully flexible array vibrations in the transverse direction in mid void fractions (40-60%): (a) non-dimensional tube rms tip vibrations, (b) frequency spectra in 60% void fraction 77

Figure 4.9 Fully flexible array vibrations in the transverse direction in high void fractions (70-90%): (a) non-dimensional tube rms tip vibrations, (b) frequency spectra in 80% void fraction. 78
Figure 4.10 Fully flexible array vibrations in the transverse direction in the 97% void fraction test: (a) tube rms vibrations, (b) frequency spectra in 80% void fraction, (c) damping ratio variation with non-dimensional flow velocity. 79
Figure 4.11 Vibration mode and phase angles referenced to tube 2 in 97% void fraction at V/fD=30. 80
Figure 4.12 Fully flexible array vibrations in the streamwise direction in mid void fractions (40-60%): (a) non-dimensional tube rms tip vibrations, (b) frequency spectra in 50% void fraction. 81
Figure 4.13 Fully flexible array vibrations in the streamwise direction in high void fractions (70-90%): (a) non-dimensional tube rms tip vibrations, (b) frequency spectra in 90% void fraction. 82
Figure 4.14 Frequency spectrum of a tube in the fully flexible array flexible in the flow direction. 83
Figure 4.15 Configurations of the tubes flexible in the streamwise directions experimented in air flow. 84
Figure 4.16 Tube vibrations of a single tube in the streamwise direction: (a) dynamic vibrations, (b) frequency spectra of the tube located in 4th row 85
Figure 4.17 Tube vibrations in the streamwise direction : (a) column configuration, (b) diamond configuration 85
Figure 4.18 Tube vibrations in the streamwise direction : (a) cluster of flexible tube located in the upstream rows of the array, (b) fully flexible array, (c) flexible array located downstream a rigid row of tubes, (d) bundle with the upstream 5 flexible rows and downstream rigid array 86
Figure 4.19 Frequency spectra of tube 3 in the fully flexible array configuration. . 87
Figure 4.20 Vibration mode and phase angles referenced to tube 3 in air flow at at the post instability flow velocity. 87
Figure 4.21 Frequency spectra of the flexible tube in the streamwise direction located in the third row for: (a) V_u/fD=4.86, (b) V_u/fD=7.64 88
Figure 4.22 Configurations of the tubes flexible in the transverse directions experimented in air flow 88

Figure 4.23 Tube vibrations of a fully flexible array in the transverse direction: (a) dynamic vibrations, (b) static deflection, (c) frequency variation, (d) frequency spectra of tube 3. 89
Figure 4.24 Flow regime map for transverse direction. 90
Figure 4.25 Stability map of the fluidelastic instability experimental data: (△,◁,◯) present study in 97% void fraction (transverse direction), and in air flow in the streamwise direction: (▽,∗,⋆) present study (P/D=1.64), (◯) Price and Kuran (P/D=2.12) [13], (◊) Païdoussis et al. (P/D=1.5) [14], (■) Nakamura and Tsujita (P/D=1.2, 1.33, 1.5) [15], (▲) Hartlen (P/D=1.3, 1.414, 1.56) [16] , (◄) Soper (P/D=1.27, 1.35, 1.52, 1.78) [17], (►) Elkashlan (P/D=1.4, 1.7) [18]; open symbols represent data from single and partially flexible arrays, filled symbols represent data from fully flexible arrays 90
Figure 4.26 Instability constant variation with tubes mass-damping parameter and array pitch spacing for fully flexible array in air flow in the streamwise direction: (⋆) present study (P/D=1.64), (■) Nakamura and Tsujita (P/D=1.2, 1.33, 1.5) [15], (▲) Hartlen (P/D=1.3, 1.414, 1.56) [16] , (◄) Soper (P/D=1.27, 1.35, 1.52, 1.78) [17], (►) Elkashlan (P/D=1.4, 1.7) [18] 91
Figure 5.1 Schematic showing of the array layout and neighbouring tubes numbers. 98
Figure 5.2 Experimental test setup showing: (a) linear motor mechanism, (b) test section. 103
Figure 5.3 Instrumented neighbouring tubes showing strain gauges fixed at tube root. 104
Figure 5.4 Test Section. 104
Figure 5.5 Variation of the lift coefficient derivative with Reynolds number. . . . 106
Figure 5.6 Variation of the drag coefficient with Reynolds number. 106
Figure 5.7 Variation of tube C lift coefficient with transverse displacement (Y/D) for: (a) single and two-phase flow for void fractions in the range $0 \leq \beta \leq 97\%$, (b) two-phase flow for $40\% \leq \beta \leq 97\%$. 107
Figure 5.8 Variation of the lift coefficient derivative of tube C with respect to Y/D for void fractions $0 \leq \beta \leq 97\%$, with a close-up view for $40 \leq \beta \leq 97\%$. 108
Figure 5.9 Variation of tube C drag coefficient with streamwise displacement (X/D) for void fractions $0 \leq \beta \leq 97\%$. 108
Figure 5.10 Variation of tube C drag coefficient derivative with respect to X/D for void fractions $0 \leq \beta \leq 97\%$. 109

Figure 5.11 Variation of the lift and drag coefficients derivatives for different arrays with flow void fraction in the: (a) transverse and (b) streamwise directions 109
Figure 5.12 Fluid lift and drag coefficients variation with respect to the central tube transverse displacement Y_c/D : (a) & (b) Tube 2, (c) & (d) Tube 3 , (e) & (f) Tube 4 112
Figure 5.13 Fluid drag and lift coefficients variation with respect to the central tube streamwise displacement X_c/D : (a) & (b) Tube 2, (c) & (d) Tube 3 , (e) & (f) Tube 4 113
Figure 5.14 Variation of the lift coefficient derivative of the neighbouring tubes for different void fractions. 114
Figure 5.15 Variation of the drag coefficient derivative of the neighbouring tubes for different void fractions. 114
Figure 5.16 Variation of the neighbouring tube drag force coefficient derivatives for the present RS array in comparison with derivatives for a triangular array [19]. 115
Figure 5.17 Configurations of flexible tubes - stability analysis. 118
Figure 5.18 Evolution of the eigenvalues with flow velocity of the single flexible tube in the transverse direction for: (a) β =70%, and (b) β =90% . . 118
Figure 5.19 Dynamic response in transverse direction in water flow showing: (a) tube vibration amplitude, (b) dominant vibration frequency and periodicity frequencies. 119
Figure 5.20 Evolution of the eigenvalues with flow velocity of the cluster case (9 flexible tubes) in the transverse direction in water flow 120
Figure 5.21 Evolution of eigenvalues for multiple cases in water flow. Tubes are free to vibrate in the transverse direction. 121
Figure 5.22 Evolution of damping ratio for multiple cases in water flow. Tubes are free to vibrate in the transverse direction. 121
Figure 5.23 Evolution of the eigenvalues with two-phase flow velocity of a single flexible and multiple flexible tubes in the transverse direction for: (a) β =40%, (b) β =70%, and (c) β =97% 122
Figure 5.24 Damping ratio variation with flow reduced velocity in the transverse direction for various flow void fractions. 124
Figure 5.25 Instability map showing the predicted reduced critical velocity for the transverse direction case of a cluster of flexible tubes. 125
Figure 5.26 Evolution of the eigenvalues with flow velocity of the single flexible tube in the streamwise direction for: (a) β =80%, and (b) β =97% . . 125

Figure 5.27 Evolution of the eigenvalues with flow velocity of a single flexible and multiple flexible tubes in the streamwise direction for: (a) β =50% and (b) β =80% 126
Figure 5.28 Evolution of the eigenvalues with flow velocity of the cluster case (9 flexible tubes) in the streamwise direction for β =80% 126
Figure 5.29 Stability map showing the predicted streamwise reduced critical velocity for the cluster of flexible tubes. 127
Figure 5.30 Damping in the streamwise direction for: (a) β =40%, (b) β =80%, and (c) β =90% 128
Figure 6.1 Variation of the tube added mass with flow void fraction in the: (a) transverse and (b) streamwise directions 132
Figure 6.2 Force coefficient and fluid phase in the transverse direction for the central tube for 6-20 Hz excitation frequencies : (a) 0%, (b) 40%, (c) 70% 134
Figure 6.3 Force coefficient and fluid phase in the transverse direction for the central tube for 6-20 Hz excitation frequencies : (a) 90%, (b) 97% . . 135
Figure 6.4 Force coefficient and fluid phase in the streamwise direction for the central tube for 6-20 Hz excitation frequencies : (a) 0%, (b) 40%, (c) 70% 136
Figure 6.5 Force coefficient and fluid phase in the streamwise direction for the central tube for 6-20 Hz excitation frequencies : (a) 90%, (b) 97% . . 137
Figure 6.6 Damping variation of central tube in the transverse direction in: (a) 60%, (b) 90% and (c) 97% void fractions 138
Figure 6.7 Single flexible tube vibrations in the transverse direction for β=97% . 139
Figure 7.1 Suggested in-plane fluidelastic instability design guideline in the fluidelastic instability map showing two-phase flow test results in the in-plane direction for: (◆) rotated square array stability boundary based on maximum flow velocity attained (present study), (◀) rotated triangle array (present study), and data from the literature: (▲) Tan et al. [20], (■, ▲) Azuma et al. [21], (▲) Mureithi et al. [10], (▲) Joly et al. [22], (▶) Violette et al. [23] 145
Figure A.1 Schematic drawing showing internal details of the APR1400 steam generator [1] 167
Figure A.2 Test loop showing the tube bundle 169
Figure A.3 Test section 170

Figure A.4 Frequency spectra of single flexible tube in water flow in the transverse direction 171
Figure A.5 Single flexible tube vibrations in water flow in the transverse direction 171
Figure A.6 Fully flexible array vibrations in water flow in the transverse direction 172
Figure A.7 Fully flexible array frequency variation in water flow in the transverse direction 172
Figure A.8 Single flexible tube water test in the streamwise direction 173
Figure A.9 Frequency spectra of single flexible tube in the streamwise direction in water flow 173
Figure A.10 Fully flexible array vibrations in water flow in the streamwise direction 174
Figure A.11 Frequency variation of the fully flexible array vibrations in water flow in the streamwise direction 174
Figure A.12 Frequency spectra at various flow reduced velocities showing the change in tube vibration frequency at reduced velocity of: (a) 0.35, (b) 0.45, (c) 0.55, and (d) 1.05 174
Figure A.13 (a) Single flexible tube response in the transverse direction for β=20%-40%, and (b) frequency spectra for β=30% 176
Figure A.14 (a) Single flexible tube response in the transverse direction for β=50%-60%, and (b) frequency spectra for β=60% 176
Figure A.15 (a) Fully flexible array response in the transverse direction for β=20%-40%, and (b) frequency spectra for β=30% 177
Figure A.16 (a) Fully flexible array response in the transverse direction for β=50%-60%, and (b) frequency spectra for β=60% 177
Figure A.17 (a) Fully flexible array response in the transverse direction for β=70%-80%, and (b) frequency spectra for β=80% 178
Figure A.18 (a) Single flexible tube response in the streamwise direction at β=20%-60%, and frequency spectra for β=: (b) 30%, and (c) 60% 179
Figure A.19 (a) Fully flexible array response in the streamwise direction for β= 20%-40%, and (b) frequency spectra for β=30% 180
Figure A.20 (a) Fully flexible array response in the streamwise direction for β= 50%-60%, and (b) frequency spectra for β=60% 180
Figure A.21 (a) Fully flexible array response in the streamwise direction for β= 70%-90%, and (b) frequency spectra for β=80% 181
Figure A.22 (a) Fully flexible array response in the streamwise direction and frequency spectra for β= 97%, and (b) frequency spectra 181

Figure A.23 Tube damping ratio estimation showing: (a) curve fitting for low flow velocity for β=50%, (b) fluid damping averaged over multiple velocity points 182
Figure A.24 Tube damping ratio in comparison with Pettigrew et al. [3] 182
Figure A.25 Hydrodynamic mass ratio for the flexible tube in the streamwise direction in comparison with Pettigrew et al. [3] 184
Figure A.26 Hydrodynamic mass ratio for the flexible tube in the transverse direction in comparison with Pettigrew et al. [3] 184
Figure A.27 Fluidelastic instability map showing test results of the present study . 187
Figure A.28 Fluidelastic instability map showing rotated triangular array test results in the transverse direction in comparison with data from the literature: (◊, ■) Pettigrew et al. [24], ◯ Sawadogo and Mureithi [25], ▲ Azuma et al. [21]. 187
Figure A.29 Flow regime map for the tube bundle. Symbols show the flow velocity at different void fractions in the streamwise direction 188
Figure A.30 Flow regime map for the tube bundle. Symbols show the flow velocity at different void fractions in the transverse direction 188

LIST OF SYMBOLS AND ACRONYMS

A	Cross sectional area
AVB	Anti-vibration bars
CANDU	Canada Deuterium Uranium
Cap	Capillary number
C_L, C_D	Coefficient of lift force and drag force, respectively
$C_{L,Y/D}$, $C_{D,X/D}$	Derivative of lift coefficient with respect to dimensionless displacement in the y direction, and derivative of drag coefficient with respect to dimensionless displacement in the x direction, respectively
C_{D_0}	Coefficient of drag force at the central position
c_f	Damping coefficient
C_R	Reaction coefficient
c_{ma}, c_{da}, c_s	Fluid added mass, added damping, and added stiffness coefficients, respectively
D, D_e	Tube outer diameter, and tube equivalent diameter, respectively
F_{da}	Damping force
f_n, f_v, f_a, f_w	Flexible tube natural frequency, flow periodicity frequency, natural frequency in air, and natural frequency in water, respectively
F_x, F_y	Force in the x and y directions, respectively
g	Gravity acceleration
G_g	Pitch mass flux
H_{Fx}	Transfer function
K	Connors constant
K_{f_x}, K_{f_y}	Fluid stiffness in the x and y directions, respectively
m, m_t	Tube mass per unit length, and total mass per unit length, respectively
m_h or m_a	Hydrodynamic (added) mass
P	Pitch spacing
P/D	Array pitch to diameter ratio
Q	Quality factor
R	Tube radius
Re	Reynolds number
Ri	Richardson number
S	Slip ratio

S_u, S_p	Strouhal number based on the upstream flow velocity, Strouhal number based on the pitch flow velocity
SONGS	San Onofre Nuclear Generation Steam
t	Time
U_g	Gas flow velocity
V_{cr}, $\bar{V}$	Flow pitch critical velocity, and dimensionless flow velocity
V_p	Flow pitch velocity
V_∞	Flow upstream velocity
β	Two-phase flow void fraction
δ	Logarithmic decrement
ϵ	Feenstra void fraction
ζ, ζ_s	Damping ratio, structural damping ratio
η_l	Liquid viscosity
λ	Eigenvalue
μ	Time delay parameter
μ_g, μ_l	Dynamic viscosity of the gas phase and the liquid phase
ρ, ρ_g, ρ_l, ρ_h	Flow density, gas flow density, and liquid flow density, and homogeneous flow density, respectively
σ	Surface tension
τ	Time delay
ϕ_f	Phase angle
ϕ_g, ϕ_l	Volumetric flow rate of the gas flow and the liquid flow, respectively
ψ	Eigenvector
ω_n, ω_d	Angular frequency ($\omega = 2\pi f$), and damped natural frequency

LIST OF APPENDICES

Appendix A Article 4: In-Plane Fluidelastic Instability Study of a Tube Bundle with a Rotated Triangular Layout and Small Pitch Ratio 163

Appendix B Uncertainty Analysis 191

CHAPTER 1 INTRODUCTION

Numerous engineering applications have structures subjected to high-speed fluid flows. In many of these applications, structures under fluid force excitation behave, either statically or dynamically, as part of a coupled fluid-structure system. This coupling has become of interest as a subject of study for designers and researchers. Vibrating structures, under certain circumstances, may fail. One of the most critical components that is subjected to cross flow is the tube bundle in industrial heat exchangers such as boilers, condensers, and most importantly, nuclear steam generators. Due to fluid-structure coupling, vibrations are induced in the tubes that are subjected to cooling fluid flow. These vibrations can potentially cause structure failures due to internal and external stresses that result in fatigue, tube wear or tube support failures.

Failures in steam generators due to tube bundle vibrations were considered to be a result of flow vorticity shedding before the 1960s. Since then, a large number of studies have conducted on this topic to provide a deeper understanding of this behaviour and to set guidelines for designers.

Tube bundles are known to be flexible in both directions; in the same direction of the flow stream, which is known as the in-plane (IP) direction (strictly, this consists of two directions within the plane of the U-tube), and transverse to the flow stream, which is commonly known as the out-of-plane direction (OOP). The out-of-plane direction (transverse to the flow and out of the plane of the tube U-bend) was found to be generally more unstable. Consequently, steam generators were fitted with so-called anti-vibration bars (AVBs), which effectively limit tube vibration in the out-of-plane direction. In January 2012, workers at the SONGS nuclear generating station in California observed a leak in one of the steam generators. A shut down was necessary to investigate the reasons and consequences of the leak. After further investigation, it was found that the leakage occurred because of an instability in the in-flow direction. IP instability in this tube bundle was wholly unexpected.

In steam generators, water flows across long supported bundles of tubes that contain contaminated flow. Water flows from the inlet at the bottom of the steam generator to cross the tube bundle at a high velocity in order to increase the heat transfer between the tubes and cooling water. During this process, the water temperature increases and gradually starts to vaporise and become a mixture of water and vapour. Figure 1.1 shows a typical design of a steam generator.

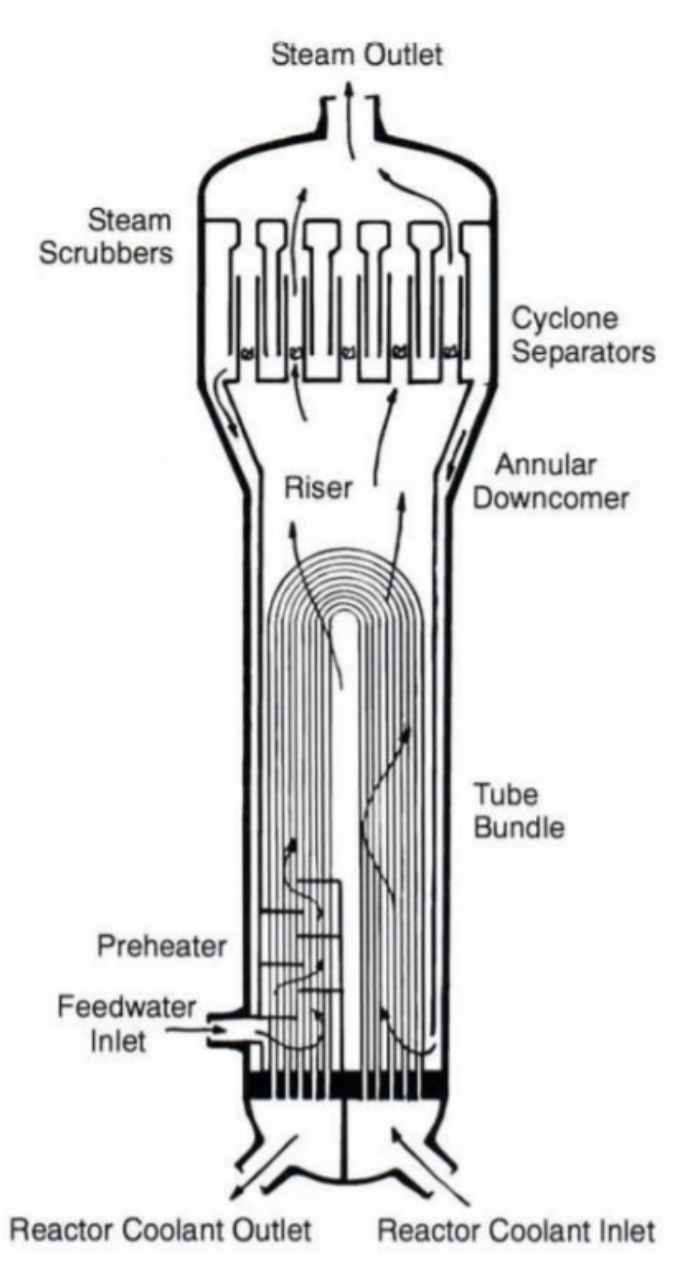


Figure 1.1 Schematic drawing showing the internal structure of a steam generator (Source: www.unene.ca/essentialcandu)

Previous studies have shown that there are three main sources of vibrations in tube bundles: Fluidelastic Instability (FEI), Vortex Shedding, and Flow Turbulence, also known as "Turbulent Buffeting". Compared to flow turbulence, both fluidelastic instability and vortex shedding produce high amplitude vibrations. However, Fluidelastic Instability (FEI) is recognized as the most important excitation mechanism that must be avoided in nuclear steam

generators (SGs) as it results in tube bundle failure within hours in extreme cases. This source of vibration, while physically well understood, remains a challenge to predict without experimentation. On the other hand, the understanding of the mechanism inducing flow periodicity (vortex shedding) in cylinder arrays is still limited.

For heat exchanger designers, it is essential to be aware of the tube array configuration effect on its fluid-structural response. Researchers have studied several arrays to provide design guidelines for new equipment. These studies covered well the common array geometries, except for rotated square arrays (this is discussed in detail in Chapter 2). Although this array shows promising dynamic stability behaviour and a more stable response in most cases, this finding is yet to be fully verified or modelled.

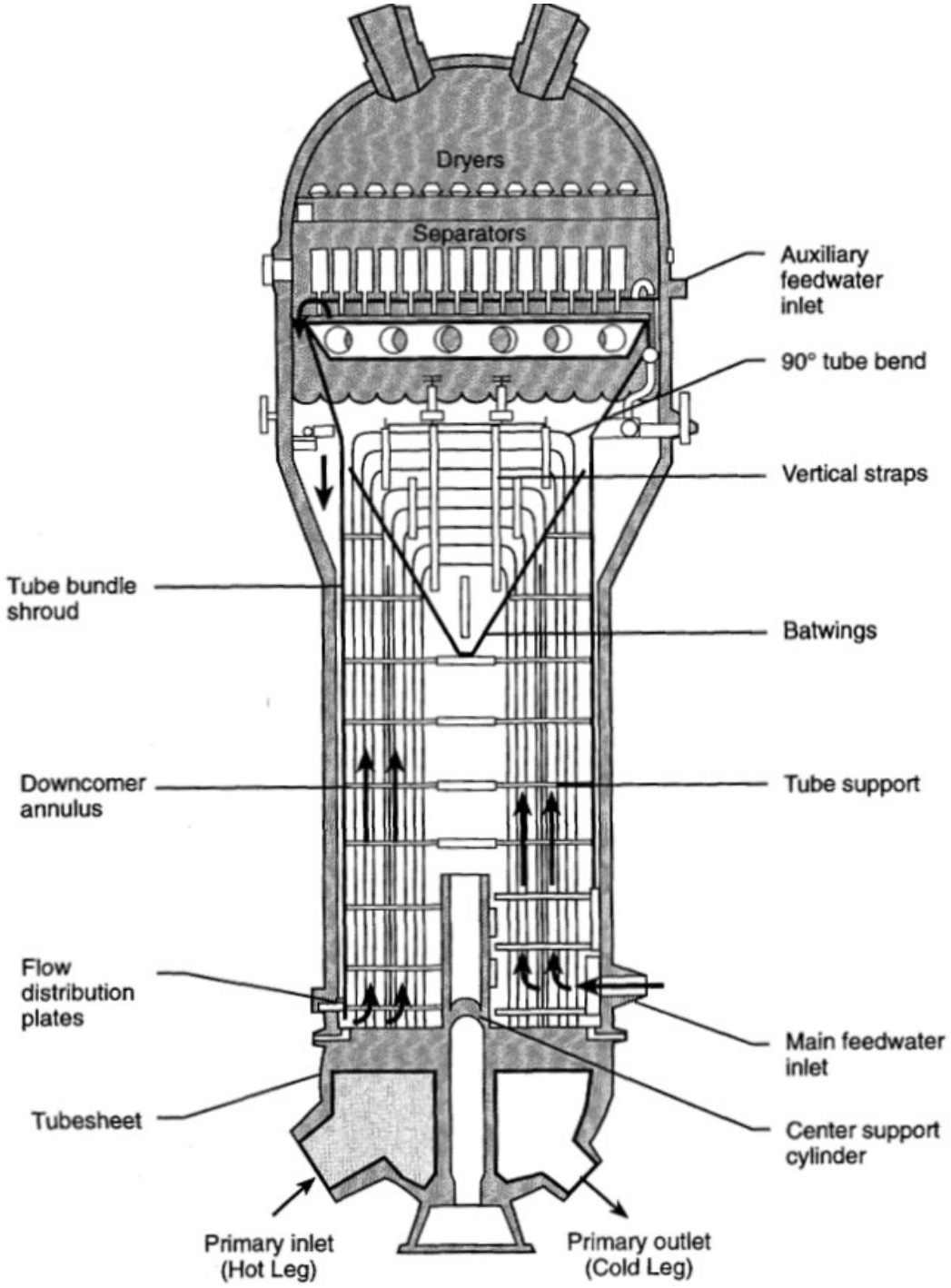


Figure 1.2 Schematic drawing showing internal details of the APR1400 steam generator [1]

1.1 Research Motivation and Objectives

During the course of the last 40 years, triangular arrays - both normal and rotated configurations - besides the normal square array have been studied extensively. The dynamic behaviour of these arrays is now generally well understood. On the other hand, rotated square array dynamic behaviour is more complex and less well understood. The published literature does not yet provide comprehensive information on the array dynamics. As the rotated square array has shown, in some previous research work, unique characteristics, in particular a tendency to be more stable than the other arrays, the motivation of this research work is to clarify further whether the rotated square array is generally stable or unstable and to what extent compared to the other arrays. This should guide designers on whether to consider this array in future steam generator tube bundle designs. The rotated square array geometry is unique due to the large spacing downstream each tube in the array. Furthermore, it has been found that random turbulence excitation in this array is significant compared to the other arrays. What is known so far is the complexity of its dynamic behaviour. Nevertheless, could this array be more suitable for stream generator tube bundles from a fluidelastic instability point of view?

The primary objective of this study is to contribute to the missing part of knowledge on the fluidelastic instability of tube bundles by examining a "new" rotated square array having P/D=1.64. Experiments are carried out in an attempt to shed new light on the missing details in the dynamic behaviour and the fluidelastic instability modelling of the rotated square array in cross-flow. This array with this exact pitch spacing is practically used in a currently operating steam generator. As part of an industrial project, the array is analyzed to provide a comprehensive understanding to its dynamic behaviour when it is subjected to cross-flow.

In order to provide these insights, an experimental program is proposed to study the dynamic behaviour of the rotated square array. A test loop design and construction is required to perform the experiments in water as well as air-water two-phase cross-flow. A stability analysis is needed to further investigate the dynamic behaviour of the array. Investigation of the effect of the number of flexible tubes on the array behaviour provides valuable insight into the instability mechanisms in the array. Another phase of the study aims to extend the fluidelastic instability measurements to the array subjected to air cross-flow, and through the analysis, investigate the fluidelastic instability behaviour of the array with various flexible tube configurations.

Another objective of this research is to analyze the array analytically and verify the applica-

bility of the quasi-steady model to predict the dynamic behaviour of this array. This requires measuring the quasi-static fluid forces in both streamwise and transverse directions in water as well as two-phase flow. The force derivatives are the key inputs needed in the model. The multiple-degrees-of-freedom model will be included by measuring the cross-coupling forces in the array. Additional experiments will provide the unsteady fluid forces which are key to determining damping variation in the array.

Specific Objectives

The specific objectives of this research project are to:

1. Experimentally study the flow-induced vibrations (FIV) of the rotated square array in single phase (water) flow to investigate the possibility of fluidelastic instability (FEI) occurrence in the in-plane and out-of-plane directions.

2. Perform fluidelastic instability vibration tests in two-phase cross-flow as the dynamic behaviour of the rotated square array in two-phase flow is poorly known compared to the other array geometries. Furthermore, to study the array behaviour in air cross-flow.

3. Experimentally measure the time-averaged forces on a static cylinder displaced in different locations as well as the unsteady hydrodynamic forces for the rotated square array. The measurements will be performed in both in-plane and out-of-plane directions. Hydrodynamic interaction in the array will be investigated for the tubes surrounding the main instrumented tube. The results will be in the form of fluid force coefficients, the phase between cylinder motion and fluid forces generated, and the fluid damping which are fundamental inputs in fluidelastic instability modelling.

4. Incorporate measured forces into a quasi-steady model to perform analysis for indepth understanding of fluidelastic behaviour of the rotated square array, concluding on its stability in various flow conditions in both in-plane and out-of-plane directions.

5. Report on the stability of the APR1400 steam generator shown in figure 1.2, especially concerning the in-plane fluidelastic instability (IPFEI). This requires studying an additional array with a rotated triangular geometry and P/D=1.33 in single phase and two-phase cross-flow.

6. Utilize the results of this study, in addition to the data provided in the literature, to propose a new design guideline for the in-plane fluidelastic instability of tube bundles operating in two-phase flow.

1.2 Thesis Outline

This thesis is divided into 8 chapters. Chapter 2 presents a detailed review of the fluidelastic instability and vortex induced vibration research for all tube array configurations, with a detailed review of work on the rotated square array. The research results are presented in the form of Journal publications. Chapter 3 presents the vortex induced vibration test results and array behaviour and dynamics in water cross-flow. The results are supported with CFD simulations showing flow structure details and verifying the test results. Array dynamics and complete fluidelastic instability analysis in two-phase flow is presented in Chapter 4. The study also showed the complexity of the array behaviour when subjected to air flow. Chapter 5 presents the fluid forces measured in this array in water and two-phase flow. The force measurement study included single tube forces and hydrodynamic coupling forces between the tubes. The measured forces are incorporated into a model to predict the fluidelastic instability onset of the array. Chapter 6 presents additional analysis and findings from unsteady measured fluid forces. A general discussion, in addition to a proposed in-plane fluidelastic instability design guideline are presented in Chapter 7. Finally, Chapter 8 addresses the conclusions, contributions, and recommended future work. The rotated triangular array test results are presented in Appendix A.

CHAPTER 2 LITERATURE REVIEW

Compared to all excitation mechanisms, FEI is considered the most crucial as it causes high amplitude vibrations that lead to tube failure in a short time. Thus, significant research effort was directed to understanding this problem and providing design guidelines to obviate instability of tube bundles. In 1962, Roberts [5] provided a study on single and double rows of tubes subjected to cross-flow. This study is considered one of the first research studies in self-excitation vibrations of tube bundles. Every tube bundle is characterised by mainly two geometrical parameters. The first is tube configuration, which defines the arrangements of the tubes in the array, and the second is the spacing between tubes. There are four tube arrangements that are commonly used in steam generators: normal triangle, rotated triangle, normal square, and rotated square (see figure 2.1). Cross sectional configuration is not the only factor that defines the array; the other factor is "pitch-to-diameter ratio", which is denoted by "P/D" (commonly referred to as pitch ratio), where P is the distance between tubes centers, and D is the outer tube diameter. This ratio represents the compactness of the array, which defines the spacing between the tubes. Common pitch ratios in steam generators are in the range of 1.2 to 1.8.

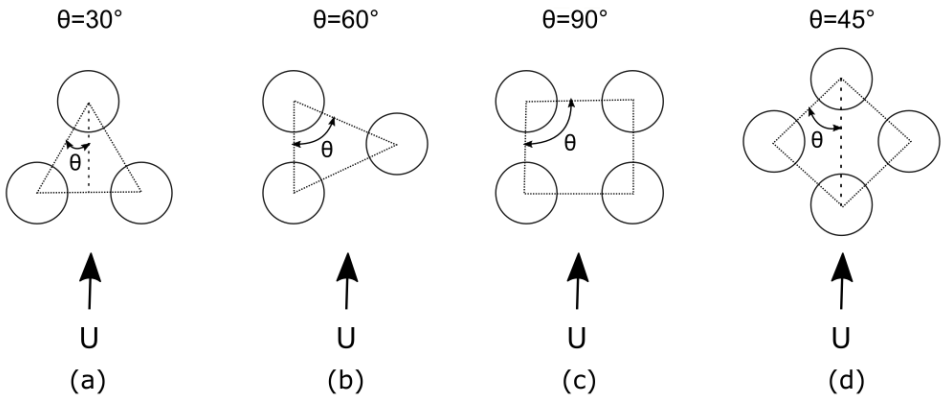


Figure 2.1 Basic cross-sectional tube array configurations: (a) normal triangle, (b) rotated triangle, (c) normal square, (d) rotated square

Flow pitch velocity (or sometimes called gap velocity) is usually used in flow calculations instead of flow upstream velocity, and it is expressed as a function of the upstream velocity, which is an easily measurable value (in experiments). Based on the continuity equation, flow accelerates while entering the bundle to keep its mass flow rate constant. Hence, its velocity increases as it crosses smaller area between the tubes. The pitch velocity is considered a

better approximation of the real velocity value that is being used in FEI and vortex induced vibration (VIV) calculations,

$$V_p = \frac{P}{P-D} V_\infty \tag{2.1}$$

where, V_p is the flow pitch velocity, V_∞, the flow upstream velocity, P, the pitch distance and D, the tube outer diameter. A first study by "Connors" in 1970 [26] introduced experimental work on a single row of cylinders and introduced the first equation that is still being used to describe the instability of flexible tubes.

$$\frac{V_{cr}}{fD} = K(\frac{m\delta}{\rho D^2})^n \tag{2.2}$$

Equation 2.2 is known as the "Connors" equation. The left hand side of the equation refers to the relative magnitude of the critical flow velocity to the tube vibration velocity. The right hand side contains the "Connors" constant (K), mass ratio, and logarithmic decrement of damping. The mass ratio is the ratio between the tube mass per unit length (including added mass) and the equivalent displaced fluid mass by the vibrating tube, which is considered the tube's inertia to moving fluid inertia. The last parameter is the logarithmic decrement (δ), which represents the amount of energy dissipated in the array by tube energy damping.

2.1 Tube Excitation Mechanisms

Forced vibrations, self-controlled vibrations, and self-excited vibrations are considered the three main steady flow-induced vibration categories, which correspond to steady state response, resonance, and instability, respectively. Paidoussis [27] classified the instability mechanisms into two classes: fluid damping-controlled mechanism and fluid stiffness-controlled mechanism. The fluid damping-controlled mechanism is dominant for low mass damping parameter and is induced by negative damping, while the fluid stiffness-controlled mechanism is dominant for high mass damping parameter and is dependent on phase difference and coupling between flexible tubes.

Tubes inside a tube bundle are affected by random turbulence excitations, or "turbulent buffeting". Rottmann and Popp [28] found that increasing turbulence intensity level inside a tube array increases the instability of the array, which reduces the flow critical velocity value. Some previous research in the literature concluded that turbulence intensity is much higher for rows deep inside the array than for upstream rows. On the other hand, Rzentkowski and Lever [29] concluded that turbulent buffeting increases tube vibrations linearly with flow

velocity but does not affect fluidelastic instability threshold.

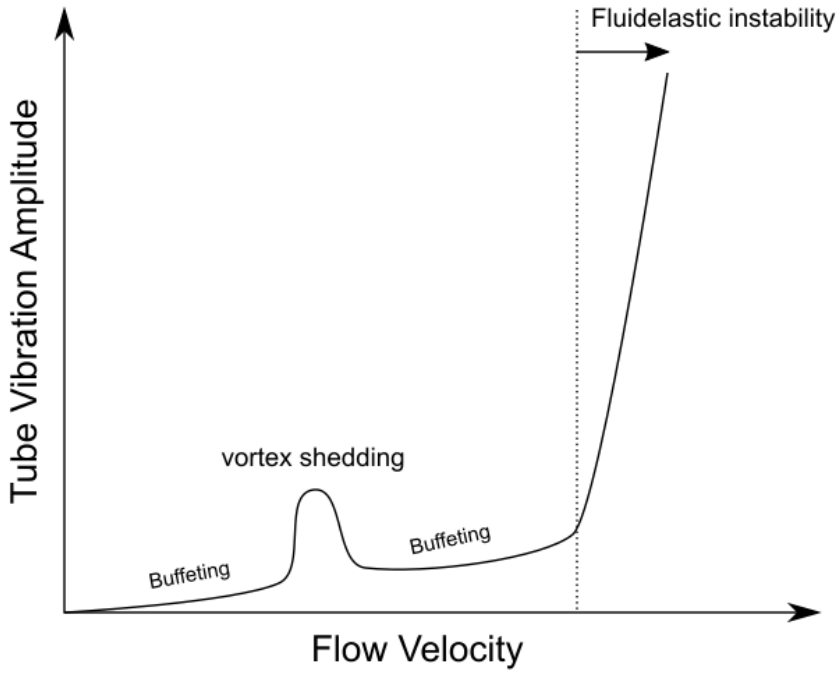


Figure 2.2 Common tube dynamic response in cross flow

Due to turbulence, vibration amplitude increases linearly with flow velocity until flow periodicity excites the tube with a relatively small amplitude. After that, it keeps increasing until the flow velocity reaches its critical value. We notice a significant increase in tube vibrations then. Figure 2.2 shows a typical instability behaviour of a flexible tube subjected to cross flow. *Critical gap velocity of fluid-elastic instability*: is when the room mean square (rms) displacement of the tube shows a sharp increase with respect to a small increase of the gap velocity.

2.2 Vortex Shedding Excitation

Vortex shedding is considered a self-controlled excitation mechanism. It is a periodic excitation in which the frequency changes linearly with flow velocity. The drag force fluctuates due to Von Karman vortices with double the frequency of lift force fluctuations [4]. Allowing the tube to move can cause some changes in the vorticity frequency. Based on Bishop and Hassan [30] this changes the shedding frequency, causing it to move to the tube's natural frequency. The effect is called synchronization, or more commonly known as "Lock-in". This effect can occur over a flow velocity range of $\pm$ 20 % of the exact resonance velocity. Tube

vibration in the transverse direction to the flow stream at a frequency close to the shedding frequency increases the ability of the tube's vibration to synchronize with the vortex shedding. It was also noticed that large amplitude vibrations can shift the shedding frequency by up to 40% [31],

$$\omega_n = \sqrt{\frac{K}{M}} \tag{2.3}$$

Vortex shedding excitation is sometimes known as Strouhal excitation. One of the common numbers used to quantify vortex shedding is the "Strouhal Number"

$$S_u = \frac{f_v D}{U} \tag{2.4}$$

where f_v is the periodicity frequency, and D is the characteristic diameter of the body, and U is flow velocity. f_v can also be the frequency of lift coefficient on a stationary cylinder. In tube bundle FIV studies, D is taken as the tube diameter. For tube arrays, the Strouhal number usually varies from 0.2 to 0.7 based on the pitch velocity, while it is constant for fixed cylinders over a wide range of Reynolds number with a value of 0.2. Tube vibration amplitude varies inversely with damping ratio and mass ratio: $A \propto [(\zeta) \times (m/\rho D^2)]^{-1}$, hence, lightly damped structures are more likely to vibrate with higher amplitudes which might cause damage more rapidly. The vortex shedding frequency follows the rule of constant Strouhal number ($S_u = f_v D/U$). For a constant Strouhal number, shedding frequency increases linearly with flow speed. As the flow speed is increased, the shedding frequency approaches the tube natural frequency and lock-in occurs. In this velocity regime, shedding frequency no longer follows the linear relationship with flow speed based on the Strouhal number equation.

The relationship between streamwise and transverse vortex-induced vibration was studied by Vandiver and Jong [32]. It was found that vibrations in both directions are strongly related and a quadratic relationship between vibrations in both directions exists during lock-in and non lock-in periods. This result provides an explanation for the doubled frequency phenomena in streamwise and transverse vibration directions. Experiments were conducted on symmetric cantilevered long cylinders with the same vibrational characteristics in both directions. The authors also observed that during the non lock-in period, spectral peak frequencies in the streamwise direction are totally equal to the summation of two spectral peak frequencies in the transverse direction, while during the lock-in, the frequency is always

doubled. By having the cross-flow time series data and nonlinear transfer function of the system, it is easy to predict the streamwise vibration.

Assi et al. [2] studied the wake-induced vibrations (WIV) of a flexible cylinder positioned in the wake of a fixed one. The authors concluded that WIV is not a resonance-induced vibration as the vibration amplitude keeps increasing when the vortex frequency is larger than the tube's natural frequency. This occurs when the energy is transferred from the fluid to the structure when the phase lag is between 0^o and 180^o. An elastically mounted cylinder was placed in the shear flow, and as can be seen in figure 2.3, without vortices, shear flow cannot excite a cylinder into WIV.

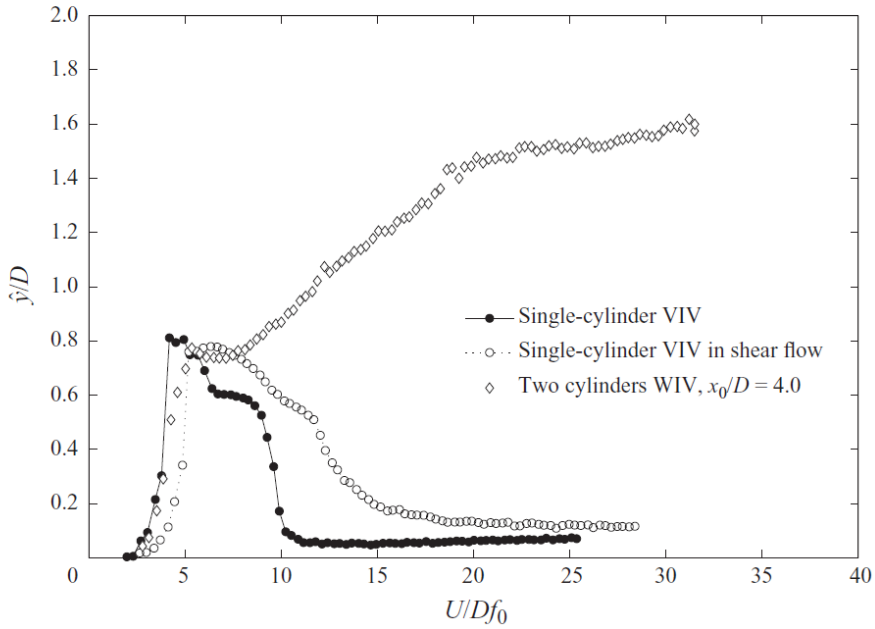


Figure 2.3 Comparison between WIV, VIV response and downstream flexible cylinder in shear flow [2]

2.3 Models of Vortex Induced Vibrations of Cylinders

Vortex shedding is known in the literature as periodicity, periodic wake shedding, or vorticity shedding. Flow periodicity causes an increase in tube vibrations in a narrow region of the operating velocity range. It becomes a problem only when the shedding frequency coincides with tubes' structural frequencies, as resonance occurs and vibration amplitude increases significantly. Vortex shedding becomes a major concern when it forces tube bundles to resonate.

However, this was observed to happen only in uniform liquid cross flow. In heat exchangers, tube bundles are subjected to cross flow at the entrance, which is normally a turbulent flow, and at the top of the bundle, which is normally more uniform. This lowers the chances of periodicity resonance to occur at the entrance as turbulence inhibits flow vorticity [33]. Available literature does not provide enough information in the area of modelling and estimating vortex shedding forces on flexible tubes. It is recommended in the case of resonance to have tube rms deflection of less than 2%D [34].

There are several semi-empirical models that have been developed over years. All developed models are trials to solve single cylinder (either rigid or flexible) forces, but previous research does not explain how that is affected if the cylinder is mounted in an array.

A nonlinear model based on experimental results was developed by Blevins [35] for a single flexible cylinder in water flow. The lift coefficient is divided into two components, in-phase and out-of-phase with cylinder motion. These two distinct coefficients, along with the mean drag coefficient, are extracted from experimental data. The model is in good agreement with transient time series data for a single cylinder in steady flow. The only difficulty with this model is that it requires a large set of experiments to cover a wide range of flow velocities and tube amplitude vibrations as VIV is known to be dependent on initial vibration amplitudes. However, the derived equation of motion can be extended to cover multiple mode responses, and force coefficients can be numerically or experimentally estimated. Model equations are shown in chapter 6.

2.3.1 Wake–oscillator models

This concept was first introduced by Birkhof [36]. Birkhof noticed that the wake oscillates from side to side, so he used a linear oscillator to describe the angle between the wake axis and the flow direction. Bishop and Hassan [30] confirmed that the wake behaves as an oscillator, and lift and drag forces respond to excitation forces as simple oscillators.

Hartlen and Currie [37] modelled the model structure system using a van der Pol nonlinear fluid oscillator using two non-dimensional differential equations, for the structure displacement,x , and lift coefficient, C_L:

$$\ddot{x} + 2\zeta\dot{x} + x = a\omega_o^2 C_L \tag{2.5}$$

$$\ddot{C_L} + \alpha\omega_o\dot{C_L}(\frac{\gamma}{\alpha\omega_o^2}\dot{C_L}^2 - 1) + \omega_o^2 C_L = \beta\dot{x} \tag{2.6}$$

Where, ζ is the damping ratio, ω_o is vortex shedding frequency to natural frequency ratio, α, β and γ are evaluated experimentally. This model is one of the empirical models that requires a single forcing function; hence, it is considered a single-degree-of-freedom model. The advantage of these empirical models is that they provide a relatively well-accepted solution to the fluid-structure coupled system as they are based mainly on experimental data. However, they lack the understanding of problem physics.

Benaroya and Wei [38] extended Hamilton's principle to model external flow-structure interaction. Some of the new model functions are experimentally based. A single equation of motion is developed assuming that system configuration is not prescribed at the end times to simplify the model. Therefore, if this assumption is not used, a series of equations can be derived to solve problems involving more complicated flow patterns.

Ogink and Metrikine [39] introduced an improved wake oscillator model to cover both free and forced vibration cases using frequency dependent coupling. The authors used the proposed modification that includes forced vibration experiments in order to search for the system nonlinearities. The frequency dependent coupling helps to reproduce the hydrodynamic forces on the cylinder, and a convolution integral is used to represent the coupling in the time domain.

2.3.2 Single-degree-of-freedom (SDOF) models

SDOF models use a differential equation of single-degree-of-freedom system to describe the tube oscillatory behavior.

$$m(\ddot{x} + 2\zeta\omega_n\dot{x} + \omega_n^2) = F(x, \dot{x}, \ddot{x}, \omega_s t) \tag{2.7}$$

A model was developed based on unsteady flow theory by Chen et al. in [40] in order to predict tube structural response and lock-in frequency. The model is based on modelling the tube as a SDOF system with excitation hydrodynamic force that includes fluid damping, and fluid stiffness effects from experimental results. Chen defined clearly the hydrodynamic forces in the lift and drag directions in two separate equations as function of added mass, fluid damping and fluid stiffness coefficients. Using experimental results, fluid force coefficients are determined using flexible tube response in water tunnel tests. Different spacings between tubes in a row are included in the study in order to show the validity of the model with different fluid forces in comparison with a single tube. This paper could not at the end predict tubes' response and compare them with experimental results. However, the work showed that the unsteady flow theory is a valid way to find a solution to the problem.

2.3.3 Force–decomposition models

The first force-decomposition model was introduced by Sarpkaya [41]. In this model, as it is called, the lift force is decomposed into fluid inertia force and fluid damping components. Sarpkaya performed a parametric study and concluded that if the mass damping parameter is larger than unity, it governs the maximum response of the cylinder. This parameter is defined as the ratio of the structural damping to mass ratio and is known as the Skop-Griffin parameter.

Later, Griffin in [42] studied a resonantly vibrating cylindrical body by vortex shedding and characterized the fluid forces inducing this vibration into: the exciting force, damping force, the added mass force, and fluid inertia force. These components can be measured separately or evaluated from total hydrodynamic forces. The equation of motion of the flexible cylinder is written as [42, 43]:

$$\ddot{y} + 2\omega_n \zeta_s \dot{y} + \omega_n^2 y = \mu \omega_{st}^2 (C_L - C_R) \tag{2.8}$$

where C_L is the lift coefficient, C_R is the reaction coefficient, μ is Skop-Griffin parameter reciprocal, and ζ_s is the viscous damping coefficient.

Wang et al [44] studied a single flexible cylinder subjected to cross-flow. Based on this study, a non-linear fluid force model was developed assuming the cylinder to be fixed at both ends. The equations of motion were obtained from Euler-Bernoulli beam theory. Auto-regressive moving average (ARMA) technique was used to obtain the fluid-force components from experimental results of the freely vibrating cylinder.

As shown in the previously discussed research papers, vortex-induced vibration of circular cylinders has been studied in order to investigate the factors influencing of lock-in, such as mass and damping, and to model the problem. The majority of these studies model the unsteady dynamic forces due to vortex shedding, including the phase of the forces relative to the cylinder deflection or velocity. As VIV is inherently nonlinear, several attempts to predict flexible tube response have been developed, but none is yet able to include the fluid-coupling effect in tube bundles. It was also noted that different models give different results, which shows that this problem is not yet fully solved.

2.4 Vibrations in Two-phase Flow

Most heat exchangers work in two-phase flow condition. Hence, it is very important to have a well-defined and clear understanding of the relation between two-phase flow parameters

and structural dynamics. Fluidelastic excitation and flow turbulence are the main excitation mechanisms known so far in two phase flow. Taylor et al. [45] indicated that flow vorticity shedding forces are absent in two-phase flow, especially in high void fractions (above 15% VF). Two-phase flow parameter measurements are more difficult than single phase. Instead, flow models are used to calculate these parameters. The simplest is the homogeneous model. This model is based on the assumption of uniformity of flow with equal velocity of air and water. In two-phase flow, flow velocity can be expressed as a function of the volumetric flow rate of water and air:

$$V_\infty = \frac{\rho_g \Phi_g + \rho_l \Phi_l}{\rho_h A} \tag{2.9}$$

$$\rho_h = \beta \rho_g + (1 - \beta)\rho_l \tag{2.10}$$

where, ρ is flow density, Φ is volumetric flow rate, A is the cross sectional area of the flow channel, subscript h indicates homogeneous quantity. For simplicity, the homogeneous model is also used by researchers to model flow mixture density in two-phase flow. The main parameter defines the state of any two phase mixture is the "Void Fraction". In two-phase flow, flow volumetric quality is calculated as the volumetric flow fraction of gas to the total of gas and liquid

$$\beta = \frac{\Phi_g}{\Phi_l + \Phi_g} \tag{2.11}$$

In the homogeneous model, The flow void fraction, ϵ, is assumed to be equal to the flow volumetric quality, β.

Feenstra et al [46] developed an improved model for two-phase flow by including the velocity ratio between gas and water. This ratio is known as the Slip Ratio

$$S = U_g/U_l = 1 + \frac{25.7}{P/D}\sqrt{Ri \times Cap} \tag{2.12}$$

where, Ri is the Richardson number, which is the ratio between the buoyancy force and the inertial force, and Cap is the Capillary number that represents the ratio between the viscous force and the surface tension force, such that

$$Ri = \Delta\rho^2 ga/G_p^2 \tag{2.13}$$

where, $\Delta\rho^2$ is the square difference of the liquid-gas densities, g is the gravity acceleration, a is the gap between the tubes, and G_p is the pitch mass flux, and

$$Cap = \eta_l U_g/\sigma \tag{2.14}$$

where, η_l is the liquid viscosity, and σ is the surface tension. These two parameters are required to calculate the Capillary number. Then, by knowing the gas-liquid velocity ratio, the two-phase flow void fraction is derived from the linear combination of the continuity equation of each phase

$$\epsilon = (1 + S\frac{\rho_g}{\rho_l}(\frac{1}{x} - 1))^{-1} \tag{2.15}$$

where, x is the flow quality, S the slipping ratio, and ϵ is the void fraction. The gas phase velocity requires a known flow void fraction such that

$$U_g = \frac{xG_p}{\epsilon\rho_g} \tag{2.16}$$

The solution is therefore requires an iterative procedure. This model agreed well with experimental measurements of Refrigerant 11 and air water mixture.

2.5 Damping Estimation

Damping is a very important parameter in FEI studies. In air, damping ratio, ζ, is usually less than 0.2 %. Damping ratio is defined as the ratio between actual damping and critical damping. Damping ratio can also be expressed as a function of logarithmic decrement, δ.

At mass fluxes before FEI threshold, tube damping decreases due to coupling between hydrodynamic forces and tube vibration. This is called "negative damping" [3]. It is a challenge to estimate the damping without the effect of negative damping. Pettigrew et al. [3] reported that damping in the lift direction decreases while it increases in the drag direction with increasing of mass flux.

A single degree-of-freedom system can be used to model the vibration response spectrum of a vibrating tube. Several methods are being used in order to estimate the damping ratio of tube bundle flexible tubes: Half-power bandwidth method (HPBW), Exponential fit method, and Frequency Response Function (FRF) fit method. Although HPBW and Exponential fit methods provide acceptable damping estimations, FRF fit method is the most accurate one.

A direct curve fit of the FRF norm can be performed, as will be shown in later sections,

$$|H(j\omega)| = \frac{1}{k\sqrt{(1-r^2)^2 + (2\zeta r)^2}} \tag{2.17}$$

where, ζ is tubes damping ratio, $r = \omega/\omega_n$, $\omega = 2\pi f$. This method can be used in all single phase and two-phase flow tests.

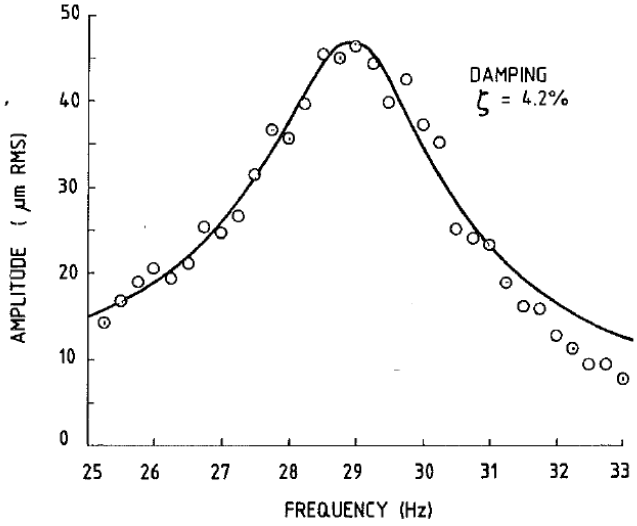


Figure 2.4 FRF fit method [3]

The half-power bandwidth method also utilizes the power spectrum in the damping estimation by calculating the quality factor, Q that represents the frequency spectrum width at half the maximum frequency response ($A_{max}/2$) from a PSD, or at $1/\sqrt{2}$ the maximum frequency response from a Fast Fourier Transform (FFT)

$$Q = \frac{1}{2\zeta} = \frac{\omega_n}{\omega_2 - \omega_1} \tag{2.18}$$

where, ω_n is the system's "damped" natural frequency, assuming it is the frequency with the maximum power. For a SDOF system, the maximum power occurs at the damped natural frequency. Hence, the assumption of the quality factor is accurate for low damping values (i.e., $\zeta < 0.05$). This method requires the frequency resolution to be relatively high in case of measuring small damping ratios, otherwise, the accuracy of the damping estimation will be significantly affected. If the damped free vibration response is known, the exponential fit method can be used as a second method to estimate the damping by having the decaying oscillation.

Generally, damping is the main energy dissipation mechanism in fluid-structure interaction

problems. There are several damping sources, but the main components may be divided into: material (structural) damping, viscous damping between tubes and fluid, flow dependent damping due to the flow surrounding the vibrating tubes, and two-phase flow damping, and when considering the tube-support interaction, the friction damping is also considerable. It is difficult to separate flow dependent energy dissipation from fluidelastic forces. However, it was shown that below the critical velocity, damping ratio is normally not affected by flow velocity [47]. Damping ratio in two-phase flow is significant compared to water and air flow. It is more complex to determine accurate damping values in two-phase flow due to measuring under some flow, the dependency on void fraction, and dependency on flow regime.

2.6 Added Mass

Commonly referred to as "hydrodynamic mass", m_h, may be interpreted as the equivalent "external mass" of fluid moving with the vibrating tube

$$m_h = m_t[(\frac{f_a}{f_w})^2 - 1] \tag{2.19}$$

where, m_t is the mass per unit length of the tube, f_a the tube natural frequency in air, and f_w the tube natural frequency in water, or in the two-phase mixture.

Rogers et al. [48] developed a theory based on the equivalent diameter (D_e) to calculate the hydrodynamic mass for two phase flow. The equation agrees well with the experimental measurements except for high void fractions :

$$m_h = \frac{\rho\pi D^2}{4}\frac{[(D_e/D)^2 + 1]}{[(D_e/D)^2 - 1]} \tag{2.20}$$

where, D_e/D can be estimated from the equation

$$D_e/D = \begin{cases} (0.96 + 0.5P/D)P/D & \text{for triangle tube bundle} \\ (1.07 + 0.56P/D)P/D & \text{for square tube bundle} \end{cases} \tag{2.21}$$

For high void fractions (above 80%), the added mass is very small since the equivalent density of the mixture is low. However, if the slip ratio, S, is high, this leads to misleading prediction of added mass from the homogeneous model, which results in a lower added mass than actually exists. Literature also showed that there is no significant difference between added mass in the streamwise and transverse directions.

2.7 Fluidelastic Instability in Tube Bundles

Fluidelastic instability is a self-excited mechanism in which the fluid forces are dependent on structure velocity and displacement. This phenomenon occurs when there is an abrupt increase in tube response with small increase in flow velocity. Tubes in heat exchangers are susceptible to extensive damage and failure if fluidelastic instability occurs. In a tube bundle, dynamic instability usually occurs when the negative fluid damping exceeds the positive damping in the system. This results in a net negative damping, thus a significant increase in tube vibrations as a result of the system energy increase. The hydrodynamic force acting on a flexible tube in an array is affected by its motion as well as neighbouring tubes motion. If this interaction causes a hydrodynamic forces proportional to tube displacements and in-phase with tube velocity, dynamic instability occurs.

Another phenomenon observed in tube bundles is static instability, also some times called "divergence". This occurs when fluid negative stiffness exceeds structural stiffness, which leads to total negative stiffness of the system. The tube natural frequency is then effectively zero. Compared to dynamic instability, this type of instability is rarely observed in tube bundles.

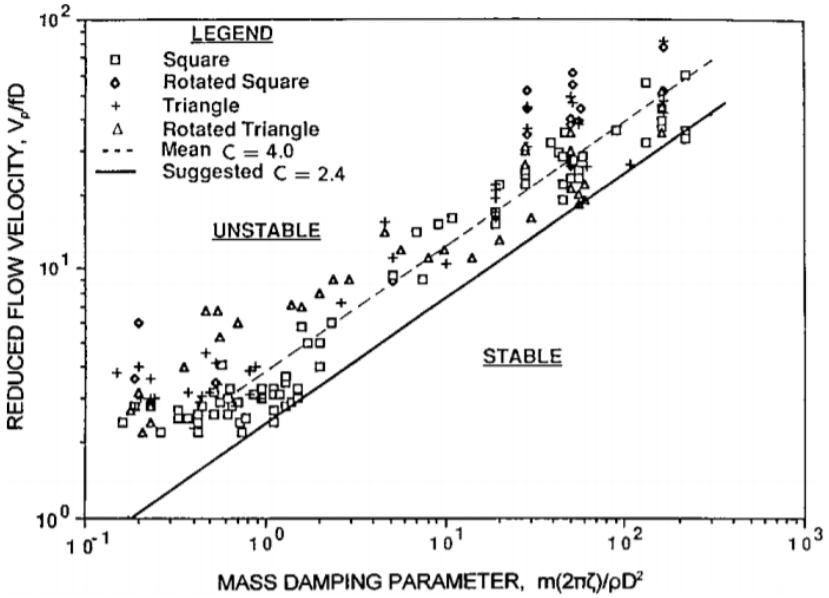


Figure 2.5 Fluidelastic stability threshold for tube bundles in heat exchangers [4]

Results reported in the literature are presented in this chapter for each configuration separately. Most studies are concerned with the single flexible tube, but some studied multiple

flexible tubes in an array. In the literature, upstream velocity is sometimes used instead of pitch velocity (gap velocity).

The unsteady models rely on directly measured dynamic fluid forces on the oscillating cylinder. Tanaka and Takahara [49, 50] measured the unsteady fluid forces on a centred tube in an in-line tube array. This tube was excited harmonically, and the fluid forces acting on the surrounding tubes were measured. They assumed that the fluid forces affecting a tube in the array are a function of the tube motion as well as that of the immediate surrounding tubes only. The experiments were conducted to measure the force amplitude and phase in the lift and drag directions.

A discontinuity in the stability boundary curves was observed for mass damping parameters in the range of $50 \leq m/\rho D^2 \leq 500$, and authors concluded that the instability mechanism is different between below and above this range. Later, Tanaka et al. [51] showed that this discontinuity is not due to a fundamental change in the instability mechanisms by conducting unsteady force measurements on a single flexible tube oscillating in the lift direction. Although Tanaka and Takahara's model showed good agreement with experimental measurements, this model is not feasible due to the effort required, which makes it unpractical for industrial applications.

Chen [52, 53] coupled the fluid forces with the tube equations of motion to develop a mathematical model from Tanaka and Takahara [49]. Chen predicted the multiple stability regions and his results were in good agreement with experimental data from Tanaka and Takahara's work. The author found that there are two main dynamic instability mechanisms in tube arrays subjected to cross-flow. One is controlled by fluid damping (commonly known as the velocity mechanism) and the other is controlled by fluid-elastic forces (commonly known as the displacement mechanism). When the modal damping becomes negative, the energy is transferred from the fluid to the tube's velocity, and the system becomes unstable. When energy is transferred from fluid to cylinder to increase its displacement, stiffness-controlled instability occurs, and modal damping decreases with tube velocity increase. When modal damping becomes zero, the system becomes unstable.

2.7.1 Jet-switching model

This is the first model that was developed by Roberts [54] to analyse the fluidelastic instability of tube arrays subjected to cross flow. This model is based on some key assumptions, such as assuming the pressure difference across the jet to be constant due to constant pressure in the wake area. Also, as shown in figure 2.6, flow separation point is at the minimum gap between cylinder centers. These assumptions are also necessary beside considering the

jet flow nonviscous. Jet- Switching model doesn't estimate the critical velocity accurately. However, the credit for identifying the first explanation as this instability is a self excited phenomenon goes to Roberts. Instability condition here is the synchronization between tube motion and jet-switching mechanism so net energy is absorbed by oscillating tube.

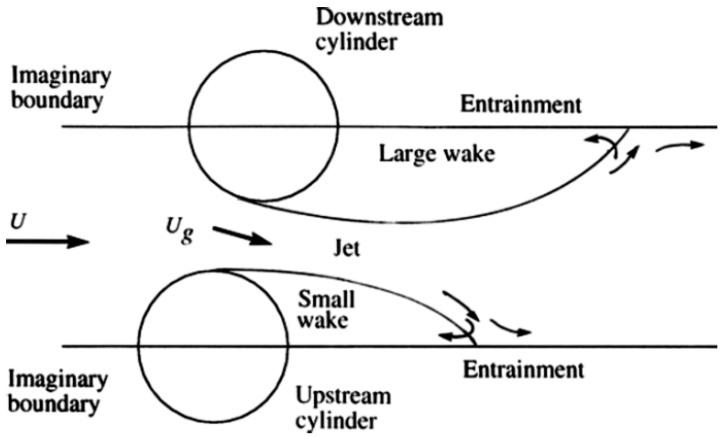


Figure 2.6 Jet-flow model between two cylinders [5]

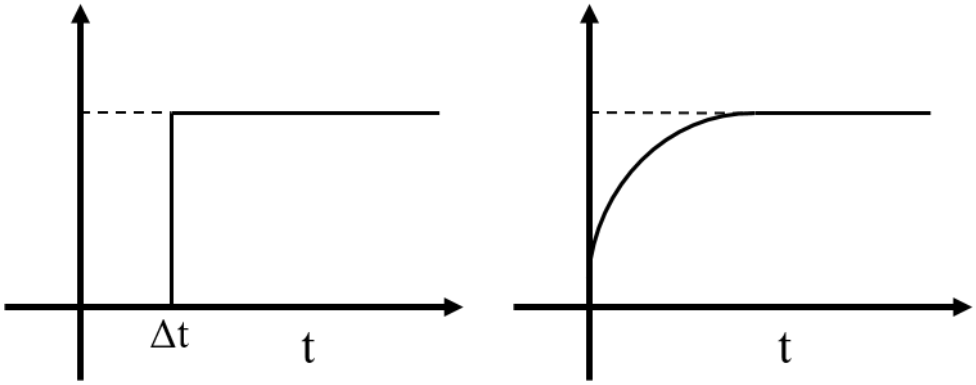
2.7.2 Quasi-steady model

Since several theoretical results in the literature are based on the quasi-steady approach, it is important to outline some of its key features. Quasi-steady models are based on the assumption that both coefficients of lift and drag are the same for flexible and rigid cylinders. In this model, moving structure fluid-dynamic characteristics with varying and constant velocities are equal. This assumption is reasonable if the cylinder deflection is relatively small. Price and Paidoussis [55] assumed that the force coefficients vary linearly with the tube displacement, the neighbouring tubes displacements and incidence flow angle. Force coefficients sensitivity to flow incidence is related directly to sensitivity of tube deflection, which is based on Price [56], might be an incorrect relation.

Price and Paidoussis [57–59] and Price et al. [60] refined this model by suggesting that the fluid forces on any cylinder in an array are directly influenced only by the cylinder's own motion and its immediate neighbours. A time delay between the tube motion and the fluid response was incorporated based on the time required for the flow to travel one row and the inclination of the wake shed from a cylinder due to its transverse motion. Price and Paidoussis multiplied the cylinder displacement by a factor, $e^{-\lambda\mu D/U}$ to consider the retardation of the flow approaching a cylinder, where λ, is the eigenvalue, and μ, the flow retardation parameter.

Granger and Paidoussis [6] modified the quasi-steady model proposed by Price and Paidoussis

[55], leading to the quasi-unsteady model. This model provides a better prediction of the fluidelastic behaviour of single tube in an otherwise rigid array. Granger and Paidoussis based their model on the Navier-Stokes equations. The study included a comparison between both the model and experimental results of the normal square and triangle arrays. While this new model proposes more accurate solution to the fluidelastic instability problem, it is more complicated and requires experimental study to provide time delay parameters. Authors concluded that disturbance is transferred from vibrating tubes to the surrounding flow field due to an existence of a finite layer of vortices. Unlike the quasi-steady model, quasi-unsteady model proposes the memory effect in the flow instead of assuming an abrupt delay effect (see figure 2.7). Although the quasi-unsteady model gives better agreement with experimental data for the fluidelastic instability critical velocity, it is limited to single-flexible cylinder analysis.



(a) (b)

Figure 2.7 Lift coefficient transient variation: (a) in quasi-steady model, (b) in quasi-unsteady model [6]

Sawadogo [61] measured both the unsteady and quasi-static fluid forces in water and two-phase air-water cross-flow in a rotated triangular array. A novel method was developed to estimate the time delay. The limitation in the function limits the experimental data to be used in a very narrow range of excitation frequencies and flow velocities. The quasi-steady stability analysis results showed fairly good agreement with experimental dynamic stability tests in the lift direction only at the high void fractions. A similar approach was adopted by Olala [62] in the streamwise direction. The study included multiple instrumented tubes to model the cross-coupling forces in the same rotated triangular array. It was necessary to model the two-phase flow using Feenestra model to have compact phase and magnitude data for the neighbouring tubes. Compared to the other models, the quasi-steady model

requires less experimental data as an input and has good agreement with the experimental measurements.

2.7.3 Analytical models

The advantage of using analytical models compared to quasi-steady and unsteady models is that they require no experimental data. Paidoussis et al [63] developed a model based on the potential flow theory. The model determined the instability threshold by considering the velocity dependent fluid-damping effect. The time lag between fluid forces and tube motion response was accounted for by adding a time delay term. The model was developed to predict the instability for a single-degree-of-freedom system. In order to extend the theory to include multiple tubes, the fluid-stiffness terms were added for better agreement with experimental data in the cost of adding empirical inputs to the model [64].

Another SDOF model was developed by Leaver and Weaver [7, 65] that does not require any empirical data (see figure 2.8). By using the unsteady Bernoulli equation and introducing the time delay effect into the model, a single flexible tube instability was predicted only in the transverse direction. The model lacked the fluid-stiffness forces effect. However, the multiple instability bands that were found to exist experimentally were first predicted using a numerical model. In a later study, Hassan and Weaver [66] included the streamwise tube motion in a newly developed model version. The transverse-to-streamwise natural frequency ratio could be changed in the array. Agreement with experimental data was acceptable for the rotated triangular geometry with a specific pitch ratio. To include other geometries, the model was extended to include normal square, normal triangle, and rotated square arrays [67]. Variable tube pitch ratio and mass damping parameters in the model could generalize the results exported from the simulations.

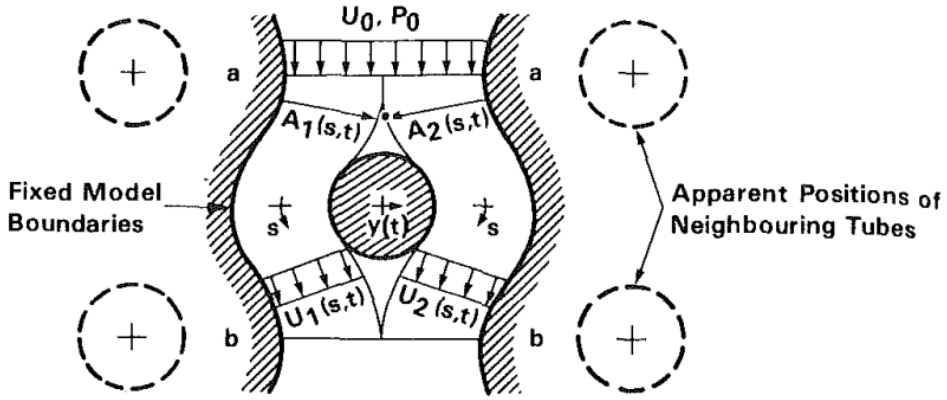


Figure 2.8 The unit cell used in the model to describe the FEI mechanism [7]

2.7.4 Nonlinear models

Due to the imperfections in manufacturing the steam generator parts, in addition to the design tolerance that may allow vibration gaps between tubes and the supports, the post-instability vibrations have been studied in the literature by several researchers for the tube arrays subjected to cross-flow. The vibrational unstable mode transition may occur as a result of the post instability contact with inactive supports. This may lead to an early fretting wear that reduces the steam generator tubes' life time. Nonlinear quasi-steady forces are incorporated in a nonlinear model developed by Price and Valerio [68]. The developed equation of motion represents a single flexible tube model, flexible only in the transverse direction. The linearized theory agreed very well with the nonlinear theory results for three different arrays. The experiments performed by Lever and Rzentkowski [69] showed that the hysteresis occurs only when the array contains multiple flexible tubes. This also agreed with the nonlinear analysis in Price's model. Meskell and Fitzpatrick [70] compared the linearized model results with experimental test results for two normal triangular arrays. It was found that the nonlinear effect is clear in the denser array, which has led to developing an empirical model. A good agreement of the critical velocity was shown from the model, but not the limit cycle that was over estimated. Nonlinear analysis considering tube-to-support contact has been done [71–73].

2.8 FEI of Rotated Square Array ($\theta = 45^o$)

In recent work, Nakamura and Tsujita [15] presented test results of rotated square arrays of different pitch-to-diameter ratios (from 1.2 to 1.5) in a wind tunnel. The authors reported the existence of fluidelastic instability only in the in-plane (streamwise) direction for all the pitch ratios studied. Tube vibration amplitudes increased in the streamwise direction more than in the transverse direction. A test velocity where an increase in response occurred was reported to be the instability velocity. Due to test facility limitations, higher test velocities could not be attained.

A larger array of rotated square tubes was studied by Price et al. [74]. This study performed both air- and water-flow experiments on a single flexible tube in a rigid array as well as a fully flexible array of pitch ratio 2.12. Results showed that fluidelastic instability does not occur in both the in-flow and cross-flow directions. However, the tube response showed a sudden increase in water flow. The authors confirmed this to be the result of a resonance effect from the lock-in between the tube natural frequency and the vorticity shedding frequency.

Price et al. [75] conducted new experiments on a single flexible tube in an array with the

same pitch-to-diameter ratio of 2.12 in a wind tunnel, in an array with two tube rows and another array with three tube rows. The flexible tube was made of a rigid cylinder attached to the walls by a piano wire at both ends, and response was recorded for both in-flow and cross-flow directions. The wires were connected to mechanical dampers in order to have the ability to vary tube damping. It was found that for the two rows array, the monitored tube remained stable for all damping values. However, the monitored tube became unstable when located in the third row only when the logarithmic decrement of damping was < 0.08. With the addition of a damping fourth row, although the monitored tube is still in the third row, it goes back to a stable state. This shows how sensitive the stability behaviour is to the tube location and number of rows in the array.

Paidoussis et al [14] presented experimental results for a rotated square array of 1.5 pitch ratio in air and water flow. The study was performed on a single flexible cylinder in an otherwise rigid array. The authors observed the static instability in this array for the first time, or as it was called, "divergence". This divergence might cause wear to deflected tubes as cylinders might chatter due to the new location in the array. Strouhal periodicities were found in the array with close frequencies to what was reported by Chen and Weaver, and with weaker coupling with the tubes. The sudden increase in tube vibration amplitude was attributed by the authors to a Strouhal periodicity. No clear fluidelastic instability was reported for the array.

Price et al [76] conducted flow visualization experiments for normal triangle and rotated square arrays of 1.375 and 1.5 pitch ratios, respectively. The study was done on a rigid tube array. For the rotated square array, symmetric vortices were clearly detected attached to all tubes in the array at low Re. Strouhal numbers are in good agreement with what was found in the literature. Strouhal number decrease was observed with flow velocity increase, but these changes are very minor. The authors suggest that flow periodicities in cylinder array might be a result of multiple mechanisms superposition effect.

Recently, an array, similar to the one reported in the current project, having 1.633 pitch ratio was studied by Chung and Chu [77]. The study covered a wide range of two-phase flow void fractions for normal and rotated square array configurations. Large amplitude vibrations of the rotated square array were attributed to hydrodynamic coupling between the tubes in the flow direction. It was found that vortex shedding exists in this array up to 50% VF as the main source of vibration. A Connors constant of 14 was reported. However, there was no clear FEI. The authors attributed this high constant to hydrodynamic coupling between the tubes.

Kuran [78] conducted a FEI study on a rotated square array of 2.12 pitch ratio in a wind

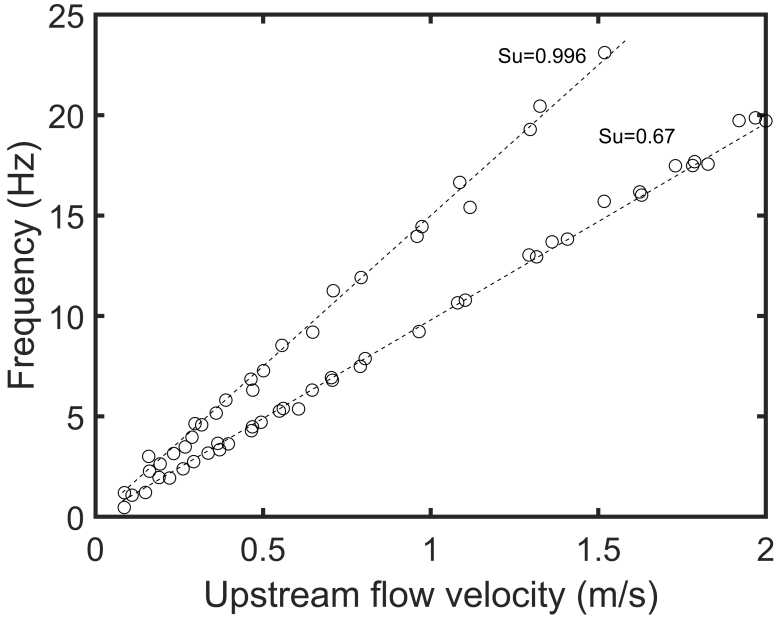


Figure 2.9 Periodicity frequencies vs. flow velocity [8]

tunnel. He confirmed that a single flexible tube in an otherwise rigid array is stable, and instability occurs when the number of flexible tubes is three or more for the studied array. Based on this result, fluid-stiffness controlled mechanism was deduced to be the cause of the flexible tube vibration. When Kuran tested multiple flexible tubes, he located two flexible tubes inside the array each time at different relative locations. It was found that fluidelastic coupling between the tubes changes significantly and that tube relocation in the array affects this interaction strength. Fluid coupling decreases significantly for flexible tubes positioned deep inside the array when compared to when they are positioned in the first few rows. Static instability (divergence) was observed in this array after observing the clear loss in transverse vibrations, which indicates a loss of stiffness.

Weaver et al. [8] studied vortex shedding in a rotated square array geometry over a wide range of pitch ratios (from 1.21 to 2.83) using hot wire measurements and flow visualization. The authors presented a comparison with previous data from the literature. It was found that two clear periodicities exist and can be detected in the first two rows of the array. For the tubes deep inside the array, it was easy to detect one of the frequencies due to the difference in local flow velocity. The authors presented a graphical representation for all periodicities captured in the tested arrays and concluded that there always exist two periodicities. It was also concluded that vortex shedding depends on row depth and Reynolds number. Figure 2.9 shows the two periodicities detected in the arrays over a wide range of flow velocities. This

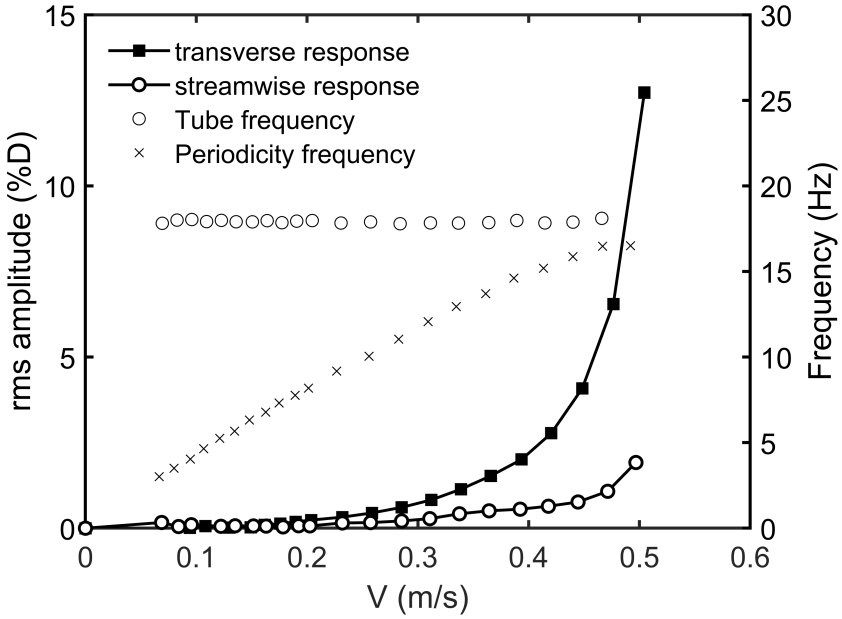


Figure 2.10 Streamwise and transverse response of single tube in rotated square array of P/D=1.7 in water cross flow [9].

study uses upstream velocity in all calculations instead of flow gap velocity.

The results of Scott [9] agreed with those of Weaver [8] who conducted water flow experiments on a rotated square array of pitch ratio 1.70. The single flexible tube and the fully flexible array showed similar behaviour. The response increases gradually and the vortex shedding frequency coincides with the tube frequency at a velocity very close to that where the vibration amplitude increases. It was not clear whether this was a resonance effect or fluidelastic instability, or both, occurring at very close velocities, as reported by the author. However, knowing that the locking effect starts even before vortex shedding and tube frequency completely match gives a different explanation, as this array might vibrate with high amplitudes due to resonance.

Generally, the rotated square array shows unique features and complex behaviour, as detailed in the research papers discussed in the foregoing. Apparently, rotated square arrays seem to be generally more stable than other arrays. Most of the experimental results in the literature showed more stable behaviour for the rotated square array over a wide range of pitch ratios. However, some research work in the literature could not clearly state the stability of the tested arrays. Also, the dynamic behaviour of the array in two-phase flow is still ambiguous.

2.9 FEI of Other Array Geometries

2.9.1 Rotated triangular array ($\theta = 60^o$)

A rotated triangular array was experimentally studied by Olala et al. [79] for a pitch-to-diameter ratio of 1.5. A quasi-steady fluidelastic instability analysis was performed in this work. Four flexible tubes were tested in an array of fixed tubes. Experimental results showed the record of lift and drag coefficients with streamwise dimensionless displacement of the mid tube in the array. Apparently, the drag force coefficient increases for the central tube starting from 0% void fraction up to around 50 %, then decreases again at high values of void fraction. The drag coefficient was found to increase when the tube is moved downstream, while it decreases when the tube is moved upstream. As the results showed, the lift force coefficient does not show any changes by moving the tube. The drag coefficient of the downstream neighbouring tube in the array was found to have a reversed variation with central tube displacement compared to the upstream tube. Results also showed that for larger number of flexible tubes, critical flow velocity has lower values.

Scott [9] conducted experiments on two arrays, one with 1.73 and the other with 1.375 pitch ratio. A single flexible tube in the compact array became unstable with a clear critical velocity and a slight shift in the tube frequency, while for the narrow spaced array a critical velocity was less clearly defined; however, instability is observed. A fully flexible array was also unstable, but with higher fluid cross-coupling between the tubes, which showed an increase in the tube vibration response with flow velocity. This coupling also results in changes in tube frequency, partly due to its effect on added mass.

Mureithi et al [10] conducted experiments on a rotated triangular array of 1.37 pitch ratio, with tubes of 40.4 mm outer diameter in air flow. The experiments are concerned with the instability in the in-flow direction as the tested array is already known to be inherently unstable in the transverse direction. The array showed an expected behaviour of tubes instability. The paper confirmed that a single flexible tube can not undergo single degree-of-freedom fluidelastic instability - in streamwise direction - in the rotated triangular arrays. Figure 2.11 shows that instability is more likely to happen with the increase in flexible tubes in the array.

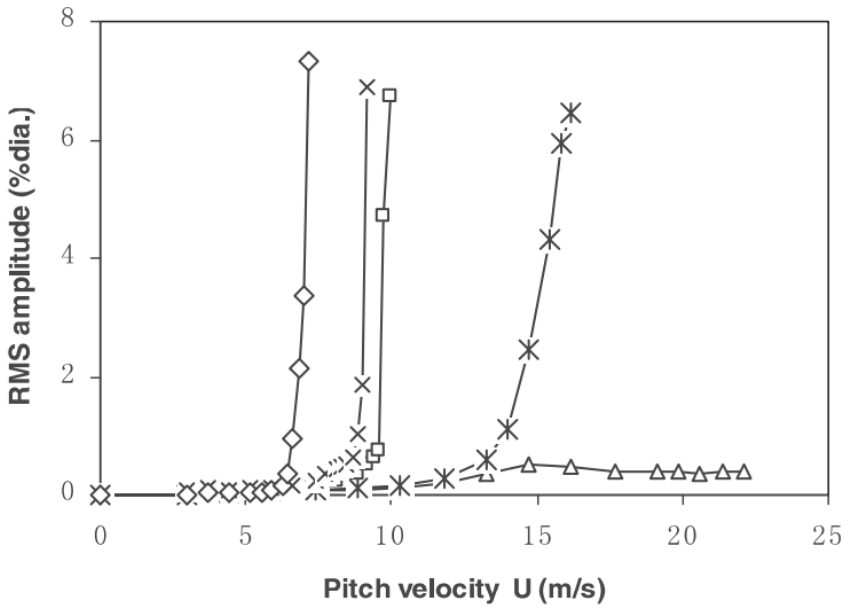


Figure 2.11 Number of flexible tubes in the array shows how this affects tubes dynamic behaviour: △, one tube flexible; ∗, two tubes flexible; □ , one column flexible; ×, seven tubes flexible; and ◊ , all tubes flexible [10].

Weaver and Elkashlan [80] conducted experiments in a wind tunnel on a rotated square array of 1.375 pitch ratio to study how stability behaviour changes with tube damping and mass ratio. It was noticed that damping in the in-flow direction is more sensitive to flow velocity. However, total damping increases gradually with flow velocity and reaches its maximum value at around 0.5 V_c, and then decreases again till it approaches zero. The authors indicated that the Connors equation is not the most adequate to define the stability threshold of a tube bundle as they found that the critical velocity is less dependent on tubes damping and mass damping parameters than indicated by Connors equation.

Austermann and Popp [81] tested rotated triangular arrays of 1.375 and 1.25 pitch ratios in a wind tunnel. The compact spacing array showed instability for the tube in the first row, while single tubes tested in other rows vibrated due to turbulence. The large spacing array of 1.375 pitch ratio was compared with the one tested in Weaver and Elkashlan [80] of the same pitch ratio. Both found that the single flexible tube located in the third row reaches instability before tubes in other rows. Tubes with low mass damping parameter had several instability thresholds, and those with higher mass damping parameter did not show high amplitude vibrations.

2.9.2 Normal triangular array ($\theta = 30^o$)

Normal triangular arrays with small pitch ratio do not usually show fluidelastic instability for the case of single flexible tube [82]. Scott [9] studied normal triangular arrays of 1.33 and 1.5 pitch ratios with a 25.4 mm tube diameter and with rigid tubes made of acrylic. For a single flexible tube in an otherwise rigid array, no FEI was observed, but only a small increase in tube vibrations due to flow turbulence. For fully flexible array of 5 rows and 17 columns, a single peak showed up with an increase in tube's frequency. That was explained by Scott as a possibility of switching in vibration modes.

Meskell and Fitzpatrick [70] conducted an experiment on two normal triangular arrays of 1.32 and 1.58 pitch ratios. Instability was observed for a case of a single flexible tube. Using nonlinear curve fitting, fluid forces were linearly modelled and agreed well with instability threshold of 1.58 pitch spacing array. However, predicted results did not agree with the array of 1.32 pitch ratio. This was explained by the significance of the nonlinear relation between fluid forces and tube motion in the 1.32 array; the model used was a linearized model.

Polak and Weaver [83] studied vortex shedding in normal triangular arrays for a wide range of pitch ratios between 1.4 and 2.67 using hot-wire measurements. This study is very similar to that by Weaver et al. [8] but with a different array configuration. This fundamental study provided a Strouhal number change with pitch ratio and a comparison with results from the literature. While spectral peak frequency increases linearly with flow velocity, it was found that a high frequency periodicity shows up in the first row and decays gradually deeper into the array, and totally disappears in the fourth row. For a large pitch ratio array of 2.67, the calculated Strouhal numbers are 0.492 and 0.349. This study shows that the first or second row in the array is the source of the vortex shedding, and some vortex shedding dissipates inside the array. For pitch ratios <2, only first row periodicity exists, but for wide spacing arrays with pitch ratios ≥ 2, second row periodicity also exists but with lower frequency and lower intensity. Note that all flow velocities used in the work of Weaver are upstream flow velocities.

2.9.3 Normal square array ($\theta = 90^o$)

Feenstra et al. [84] studied a group of 12 tubes in a normal square array with a pitch ratio of 1.485. The operating fluid was Refrigerant 11, and vapour was generated by heating up the fluid using electric heaters. Both single flexible and fully flexible array tests were performed in single phase and two-phase flow. A single flexible tube was observed to be unstable in the lift direction, while in the drag direction, symmetric vortex shedding caused an increase

in tube response, but no instability was observed. A fully flexible tube array test was also conducted, and instability occurred in both lift and drag directions. The stability threshold of the fully flexible array was 25% less than the single flexible tube threshold. Tubes response in the drag direction was quite high (up to 6% D) due to vortex shedding for the case of the fully flexible array. Two-phase flow tests did not show instability in the case of a single flexible tube. However, they showed instability for all tested void fractions in the fully flexible array, which means that the instability mechanism in this case is due to hydrodynamic coupling between neighbouring tubes (negative stiffness mechanism).

Weaver and Abd-Rabbo [85] conducted a flow visualization study on another normal square array of 1.5 pitch ratio, as well as instability analysis. Large vibration response resulted from vortex shedding resonance and resulted in 6%D vibration amplitudes in water. Flow visualization results of the first two rows showed different flow patterns from those deep rows inside the array.

Weaver and Young in [86] conducted a water tunnel experiment on a 1.5 pitch ratio square array. The array could be rotated from 0^o to 45^o, so both normal and rotated square geometries were tested. The array consisted of four rows of flexible tubes. With the change of the incidence angle, the flow periodicity frequency was observed to change.

Price and Paidoussis [87] conducted experiments to study the instability of a normal square array of 1.5 pitch ratio in air and water flows. The study covered several locations for the flexible tube inside the array. For all locations, tube was unstable in the transverse direction, and changing tube's location had negligible effect on tube stability. Moreover, critical velocity was insensitive in water flow. Vortex shedding with low frequency occurred in air and water flows with Strouhal number less than 0.1.

2.10 Numerical Solutions of Fluidelastic Instability

The majority of the research work in the numerical area of solving this problem and investigating fluidelastic instability has studied the instability in the flow transverse direction. The reason is that instability is dominant in this direction even in the case of a single flexible-centered cylinder. Shinde et al. [88] performed a LES simulation with a comparison to experimental results of his own test section. LES is still a challenge for high Re as it requires expensive computational power, hence, this paper studied the instability for low range of Re. Again, recent research work shows that a single flexible tube in either a set of fixed or flexible array of cylinders will have the same critical velocity. The domain is discretized into 25.3 million elements (structured mesh) to perform this LES simulation.

Shinde et al. [89] showed numerical simulation results of the same problem for high Re (up to $Re = 20,000$). The NSMB (Navier–Stokes Multi Block) code was used in the simulation of the "CEA-DIVA" configuration, which is composed of 20 cylinders with P/D=1.5. The authors simply explained the instability to occur by change of sign of the phase difference between the fluid force and the cylinder movement when the transverse flow velocity increases. A 2-D simulation here is performed to predict the unsteady forces for a static tube array. Unsteady loads on the central cylinder is presented vs. time for different turbulence models. The phase lag can be easily predicted by the numerical simulation, as was shown in the results. For high Reynolds numbers, 3-D simulation more efficiently predicts the instability due to the existence of highly turbulent flow. The authors, at the end, showed that 3-D simulation can efficiently estimate the displacement amplitudes better than the 2-D simulation.

Hassan et al. [90] predicted the fluidelastic instability numerically for inline square and normal triangle tube arrays. This paper provided a good explanation of the problem with a neat literature survey. Tanaka and Takahara's unsteady flow model in [50] requires the availability of fluid force coefficients. While these coefficients are usually investigated experimentally, they are estimated numerically in this work. The authors suggested using CFD simulations to predict the parameters of fluid forces for theoretical FEI models, as simulating such an unsteady problem using CFD is computationally very expensive. However, in this paper, CFD is coupled with UFM to get the unsteady fluid forces and coefficients. ANSYS-CFX is used to perform these simulations. The pitch to diameter ratios of the studied arrays are 1.33 and 1.35 for square and normal triangle arrays, respectively.

For a pitch-to-diameter ratio of 1.28, Tan et al. [20] performed another LES numerical simulation using CFX to verify their own experimental results. Tube natural frequency and damping were measured in air, while in water it was difficult for the authors to do so. Instead of measuring in water, damping was numerically estimated by CFD. Tube motion was assumed to be rigidly moving and supported by a spring with stiffness k. Spring coefficient k was calculated as $k = \omega^2 m$. Results showed good agreement between experimental and numerical results, however, the match is not good enough.

Jafari et al. [91] predicted the threshold of fluidelastic instability of a normal triangular array. The solver used is a finite volume based algorithm. This algorithm is validated by results presented in the literature. Geometry and dynamic conditions are chosen based on previously published experimental work. The flow field is two-dimensional, viscous, unsteady, and turbulent, with density of $1000 kg/m^3$ (water flow). The fluid-structure coupling is solved by including feedback between the flow field and structure equations of motion at each time step, which is done by getting the flow-induced forces by solving a RANS model. Then, by

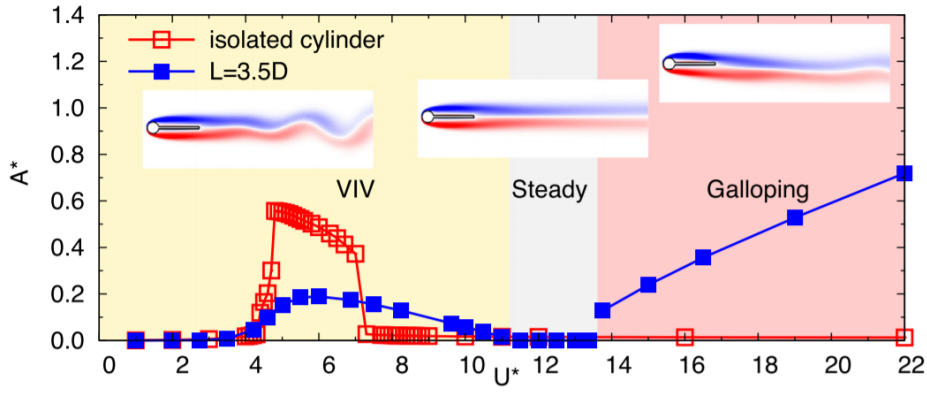


Figure 2.12 FIV regimes with and without splitter plate for single cylinder [11]

solving the equations of motion of the structure, and based on the new position of each node in the domain, the mesh is refined. The time step used is 1 ms. The dynamic properties of the flexible cylinder are chosen based on an experiment from the literature (with Re of 10^4).

Flow induced vibration (FIV) was studied by Sahu et al. [11] for a wide range of flow velocities. This study has been numerically conducted on a single cylinder with and without a splitter plate. Several splitter plates have been used to show the effect of plate length and width on the wake area. As shown in figure 2.12, FIV regimes are defined as VIV, steady and galloping regimes. As expected, the vibration response of an isolated cylinder increases due to lock-in. During lock-in, the vibration frequency is close to the cylinder natural frequency. Numerical results showed a significant reduction in cylinder peak amplitude response due to the existence of the splitter plate in the wake region.

Longatte et al. [92] presented a newly built numerical tool to predict tube vibration in fluid at rest and in cross-flow. Numerical simulations were carried out on Granger's test results on a normal square array [93] of 9 rows and 7 columns of fixed tubes except for a central flexible tube that is moving due to hydrodynamic forces. Simulation was carried out first for the tube in water at rest in order to evaluate added mass and damping. Numerical simulation results were compared fairly to those conducted experimentally.

2.11 Concluding Remarks

Over the last 40 years, experimental studies have been done on normal and rotated triangular arrays, and some on normal square arrays. Rotated square arrays have not received significant attention from researchers. This has led to a lack of knowledge of this array's dynamic behaviour. Thus, a reliable prediction of fluidelastic instability in the rotated square array

has not yet been achieved. Previously discussed studies on the rotated square array showed more stable behaviour than for other configurations. However, no one is yet able to confirm its stability in single phase and two-phase flow. Although some studies observed a change in the critical flow velocity with increasing the number of flexible tubes, no one could provide details on the existence of multiple tubes instability condition as in some cases, a single flexible tube does not undergo instability.

CHAPTER 3 ARTICLE 1: FLOW-INDUCED VIBRATIONS OF A ROTATED SQUARE TUBE ARRAY SUBJECTED TO SINGLE-PHASE CROSS-FLOW

Sameh Darwish, Abdallah Hadji, H.P. Pham, Njuki Mureithi, Minki Cho

This article was published in the "Journal of Pressure Vessel Technology", volume 144(4), pages 041405, January 13, 2022.

In this chapter, the flow-induced vibration (FIV) of the rotated square array is studied in water flow. This is to meet the specific objectives to:

- Investigate the susceptibility of the array to streamwise and/or transverse fluidelastic instability in water flow.
- Study the vortex-induced vibration (VIV) of the tube array and find the Strouhal numbers.

The paper presents a series of flow-induced vibration tests in water cross-flow. Single and multiple flexible tubes were examined in both the transverse and streamwise directions separately. It was found that a flexible tube frequency synchronizes with the flow vortex shedding frequency. This synchronization results in a strong lock-in causing the tube to violently vibrate. Despite of the strong vibrations, no transverse or streamwise fluidelastic instability was reported. Similar observation was made when tested a column of flexible tubes. In the case of fully flexible array, at low range of flow velocities, same behaviour was seen. In the transverse direction, however, no reduction in the tubes vibration amplitudes was noticed after the flow periodicity de-synchronized with the tube natural frequency. This was further discussed in detail in chapter 5. Using Computational Fluid Dynamics (CFD), the measured Strouhal numbers were confirmed using unsteady simulations. A third low Strouhal number was found. However, it is less concerning as it never interferes with the tube frequency at the practical operating range of flow velocities.

Abstract

This paper investigates the flow-induced vibration (FIV) and possibility of fluidelastic instability occurrence in a rotated square geometry tube array through a series of experimental tests. All experiments presented here were conducted in water cross-flow. The array's pitch spacing ratio of approximately P/D=1.64 is somewhat larger than that commonly found in typical steam generators. The stability of a single flexible tube as well as multiple flexible tubes were investigated. The tubes were free to vibrate purely in the streamwise direction or the transverse direction relative to the upstream flow. A single flexible tube, in the otherwise rigid tube array, was found to undergo large amplitude vibrations (up to 40% D) in the transverse direction. Tube vibration frequency analysis indicated the presence of two frequency components related to vorticity shedding in the array. This potential vorticity-induced-vibrations (VIV) and potential coupling between VIV and FEI are discussed in the paper. Test results for streamwise flow-induced vibrations are also presented. Results in water flow show a possible effect related to flow periodicity at low velocity. At significantly high flow velocities, the tubes are found to fully restabilize. This restabilization after VIV locking has not been previously reported as an unlocking result. The present results suggest that the flow-induced vibration of tubes in a rotated square array configuration is significantly more complex than in other geometries, particularly for the streamwise vibration case.

3.1 Introduction

Shell-and-tube heat exchangers are subjected to high-speed flows, which may result in large amplitude structural oscillations and possibly tube failure when supports are ineffective. Tube bundles are susceptible to fluidelastic instability (FEI), vortex shedding and flow turbulence as three main sources of vibrations in fluid cross-flow. Compared to flow turbulence, both fluidelastic instability and vortex shedding can produce high amplitude vibrations. Fluidelastic instability (FEI) is recognized as the most important excitation mechanism that must be avoided in nuclear steam generators (SGs). The instability has been the subject of study over the past 50 years. The transverse direction (transverse to the flow, and out of the plane of the tube U-bend) was found to be generally more unstable. Consequently, steam generators are fitted with so-called anti-vibration bars (AVBs) which effectively limit tube vibration in the transverse direction. The failure of the SONGS steam generators in 2012 [94] confirmed for the first time the possibility of streamwise (in-plane) fluidelastic instability (IPFEI) in an operating steam generator.

Vorticity shedding and associated flow periodicity is the second potentially important cause

of flow-induced vibration in tube arrays. In SGs, vortex shedding excitation is important in the single phase flow regions. As detailed further below, vortex shedding in tube arrays is strongly dependent on tube array geometry. Rotated square arrays with large tube pitch spacings have been found to be particularly susceptible to vortex shedding resonance. While vortex shedding excitation is generally considered as a resonance excitation distinct from fluidelastic instability, some recent work [95,96] has suggested the excitation (lock-in) can be modelled as a coupled mode flutter phenomenon based on a linear wake oscillator model. In this case, however, one of the degrees-of-freedom derives from the fluid (lift force coefficient). While the problem of flow-induced vibration has been intensively studied experimentally and modeled analytically for normal triangular, rotated triangular and normal square arrays, fewer studies to date have dealt with rotated square arrays in details. The dynamic behaviour of this array geometry in different flow conditions and for different pitch ratios remains, at best, only partially understood.

In recent work, Nakamura and Tsujita [15] presented wind tunnel test results for rotated square arrays of different pitch-to-diameter ratios (from 1.2 to 1.5). The authors reported the existence of streamwise fluidelastic instability for all the pitch ratios studied. Tube vibration amplitudes increased in the streamwise direction more than in the transverse direction. A test velocity where an increase in response occurred was reported to be the instability velocity. The possibility of vortex shedding resonance was not investigated. Due to test facility limitations, higher test velocities could not be attained. A larger array of rotated square tubes was studied by Price et al. [97]. This study performed both air and water flow turbulence measurements as well as flow induced vibration experiments on a single flexible tube in an otherwise rigid array of pitch ratio 2.12. Results showed that fluidelastic instability does not occur, in either the in-flow or cross-flow direction. The tube response, however, showed large amplitude vibrations in water flow. The authors confirmed this to be the result of a resonance effect from the lock-in between the tube natural frequency and a vorticity shedding frequency. Price et al. [98] conducted further experiments on a single flexible tube with the same pitch-to-diameter ratio of 2.12, in an array with two tube rows and a second three tube row array. It was found that for two rows, the monitored tube remained stable, however, instability existed in the transverse direction when the tube was located in the third row. With the tube in a middle row, the tube showed stable behaviour. No streamwise instability was reported for any array configuration or tube damping. Static instability (or divergence) was first experimentally observed by Paidoussis et al. [14] in a rotated square array of 1.5 pitch ratio in air and water flow tests, in both in-flow and transverse directions. Fluidelastic instability was observed in air tests for different mass damping parameters, and different locations for the flexible tube in the array. For water flow, the sudden increase

in tube vibration amplitude was attributed to a Strouhal periodicity by the authors. No clear fluidelastic instability was reported for the array. Price et al. [99] conducted flow visualization experiments for normal triangle and rotated square arrays of 1.375 and 1.5 pitch ratios, respectively. The study was done on rigid tube arrays. For the rotated square array, symmetric vortices were clearly detected attached to all tubes in the array, for low Re.

Recently, an array, similar to that reported here, having 1.633 pitch ratio was studied by Chung and Chu [77]. The study covered a wide range of two-phase flow void fractions for normal and rotated square array configurations. Large amplitude vibrations of the rotated square array were attributed to hydrodynamic coupling between the tubes in the flow direction. Weaver et al. [8] studied vortex shedding in rotated square array over a wide range of pitch ratios (from 1.21 to 2.83). The authors also presented a comparison with previous data from the literature. It was found that two clear periodicities exist and can be detected in the first two rows of the array. The results agreed with those by Scott [9] who conducted water flow experiments on a rotated square array of pitch ratio 1.70. The single flexible tube and the fully flexible array showed similar behaviour. The response increases gradually and vortex shedding frequency coincides with the tube frequency at a velocity very close to that where the vibration amplitude increases. It was not clear whether this was a resonance effect or fluidelastic instability, or both occurring at very close velocities. Generally, the rotated square array shows unique features and complex behaviour as detailed in the papers cited in the foregoing. Theoretically, Price and Paidoussis [100] showed that the occurrence of fluidelastic instability in a rotated square array of 2.12 pitch ratio requires the existence of multiple flexible tubes (at least two degrees-of-freedom). This was later confirmed by Price and Kuran [13], where the instability mechanism found in the same array subjected to air cross-flow is the stiffness mechanism. This conclusion was based on the occurrence of instability when multiple flexible tubes are tested, while a single flexible tube did not undergo instability. A closely packed array was studied by Abd Rabbo and Weaver [101] of a 1.41 pitch ratio. The work included a flow visualization study. The authors reported that both single and multiple flexible cases showed became unstable, although the observed periodicities in the array.

Based on the findings discussed in the previous section, It is clear that much remains to be done for a clear understanding of the rotated square array behaviour. The present study contributes results on a rotated square array of pitch ratio 1.64 in water cross-flow. Both streamwise and transverse direction tube responses are measured. Different configurations of the flexible tubes are studied to investigate the array behaviour with different number of flexible tubes.

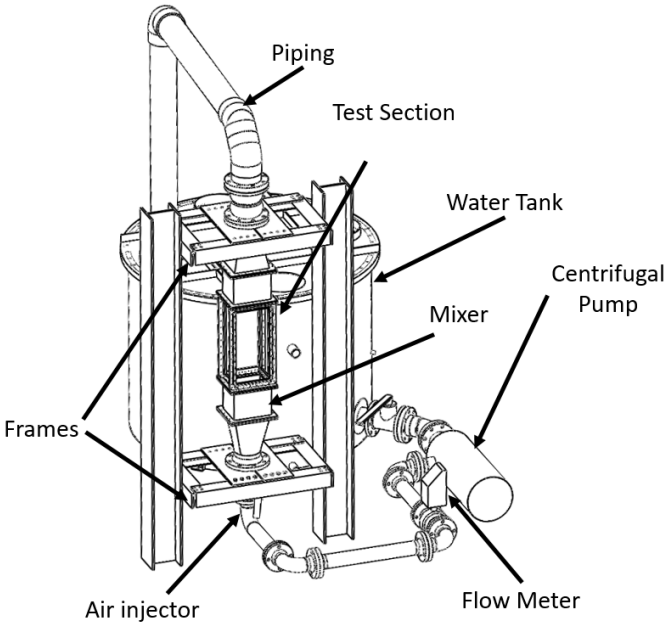
In order to arrive to a clear conclusion about the dynamic behaviour of the tube bundle in

the steam generator, two-phase flow and air flow tests are necessary. The present research work is part of a test program which includes test results for a range of flow conditions. The results of tests in water flow are presented here.

3.2 Experimental Apparatus

The experiments are conducted in a water tunnel loop with water circulated by a 7.5 HP pump, with a capacity of 25 l/sec (see Fig. 3.1). An electromagnetic water flowmeter is installed in the loop for accurate flowrate monitoring. The flow loop is instrumented with a thermocouple to monitor fluid temperature during the tests. The tube bundle is mounted in a test section of cross sectional dimensions 220x190.5 mm^2.

The tube array consists of 32 tubes, either rigid or flexible, arranged in 9 rows an 9 columns, Fig. 3.2. This allows for a wide range of test configurations. Side half tubes are mounted on both side walls of the test section to reduce wall effect. All flexible tubes are instrumented with full bridge strain gauges type 2 (Tee Rosette). This type of bridge contains 4 active elements. The chosen setup is sensitive to bending only (rejects axial strain), is compensated for temperature, compensated for aggregate material (due to Poisson's ratio), and compensated for lead resistance.



(a)



(b)

Figure 3.1 Test loop showing: (a) loop components and (b) test section with tube bundle assembly

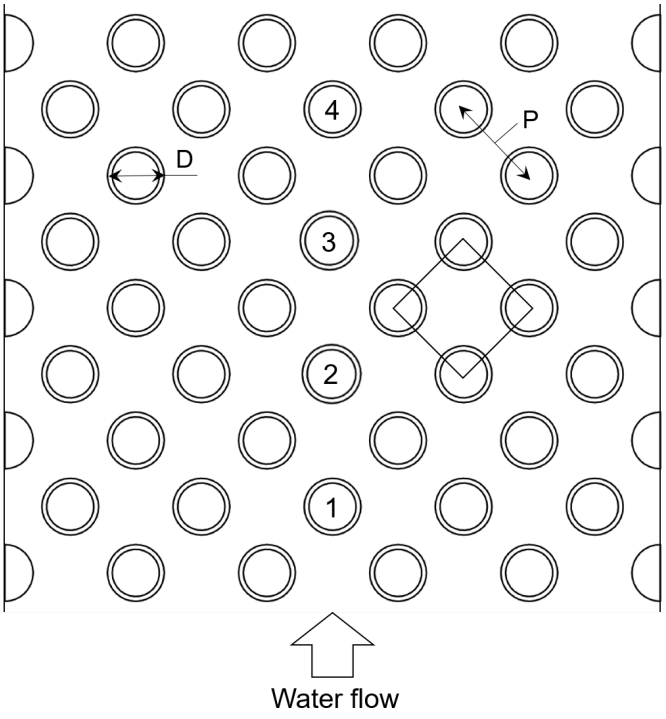


Figure 3.2 Schematic of the rotated square array tubes layout

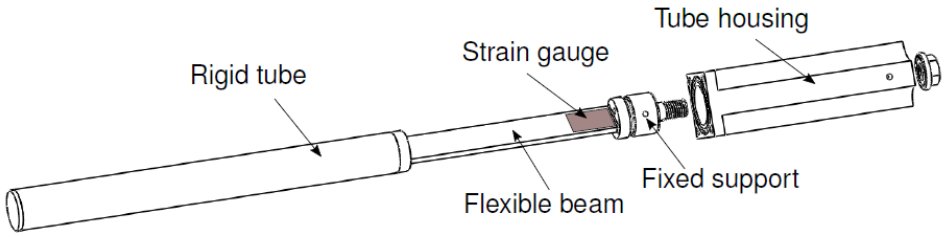


Figure 3.3 Flexible tube design with its mounting

The 'flexible tubes' consist of a rigid tube made of Inconel alloy, mounted on a flexible Aluminium support plate, Fig. 3.3. Due to the rectangular plate having a small thickness-to-width ratio, the flexible tubes vibrate in only one direction, either streamwise or transverse, depending on support plate orientation relative to the flow. The normal direction frequency is five times higher and thus effectively rigid. Each flexible tube is fixed to the test section using a tube housing to mount the rectangular plate for the purpose of subjecting the cylindrical part only to the flow. The natural frequency and damping ratio of all flexible tubes are measured in air prior to the the tests in order to have well tuned tubes with the same dynamic properties. Fig. 3.4 shows the tube in-air response and frequency spectrum. The

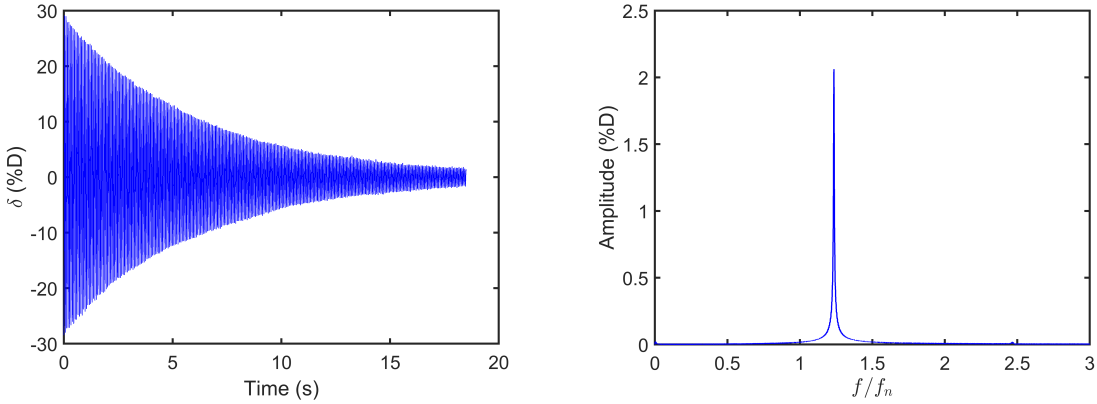


Figure 3.4 Sample of tube response and frequency spectrum in air

average tubes damping ratio is 0.23 % damping ratio in air (δ=0.0145), with mass damping parameter ($m\delta/\rho D^2$) of 20.6 in air, and 0.24 in water.

Three different configurations of flexible tubes are studied in order to give better understanding to the array in water cross-flow direction: (i) single flexible tube, located in the middle column, surrounded by rigid tubes. In this test the tube was located in the 4th row and in a later test in the 6th row. (ii) column of four flexible tubes, (iii) fully flexible array of 32 flexible tubes. Figure 3.2 shows a schematic drawing of monitored flexible tubes locations in the array. The numbered flexible tubes located in the 2nd, 4th, 6th, and 8th rows are monitored. Before the tubes are mounted into the test section, all instrumented tubes are calibrated to have a relation between strain and displacement using CMCP610 benchtop calibrator.

To present the tube dynamic behaviour, the root mean square (rms) of tube tip dynamic displacement is used. All flow velocity values used in the analysis correspond to the pitch flow velocity (V_p). This velocity is related to the upstream velocity (V_∞) by

$$V_p = V_\infty \frac{P/D}{P/D - 1} \tag{3.1}$$

where, P is the pitch gap between the tubes, D is the tube (outer) diameter, and V_∞ is the upstream flow velocity entering the test section. This equation is based on the continuity equation and most commonly used in the literature to describe the mean interstitial flow velocity for all the arrays. All velocity values are presented in the non-dimensional form.

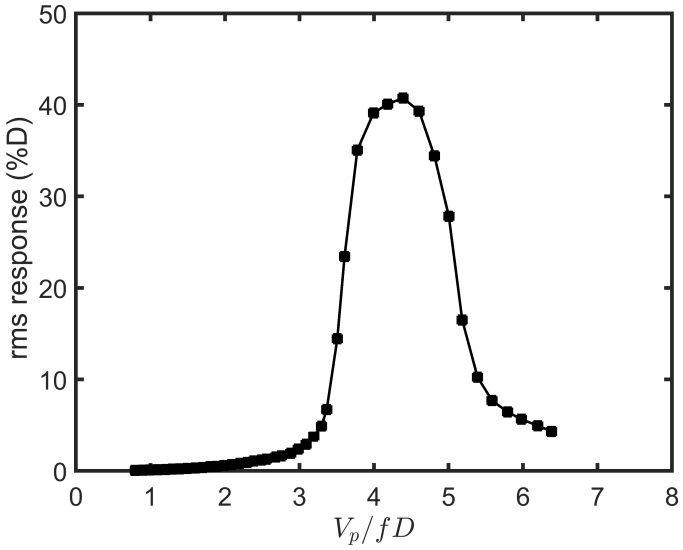


Figure 3.5 Vortex-induced vibrations of a transverse single flexible tube located in the 6th row

The dimensionless flow velocity $\bar{V_p}$ is defined as

$$\overline{V_p} = \frac{V_p}{fD} \tag{3.2}$$

The dimensionless flow velocity is often be referred to as the 'reduced velocity'. A high (2kHz) sampling rate is used in the flow-induced vibration tests. Strain and flow velocity data were collected using a calibrated data acquisition system, along with the water temperature and pressure gauge for monitoring. Before the tubes are mounted into the test section, strain-to-displacement factor is accurately measured using a calibrated device, and used to present the tube dynamic response as a ratio of its outer diameter (%D). All tests are conducted up to the flow capacity of the test loop.

3.3 Experimental Results

3.3.1 Transverse FIV results

Single flexible tube

The single flexible tube in an otherwise rigid array was tested first. The effect of the tube location in the array was also investigated. The flexible tube was first located in the 4th row and later in the 6th row (this corresponds to tube numbers of 2 and 3 in Fig.3.2,

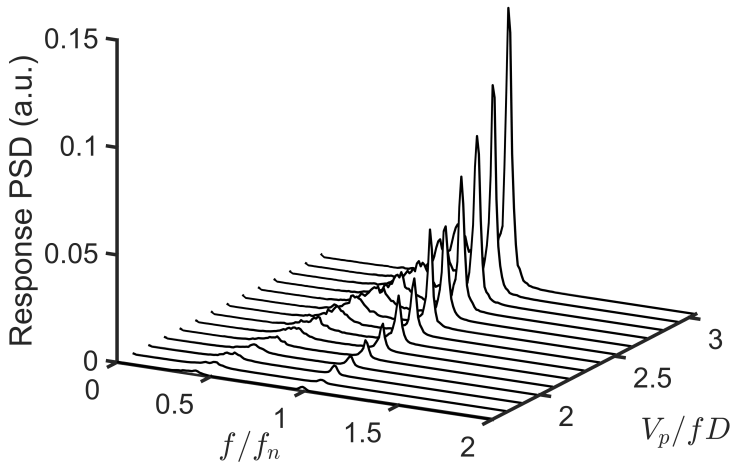


Figure 3.6 Response spectra of single flexible tube in the transverse direction - 6th row

respectively). The rms response of a single flexible tube located in the sixth row is plotted against flow velocity in Fig. 3.5. In the transverse direction, tube response is found to be low in the (reduced) velocity range 0.8 to 3. For velocities above 3.3, the tube response increases significantly. An initial, possible, explanation for this might be the occurrence of fluidelastic instability at this flow velocity. When the flow velocity increases after velocity of 4.5, the tube vibration amplitude was found to be reduced.

The tube response frequency spectres, Fig. 3.6, provide insight into the observed tube response. The response PSDs show that, in addition to the response at the natural frequency, a second periodicity exists. This flow periodicity frequency approaches the tube natural frequency as flow velocity increases. The Strouhal number for this periodicity, calculated based on the flow pitch velocity, is S_p=0.26, based on the definition

$$S_p = \frac{f_v D}{V_p} \tag{3.3}$$

where, f_v is vortex shedding frequency, D is tube diameter, and V_p is flow pitch velocity. Figure 3.7 confirms this Strouhal number when the periodicity frequency and tube (natural) vibration frequency are plotted versus the flow velocity. Based on the results presented in Fig. 3.5 and Fig. 3.7 , in addition to the PSDs in Fig. 3.6, it is clear that lock-in occurs between the vorticity shedding frequency and the tube natural frequency. Lock-in starts near a reduced velocity of 3.3 and causes a significant increase in tube dynamic response which

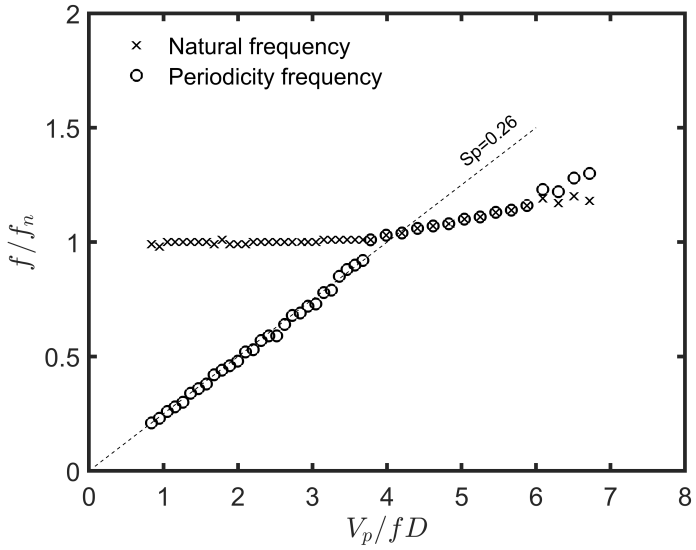


Figure 3.7 Natural frequency of the tube and periodicity frequency in the transverse direction

peaks near reduced velocity of 4. The frequency lock-in is clearly in Fig. 3.7 for the velocity range $3.7 < V_p/fD < 5.9$. This is also the range of the highest response in Fig. 3.5. For $V_p/fD > 6$ the vortex shedding frequency separates from the tube natural frequency, f_n. Coincidentally, the tube response decreases to below 5%D. The foregoing strongly suggests that the large amplitude tube vibrations in Figs. 3.5 and 3.6 are mostly likely onset by flow periodicity rather than the fluidelastic instability. In a later section in this paper, CFD simulation results of the flow in the tube array are presented. The results provide further evidence supporting flow periodicity excitation rather than the fluidelastic instability. The periodicity frequency cannot be clearly detected beyond $V_p/fD = 3.3$ as it merges with the tube frequency at higher velocities.

When the flexible tube was placed in the 4th row, a similar dynamic response was observed. However, the lock-in occurrence was relatively earlier as seen in Fig. 3.8. This is attributed to the existence of a second flow periodicity at a higher frequency. This also explains the moderate tube vibration change at $V_p/fD = 4.5$. Figures 3.9 and 3.10 depict the two periodicities having Strouhal numbers 0.27 and 0.4, respectively, observed in the 4th row.

Four flexible tubes - column configuration

The second array configuration tested had four flexible tubes, all instrumented and aligned in a column as shown in Fig. 3.2. Tubes are referred to as tube 1 ,2 ,3 and 4, respectively, according to the row location in the array. The vibration response of the four tubes is

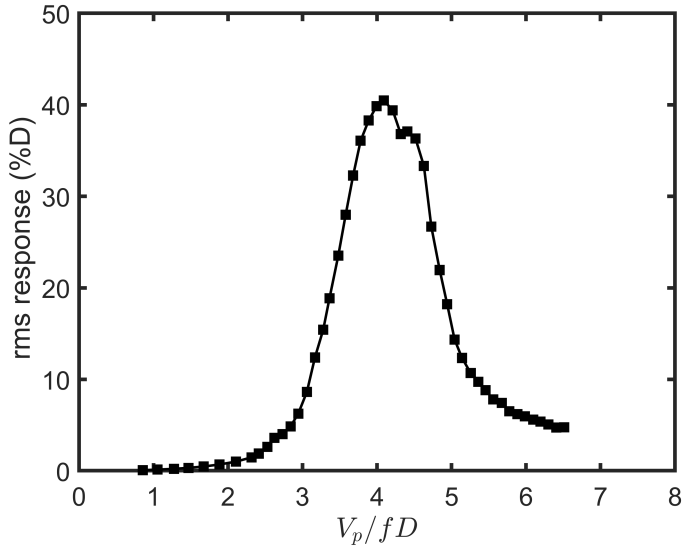


Figure 3.8 Vortex-induced vibrations of a transverse single flexible tube located in the 4th row

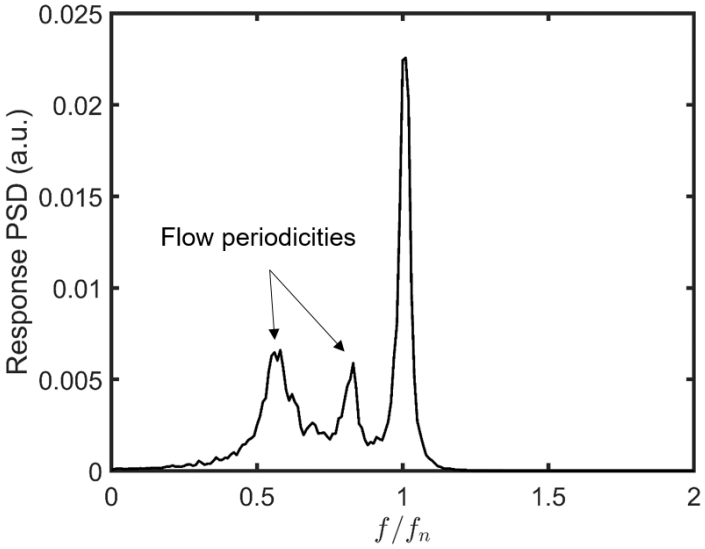


Figure 3.9 Response spectra of single flexible tube in the transverse direction - 4th row

presented in Fig. 3.11. The increase in the rms response for all four tubes is seen to start at a reduced flow velocity of 2.5, reaching a maximum value at 4.5, followed by the same sudden decrease in the vibration amplitude observed in the single flexible tube case. Compared to the single flexible tube, the large excitation onset velocity decreased to 2.5 from 3.3. In addition to this, an early peak showed up at a reduced velocity of 3 before the tube reaches

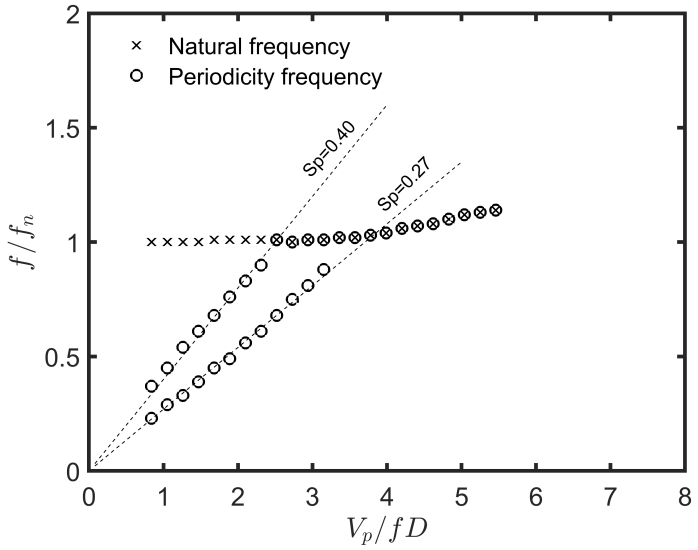


Figure 3.10 Natural frequency of the tube and periodicity frequency in the transverse direction

its maximum vibration amplitude at 4.5. This is apparent in Fig. 3.12a, which shows the response PSDs for tube 2.

The nature of the flow excitation mechanism can be inferred from Fig. 3.13 where similar Strouhal numbers to the case of the single flexible tube (S_p=0.25) are found in this test. In addition, a second flow periodicity appears, but only in the frequency spectra of the first two flexible tubes (S_p= 0.39). This second frequency approaches the tube frequency near V_p/fD=2.5; this is also observed in the frequency spectra in Fig. 3.12. The result closely agrees with what Weaver et al. [8] reported by capturing the two periodicities found in their experiment in the first few rows, and also only one of the periodicities further inside the array. The two Strouhal numbers also agree well with those reported by Scott [9] and Weaver et al. [8] for an array of pitch ratio 1.7.

We note a slight increase in the two Strouhal numbers compared to those reported in these two related works. This is an expected behavior as Strouhal numbers typically increase with decreasing pitch ratio. A remarkable finding is that a third periodicity is observed at very low frequency corresponding to Sp=0.15, as shown in Fig. 3.13. However, this low frequency perturbation did not have noticeable excitation on the tubes; the expected lock-in velocity was higher than the maximum velocity possible in the test loop. Results show that the vortex shedding at Sp=0.25 or 0.26 has significant higher strength than the others. The dominant peak response frequencies obtained from the test results and plotted in Fig. 3.14. It is apparent that the divergence of tube dominant frequencies ends at V_p/fD=2.5 flow velocity

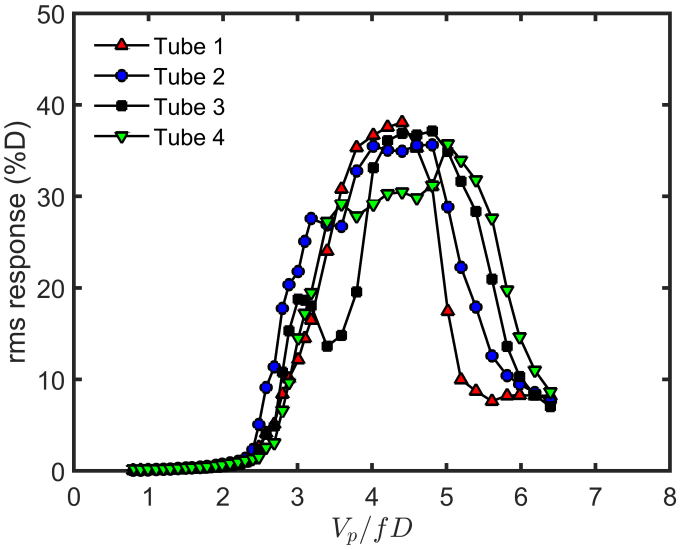


Figure 3.11 Dynamic behaviour of four flexible tubes in the transverse direction

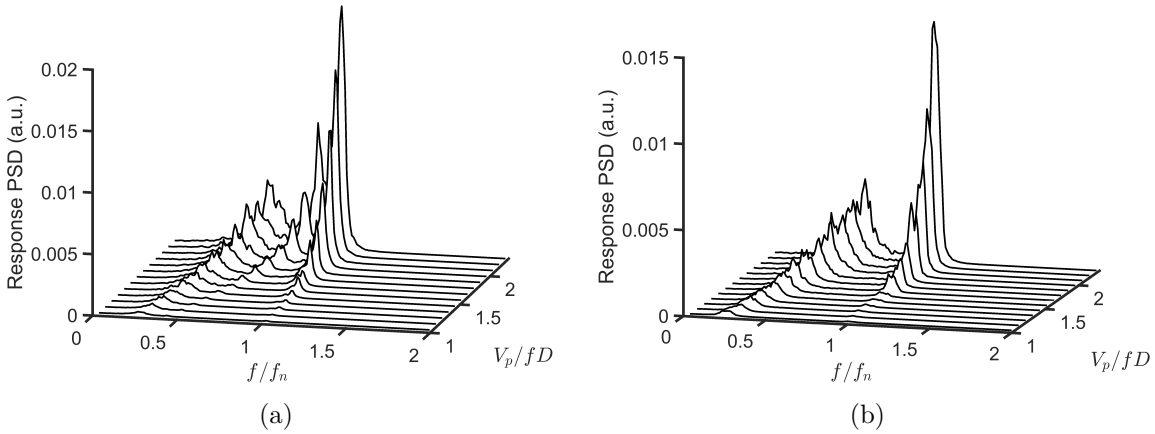


Figure 3.12 Frequency spectra for the column configuration of : (a) tube 2, (b) tube 3

and all tubes start resonating with a single frequency for higher reduced velocities. The coalescence of the tube response frequencies is directly coincident with the lock-in phenomena for S_p=25.

Fully flexible array

The FIV behaviour of the fully flexible array was also investigated. The response of the tubes in the post lock-in velocity range is completely different for the array of flexible tubes. Strong hydrodynamic coupling violently excites the tubes and, even for high flow velocity,

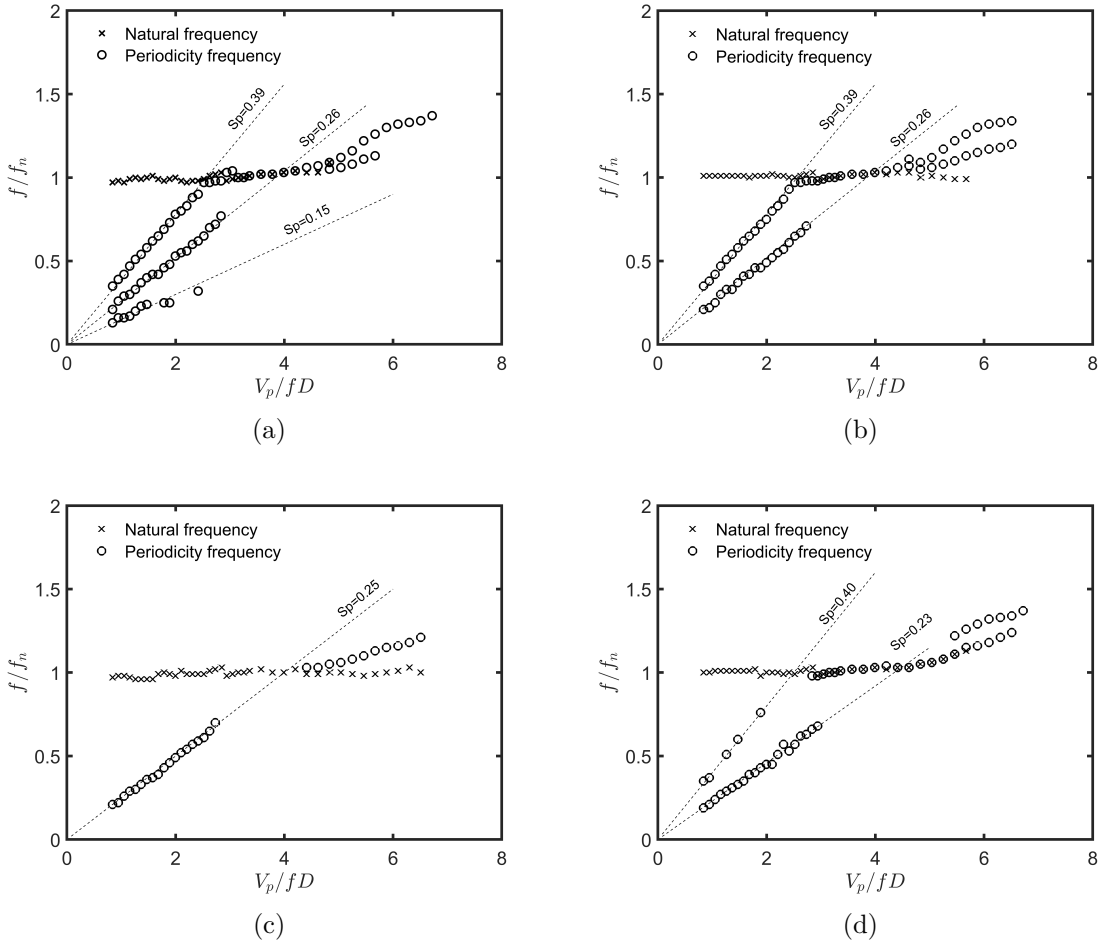


Figure 3.13 Flow periodicity frequencies and tubes natural frequencies; (a) tube 1, (b) tube 2, (c) tube 3, and (d) tube 4

the vibrations did not go below 30%D, see Fig. 3.15. In this test, tube frequencies decoupled from the shedding frequency, such that the vortex shedding frequency was clearly detected, in the post lock-in velocity range (for reduced velocities above 4.4) as shown in Fig. 3.16b. However, large amplitude vibrations in this test above a reduced velocity of 5 is attributed to strong coupling in the water due to the large number of flexible tubes. Figure 3.17 shows the effect of array flexibility on the lock-in range and coupling velocity in the transverse direction for the tube located in the same location (4th row). Compared to the column case discussed earlier, the vibrations start at a flow velocity of $V_p/fD = 2$ instead of 2.5. Frequency analysis showed the similar vortex shedding as previously discussed in the column test.

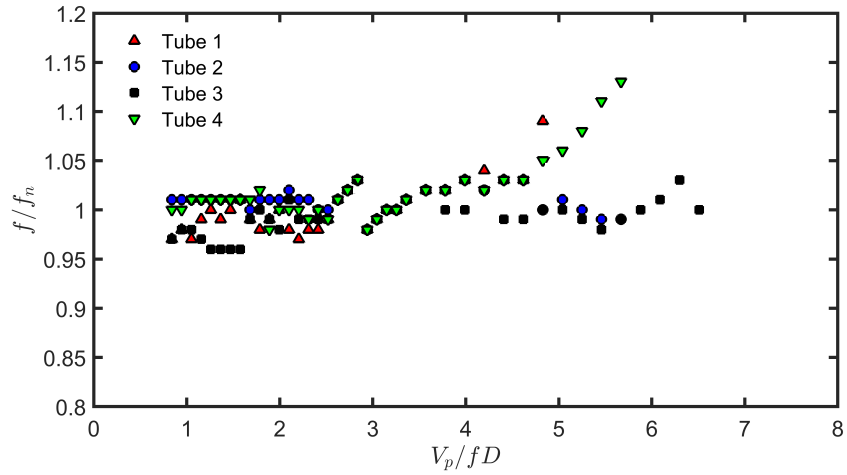


Figure 3.14 Response frequencies vs. flow velocity, for the flexible tubes in a column, vibrating in the transverse direction

3.3.2 Streamwise FIV results

Single flexible tube

The tube behavior in the streamwise direction, on the other hand, is stable as seen in Fig. 3.18 and 3.19. We do remark, however, some mild increase in vibration response which occurs near the reduced velocity of $V_p/fD = 3.0$. The tube response remains, however, much

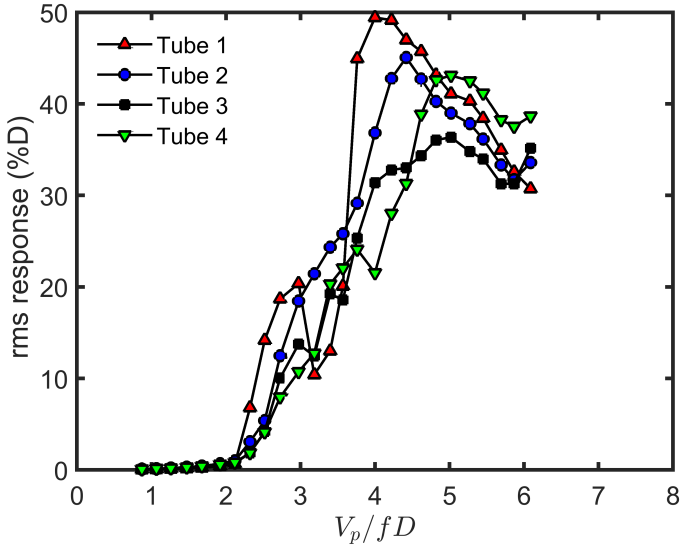


Figure 3.15 Fully flexible bundle behaviour in the transverse direction

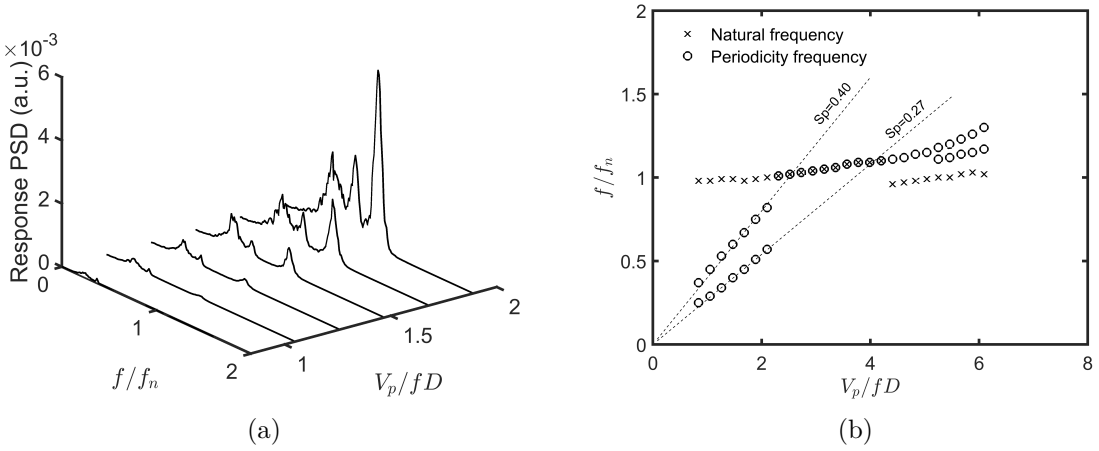


Figure 3.16 Frequency analysis of tube 2 in the fully flexible array : (a) frequency spectra at low velocities, (b) tube natural frequency syncronization with shedding frequencies

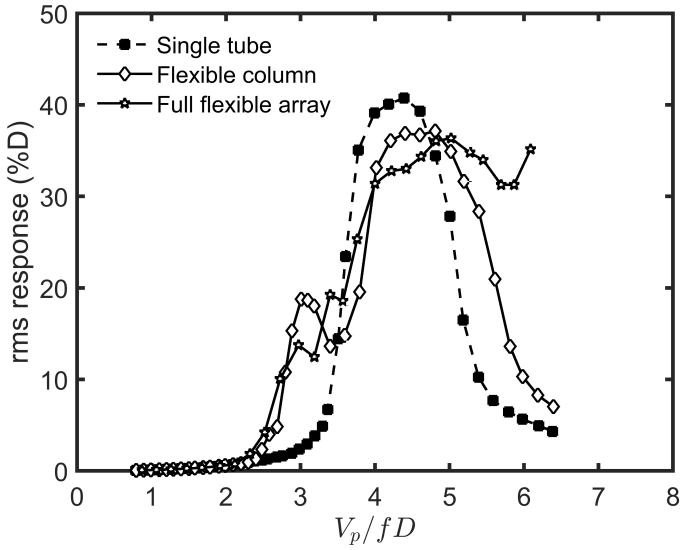


Figure 3.17 Flexible tube dynamic response in different arrangements

lower than that found in the transverse direction. In the streamwise direction, there is no strong vorticity shedding-induced excitation detected in the array. The presence of the flow periodicity, responsible for strong transverse resonance is lower, but clearly detected in the streamwise direction tests. Similar Strouhal number of 0.23 is detected clearly in Fig. 3.20.

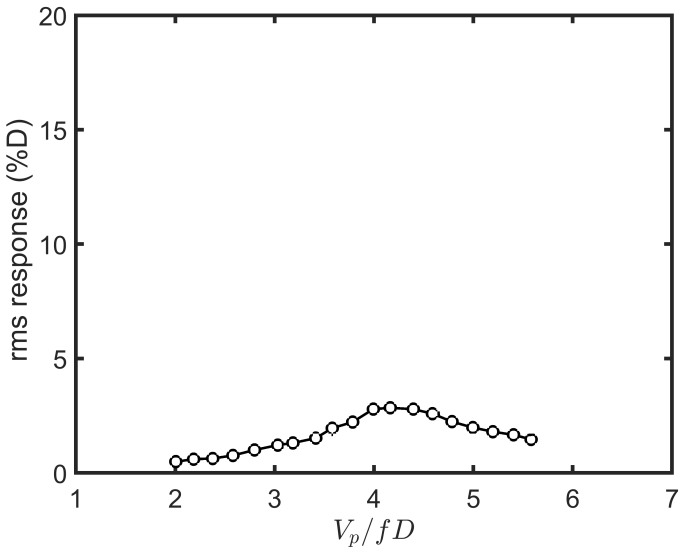


Figure 3.18 Vortex-induced vibrations of a streamwise single flexible tube located in the 6th row

Four flexible tubes - column configuration

The same configuration of four tubes flexible in the streamwise direction was also tested. The rms tube vibration response is presented in Fig. 3.21. The effect of the two flow periodicities shown in Fig. 3.23 is clearly manifested in the response of first two (upstream) flexible tubes via the sudden increase in tubes 1 and 2 rms response values near $V_p/fD = 2.5$. Downstream tubes, 3 and 4, responses show a rapid increase at the coincidence of the second flow periodicity frequency with the tube frequencies, near the reduced velocity of 3.3. This second periodicity-induced response increase also occurs for the first two (upstream) flexible tubes.The coupling strength in both flexibility directions is depicted in Fig. 3.22. It is clear that due to flow pressure perturbations, tubes are more excited in the transverse direction, with a clear longer lock-in velocity range. Strong coupling (or lock-in) is observed between the flow periodicity frequency and tube frequencies occurs in the velocity range from 2.7 to 4.2 as seen in Fig. 3.24. In this velocity range, the four flexible tubes vibrate with the same frequency due to the coupling with the flow periodicity. It can be seen that tube response in the flow direction is less than that observed in the transverse direction.

Fully flexible array

The behaviour of the array in the streamwise direction is similar to what was found in the transverse direction experiment except that the bundle shows a sudden decrease in the post

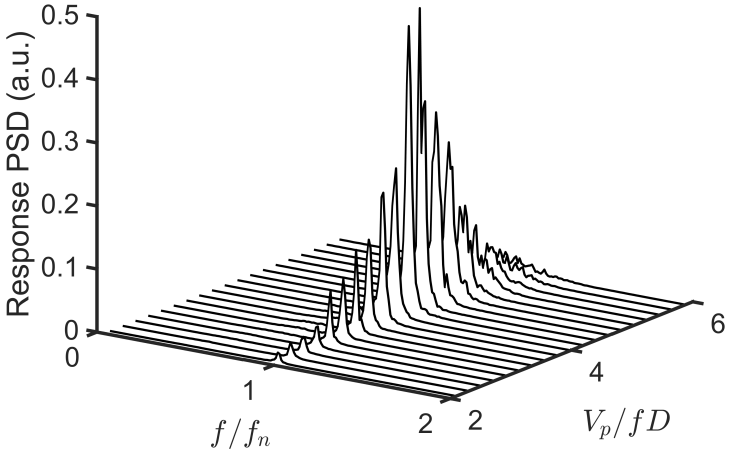


Figure 3.19 Response spectra of single flexible tube in the streamwise direction

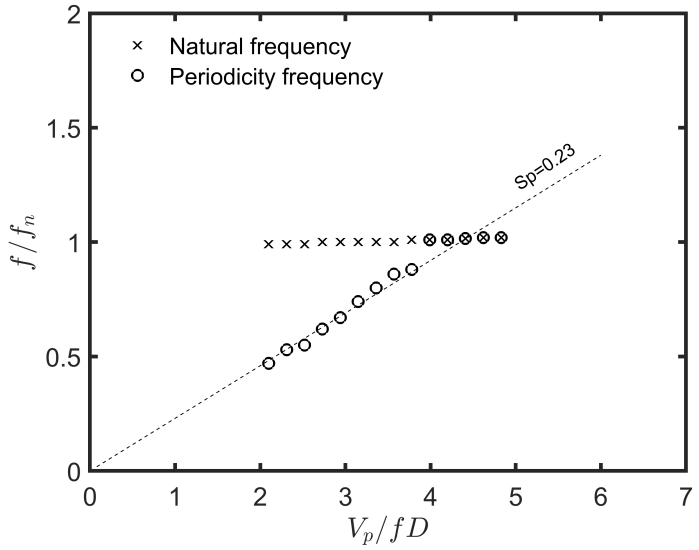


Figure 3.20 Vortex-induced vibrations of a streamwise single flexible tube located in the 6th row

lock-in region, see Fig. 3.25. In the streamwise direction, the peak vibration velocity is shifted from around 3.8 with 4 flexible tubes to 4.5 with the 32 flexible tubes case.

Compared to the transverse direction, it seems that tube lock-in strength is greatly affected by the number of flexible tubes. Fig. 3.27 shows that a single flexible tube does not undergo large amplitude vibrations, however, with the 4 and 32 flexible tubes vibrations significantly

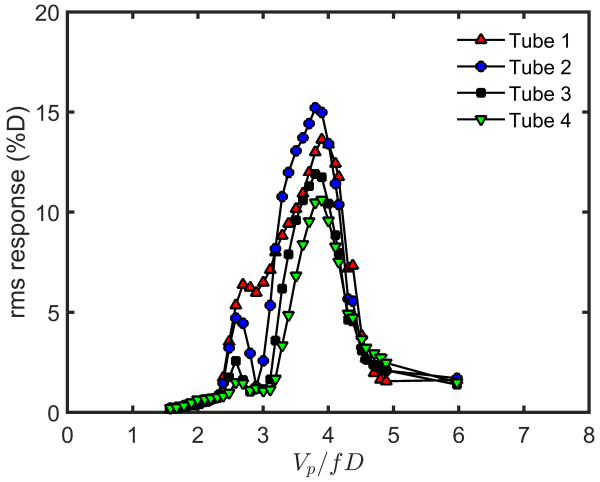


Figure 3.21 Dynamic behaviour of four flexible tubes in the streamwise direction

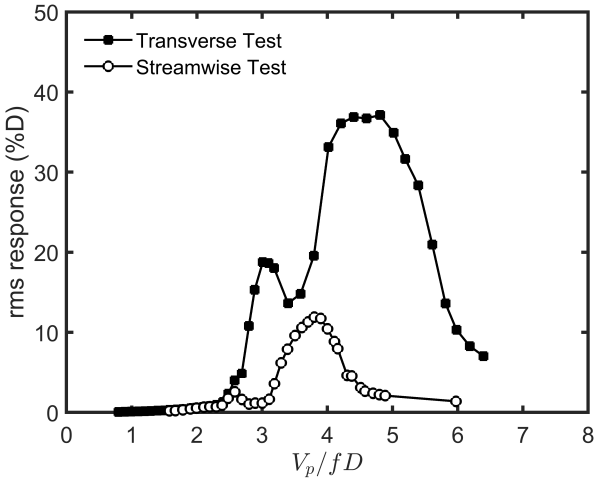


Figure 3.22 Flexible tube in a column located in the 6th row

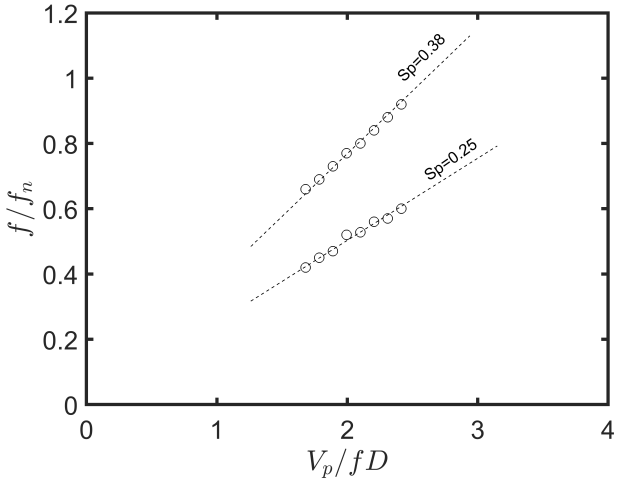


Figure 3.23 Flow periodicity frequencies of tube 1. Only the smaller Strouhal number is found for the other tubes in the array

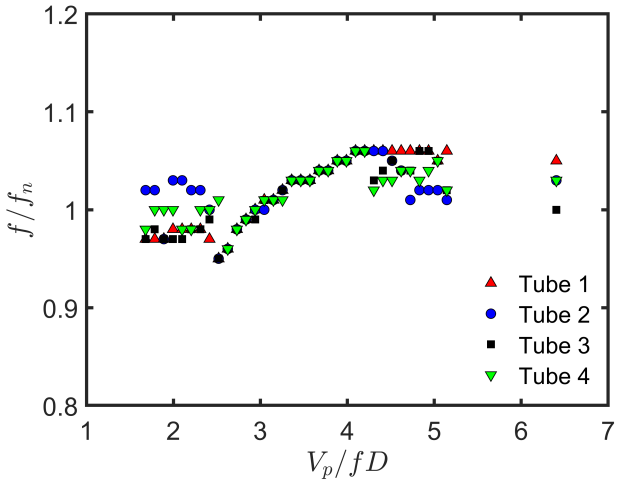


Figure 3.24 Response frequencies, of all flexible tubes in a column, in the streamwise direction vs. flow velocity

increased. Furthermore, it is noticed that when the full array of flexible tubes are tested, peak-vibration velocity differed from the column case and the lock-in range became slightly wider. In the streamwise direction, tube located in the 6th row always synchronizes with a vortex associated with Strouhal number of 0.22, compared to 0.26 for the rest of the tubes. In the column case, all the four tubes vibration peaks correspond to $S_p = 0.26$, while in the full bundle, vibration peaks correspond to $S_p = 0.22$. Apparently, the increase in the number

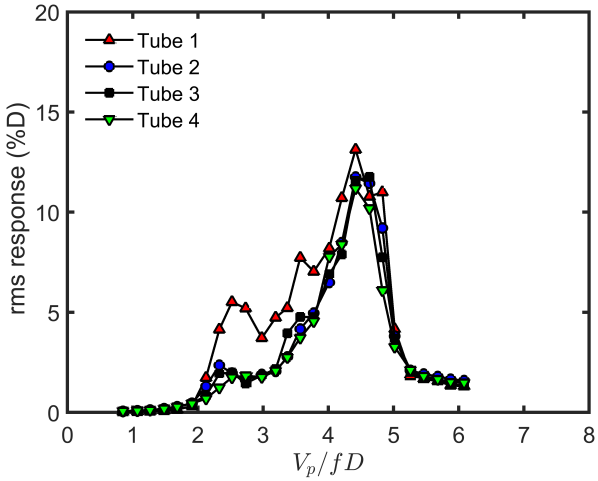


Figure 3.25 Fully flexible bundle behaviour in the streamwise direction

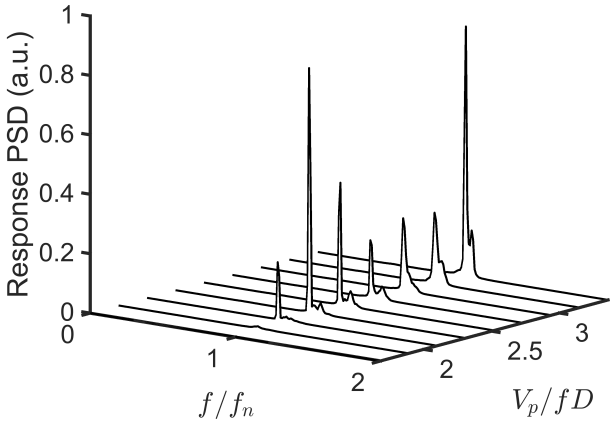


Figure 3.26 Frequency spectra of tube 2 in the fully flexible configuration

of flexible tubes could lead to a slight shift in the syncronization frequency. However, the reason behind this is still not very clear. This was not noticed in the transverse tests as transverse tube vibration near the shedding frequency organizes the wake and increases the vortices strength.

3.4 Investigation/Further Evidence of Excitation Mechanisms

3.4.1 Effect of splitter plate on single flexible tube - transverse response

The single flexible tube underwent large amplitude transverse vibrations starting at a reduced flow velocity coinciding with the lock-in between a flow periodicity frequency and the tube natural frequency. To ascertain that the large amplitude response is due to a lock-in resonance, a flow splitter was designed and installed to reduce the vorticity shedding effect in the wake region of the flexible tube. The splitter is a thin flat plate that is fixed on the rigid tube downstream the flexible tested tube, see Fig. 3.28. With the splitter plate in place, Fig. 3.29 shows that the rms amplitude of vibration does not exceed 4% of tube diameter. This is significantly lower than the response of the flexible tube behavior in the same location without the splitter. The corresponding vibration response spectra are shown in Fig. 3.30 for a wide range of pitch velocities. In contrast to the case with the flow splitter, the vibration amplitude goes up to 40% without the splitter. The results provide additional confirmation that flow periodicity lock-in is the mechanism underlying the observed large vibration amplitudes.

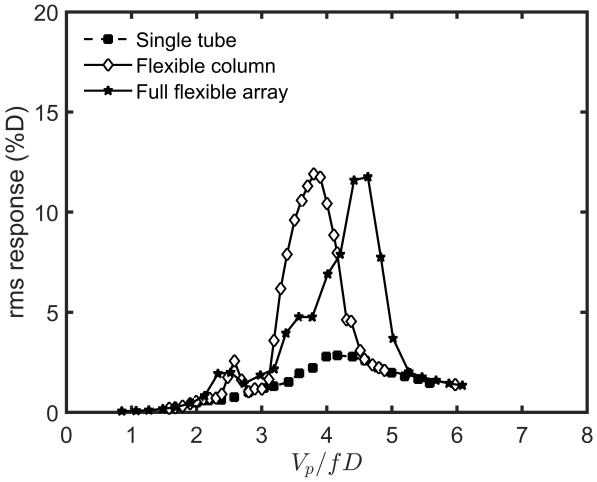


Figure 3.27 Flexible tube dynamic response in different arrangements in the streamwise directions

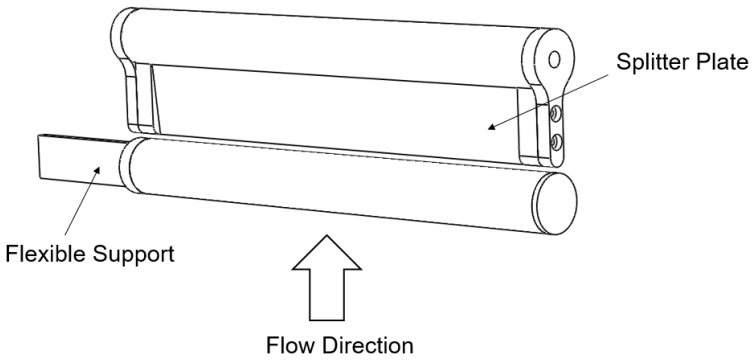


Figure 3.28 Splitter Plate downstream flexible tube to suppress vortex induced vibrations

The physical nature of the lock-in phenomenon is complected. Therefore, more detailed analysis could be able to provide insights into the details of the interstitial flow in the array.

3.4.2 Numerical results

The tube vibration, especially in the transverse direction, affects the vortex shedding by altering the phase and pattern of the vortex street in the tube wake area. Hence, the generated periodicities in the interstitial flow through the array ought to be investigated when using stationary cylinders.

A numerical study of the presented tube array was conducted to investigate the flow periodicity and related frequencies. The Unsteady Reynolds Averaged Navier-Stokes (URANS) equations have been solved to calculate the time dependent flow pressure and velocity, using

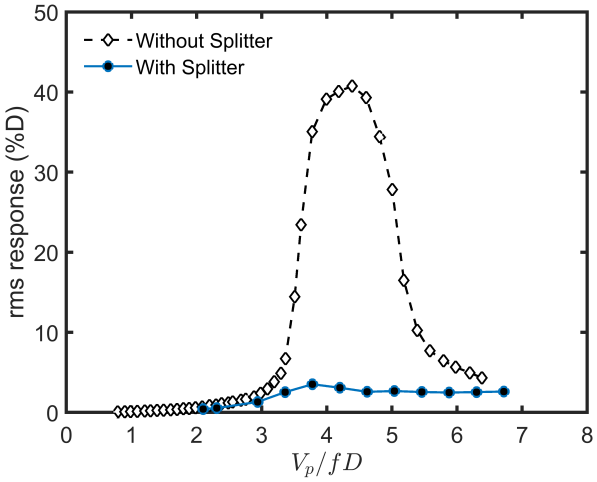


Figure 3.29 Dynamic behaviour of single flexible tube followed by a splitter plate in transverse direction vs its behaviour without the splitter

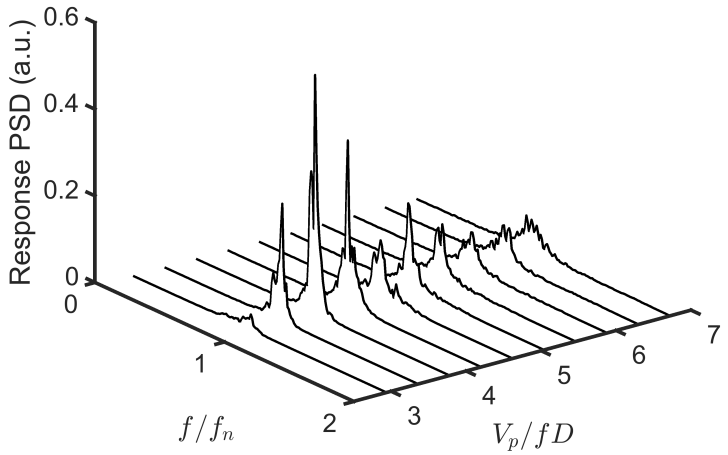


Figure 3.30 Vibration spectra in the cross-flow direction of the single tube configuration using a plate splitter

the commercial package ANSYS-FLUENT. The solver equations adopted to solve similar problems have been severally presented in the literature [90, 102].

A velocity inlet is chosen as the boundary condition at the domain inlet. The flow velocity is chosen to be relatively low (upstream velocity $V_\infty/f_nD = 0.8$) in order to have a subcritical Reynolds number. In this range, the vortex shedding is strong and periodic. This allows the numerical solver to easily capture the pressure fluctuations downstream of the tubes.

At higher velocities, vortex shedding may become disrupted and have a broad frequency spectrum [31]. Side walls of the domain are defines as walls with zero shear stress in order to reduce the wall effect. Tube surfaces are stationary and treated as walls with a no slip condition. The domain outlet boundary condition is pressure outlet. The real tube diameter and pitch spacing between the tubes is implemented here in the numerical model.

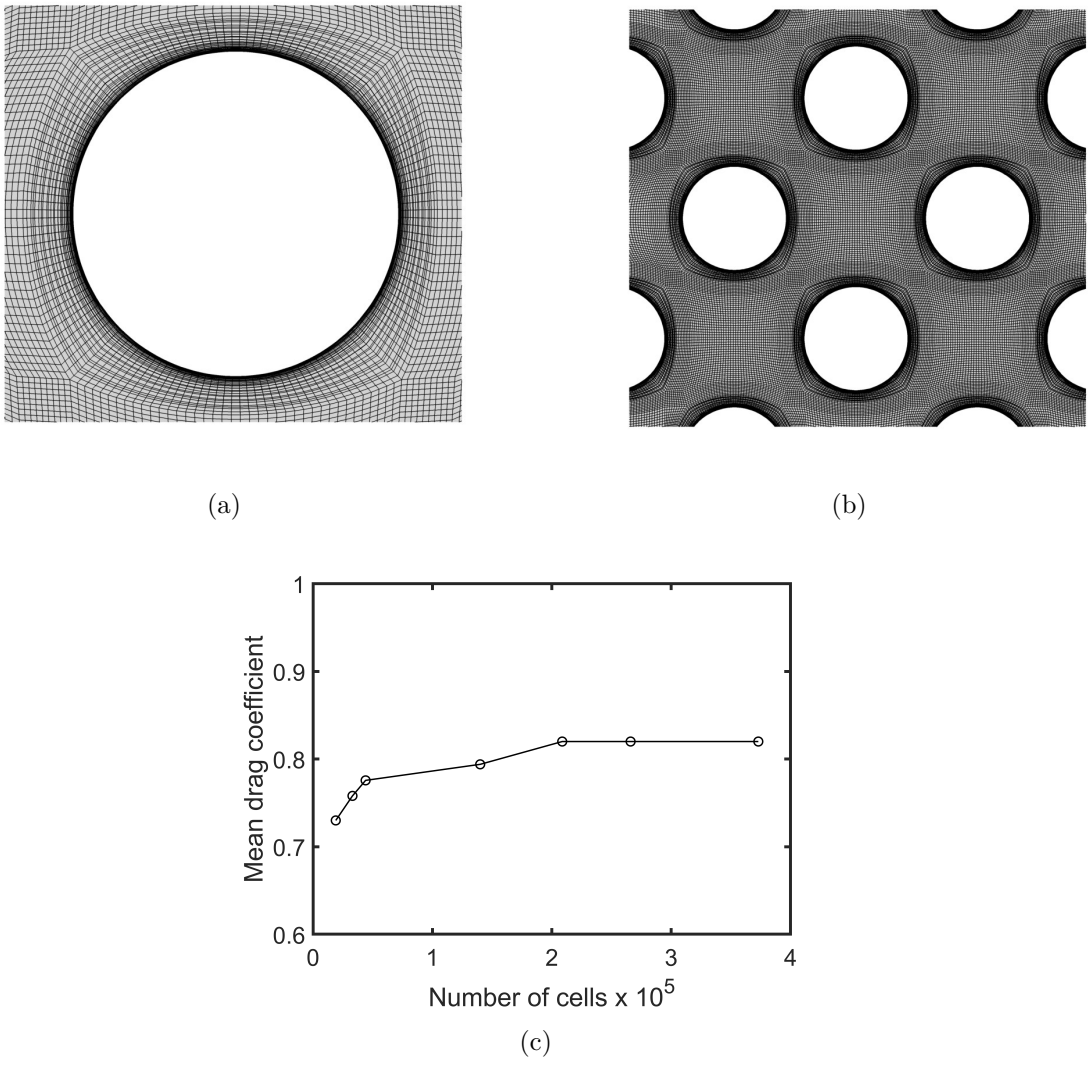


Figure 3.31 Grid overview: (a) inflation layer around cylinders, (b) computational domain meshing, (c) grid independence study

The domain simulation mesh is presented in Fig. 3.31 with details in the tube vicinity shown. In order to provide a grid-independent results, a mesh resolution study was performed as shown in Fig. 3.31(c). This showed that for a finer grid than a 200k cells grid, No change is seen to the mean force coefficient in the flow direction. Hence, the number of elements

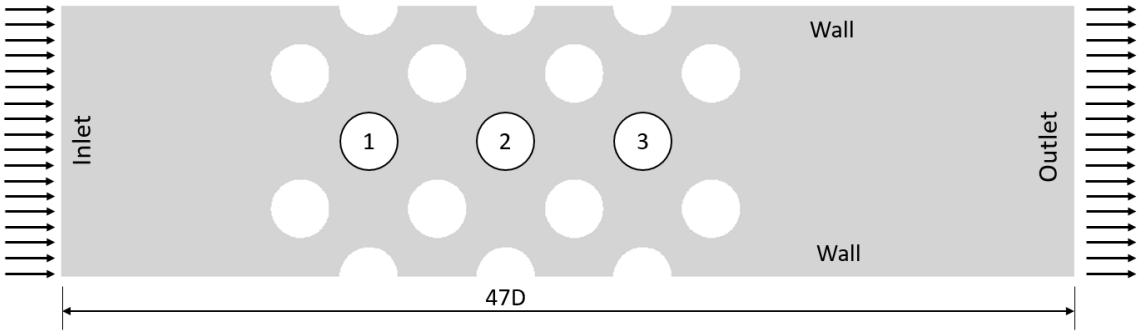


Figure 3.32 Domain and boundary conditions of the CFD model

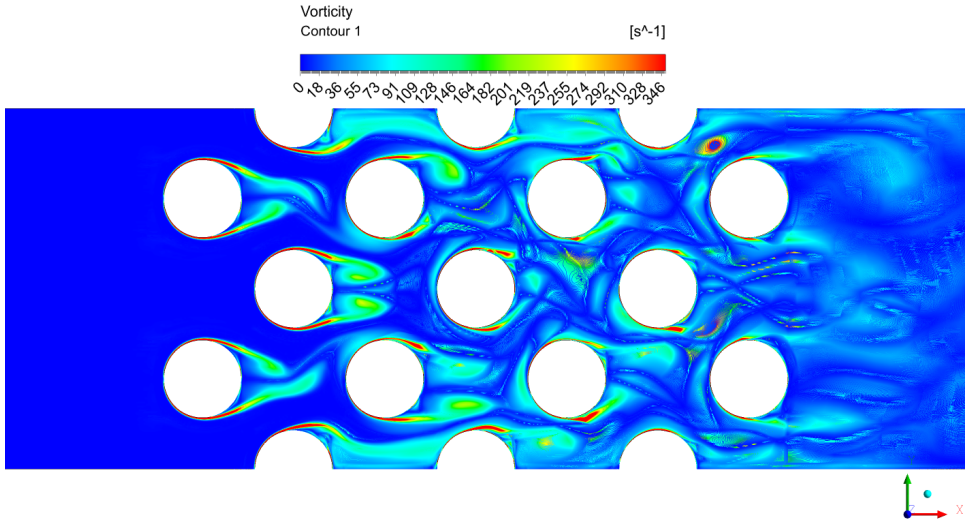
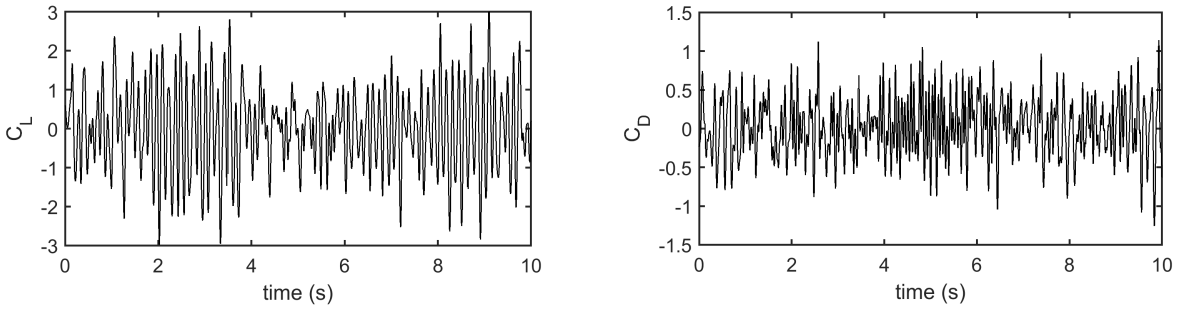


Figure 3.33 Flow vorticity field inside the array ($Re = 10702$, $V_p/fD = 2.1$)

used in the simulation is approximately 281k. The domain elements around the tubes are very fine relative to the average cell sizes in the domain and inflated in order to properly model the boundary layer on the tubes surfaces. The array geometry considered is shown in Fig. 3.32. In order to reduce the domain size and the required computational power, the number of tubes in the array is reduced. Time step is a significant parameter in the unsteady simulations for the accuracy of the results. Therefore, based on the expected vortex shedding frequency, a 0.5 ms time step is adopted in this work. This is to ensure the accurate capturing of the flow periodicity frequencies in the array. While considering 30 sample points per vortex cycle is satisfactory (see [103]), having 2000 sample points per second makes it possible to capture periodicity frequencies up to 60 Hz with high resolution.

The turbulence model selected for the simulations is the Shear Stress Transport (SST) model developed by Menter [104]. This model has been widely adopted in similar problems due to



(a) (b)

Figure 3.34 Time sample of tube 2 unsteady (a) lift coefficient and (b) drag coefficient

Table 3.1 Central tubes numerical results

Coefficient	Tube 1	Tube 2	Tube 3	S_p
$C_{L,rms}$	0.27	1.06	0.87	———
f_{l1}	2.96 Hz	2.86 Hz	2.90 Hz	0.11
f_{l2}	7.72 Hz	7.72 Hz	7.72 Hz	0.29
f_{l3}	9.55 Hz	9.55 Hz	9.55 Hz	0.36
f_{d1}	———	6.68 Hz	———	———
f_{d2}	10.59 Hz	10.59 Hz	10.59 Hz	———
f_{d3}	———	15.14 Hz	15.14 Hz	———

its applicability in the near wall regions. Furthermore, in the free stream region, the $k-\epsilon$ turbulence model is employed in the SST formulation to avoid the ω formulation sensitivity to free stream turbulence.

Figure 3.33 shows the instantaneous vorticity field in the tube array. Clearly seen are the sharply defined vortices in the wakes of nearly all the tubes in the array. For tubes in the first three rows, clear formation and shedding of large vortices is evident. Deeper in the array, the vortices are smaller and appear to break up. From the complex vortex structures, multiple frequencies can be expected following vortex breakdown.

The wake oscillation throughout the array is clearly apparent and provides clear evidence of periodic vorticity shedding and associated pressure perturbations in the array. Additional analysis was performed for the pressure field around the tubes in the center column; these tubes are identified as tube 1 to 3 starting with the upstream-most tube. The computed tube unsteady lift coefficient frequency spectra along with the corresponding drag coefficients are presented in Fig. 3.34. Tab. 3.1 summarizes the flow periodicity frequencies extracted from the frequency spectra in the lift direction, f_{li}, and the drag direction ,f_{di}, where i denotes

the tube number in the array.

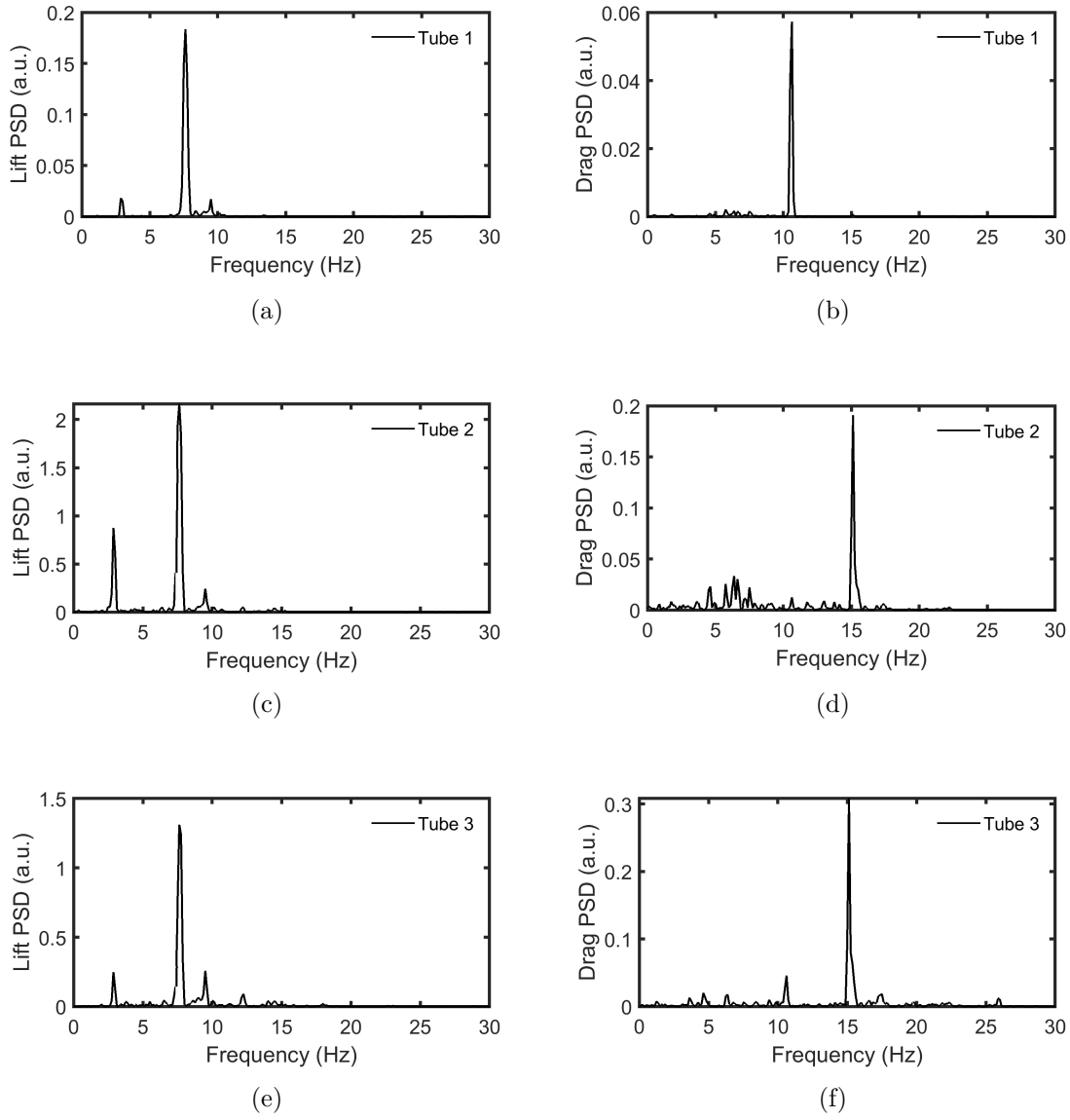


Figure 3.35 Fluid forces frequency spectra of the central tubes: (a & b) tube 1, (c & d) tube 2, (e & f) tube 3

The frequencies obtained from the unsteady lift spectra correspond to the experimentally measured frequencies. The two higher frequencies (7.72 Hz and 9.55 Hz) yield the Strouhal numbers of 0.29 and 0.36 which match the experimentally measured Strouhal numbers (see Fig. 3.13). In addition to these two main frequencies, a third frequency at approximately 2.9 Hz was also found. The related Strouhal number for this low frequency is $S_p = 0.11$. This weak periodicity was detected in the second row of the array. However, it was not observed

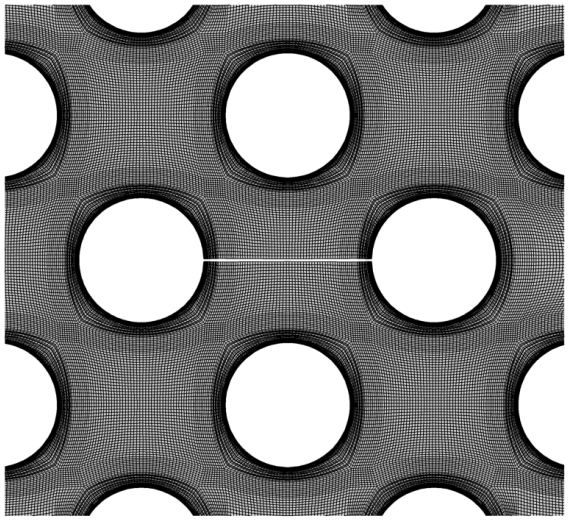
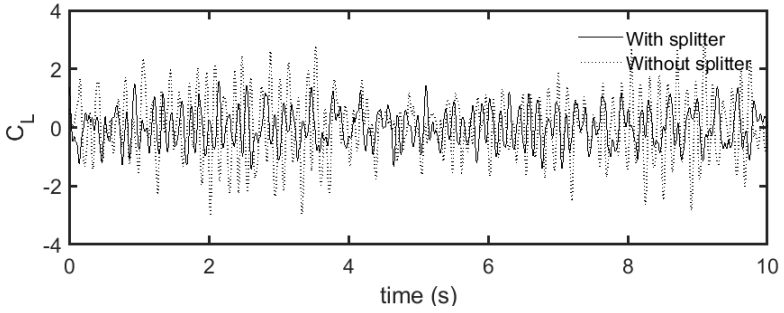
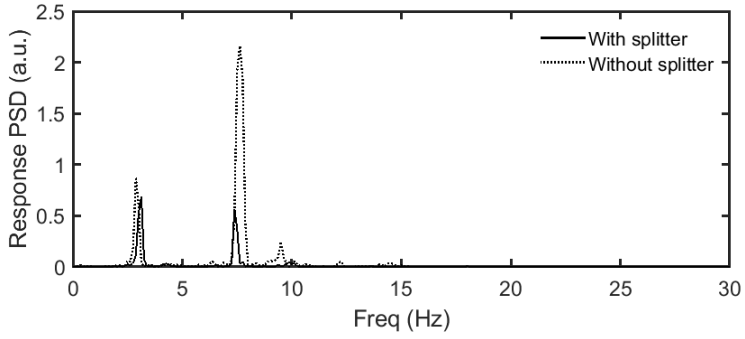


Figure 3.36 Domain grid showing splitter plate placed between tube 2 and tube 3



(a)



(b)

Figure 3.37 Comparison of the lift coefficient signals for the same flow velocity

in the downstream flexible tubes region. An initial explanation is this periodicity is obscured by tube vibration. However, it might be showing only at very low flow velocities. Clearly, this weak periodicity does not affect the tube vibration response during the tests.
The frequency spectra of Fig. 3.35 show all periodicity frequencies in the transverse (lift) and streamwise (drag) directions. While oscillations in the transverse direction occur at the shedding frequency, streamwise periodicities have double the shedding frequencies in the transverse direction. This is true for tubes 2 and 3. For the tube 1, the drag frequency is not double the lift frequency. This suggests that the tube 1 drag frequency may be related to the upstream forces of tube 1.

A splitter plate can suppress or weaken vortex shedding. Hence, a thin splitter plate was placed between tubes 2 and 3 as shown in Fig. 3.36 investigate this. The plate is defined as a wall with components of shear stress are equal to zero in the CFD model. This allows consideration of the effect of the plate as only a separate of the domain which prevents flow pressure perturbations without adding any additional shear stresses. Results showed that the central tube (tube 2) lift coefficient rms value dropped from 1.06 to 0.642. Frequency spectra of lift and drag coefficients of tubes 2 and 3 show the same frequency with lower amplitude values.

3.5 Conclusions

In the work reported here, the dynamic behaviour of a large spacing (P/D=1.64) rotated square tube array subjected to water flow was investigated experimentally. The test results showed that the vortex shedding was the dominant excitation mechanism in this array. The array was found to violently vibrate in the transverse direction when lock-in occurred. The vortex shedding resonance was found to be strongly dependent on array flexibility. Tube array flexibility clearly enhanced the strength of vortex shedding. Lower vibration amplitudes were observed in the streamwise direction as expected. Frequency analysis revealed the existence of up to three distinct flow periodicity modes with associated Strouhal numbers also confirmed by CFD analysis. The numerical simulations also showed the existence of well defined vortex shedding, facilitated by the large tube pitch spacing. The strength of the vorticity shedding was such that successive lock-ins occurred as two of the Strouhal frequencies approached the tube natural frequency. Multiple lock-ins were found for the case of multiple flexible tubes but not in the case of a single flexible tube. No fluidelastic instability (static or dynamic) was found for this array. The present results confirm previous observations that rotated square arrays have unique and complex behaviour compared to the normal square and triangular arrays. Based on the findings in this paper, in conjunction with related literature work, this

array deserves further study. Future work should also include fluidelastic instability studies of this array in two-phase flow.

CHAPTER 4 ARTICLE 2: EXPERIMENTAL INVESTIGATION OF FLUIDELASTIC INSTABILITY OF A ROTATED SQUARE ARRAY SUBJECTED TO TWO-PHASE AND AIR CROSS-FLOW

Sameh Darwish, Njuki Mureithi, Abdallah Hadji, Minki Cho

This article has been submitted to "Journal of Nuclear Engineering and Design", is accepted pending revision. This is the revised version. It was submitted on October 15, 2022.

In this chapter, the fluidelastic instability (FEI) of the rotated square array is studied in two-phase (air-water) cross-flow. This is to meet the specific objectives to:

- Investigate the susceptibility of the array to streamwise and/or transverse fluidelastic instability in two-phase flow.
- Investigate the array fluidelastic behaviour in the streamwise and transverse directions in air flow.
- Determine the instability mechanism by testing multiple configurations of flexible tubes.

The paper presents a series of fluidelastic instability tests in air-water two-phase cross-flow. The tests covered a wide range of two-phase flow void fractions up to 97%. A single and multiple flexible tubes were examined in both flexibility directions, streamwise and transverse to the flow. It was found that a single flexible tube never becomes unstable in the tested range of flow velocities, either in the flow direction or transverse to the flow. Similarly, the fully flexible bundle never became unstable in the streamwise direction. However, the flexible bundle in the transverse tests, only in the 97%, showed an increase in tube vibrations. This increase is gradual, followed by a decrease in tube vibrations at high flow velocities. Maximum vibration amplitude was seen to be a function of the number of flexible tubes, the more flexible tubes existed, the higher the vibration amplitude is. As a complementary work, air flow experiments were also conducted. Results showed that an in-plane instability arises only when the number of flexible tubes are more than four. Also, instability occurrence is sensitive to tube location in the array. When tubes are located in the upstream rows, instability arises. The coupling between the tubes show that the stiffness-controlled mechanism is the mechanism leading the instability in this array.

Abstract

This paper reports laboratory experiments to investigate the fluidelastic instability of a rotated square array with a pitch ratio of 1.64 subjected to cross-flow. A series of air-water two-phase flow, as well as air flow, experiments were conducted. Test done for a range of array flexibilities yielded valuable insight into the array dynamics over a wide range of flow void fractions from 40% to 97%. The study revealed the existence of transverse fluidelastic instability for 97% void fraction, with variable vibration strength based on the number of flexible tubes, and stable behaviour for lower void fractions. Generally, a significant increase in fluid damping was noted in the transverse and streamwise directions in two-phase flow. In air flow, a series of experimental tests showed complex fluidelastic behaviour for this array. Fluidelastic instability was found in air flow tests in the streamwise direction only, while divergence, associated with negative fluid stiffness force, was observed in the transverse direction. Dynamic instability in air required coupling between adjacent tubes; confirming the stiffness controlled instability mechanism. For air flow, fluidelastic behaviour was strongly dependent on tube location within the array.

4.1 Introduction

For the first time in a nuclear steam generator in service, fluidelastic instability (FEI) in the in-plane (streamwise) direction was reported in the San Onofre Nuclear Generating Station (SONGS) in the steam generator (SG) U-bend region. The instability resulted in significant tube-to-tube wear (TTW) [94]. The instability resulted from high flow velocity at high flow void fractions, combined with insufficient contact forces between tubes and anti-vibration bars (AVBs). This has led to increased focus on the risk of streamwise fluidelastic instability in other operating SGs. Fluidelastic instability is classified as the most significant potential cause of tube failure in heat exchangers. Tube arrays in commercial heat exchangers have simple geometrical patterns, either based on a square or triangular layout. This is used to classify the tube array geometry, hence, its dynamical properties. Besides the array layout, the tube pitch spacing to tube diameter ratio (P/D) is a second important parameter classifying the array. Based on these two parameters, a heat exchanger tube array dynamic characteristics is defined. Over the past decades, considerable effort has been made to experimentally investigate the fluidelastic stability behaviour of various tube array geometries. Much of the current literature focused on the triangular and normal-square arrays, however, far too little attention has been paid to the dynamics of the rotated square (RS) geometry.

Early work investigating the in-plane fluidelastic instability (IPFEI) was presented by Weaver

and Schneider [105]. The flat bar supports effect on The U-tubes was studied in a wind tunnel with different sets of supporting conditions. Results showed that the out-of-plane modes were more critical, and no IPFEI has occurred even when increasing the flow velocity significantly above the expected in-plane critical velocity. Haslinger and Steininger [106] also performed experiments on U-tubes supported with AVBs. The out-of-plane vibrations were found to be always higher than the in-plane. Despite the increase in the in-plane vibrations with the flow velocity, no FEI was observed in the IP direction. In water flow, Weaver and Yeung [107] studied the vorticity response variation with the tube mass damping parameter in a RS array with P/D=1.5. The Connors-type instability relationship was found not to be applicable in the provided test results. This was followed by a more detailed study for a closely packed array with P/D=1.41 using flow visualization by Abd-Rabbo and Weaver [101]. The study reported on all the Strouhal numbers that were found in the array. Later, work on a RS array with spacing ratio P/D=2.12 was reported by Price and Kuran [13]. According to the authors, a single flexible tube in this array did not undergo fluidelastic instability; instability was only triggered in the case having three or more flexible tubes in the array. The results provided strong evidence of a fluid stiffness-controlled instability as the underlying mechanism in the tested array. The stiffness mechanism requires coupling between multiple degrees-of-freedom (typically adjacent tubes) in the array. It was found that combining tube structural damping and nondimensional mass could be a misconception since the critical flow velocity was found to strongly vary depending on tube mass, compared to mechanical damping that has much lower effect. The authors also indicated that natural frequency reduction of one tube in a group of unstable tubes led to an early (lower flow velocity) FEI onset. Furthermore, static instability (or "divergence"), which is rare in other array geometries, was observed in the rotated square array. Price et al [75] found that, in a RS array of 2.12 pitch ratio, a downstream single flexible tube was stable in a double row array. Interestingly, when the array was extended with a third row, and when the flexible tube was placed in this row, fluidelastic instability occurred. In a later study [74], the same array was tested with more downstream tubes, and results showed that a single flexible tube never went unstable. In contrast to the earlier findings, Païdoussis et al. [14] confirmed the existence of dynamic fluidelastic instability of a single flexible tube subjected to air flow, located in the first or second row, in an otherwise rigid array for a RS array of pitch ratio 1.5. All the previously mentioned studies conducted the experiments with axis-symmetric tubes, indicating that the instability is observed predominantly in the flow direction, particularly in the first few rows of the array. Rotated square arrays are generally found to be dynamically unstable in air. Previous work by Nakamura and Tsujita [15] focused on RS arrays having pitch ratios 1.2-1.5, in air flow, for both in-flow and transverse direction flexibility. Strong instability in the

in-flow direction was found. The largest array spacing showed a significantly high Connor's constant compared to the tighter arrays. The instability was attributed to change of the flow path in the rotated square array, compared to the normal square and normal triangle geometries. The experimental data showed strong vibrations in the upstream rows, while downstream tubes did not vibrate violently. For a more tightly spaced array, Austermann and Popp [81] investigated the single tube dynamics in an array of P/D=1.25 in air flow. The tube response was studied for the first four rows, and turbulence buffeting was found to be the only source of vibration in the array. Chung and Chu [77] tested normal and rotated square arrays with pitch ratio 1.63. In the case of the normal square array, the instability was observed in the transverse direction only with two instability regions. This transition in the stability region was attributed to the change in the two-phase flow regime. On the other hand, the rotated square array showed a more stable behaviour. However, the authors reported an instability for mid void fractions. This could be a result of calculating the tube vibrations from the total frequency spectrum. When the array was part of a U-bend structure, and by subjecting the whole array to two-phase flow, instability was observed at void fractions higher than 65%.

The analysis by Price and Païdoussis [100] agreed with the previously discussed experimental results. Also, Price and Païdoussis [108] experimentally discovered that a single degree-of-freedom did not induce instability, in addition to the findings by Kuran and Price where dynamic instability was found only in a multiple degree of freedom array [13]. In Lever and Weaver theoretical analysis [7, 65], the existence of fluidelastic instability of a single tube in the rotated square arrays was predicted regardless of the array pitch ratio. The negative damping mechanism in the theoretical modelling, that requires only one flexible tube to develop instability, was considered, presumably it is the only mechanism leading to instability.

The studies presented thus far show that the rotated square geometry generally remains a complex and not fully understood area in the experimental fluidelastic instability research. An experimental program has therefore been developed with the goal of shedding more light on the fluidelastic behaviour of this array geometry. The aim of the work reported here is to experimentally investigate the dynamic behaviour of a rotated square array of pitch ratio 1.64 in two-phase, as well as, air cross-flow, see Fig. 4.1. The same array has been studied in water flow in previous research work [12].

4.2 Experimental Apparatus

The fluidelastic instability experiments were conducted in both air-water and air flows in different test loops. The two-phase flow experiments were conducted in a test loop fed by compressed air with flow rate up to 260 l/s in standard conditions, and water provided by a 7.5 HP (5.6 kW) centrifugal pump provides up to 25 l/s. Both air and water flow are mixed upstream of the test section, passing by a double honeycomb mixer for flow homogeneity. Flows entering the test section are measured using an electromagnetic water flowmeter and air flowmeter. Water temperature is monitored using a Kimo Instruments T-type thermocouple probe. All air flow characteristics (pressure, temperature, and flow rate) are measured for flow monitoring during the tests.

The air experiments were conducted in a recirculating subsonic wind tunnel (Model 407-B, ELD, Lake City, MN, USA) with a 60 x 60 cm^2 test section in the Fluid-Structure Interaction Laboratory of Polytechnique Montréal. This large cross-section was reduced using reduction panels to maintain the array internal dimensions. Air flow dynamic pressure was monitored using a pitot tube attached to a Dwyer 647 calibrated differential pressure transmitter. The test section was designed to monitor the number of flexible tubes in order to allow variation of the number of flexible tubes, see Fig. 4.1. The cross section area of the test section is 0.04191 m^2. In both test setups, tubes are arranged in 9 rows and 9 columns with half tubes attached to the test section wall to reduce wall effect.

Flexible tubes are composed of straight Inconel cylinders mounted on a flexible beam with a rectangular cross-section as shown in Fig. 4.2. This allows for tube flexibility in one direction, whether in-flow or cross-flow depending on the tube orientation, while effectively rigid in the normal direction. Tube vibration signal is measured via strain gauges. The flexible tube logarithmic decrement of damping was measured in air and resulted in an average tube mass damping parameter ($m\delta/\rho D^2$) of 20.6. The average mass damping parameter in water was found to be 0.24.

In the following sections, flow velocity used in the analysis is the pitch velocity, defined as,

$$V_p = V_\infty \frac{P/D}{P/D - 1} \tag{4.1}$$

where V_∞ is the homogeneous free-stream velocity at the test section entrance, and P/D the array pitch-to-diameter ratio. The homogeneous flow velocity is determined by dividing the flow rate by the test section cross-sectional area.

The homogeneous void fraction β is calculated from the air and water volumetric flow rates to determine the mixture properties. The homogeneous model assumes uniform two-phase

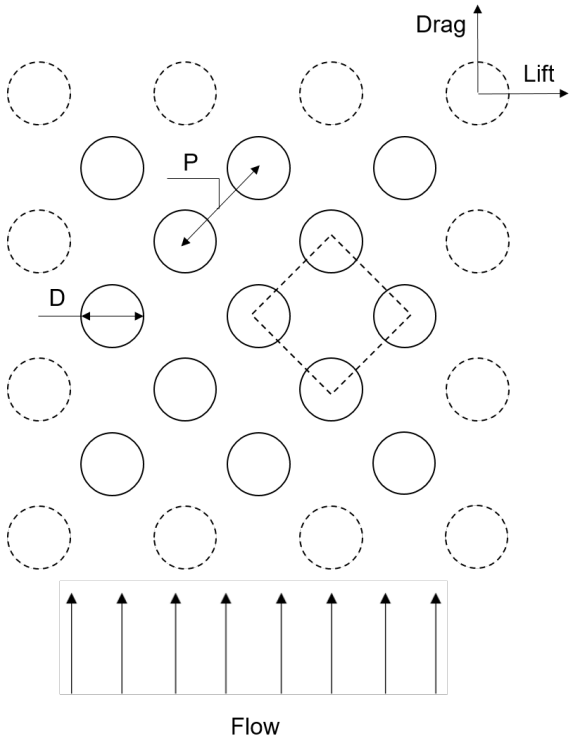


Figure 4.1 Tube array layout showing flow direction.

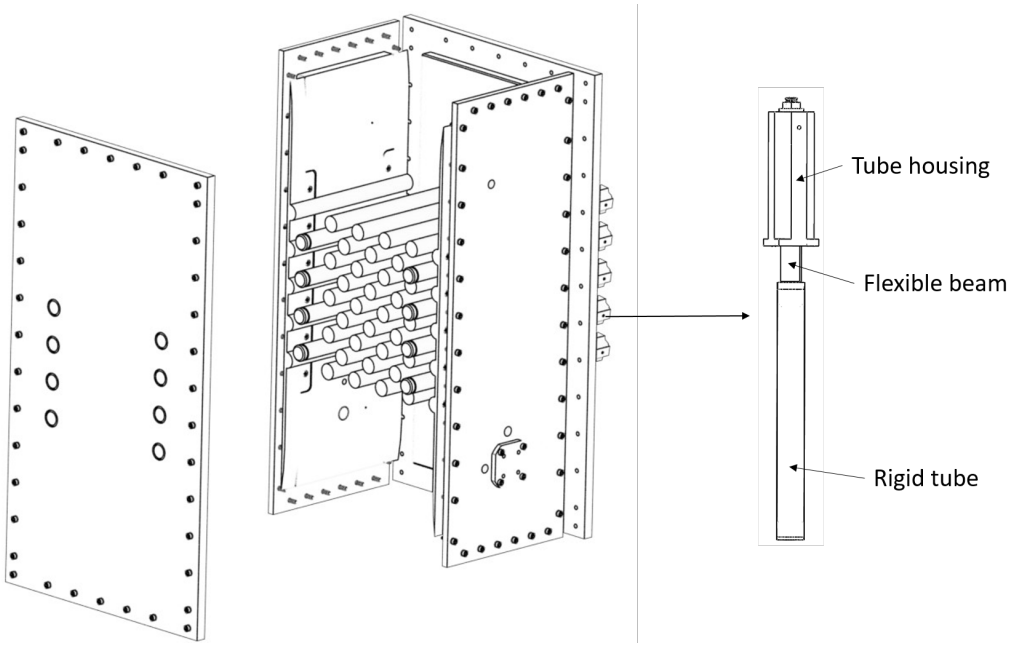


Figure 4.2 Test section showing tube bundle and flexible tube structure.

flow across the test section.

$$\beta = \frac{Q_g}{Q_g + Q_l} \tag{4.2}$$

where, Q is the volumetric flow rate, and g and l subscripts denoting the gas and water, respectively. The time-averaged homogeneous two-phase flow density, ρ_h is calculated by

$$\rho_h = \beta\rho_g + \rho_l(1 - \beta) \tag{4.3}$$

where, ρ_h is flow mixture density, and g and l subscripts denoting the gas and water, respectively.

4.3 Array Dynamics in Two-phase Flow

In two-phase flow, three main configurations are examined: (i) a single flexible tube, surrounded by rigid tubes, located in the fourth row, (ii) a column of four flexible tubes located in the centre of the array arranged in the flow direction, and (iii) a full bundle of 32 flexible tubes. In the last configuration, the responses of the four tubes in the central column are monitored. A given test is performed by subjecting the tube bundle to gradually increasing two-phase flow while keeping the (homogeneous) void fraction constant. The flow velocity is increased in sufficiently small increments in order to capture the instability onset accurately. The results are presented as tube root mean square (rms) vibration response versus non-dimensional pitch flow velocity (V_p/fD).

4.3.1 Transverse vibration response

Single flexible tube

For single phase flow (Fig. 4.3(a)), large amplitude vibrations reaching 50%D are found. This was found to be the result of vortex shedding lock-in as reported in [12]. At low flow velocity, tube dominant frequency and vorticity shedding frequencies are clearly distinct. Two vortices are captured by the tube vibrations, with frequencies linearly increasing with flow velocity, until the vorticity with the high Strouhal number coincides with the tube vibration frequency at velocity near 2.4. The evolution of vortex shedding with flow velocity is seen in the frequency spectra in Fig. 4.3(b) at low flow velocity (before lock-in), and for the full range of flow velocity in Fig. 4.3(c). Figures 4.4 and 4.5 show the vibration response of the single flexible tube located in the fourth row for all void fractions tested. The stable behaviour for two-phase flow tests is very clear up to the maximum velocity tested. For the mid range

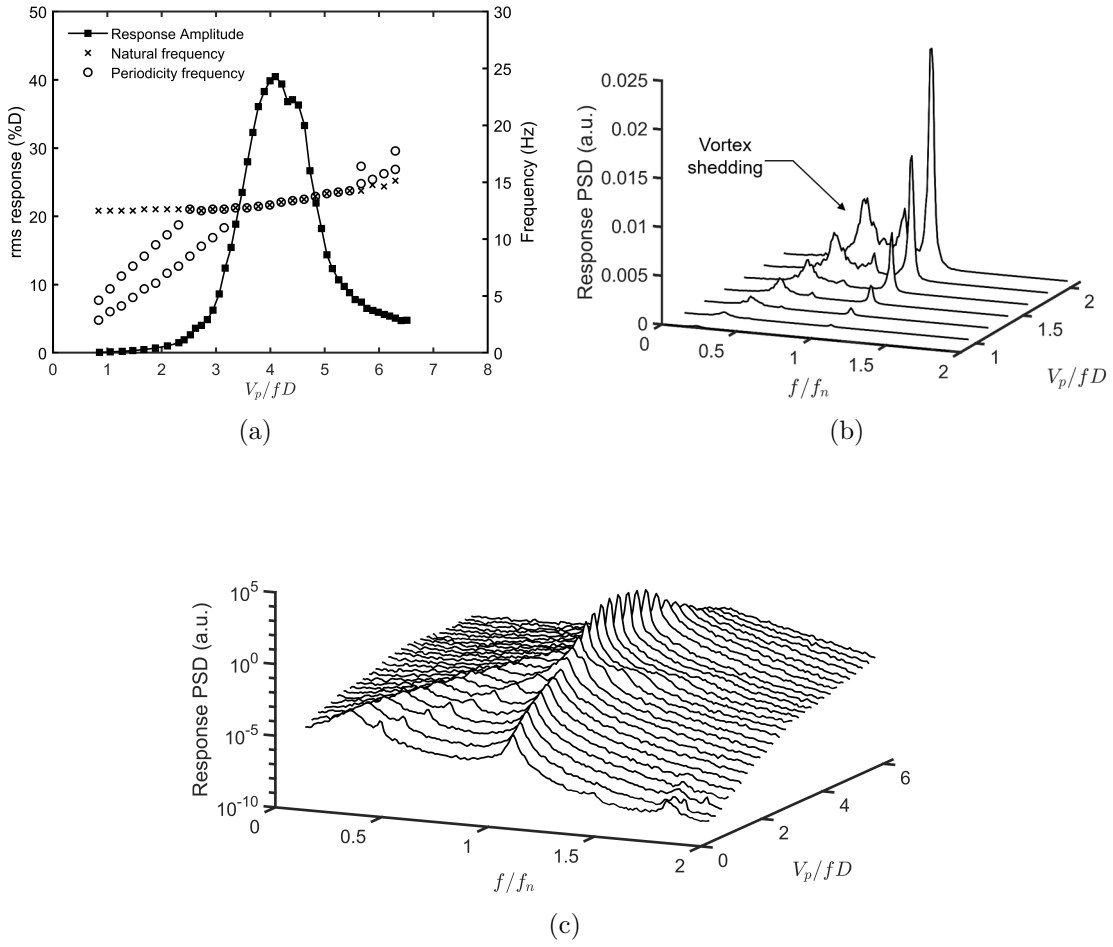
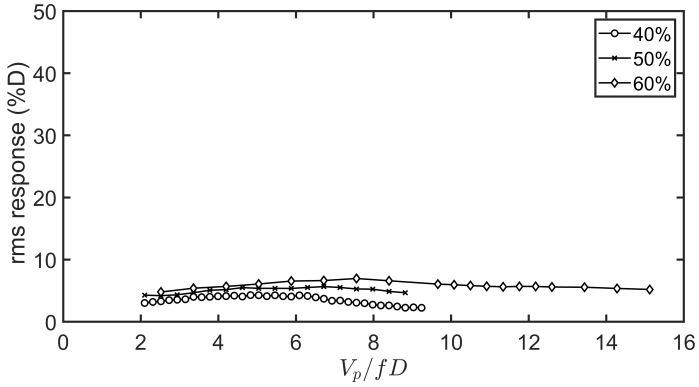
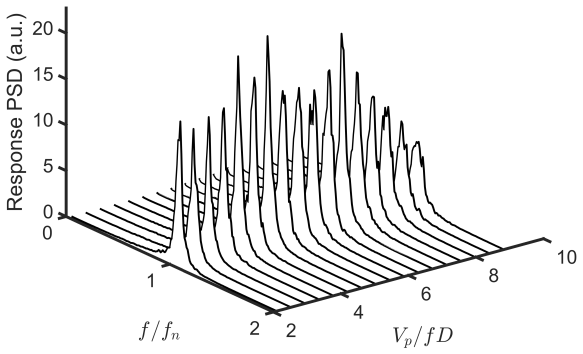


Figure 4.3 Transverse vibration response of a single flexible tube in water flow [12]: (a) non-dimensional tube rms tip vibrations, (b) frequency spectra at low flow velocities showing vortex shedding frequency, and (c) frequency spectra for the full range of flow velocity in log scale.

two-phase flow void fractions (40-60%), Fig. 4.4(a), tube rms values did not exceed 10% of the tube diameter. This is also the case for high void fractions (70-97%), Fig. 4.5(a). These low amplitude random vibrations are attributed to two-phase flow turbulence excitation only. For the highest void fraction (97%), an increase in tube vibration is visible near V_p/fD=25, suggesting a possible fluidelastic unstable behaviour of the tube at this void fraction, which is however, relatively weak. This is followed by a decrease in the tube rms vibration amplitude. Compared to the lower void fractions, the frequency response in the 97% test is significantly different (Fig. 4.5(b)). The PSDs show that starting at V_p/fD=10, the tube response peak is increasingly sharp and does not correspond to a wide-banded turbulence excitation response as was found for lower void fractions. This is a characteristic of the fluidelastic instability



(a)



(b)

Figure 4.4 Single flexible tube vibrations in the transverse direction when surrounded with rigid tubes in mid void fractions (40-60%): (a) non-dimensional tube rms tip vibrations, (b) frequency spectra in 50% void fraction

occurrence, where the fluidelastic forces become dominant. Therefore, the dynamic response of the single tube in the transverse direction at 97% void fraction is considered to show weak unstable behaviour, with fluidelastic forces only causing relative low amplitude vibration. As the tube response does not undergo a sudden increase at a well defined critical velocity, the apparent tube damping values are used to estimate a critical velocity, when the damping becomes lower than 1%, in addition to the critical velocity estimated from the rms response graphs, when the rms value becomes higher than 10%D (turbulence excitation level of the tubes in the two-phase flow). The final critical velocity is an averaged value of the estimated critical velocities from the damping ratio and the tube vibration response graphs. It is noted, however, that for higher flow velocity, the tube damping ratio dramatically increased. At

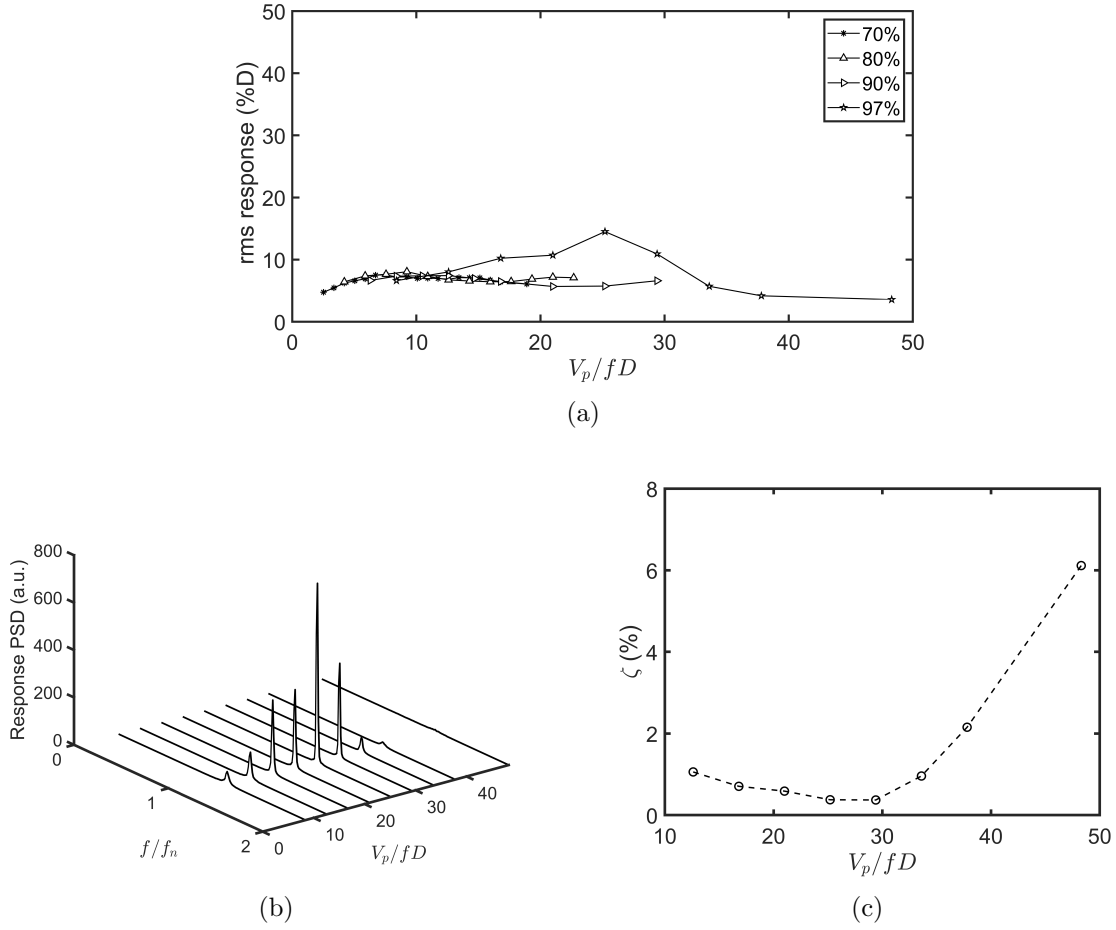
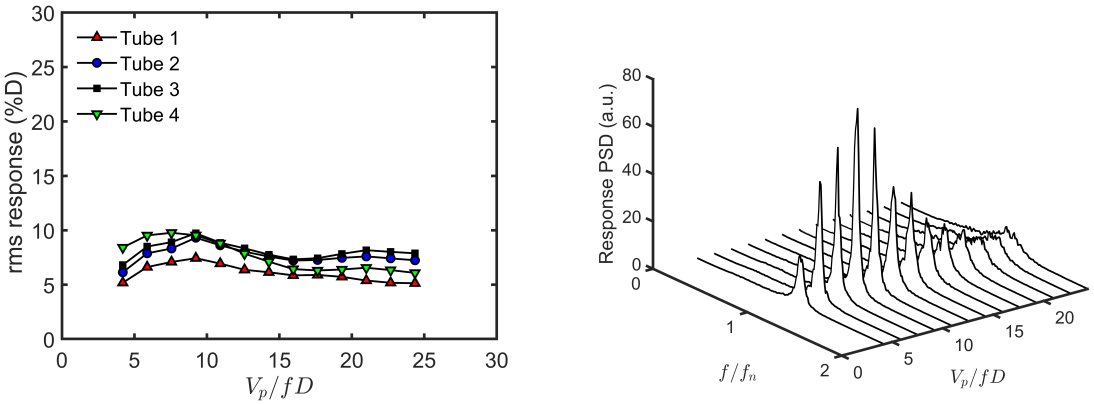


Figure 4.5 Single flexible tube vibrations in the transverse direction when surrounded with rigid tubes in high void fractions (70-97%): (a) non-dimensional tube rms tip vibrations, (b) frequency spectra of 97% void fraction, and (c) damping ratio of 97% void fraction

the highest flow velocity the damping reached 6 times its value at low flow velocity (see Fig. 4.5c).

Column dynamics

Tests with the central column of four flexible tubes were performed using the same flexible tubes having the same dynamic characteristics (with standard deviation of the natural frequency and damping ratio of 0.1 Hz and 0.07%, respectively). Results obtained for this configuration are very similar to the single flexible tube case, except that at 97% void fraction, tube vibration rms showed slightly higher increase. This is explained by increased fluid coupling between the tubes. No instability is observed for lower void fractions in the trans-



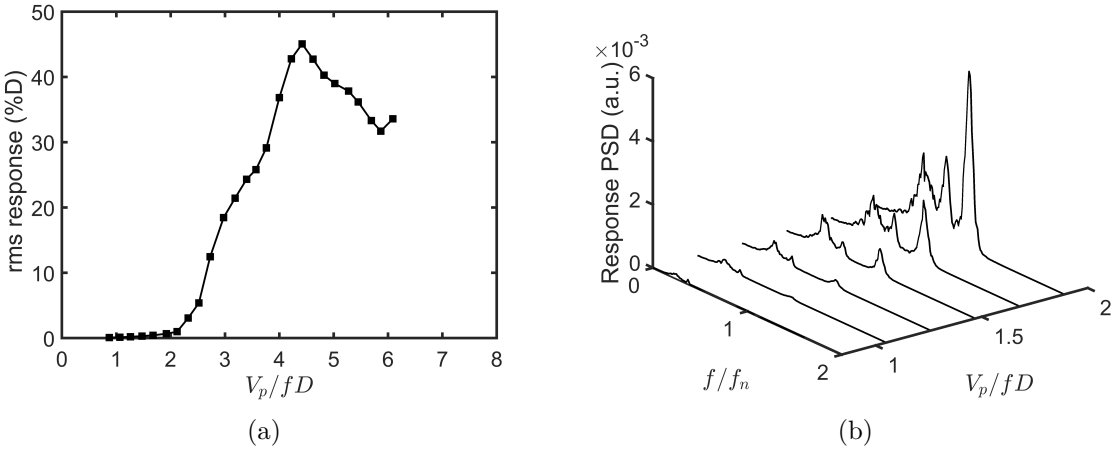
(a) (b)

Figure 4.6 Column of flexible tubes vibrations in the transverse direction for 80% void fraction: (a) tube rms vibrations, (b) frequency spectra.

verse direction for this configuration. Fig. 4.6 shows an example of test results for 80% void fraction.

Flexible bundle dynamics

The large amplitude vibrations in water flow (Fig. 4.7) are here also attributed to vortex induced vibrations (VIV) as detailed in [12]. The water flow results are included here for completeness. For 40% void fraction, the results show a small increase in tube vibration starting near a reduced velocity of 4. As in water flow, this increase in vibration is attributed to flow periodicity, related to vorticity shedding for liquid flow. This is a remnant of vortex shedding, weakened by two-phase flow. For 50%-90% void fraction, no fluidelastic instability is observed, see Figs. 4.8 and 4.9. Unlike the single and flexible column cases, the fully flexible bundle showed a significant increase in vibration amplitudes when subjected to 97% void fraction flow as shown in Fig. 4.10. The response amplitude increases monotonically, reaching as high as 40%D near a reduced velocity of 30. These violent vibrations indicate that the array is fluidelastically unstable. We remark, however, that the instability (amplitude) growth rate with flow velocity is very slow, reaching maximum amplitude at approximately three times the critical velocity. As the flow velocity increases, the vibration amplitude shows a gradual decrease, indicating gradual restabilization but for very high velocities above 30. Since the variation of mass-damping parameter in this study is via changing the void fraction, the decrease in tube response might be a result of the change in flow regime. For a better estimation of flow critical velocity, damping analysis is used, along with tube rms response, to



(a) (b)

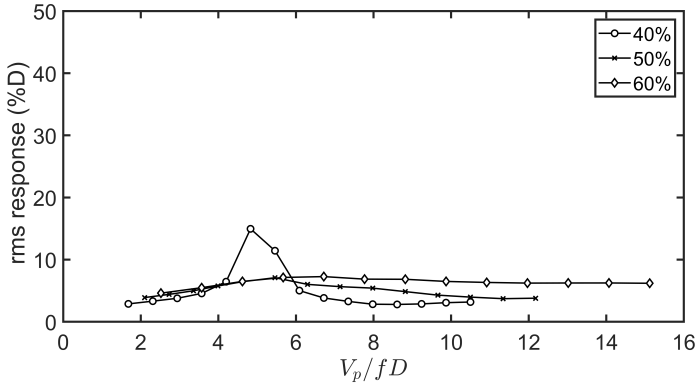
Figure 4.7 Fully flexible array vibrations in the transverse direction in water flow [12]: (a) non-dimensional tube rms tip vibrations, (b) non-dimensional tube rms tip vibrations, (c) frequency spectra at low flow velocities showing vortex shedding frequency

assess in accurately estimate the stability onset, as previously discussed in the single flexible tube results. The vibration mode of the tube bundle is shown in Fig. 4.11 at the reduced velocity of the maximum vibration amplitude (V/fD=30). The mode shape is determined from the phase angles of the tubes. The phase angles are obtained form the cross power spectral density at the dominant vibration frequency. For a practical representation, all phase angles are estimated in reference to the central tube, tube 2. In Fig. 4.11 white dot circles represent the tubes equilibrium position, and the solid white circles represent the tube position at an arbitrary time. Tube movement direction is illustrated by the arrows. Tube movement limits represent a sine wave angles with maximum and minimum vibration amplitudes. The sign of the phase angle is an indication whether the tube leads or lags the motion of tube 2. The pattern of the bundle vibration is clearly seen to be well defined. Tubes in the central column are almost out of phase.

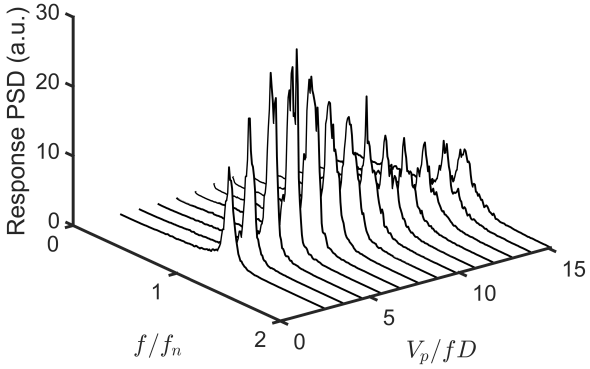
4.3.2 Streamwise vibration response

Flexible bundle dynamics

Figs. 4.12 and 4.13 depict the response of the tube located in the fourth row in a fully flexible bundle. No fluidelastic instability occurred in this array in the streamwise direction. The 90% void fraction test result shows an increase in tube rms vibrations, however, this does not indicate any occurrence of fluidelastic instability. This is confirmed from the frequency spectrum analysis that shows a wide frequency band response of the tubes. Since this study



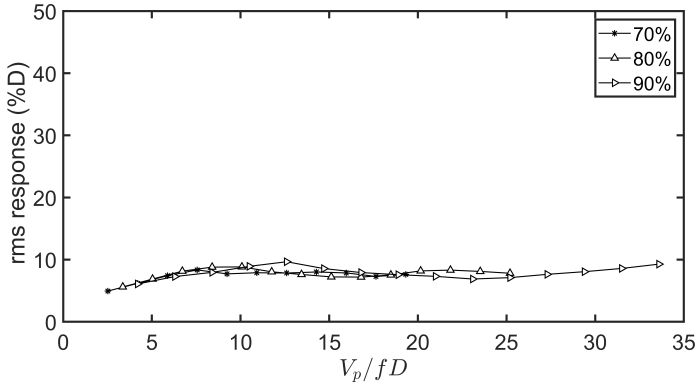
(a)



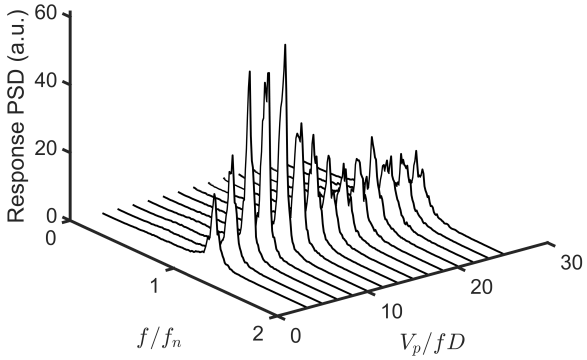
(b)

Figure 4.8 Fully flexible array vibrations in the transverse direction in mid void fractions (40-60%): (a) non-dimensional tube rms tip vibrations, (b) frequency spectra in 60% void fraction

focuses mainly on the fluidelastic instability, it is worth mentioning that all rms response in the streamwise direction is calculated in a small frequency band at the tube natural frequency. This is in order to exclude the quasi-periodic excitation of the tubes at low frequency. In this set of experiments, the tubes are quasi-periodically excited at a nondimensional frequency near 0.25 as shown in Fig. 4.14. As these periodic forces excite the tubes at a frequency clearly distinguished from natural frequency vibration in two-phase flow, the existence of such a vibration excitation mechanism should be excluded in the analysis of a fluidelastic instability. Pettigrew et al. [109] showed the existence of large swings in void distribution inside a rotated triangle array. This was shown to lead the strong fluctuating (quasi-periodic) fluid forces. More detailed studies and test results of the same array were presented by Zhang



(a)



(b)

Figure 4.9 Fully flexible array vibrations in the transverse direction in high void fractions (70-90%): (a) non-dimensional tube rms tip vibrations, (b) frequency spectra in 80% void fraction.

et al. [110, 111].

4.4 Array Dynamics in Air Flow

Different configurations of flexible tubes were tested in air, starting from a single flexible tube, to fully flexible tube array. All test configuration results are discussed below, however, for brevity, only the most significant results are graphically presented.

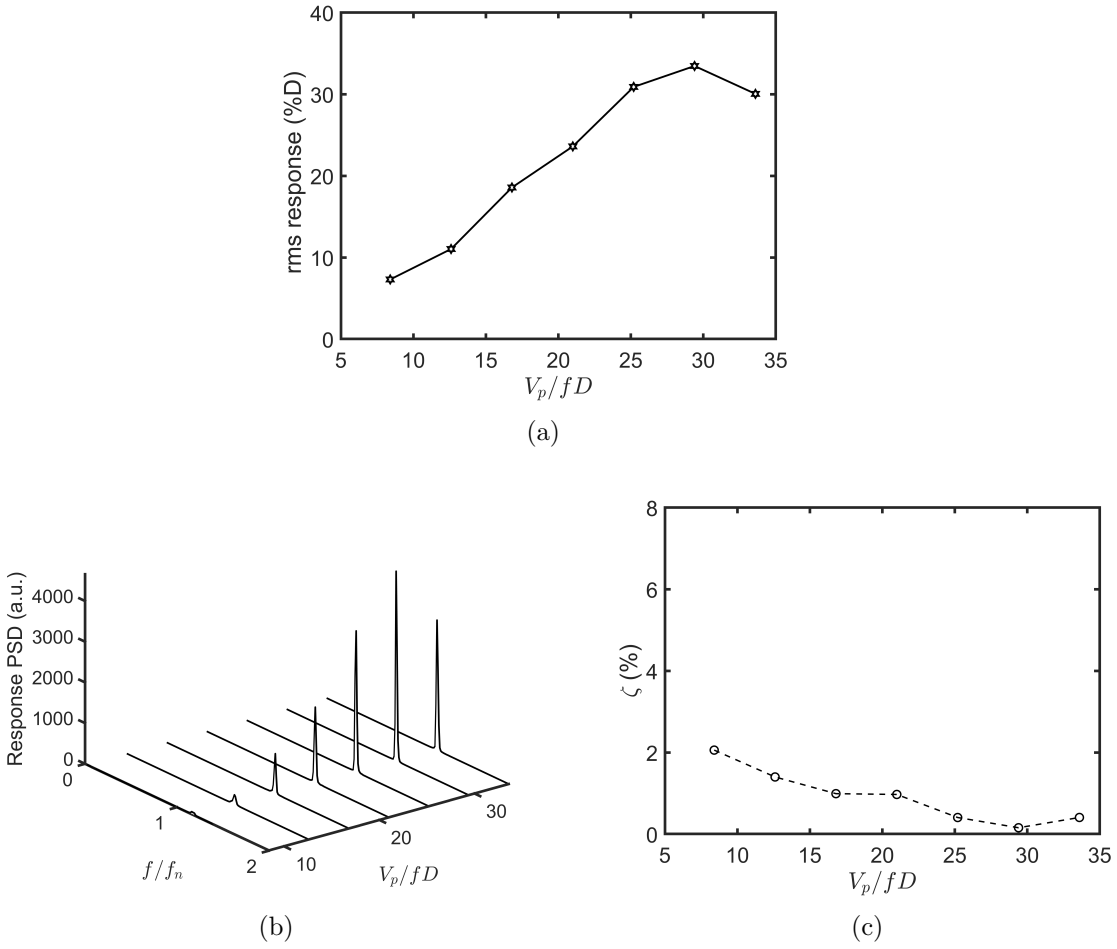


Figure 4.10 Fully flexible array vibrations in the transverse direction in the 97% void fraction test: (a) tube rms vibrations, (b) frequency spectra in 80% void fraction, (c) damping ratio variation with non-dimensional flow velocity.

4.4.1 Streamwise direction dynamics

The tested array configurations and flexible tube IDs are presented in Fig. 4.15. Multiple test configurations were tested, primarily in the streamwise direction.

In the first set of experiments, all tubes were rigid with only one flexible tube mounted in different rows in the array; this is to investigate the effect of the tube location in the array on its dynamic behaviour. A single flexible tube positioned in any of the first 6 rows as the one shown in Fig. 4.15a did not become fluidelastically unstable, see Fig. 4.16(a). In Fig. 4.16(b) the frequency spectra of the tube located deep in the array is presented. A significant difference in the tube static deflection is observed for the first two rows, compared to rows deeper in the array. By increasing the number of flexible tubes to two or three,

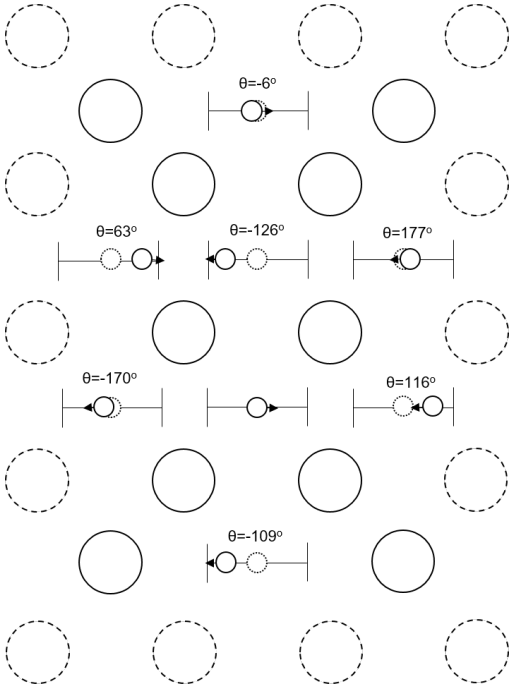
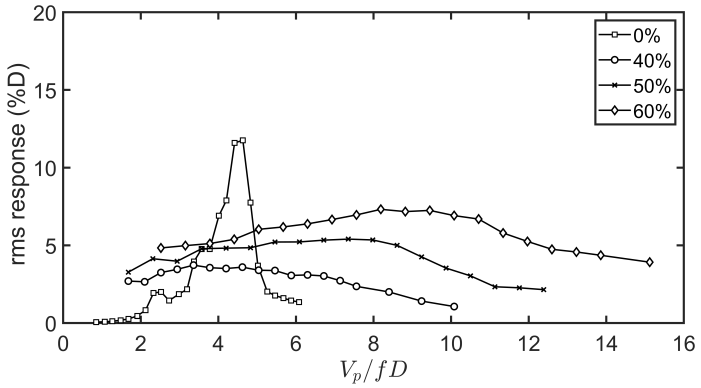


Figure 4.11 Vibration mode and phase angles referenced to tube 2 in 97% void fraction at V/fD=30.

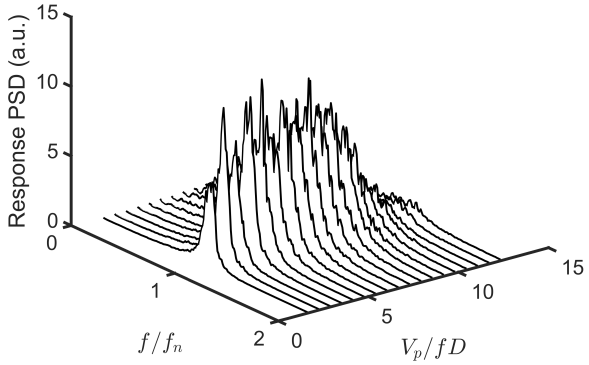
positioned in the first two rows, it seems very apparent that the array will not become unstable. However, in the case of three flexible tubes, low amplitude random vibrations showed up above V/fD=117. A column of flexible tubes also did not undergo instability (Fig. 4.17(a)).

Other experiments were done with multiple flexible tubes, arranged in a diamond, placed in the upstream rows as shown in Fig. 4.15e. In this case, fluidelastic instability was observed at relatively high flow velocity near 140. A direct comparison was made to compare the same configuration but with 4 tubes instead of 9. It was found that adding more flexible tubes downstream delays the instability. The main difference was the pattern of tube motion as downstream tubes were noticed to be stabilizing the upstream tubes, causing multi stage instability as shown in Fig. 4.17(b). When the tubes are regrouped to form a cluster as shown in Fig. 4.15f, the array underwent fluidelastic instability at fairly high flow velocity V/fD=118, see Fig. 4.18(a).

It should be mentioned that, when fluidelastic instability occurs, tubes vibrations are seen to be violent to the extent that they impact each other in such a wide spacing array. Furthermore, once instability is initiated, it cannot be stopped unless the test loop is shut down and air flow stops.



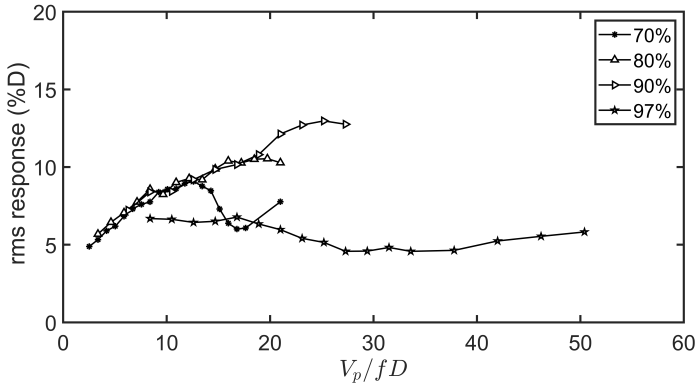
(a)



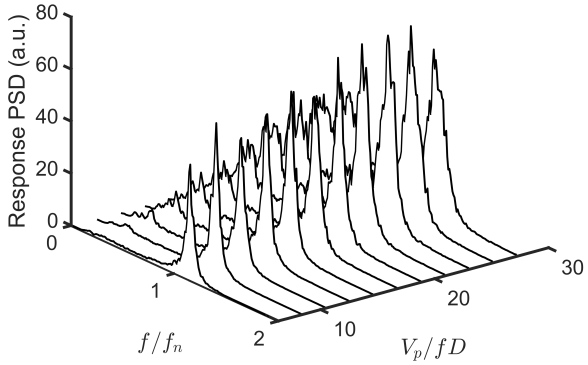
(b)

Figure 4.12 Fully flexible array vibrations in the streamwise direction in mid void fractions (40-60%): (a) non-dimensional tube rms tip vibrations, (b) frequency spectra in 50% void fraction.

Following the cluster configuration tests, experiments with more flexible tubes were performed. A partially flexible array (Fig.4.15g) with flexible tubes placed in the 5 upstream rows, followed by 4 rows of rigid tubes, was tested. The array was fluidelastically unstable at a reduced velocity of 75. For tests on the fully flexible array (Fig. 4.15h), a slight decrease in the instability threshold was observed; where the array became unstable at a reduced velocity of 72, see Fig. 4.18. The importance of the effect of tube-tube coupling on fluidelastic instability is clearly evident. The tests suggest that fluidelastic instability is predominant in the upstream rows. To further investigate this, an experiment was repeated with the upstream tube row fixed. The resulting instability onset was significantly delayed as shown in Fig. 4.18(c), with approximately 78% increase in the reduced velocity. The



(a)



(b)

Figure 4.13 Fully flexible array vibrations in the streamwise direction in high void fractions (70-90%): (a) non-dimensional tube rms tip vibrations, (b) frequency spectra in 90% void fraction.

vibration mode of the fully flexible array is shown in Fig. 4.20. In this figure the phase of all tubes is referenced to tube 3. Tubes in adjacent columns and same row seem to have similar phase angle. This is clearly noticed in rows 1 and 3. However, in the central column, downstream tube always leads the upstream one with the same phase angle except tube 8. Note that tube 8 is not significantly affected by the fluidelastic instability forces and can not be confirmed to be unstable.

The results are very significant, since array stabilization is achieved by fixing the upstream tube row in this case. The streamwise fluidelastic instability requires synchronized motion between the flexible tubes. The stiffness-controlled instability, that requires coupling motion between the tubes, is confirmed to be the fluidelastic instability mechanism for this array.

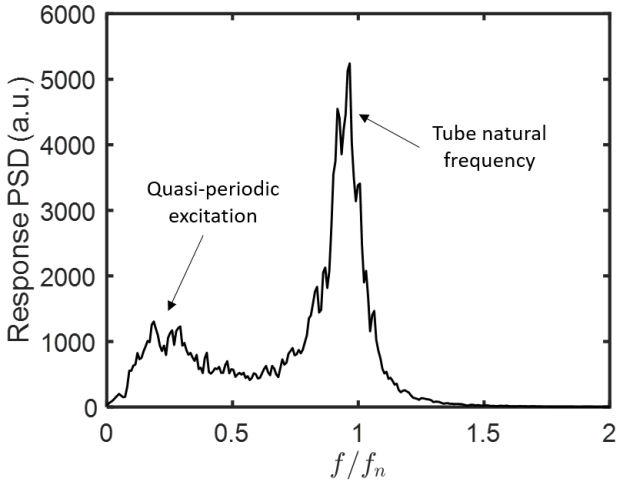


Figure 4.14 Frequency spectrum of a tube in the fully flexible array flexible in the flow direction.

This agrees well with results from the literature for larger spaced arrays with the same array geometry.

Further analysis revealed that several distinct flow periodicities exist in this array with a wide range of Strouhal numbers. For comparability of the test results, Strouhal numbers here are calculated based on the upstream flow velocity ($S_u = f_v D/V_u$). Generally, three periodicity frequencies could be observed, (however, not necessarily at the same flow velocity), that correspond to S_u of 0.10, 0.19, and 0.32. Figure 4.21 shows the frequency spectrum at two different flow velocities with the three flow periodicities. In these results that are obtained in air flow, there is no resonance-like vibrations observed. Price et al. [74] also reported three periodicities in a wider RS array with pitch ratio of 2.12. These periodicities correspond to low Strouhal numbers. This was attributed to the limitation in the minimum flow speed achievable in the wind tunnel. It is worth mentioning that these results are obtained from the streamwise tests, as flow periodicity frequencies could not be picked up from the transverse vibration test frequency spectra.

4.4.2 Transverse direction dynamics

Generally, transverse vibration tests did not reveal any existence of "dynamic" instability in this array. A single flexible tube located in the 4th row was first tested and found to be dynamically stable. Similarly, when a full bundle of flexible tubes was tested, no dynamic instability was observed. The configurations tested are presented in Fig. 4.22. The fully

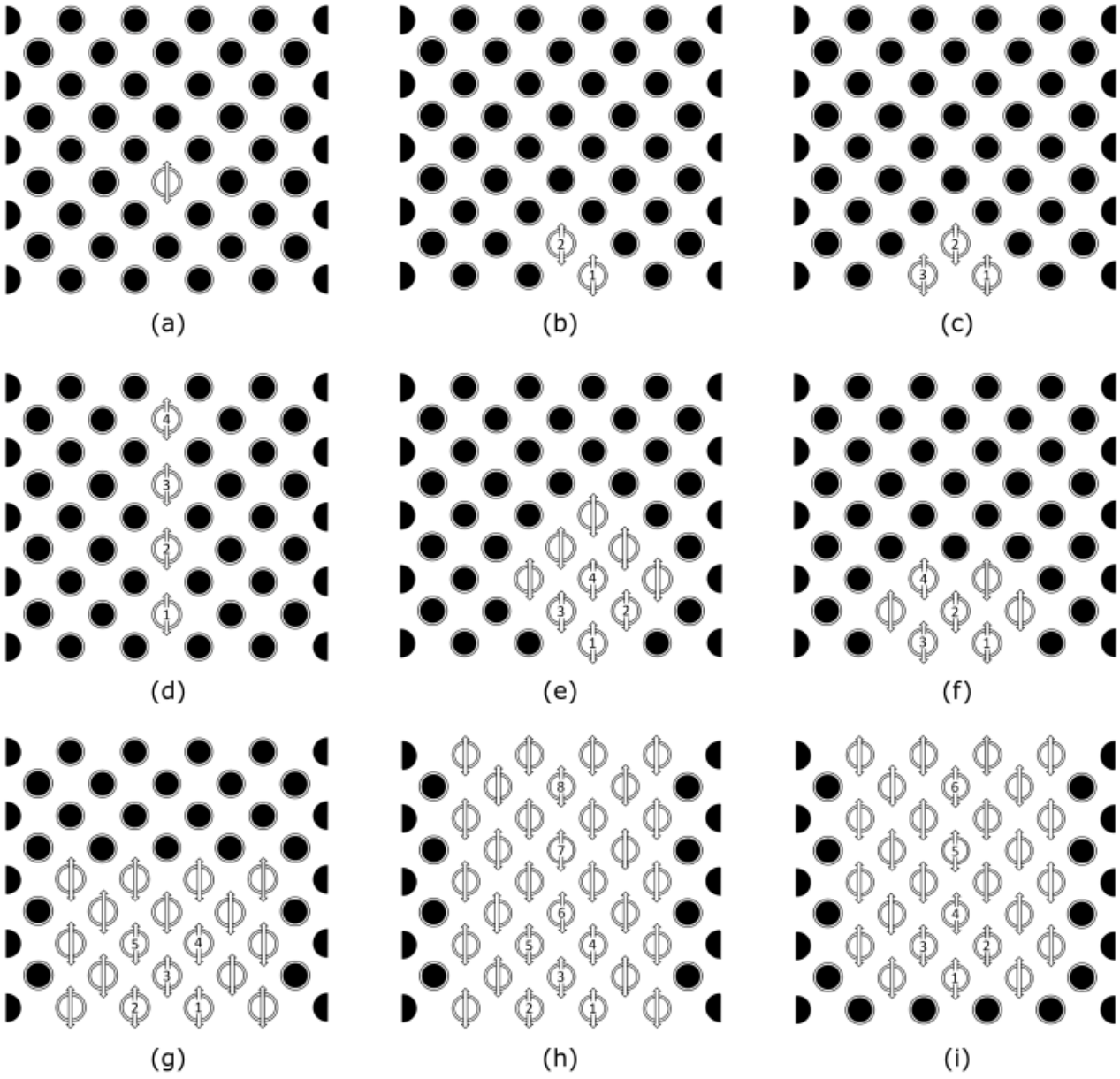
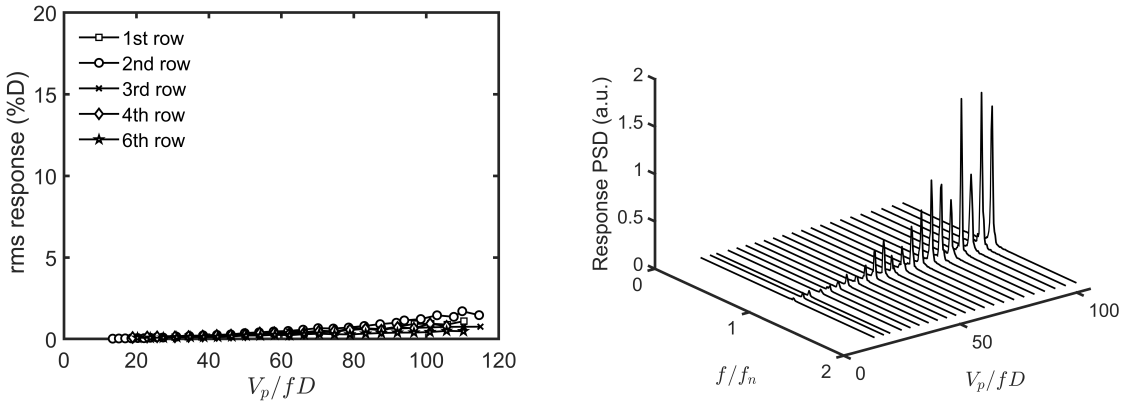


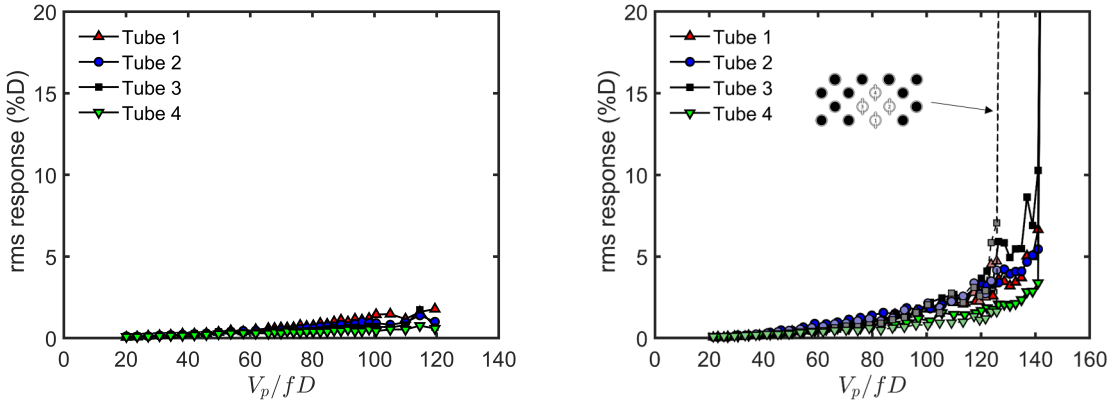
Figure 4.15 Configurations of the tubes flexible in the streamwise directions experimented in air flow.

flexible array was found to be dynamically stable as seen in Fig. 4.23. However, a sudden static deflection was observed for tube 3 (tube located in the 2nd row) near V/fD=85. Fig. 4.23c shows that tube 3 frequency gradually decreased for high flow velocity. This indicates that a loss of net stiffness caused negative fluid stiffness forces, leading to a static instability (divergence) in the array, and suggesting the onset of static instability for this tube. The fluid stiffness effect in the first few rows of the array is therefore significant.



(a) (b)

Figure 4.16 Tube vibrations of a single tube in the streamwise direction: (a) dynamic vibrations, (b) frequency spectra of the tube located in 4th row



(a) (b)

Figure 4.17 Tube vibrations in the streamwise direction : (a) column configuration, (b) diamond configuration

4.4.3 Discussion

The Connors equation expresses the relationship between the non-dimensional (or reduced) critical pitch velocity and "tube mass-damping parameter". The equation takes the form

$$\frac{V_{pc}}{fD} = K\sqrt{\frac{m\delta}{\rho D^2}} \tag{4.4}$$

The tube rms response and response PSD presented above confirmed the occurrence of transverse direction FEI for 97% void fraction. Damping analysis was used along with tube re-

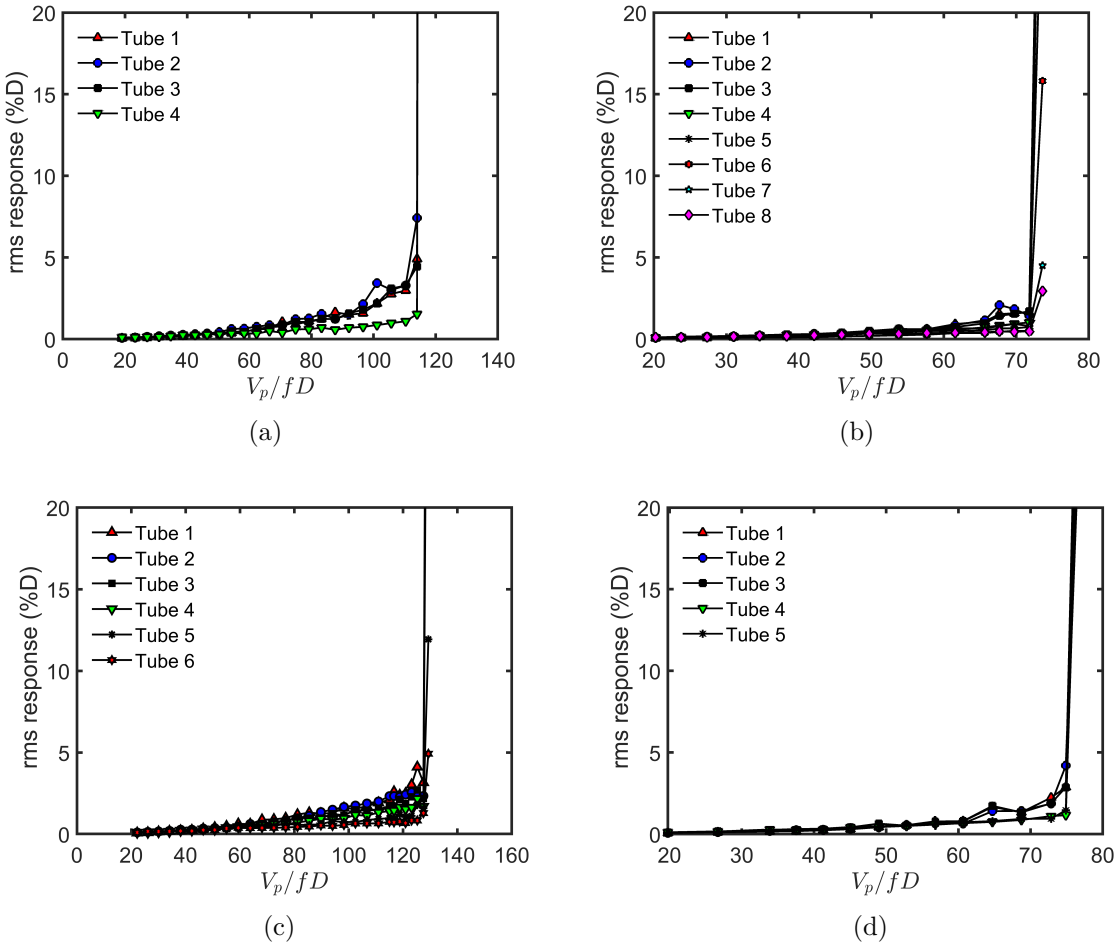


Figure 4.18 Tube vibrations in the streamwise direction : (a) cluster of flexible tube located in the upstream rows of the array, (b) fully flexible array, (c) flexible array located downstream a rigid row of tubes, (d) bundle with the upstream 5 flexible rows and downstream rigid array

sponse data to determine the average critical velocity. For the fully flexible array, a Connors constant of K=4.4 was estimated for V_{pcr}/fD=13.2. For the single flexible tube and flexible column configurations, values of K= 5.3 and 4.9, were respectively, obtained.

Figure 4.24 shows two flow regime maps proposed by Noghrehkar et al. [112] and Ulbrich and Mewes [113]. The experimental test conditions are also superposed on maps. Noghrehkar et al. [112] distinguished three different flow regimes by analysing the two-phase flow void fraction probability density: Bubbly, Intermittent, and Dispersed flow. Since these maps to do not correspond to the rotated square array studied in the present work, they provide an estimate of the expected flow pattern. Figure 4.24 shows that for void fractions of 40% - 60%, the flow pattern is primarily bubbly flow. For 70%-80% void fraction, the flow pattern is at the transition boundary between bubbly and intermittent flow patterns (according to

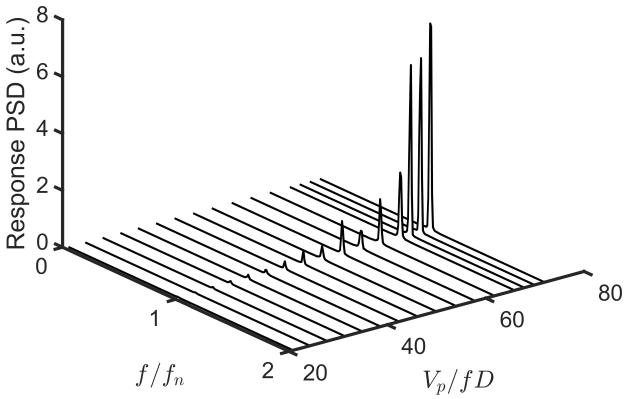


Figure 4.19 Frequency spectra of tube 3 in the fully flexible array configuration.

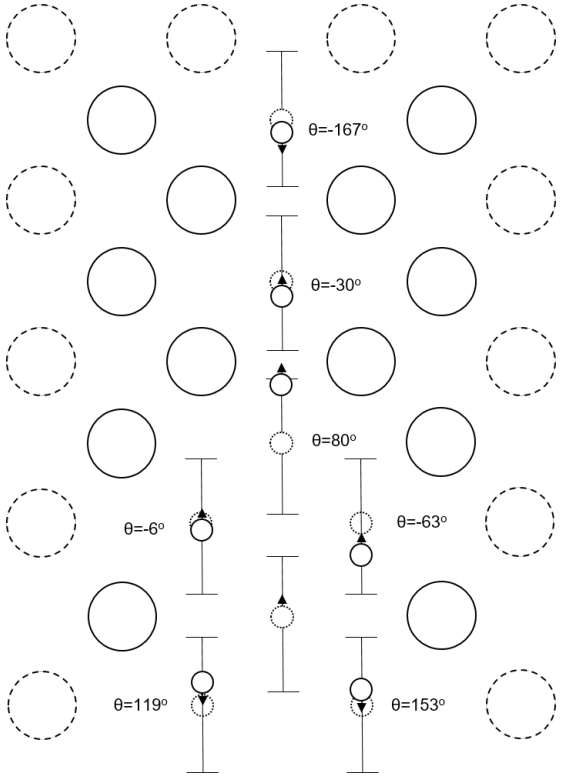


Figure 4.20 Vibration mode and phase angles referenced to tube 3 in air flow at at the post instability flow velocity.

Ulbrich and Mewes [113]) particularly in the mid-velocity range. For the void fractions of 90% and 97%, the flow conditions are primarily in the intermittent flow regime; for 97% void fraction the highest velocity conditions approach the transition boundary to dispersed flow.

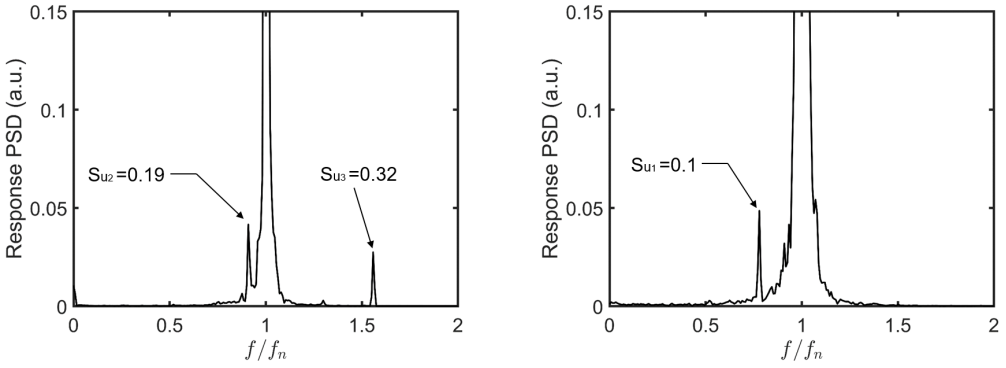


Figure 4.21 Frequency spectra of the flexible tube in the streamwise direction located in the third row for: (a) V_u/fD=4.86, (b) V_u/fD=7.64

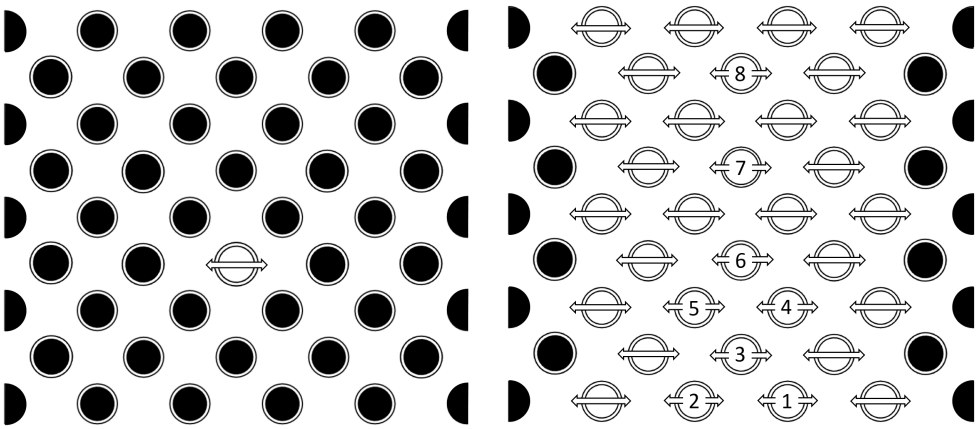


Figure 4.22 Configurations of the tubes flexible in the transverse directions experimented in air flow

The reduced critical velocity for the two-phase flow and air flow unstable cases are plotted in Fig. 4.25 as a function of mass damping parameter, $m\delta/\rho D^2$. In addition to the test results presented above, previously published data is included in Fig. 4.25 for comparison. The published data includes a range of pitch spacings and flow types.

In Fig. 4.26, the same data is plotted to show the relation between the stability constant K and array spacing ration P/D. Due to the complexity of the dynamic behaviour in air flow compared to water and two-phase flow, the diagrams shown in Figs. 4.25 and 4.26 show only arrays tested in air. It is apparent, from the current work and previous work from the literature, that a single flexible tube is stable in this layout, and fluidelastic stiffness coupling

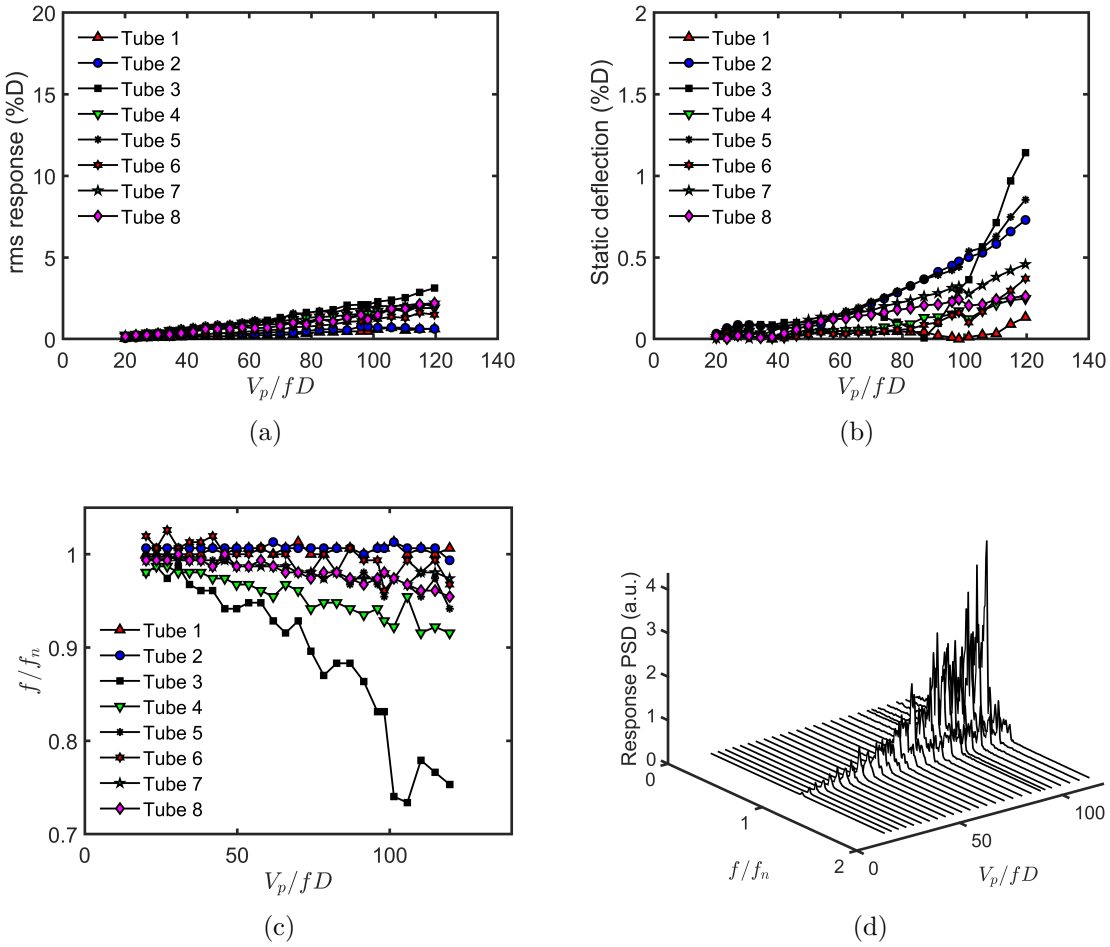


Figure 4.23 Tube vibrations of a fully flexible array in the transverse direction: (a) dynamic vibrations, (b) static deflection, (c) frequency variation, (d) frequency spectra of tube 3.

is necessary for instability. For the fully flexible array, the critical reduced velocity increases rapidly with pitch spacing, reaching its maximum value near P/D=1.6 as reported in [17], then it does not show a clear increase at higher pitch ratios. This can not be confirmed yet as there is very few data published for this layout with wide spacing in air flow.

Single flexible tube array, as well as partially flexible arrays, have delayed instability onset due to the relatively weak tube-tube coupling. This is incomparable to the fully flexible array cases where the array could become unstable at lower velocity due to the strong fluidelastic coupling between the tubes. Hence, data showing fully flexible array instability in Fig. 4.25 are distinguished with filled symbols. Price and Kuran [13] provided data for up to four flexible tubes, located in the upstream rows. For such a small number of flexible tubes, and widely spaced array (P/D=2.12), the critical velocity is found to be the highest among the

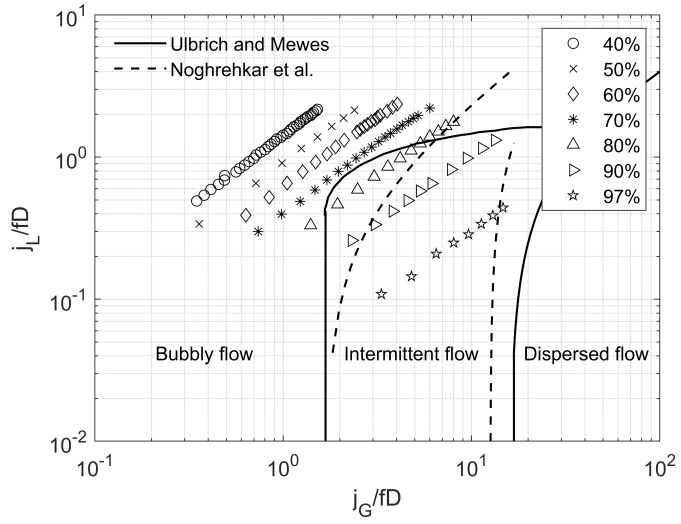


Figure 4.24 Flow regime map for transverse direction.

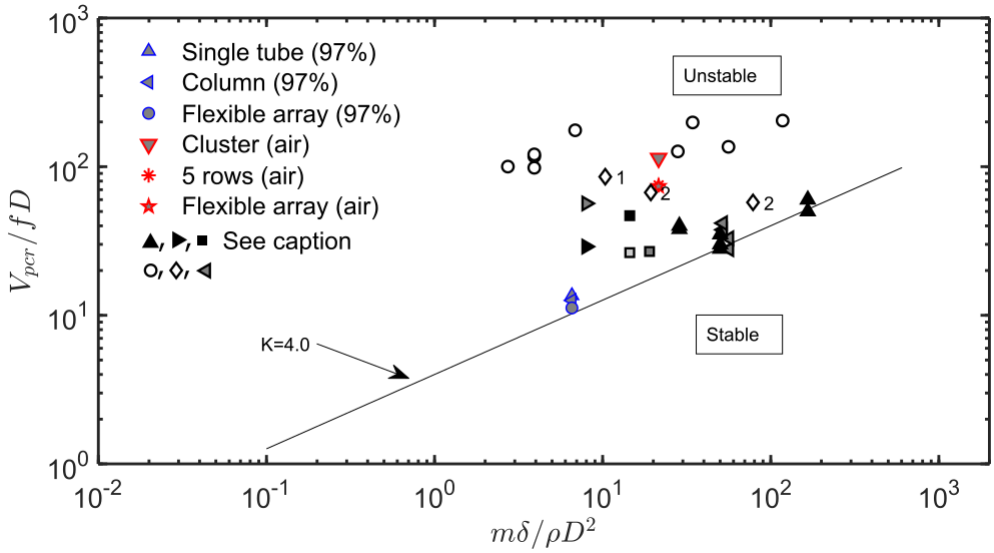


Figure 4.25 Stability map of the fluidelastic instability experimental data: (△,◁,◯) present study in 97% void fraction (transverse direction), and in air flow in the streamwise direction: (▽,∗,⋆) present study (P/D=1.64), (◯) Price and Kuran (P/D=2.12) [13], (◊) Païdoussis et al. (P/D=1.5) [14], (■) Nakamura and Tsujita (P/D=1.2, 1.33, 1.5) [15], (▲) Hartlen (P/D=1.3, 1.414, 1.56) [16] , (◀) Soper (P/D=1.27, 1.35, 1.52, 1.78) [17], (▶) Elkashlan (P/D=1.4, 1.7) [18]; open symbols represent data from single and partially flexible arrays, filled symbols represent data from fully flexible arrays

data in the literature. This was also the case for the present tighter array; where a cluster of four flexible tubes becomes unstable at much higher critical reduced velocity than the fully flexible case.

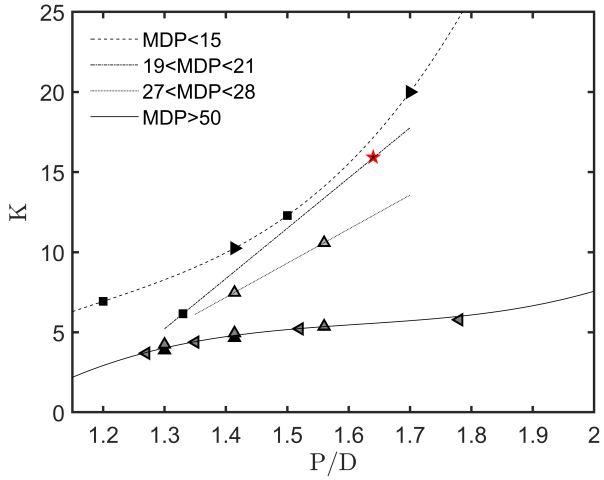


Figure 4.26 Instability constant variation with tubes mass-damping parameter and array pitch spacing for fully flexible array in air flow in the streamwise direction: (⋆) present study (P/D=1.64), (■) Nakamura and Tsujita (P/D=1.2, 1.33, 1.5) [15], (▲) Hartlen (P/D=1.3, 1.414, 1.56) [16] , (◄) Soper (P/D=1.27, 1.35, 1.52, 1.78) [17], (►) Elkashlan (P/D=1.4, 1.7) [18]

The pitch ratio is a key parameter affecting the stability threshold. For the rotated square array, this effect is significant. As seen in Fig. 4.26, the critical velocity increases for large spacing arrays when the mass damping parameter is relatively small (MDP<30), while this increase is considerably small for large mass damping parameters. Soper [17] and Harlten [16] test results are conducted for different mass damping parameters, 50 and 166 respectively, and stability constant does not vary significantly for multiple pitch ratios, compared to lower mass damping parameters.

4.5 Conclusions

A fundamental experimental program was carried out to investigate the stability behaviour of a rotated square tube array of pitch ratio P/D=1.64. The study is comprised of extensive fluidelastic vibration experiments in air-water two-phase flow, as well as air flow. In two-phase flow, of up to 90% void fraction, with single or multiple flexible tubes, the array was found to be fluidelastically stable in both transverse and streamwise directions. For a very high void fraction of 97%, unstable behaviour in the transverse direction was induced by the flow. The strength of the vibrations varied depending on the number of flexible tubes in the array. The amplitude growth rate with flow velocity was low compared to typically observed fluidelastic instability. Damping analysis showed a significant increase in damping ratio in the

streamwise direction. This explains the strongly stable behaviour in the streamwise direction for this array in two-phase flow.

In air flow, a single flexible tube was found to be stable in both the transverse and streamwise directions. This led to the conclusion that the damping controlled mechanism is incapable of inducing fluidelastic instability in this array. Experiments with multiple tubes flexible in the streamwise direction showed stable dynamic behaviour, unless more than two flexible tubes are located in the first row. However, by increasing the number of degrees-of-freedom, upstream rows underwent fluidelastic instability, with instability threshold related to the number of flexible tubes. Transverse fluidelastic loss of stiffness was observed in the second row that led to a 30% drop in natural frequency, accompanied by static deflection, indicating the possibility of static instability (divergence) in this array. Taken together, results show that the leading instability mechanism in this array is the stiffness-controlled fluidelastic instability mechanism for air flow. In the array, streamwise fluidelastic instability (in air flow) could be restrained by fixing the upstream tube row. For two-phase flow, the array is fluidelastically stable in the streamwise direction.

CHAPTER 5 ARTICLE 3: STABILITY BEHAVIOUR OF A ROTATED SQUARE TUBE ARRAY SUBJECTED TO TWO-PHASE CROSS-FLOW

Sameh Darwish, Njuki Mureithi, Minki Cho

This article has been submitted to the "Journal of Nuclear Engineering and Design" on October 26, 2022.

In this chapter, the stability analysis of the rotated square array is performed in single phase (water) and two-phase (air-water) cross-flow. This is to meet the specific objectives to:

- Measure the quasi-static fluid forces of the tubes in the array in the lift and drag directions.
- Perform stability analysis of the array to study its fluidelastic behaviour.
- Verify the applicability of the quasi-steady model to the rotated square array in two-phase flow.

The paper presents the time-averaged quasi-static fluid force measurements of the rotated square array in single and two-phase flow. A test apparatus is designed to measure the forces in both the transverse and streamwise directions. Central tube is instrumented using an accurate force sensor to measure the fluid forces. This tube is mounted on a mechanism with a feedback and a laser sensor to control its displacement. Cross-coupling fluid forces were also measured by instrumenting the neighbouring tubes with strain gauges. Lift and drag force coefficients are measured at high reduced velocity for each void fraction. Results show that lift force coefficient derivative is positive in water flow, while it is significantly low in two-phase flow. Results are compared with a rotated triangular array fluid forces, an array that is known to be inherently unstable, especially in the transverse direction. The measured fluid forces were incorporated into a quasi-steady model to study the array stability behaviour. The model confirmed that the array is generally stable in both the transverse and streamwise directions in two-phase flow. Despite the stable behaviour in two-phase flow, instability was detected when a multiple flexible tubes existed in the array in water cross-flow. This observation made it clear that the previously reported vibrations in water cross-flow at high flow velocity when fully flexible array is tested resulted from fluidelastic instability. The complex behaviour in water flow due to the tube-vortex interaction made it unclear to predict the fluidelastic instability. Interestingly, the model was able to predict the fluid damping variation with the flow velocity.

Abstract

Theoretical analysis of fluidelastic instability of tube arrays operating in two-phase flow, in particular, for rotated square arrays, remains limited. In this paper, an experimental program was carried out to gain insight into the rotated square array fluidelastic forces. The quasi-steady model is used to predict the fluidelastic behaviour of a rotated square array having pitch spacing ratio P/D=1.64. A test apparatus is designed to measure the quasi-static fluid forces in single phase (water) and two-phase (air-water) flow for a wide range of void fractions. Both streamwise and transverse directions are considered in the study by measuring the forces and their derivatives with respect to tube finite displacement in both the lift and drag directions. The cross coupling fluid forces are incorporated into the quasi-steady model to investigate the existence of the stiffness-controlled instability mechanism in this array. The results of the theoretical analysis were compared with fluidelastic instability experimental data for the same array. Agreement between the theoretical results and the experiment is shown to be good. In general, the stable behaviour of this array in two-phase flow was confirmed. The analysis showed the vulnerability of this array to transverse fluidelastic instability in water flow in the case of the fully flexible array. This analysis is also used to investigate the array behaviour in the 97% void fraction and results are compared with those exported experimentally. Compared to the lower void fractions, the damping is, uniquely in the 97%, invariably behaving with the flow velocity increase. This is relatively consistent with the observed fluidelastic instability from the experiments.

5.1 Introduction

Fluidelastic instability (FEI) in steam generators has been a major concern in the last decade due to an unexpected repeat occurrence. In 2012, two steam generators in the San Onofre Nuclear Generating Station (SONGS) in California suffered significant tube failures due to fluidelastic instability induced vibrations. Despite the extensive experimental effort and significant advances in understanding tube arrays dynamics in two-phase flow, significant work is still needed to develop theoretical models to predict the fluidelastic instability for different tube arrangements. To elucidate the physics of the problem, Roberts [5] provided the first modeling approach by considering a jet switching mechanism in the tube bundle and assuming that flow separation occurs at minimal inter-tube gaps while pressure is constant in the wake regions of the tubes. Robert's theory could not, however, predict transverse fluidelastic instability, although research has shown this to be the dominant instability direction. A different approach was followed in the quasi-static model developed by Connors [26] and

Blevins [114] who proposed using measured quasi-static fluid forces on a tube. The model assumes that fluid forces exerted on a flexible tube could be predicted (approximately) by statically displacing the tube relative to its neighbours. This assumption allowed the experimental measurement of the fluid force coefficients using a rigid tube in an array. In the quasi-static model, the flow adjusts to tube motion with no retardation. Considering the retardation of the flow approaching the cylinder, a significant improvement was proposed by Price and Paidoussis [55, 57, 115] by including the resulting time lag between tube motion and fluid forces. Granger and Paidoussis [6] and Meskell [116] introduced the quasi-unsteady model by modelling the memory effect. This improvement has led to better agreement with the experimental FEI test results. However, it introduced more parameters to be determined, which are array-dependent.

The general unsteady model was developed by Tanaka and Takahara [49,50], and Chen [117]. The method is based on unsteady fluid forces measured on an oscillating cylinder. Despite the method's accuracy predicting the 1 d.o.f damping-controlled induced FEI, the method encounters challenges predicting stiffness-controlled instabilities for two-phase flow. This is due to the difficulty measuring dynamic (cross-coupling) forces in two-phase flow which requires strong coherence between the tube motion and the neighbouring tubes cross-coupling forces. Nakamura et al. [118], Mureithi et al. [119], and Hirota et al. [120] applied the unsteady model and presented the time-frequency analysis developed to calculate the tube displacement-fluid force phase difference. Despite the difficulty in measuring the time delay in two-phase flow due to high flow turbulence, Sawadogo and Mureithi [25, 121] showed that the time delay could be deduced by equating the quasi-steady with a time delay to measured unsteady fluid forces. While their work was innovative, difficulties were, however, encountered when extracting the time delay parameter from the deduced equation for some test flow velocities and excitation frequencies.

Lever and Weaver [7] developed a tube-in-channel model to describe the transverse dynamics in tube bundles. The model is based on the analysis of a single flexible tube in a so-called unit cell consisting of a wake and channel region. The model considered only single degree-of-freedom (SDOF) instability, where transverse and streamwise motions are mechanically decoupled. With some later modifications reported in Lever and Weaver [65], static instability (divergence) and streamwise instability were taken into account in a modified version of the equations. Later, Hassan and Weaver [66] extended the theory with a simplified model to couple the streamwise and transverse motion of the tubes in a flexible bundle. This improvement allows the theory to predict FEI due to the stiffness mechanism (FEI with coupled multiple degrees-of-freedom). The authors later studied the stability behaviour of the rotated square array in the streamwise direction [122]. Simulations were carried out to

compare a single flexible tube in an otherwise rigid array with experimental results. The work cited in the foregoing is a small subset of the work done on fluidelastic instability. Price [56] did an excellent review addressing the historical progress of FEI model development for tube arrays, discussing in details the relative strengths and limitations of the various models.

Staggered arrays, especially the rotated square, have shown complex dynamic behaviour in single and two-phase flows. Previous experimental results revealed that the rotated square array has an even higher level of dynamic complexity when subjected to air cross-flow. Yet, the data existing for this array, in addition to modelling research in the literature is scarce. The only theoretical study comprising experimentally measured forces in a rotated square array was performed by Kuran [123] for air flow. The results were incorporated into a multi-degree-of-freedom quasi steady model. However, the model provided by the author could not fully reveal the physical mechanisms governing several phenomena observed in the array.

The purpose of the present work is to contribute to a deeper understanding of the complex dynamics of the rotated square array. The main objectives of the work is to explicitly determine the fluid force coefficients in the array in the streamwise as well as the transverse directions, and to verify the applicability of the simple quasi-steady model in predicting the FEI onset for the rotated square array. Fluidelastic instability tests performed in single and two-phase flow form the basis for the work presented here. In addition to stability testing, a careful study is needed to measure the fluid forces acting on a flexible tube in this array. In the case of multiple flexible tubes, the fluid coupling resulting from tube motion is significant based on previous findings for this array. In the present study, the time-averaged quasi-static forces acting on a bundle of rigid tubes as a function of tube displacement are measured in a rotated square array of pitch spacing ratio P/D = 1.64. The study is conducted for both the transverse and streamwise directions in water flow, and two-phase flow for void fractions ranging from 40% to 97%. These results are used in the quasi-steady model to predict the fluidelastic instability boundary.

5.2 Theoretical Formulation

The quasi-steady model is used in this work in view of its moderate complexity and applicability in predicting the fluidelastic instability onset for different arrays for a wide range of mass damping parameters. The quasi-steady model is based on the following assumptions: tube non-dimensional displacement (y_0/D or x_0/D) is small, flow reduced velocity (V/fD) is high, implying that tube velocity is relatively small compared to flow pitch velocity, and a time delay exists between tube displacement and fluid forces. One main advantage of using the quasi-steady model is to model the multi-degree-of-freedom array. This is achieved by

measuring the fluid forces on the surrounding tubes resulting from central tube displacement. This is easily done when measuring the steady fluid forces. It is significantly more difficult to measure dynamic forces (for the unsteady model) due to weak correlation of the cross-coupling forces on the surrounding tubes.

5.2.1 Quasi-steady model formulation

In the following, the equations governing the motion of a tube that is assumed to be flexible in one direction only are presented. In this formulation the x- and y-directions are mechanically decoupled. This is also the case for the multiple flexible tubes conditions. Here, the quasi-static lift and drag coefficients are determined using the pitch flow velocity for practical purposes. All equations that follow are also based on the pitch flow velocity defined as

$$V_p = V_\infty \frac{P/D}{P/D - 1} \tag{5.1}$$

where V_∞ is the homogeneous free-stream velocity at the test section entrance and P/D the array pitch-to-diameter ratio. Due to the vibrational motion of the flexible tube, the velocity vector becomes at an induced angle, α, relative to the tube as shown in Fig. 5.1(b). The velocity relative to the tube motion can be expressed as:

$$V_r = \sqrt{(V_p - \dot{x})^2 + \dot{y}^2} \tag{5.2}$$

By neglecting the higher order terms

$$\frac{V_r}{V_p - \dot{x}} = \sqrt{1 + (\frac{\dot{y}}{V_p - \dot{x}})^2} \simeq 1 \tag{5.3}$$

For small displacements, the angle of incidence can be defined as

$$\alpha \simeq \frac{\dot{y}}{V_r}; \quad \cos\alpha = \frac{V_p - \dot{x}}{V_r} \simeq 1 \tag{5.4}$$

The quasi-steady fluid forces in the x- and y- directions can be expressed as

$$\begin{aligned} F_x &= F_D \cos\alpha + F_L \sin\alpha \\ F_y &= F_L \cos\alpha - F_D \sin\alpha \end{aligned} \tag{5.5}$$

where the drag and lift forces are

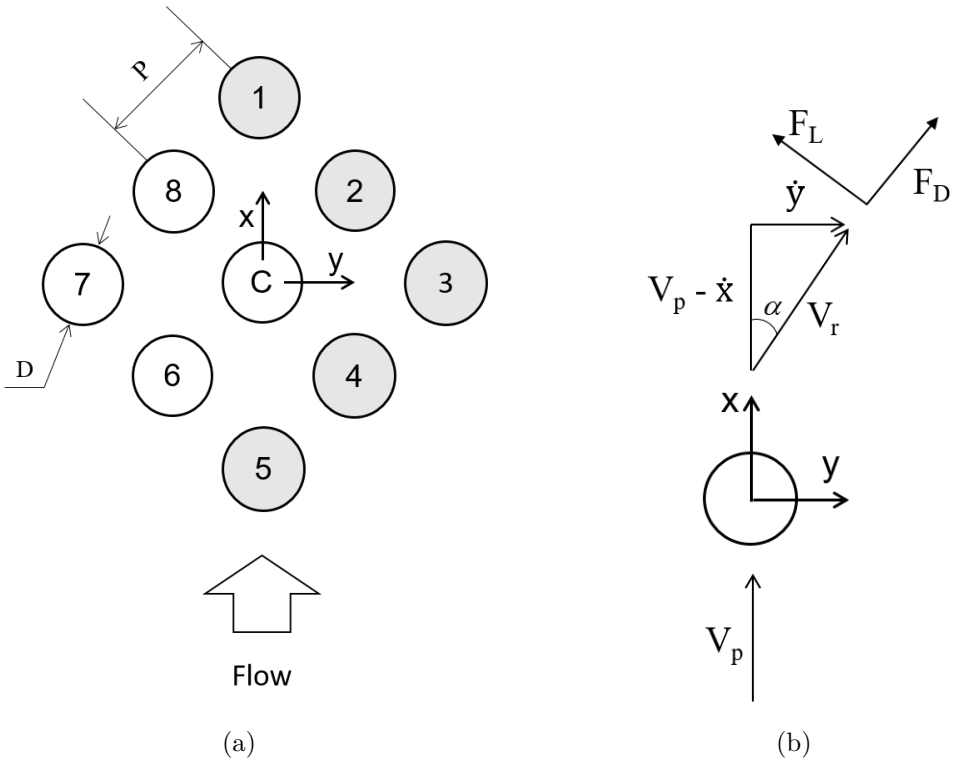


Figure 5.1 Schematic showing of the array layout and neighbouring tubes numbers.

$$F_D = \frac{1}{2}\rho_h V_r^2 D C_D$$
$$F_L = \frac{1}{2}\rho_h V_r^2 D C_L \tag{5.6}$$

By combining equations 5.4, 5.5, and 5.6, the expression of the fluid forces in the streamwise direction can be written as

$$F_x = \frac{1}{2}\rho_h V_p^2 D[C_D - \frac{2}{V_p}C_D\dot{x} + C_L\frac{\dot{y}}{V_p}] \tag{5.7}$$

and in the transverse direction as

$$F_y = \frac{1}{2}\rho_h V_p^2 D[C_L - \frac{2}{V_p}C_L\dot{x} - C_D\frac{\dot{y}}{V_p}] \tag{5.8}$$

Considering an array having N flexible tubes, the drag and lift coefficients can be described using first order Taylor's approximation

$$C_{Di} = C_{D0i} + \sum_{i=1}^{n} \frac{\partial C_{Di}}{\partial x_j} x_j + \sum_{j=1}^{n} \frac{\partial C_{Di}}{\partial y_j} y_j$$
$$C_{Li} = C_{L0i} + \sum_{i=1}^{n} \frac{\partial C_{Li}}{\partial y_j} y_j + \sum_{j=1}^{n} \frac{\partial C_{Li}}{\partial x_j} x_j \tag{5.9}$$

where, the C_{Di} and C_{Li} are the drag and lift coefficients for tube i, x_j and y_j are the streamwise and transverse tube displacements of tube j. Thus, the linearized streamwise fluid force per tube unit length, for a tube in figure 5.1(a), may be expressed as:

$$F_x = \frac{1}{2}\rho_h V_p^2 D \left[C_{D0} + \frac{\partial C_D}{\partial x} x - \frac{2}{V_p} C_{D0} \dot{x} \right] \tag{5.10}$$

Similarly in the transverse direction

$$F_y = \frac{1}{2}\rho_h V_p^2 D \left[\frac{\partial C_L}{\partial y} y - \frac{C_{D0}}{V_p} \dot{y} \right] \tag{5.11}$$

where, ρ_h is the homogeneous fluid density, D is the tube outer diameter, C_L is the lift coefficient, C_D is the drag coefficient, C_{D0} is the drag coefficient at the tube central location. The equation of motion of the tube array flexible in the transverse direction, considering linearized quasi-steady fluidelastic forces, can be written as

$$([M_s] + [M_{f_y}])[\ddot{\vec{\mathbf{y}}}] + ([C_s] + [C_{f_y}])[\dot{\vec{\mathbf{y}}}] + ([K_s] + [K_{f_y}])[\vec{\mathbf{y}}] = 0 \tag{5.12}$$

and in the streamwise direction

$$([M_s] + [M_{f_x}])[\ddot{\vec{\mathbf{x}}}] + ([C_s] + [C_{f_x}])[\dot{\vec{\mathbf{x}}}] + ([K_s] + [K_{f_x}])[\vec{\mathbf{x}}] = 0 \tag{5.13}$$

where:

$$[M_s] = m_s[I]_{nxn}; [M_f] = m_f[I]_{nxn}; C_s = 2\omega\zeta m_s[I]_{nxn}; [K_s] = m_s\omega^2[I]_{nxn};$$

where, m is the mass, K is the stiffness, and C is the damping, and subscripts s and f indicate structure and fluid quantities, respectively, ω is tube natural frequency, and ζ is tube damping. The fluid damping induced by the flow drag force on the tube flexible in the transverse direction in the array is

$$[C_{f_y}] = \frac{1}{2}\rho_h D V_p C_{D0}[I]_{nxn} \tag{5.14}$$

and for the tube flexible in the streamwise direction

$$[C_{f_x}] = \rho_h D V_p C_{D0} [I]_{nxn} \tag{5.15}$$

This flow dependent damping always has a positive value as C_{D0} is always positive. A time lag is introduced into the fluid forces that describes the delay between fluid adjusting continuously around the tube due to changing location of the vibrating cylinder. In the case of a single flexible tube, previous work has shown that the time delay is necessary to predict the fluidelastic instability that is induced by the damping controlled mechanism. For a simplified first order model, the time lag between the fluid dynamic force and tube displacement can be expressed as [57]

$$\tau = \mu \frac{D}{U} \tag{5.16}$$

where μ is the time lag parameter estimated to be of order of magnitude of 1. Recent measurements by Sawadogo and Mureithi [121] found values of μ in the range $1.2 \leq \mu \leq 2.7$ for a rotated triangular array in two-phase flow of void fractions in the range 60%-90%. Generally, fluid force measurements of the rotated square arrays have not been reported in the literature except for the quasi-static forces measured in air flow by Kuran [123]. Taking into account the time delay, the fluid stiffness in the transverse direction is written as

$$[K_{f_y}]_{i,j} = -\frac{1}{2} \rho_h V_p^2 D \left[\frac{\partial C_{L_i}}{\partial y_j} \right] e^{-i\omega\tau} \tag{5.17}$$

while in the streamwise direction

$$[K_{f_x}]_{i,j} = -\frac{1}{2} \rho_h V_p^2 D \left[\frac{\partial C_{D_i}}{\partial x_j} \right] e^{-i\omega\tau} \tag{5.18}$$

The fluid stiffness is composed of a real and imaginary parts introduced from the $e^{-\omega\tau}$ term. This generates an additional fluid damping term proportional to $\partial C_L/\partial y$ or $\partial C_D/\partial x$ depending on the flexibility direction. Considering an array having n flexible tubes, with all tubes flexible in one direction only, the equation of motion of tube i flexible in the streamwise direction will be expressed as

$$\ddot{x_i} + \left[\frac{\delta}{\pi}\omega_n + \frac{\rho V D}{m} C_{D0}\right]\dot{x_i} + \left[\omega_n^2 - \frac{1}{2}\frac{\rho V^2 D}{m}\frac{\partial C_{D_i}}{\partial x_i} e^{-i\omega\tau}\right] x_i - \left[\frac{1}{2}\frac{\rho V^2 D}{m} e^{-i\omega\tau} \sum_{\substack{j=1 \\ j\neq i}}^{n} \frac{\partial C_{D_i}}{\partial x_j}\right] x_j = 0 \tag{5.19}$$

and in the transverse direction

$$\ddot{y_i} + \left[\frac{\delta}{\pi}\omega_n + \frac{1}{2}\frac{\rho V D}{m} C_{D0}\right]\dot{y_i} + \left[\omega_n^2 - \frac{1}{2}\frac{\rho V^2 D}{m}\frac{\partial C_{L_i}}{\partial y_i} e^{-i\omega\tau}\right] y_i - \left[\frac{1}{2}\frac{\rho V^2 D}{m} e^{-i\omega\tau} \sum_{\substack{j=1 \\ j\neq i}}^{n} \frac{\partial C_{L_i}}{\partial y_j}\right] y_j = 0 \tag{5.20}$$

From 5.20, assuming one degree-of-freedom transverse vibration, $y = y_o e^{i\omega t}$, the total damping becomes

$$\zeta_{tot} = \frac{1}{2\omega_n}\left[\omega\left(\frac{\delta}{\pi}\omega_n + \frac{1}{2}\frac{\rho V D}{m} C_{D0}\right) + \frac{1}{2}\frac{\rho V^2 D}{m}\frac{\partial C_L}{\partial y}\sin\omega\tau\right] \tag{5.21}$$

For the damping controlled instability to occur, the flow-induced negative damping must be negative enough to overcome the structural damping and flow independent damping expressed in equations 5.14 and 5.15 [124]. The last terms in equations 5.19 and 5.20 represents the coupling factor in the model. It is noteworthy to mention that the fluid damping and fluid stiffness are flow velocity dependent values and clearly on the damped harmonic frequency of the tubes.

5.2.2 Derivatives of fluid force coefficients

The drag and lift force coefficients are defined as

$$\begin{aligned} C_D &= \frac{F_D}{0.5\rho_h V_p^2 A} \\ C_L &= \frac{F_L}{0.5\rho_h V_p^2 A} \end{aligned} \tag{5.22}$$

From the symmetry of the array, one may deduce that

$$C_{Li0} = C_{Lc0} = 0 \tag{5.23}$$

In addition, the lift coefficient remains invariant as the tube is displaced in the streamwise

direction. The drag coefficient on the other hand is symmetrical with respect to tube displacement in the transverse direction. This leads to the relation

$$\begin{aligned} \frac{\partial C_{Di}}{\partial y_i} &= \frac{\partial C_{Dc}}{\partial y_c} = 0 \\ \frac{\partial C_{Li}}{\partial x_i} &= \frac{\partial C_{Lc}}{\partial x_c} = 0 \end{aligned} \tag{5.24}$$

In the force measurement tests, only the central tube in the array is displaced. The force derivatives of the neighbouring tubes as well as the central tube are deduced from tests with central tube displacement. Tubes C, 1-5 (Fig. 5.1(a)) are instrumented for force measurements. Array symmetry is used to determine force derivatives on the non-instrumented tubes 6-8, as well as all cross-coupling force derivatives for all the nine tubes in Fig. 5.1(a). Tables 5.1 and 5.2 show the force coefficient derivative relations deduced from array symmetry. The fluid induced stiffness is determined based on the derivatives, which determine the tube-to-tube fluid stiffness coupling.

It should be noted that the quasi-steady model implemented here does not explicitly consider unsteady fluid effects. Also, it assumes that the two-phase flow is perfectly homogeneous inside the tube array. The homogeneous model is used to provide the estimate of the two-phase flow condition, while the model utilized here does not make any assumption on the flow distribution.

5.3 Experimental Apparatus

A two-phase flow test section was designed to run stability experiments as well as the force measurement tests. The test section is supported by two steel columns to ensure its rigidity. Air is injected into the test section with a capacity of up to 500 scfm, while a 7.5 HP centrifugal pump is connected to the loop to circulate the water flow with a flow rate up to 25 l/s. Water flow rate is measured with MAG500 magnetic flow meter. Air flow rate, in addition to air pressure and temperature, are measured and monitored during the tests using Rosemount 3095 flow meter. The static pressure of the mixture is measured at the inlet of the test section using a differential pressure transducer to accurately correct for air flow compressibility in the two-phase flow rate measurement. Both the air and water streams are mixed upstream of the test section entrance by a two-stage two-phase flow honeycomb mixer to ensure homogeneity of the flow across the test section.

The test section measures 220 x 190.5 mm^2 in cross-section. Rigid tubes in the array are arranged in 9 rows and 9 columns. Half tubes are mounted on the side walls to reduce the

Table 5.1 Transverse fluid force derivatives.

Measured variable	Equivalent
$\frac{\partial C_{Lc}}{\partial Y_c}$	$\frac{\partial C_{Li}}{\partial Y_i}$
$\frac{\partial C_{L2}}{\partial Y_c}$	$-\frac{\partial C_{L8}}{\partial Y_c}$
$\frac{\partial C_{L3}}{\partial Y_c}$	$-\frac{\partial C_{L7}}{\partial Y_c}$
$\frac{\partial C_{L4}}{\partial Y_c}$	$-\frac{\partial C_{L6}}{\partial Y_c}$

Table 5.2 Streamwise fluid force derivatives.

Measured variable	Equivalent
$\frac{\partial C_{Dc}}{\partial X_c}$	$\frac{\partial C_{Di}}{\partial X_i}$
$\frac{\partial C_{D2}}{\partial X_c}$	$\frac{\partial C_{D8}}{\partial X_c}$
$\frac{\partial C_{D3}}{\partial X_c}$	$\frac{\partial C_{D7}}{\partial X_c}$
$\frac{\partial C_{D4}}{\partial X_c}$	$\frac{\partial C_{D6}}{\partial X_c}$

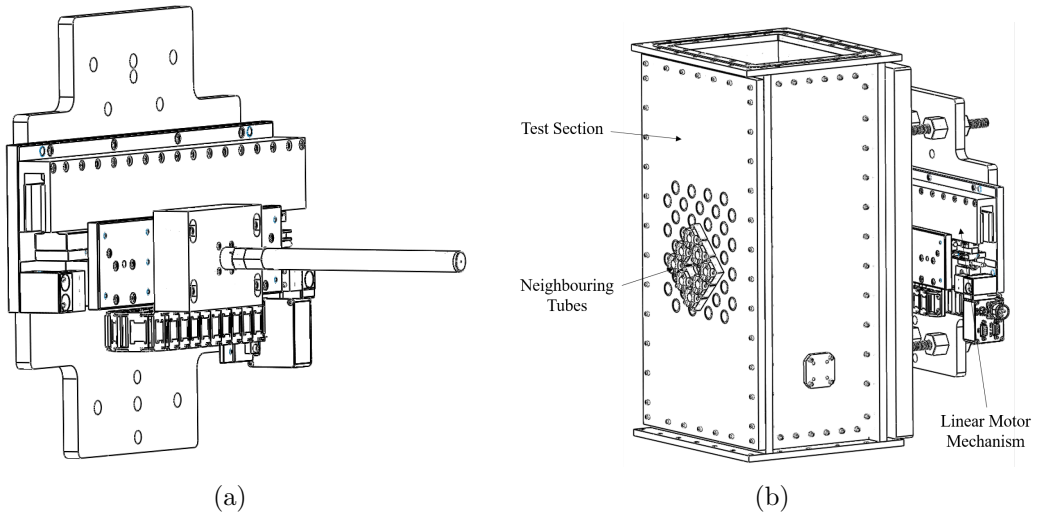


Figure 5.2 Experimental test setup showing: (a) linear motor mechanism, (b) test section.

wall effects. The test apparatus is designed to operate with tube vibration in the transverse and streamwise directions. For the force measurement tests the central tube is located in the fourth row and is surrounded by rigid tubes. This tube is mounted on a linear motor delivering up to 3KN peak force and 660 N of continuous force. The motor is controlled by an Aries smart AR-04CE servo-drive. This motor is designed to generate a direct linear motion. A linear magnetic encoder ensures motor motion with an accuracy of ± 30 μm. The quasi-static force measurement is done by moving the tube with predefined finite static displacements of 0.25 mm (0.013D). In the case of a transverse displacement of the tube, this shows the variation of the lift and drag coefficients of the tubes with the transverse movement of the central tube (y_c). The same applies to the streamwise direction by determining the force coefficients variation with central tube streamwise displacement. Force measurement tests are performed for single phase flow (water flow, 0% void fraction), and two-phase flow with void fractions from 40% to 97%. During the test, the steady-state condition of the fluid force is attained by allowing enough time at each tube location.

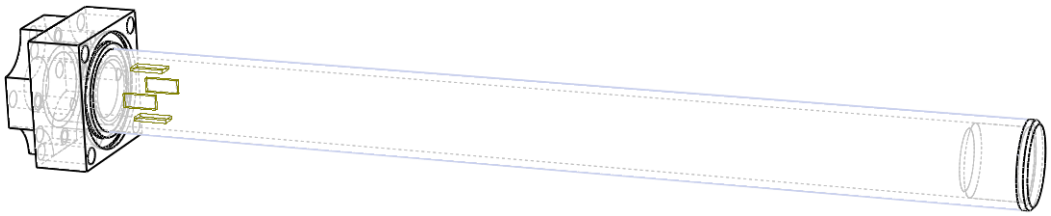


Figure 5.3 Instrumented neighbouring tubes showing strain gauges fixed at tube root.



Figure 5.4 Test Section.

Figure 5.2 shows the test section and the tube mounted on the force sensor. The central tube is surrounded by eight instrumented tubes. These tube are effectively rigid in order to avoid any vibration and coupling between the neighbouring tubes and the central tube. The neighbouring tubes are made of plexiglass, and hydrodynamic forces are measured using strain gauges mounted near tube root as shown in Fig. 5.3. Considering the symmetry in the tube array, the force measurements are only preformed on tubes labeled 1-5 in Fig. 5.1(a).

The quasi-static forces are measured using an ATI Nano17 force transducer. The transducer has high signal-to-noise ratio via using silicon strain gauges technology. The force resolution by the sensor is 0.0125 N. Tube location and time dependent vibratory displacement is measured using an optical sensor. All signals are monitored via an inhouse Labview program and collected through National Instruments Data Acquisition System (DAQ) with a high

sampling rate of 2 kHz. All instrumentation transducers and devices are calibrated to ensure the validity of the collected data.

Two-phase flow parameters

The homogeneous void fraction, β, is calculated from the air and water volumetric flow rates to determine the mixture properties. The homogeneous model assumed uniform two-phase flow across the test section.

$$\beta = \frac{Q_g}{Q_g + Q_l} \tag{5.25}$$

where, Q is the volumetric flow rate, and g and l subscripts denoting the gas and water, respectively. The time-averaged homogeneous two-phase flow density, ρ_h is calculated by

$$\rho_h = \beta\rho_g + \rho_l(1 - \beta) \tag{5.26}$$

where, ρ_h is flow mixture density, and g and l subscripts denoting the gas and water, respectively. The two-phase flow Reynolds number (Re) is determined as

$$Re = \frac{\rho_h V D}{\mu_h} \tag{5.27}$$

$$\mu_h = \left[\frac{x}{\mu_g} + \frac{(1-x)}{\mu_l}\right]^{-1} \tag{5.28}$$

$$x = \frac{\beta}{\beta + (1-\beta)\rho_l/\rho_g} \tag{5.29}$$

where, x is mass quality, and μ_l and μ_g are the fluid dynamic viscosity, for the liquid phase and the gas phase, respectively.

5.4 Experimental Results

5.4.1 Quasi-static force measurements

The procedure followed for the tests starts with determining the test velocity for each void fraction. All tests performed here are done for $Re \simeq 1 \times 10^4$. Quasi-static force coefficients are the key inputs needed in the quasi-steady model. Roshko [125] has shown that the drag coefficient decreases at low Reynolds number, and reaches an approximately constant

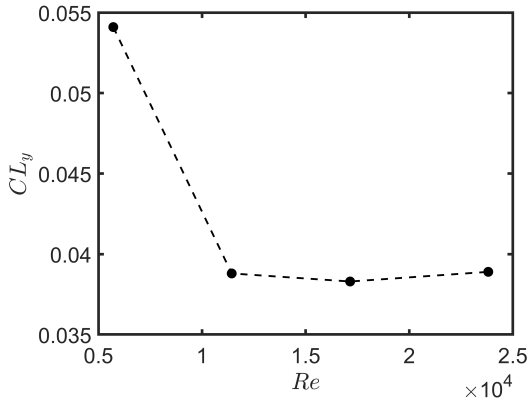


Figure 5.5 Variation of the lift coefficient derivative with Reynolds number.

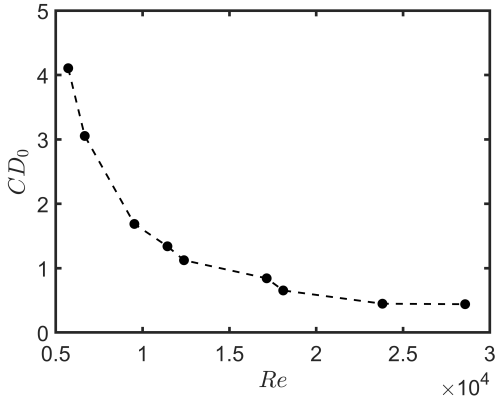


Figure 5.6 Variation of the drag coefficient with Reynolds number.

value at mid and high Reynolds number. Recently, it was shown that quasi-static force coefficients have near constant value for a rotated triangular array of P/D=1.5 in single phase for Shahriary et al. [126], and two-phase flow Sawadogo and Mureithi [127], for high Re. Similarly, Tanaka and Takahara [49] showed that tube phase and lift force coefficient change with tube transverse displacement for an in-line square array having pitch ratio P/D=1.33.

In the present work, the effect of the flow velocity on the quasi-static force coefficients is studied. The variation of the force coefficients is investigated in single (water) and two-phase flow. Figure 5.5 presents the lift coefficient derivative dependence on reduced flow velocity. The derivative is seen to be nearly constant for mid and high flow velocities. The drag coefficient at the tube central position is plotted versus reduced velocity in Fig. 5.6. It is clear that the drag coefficient tends to be constant at high flow velocity.

The variation of the lift coefficient, C_L, with respect to tube non-dimensional displacement

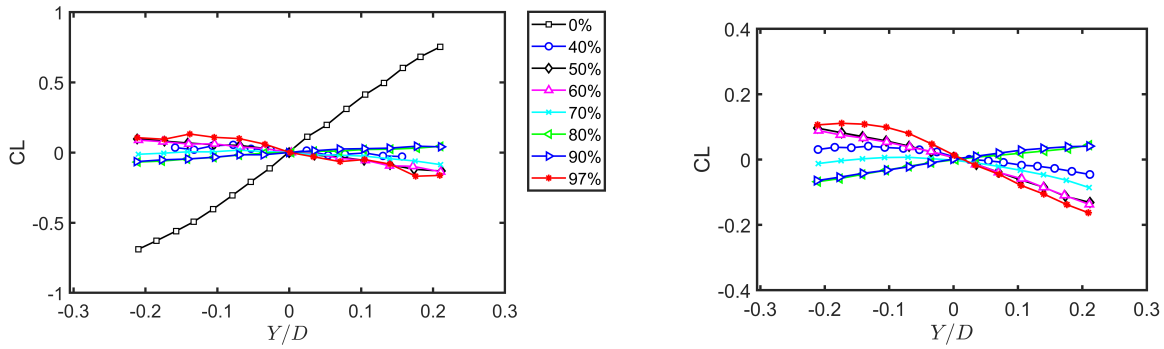


Figure 5.7 Variation of tube C lift coefficient with transverse displacement (Y/D) for: (a) single and two-phase flow for void fractions in the range $0 \leq \beta \leq 97\%$, (b) two-phase flow for $40\% \leq \beta \leq 97\%$.

in the lift direction, Y/D, in water flow and two-phase flow is presented in Fig. 5.7, for 0%-97% void fractions, Fig. 5.7a. The variation was considered over a displacement range of the central tube of -0.2 to 0.2. In water flow ($\beta = 0\%$), the change in C_L is large and positive, so lift force is directed away from tube equilibrium position. For two-phase flow (Fig. 5.7b), C_L is much lower. Figure 5.8 shows the derivative ($C_{L,Y/D}$) of the lift force coefficient with respect to the tube non-dimensional displacement, Y/D. It is seen that the derivative changes from positive in water flow to negative in two-phase flow having significantly lower values in the latter case. The same trend was observed by Sawadogo and Mureithi [121] and Shahriary et al. [126]. The lift derivative is the main indicator of stabilizing or destabilizing fluid forces in the array, for a single flexible tube case. Results show that in water flow, a large positive lift derivative is measured. It was previously suggested that the magnitude of the lift derivative must be large and the sign must be negative in order for the damping controlled fluidelastic instability to occur based on the quasi-steady model [124]. This would imply that the negative-damping induced instability may not be possible in this array, in particular, for water flow. However, in a recent study by Li and Mureithi [128], the negative lift coefficient instability condition was shown not to be necessarily true in general. A new time delay formulation improving on the constant time delay model showed that negative-damping induced instability was even for positive $C_{L,Y/D}$, when the Re effect is considered. Hence, the instability of the present RS array cannot be judged simply from the force coefficient derivative, and stability analysis is required to determine the dynamic behaviour of the array. Solving the system of governing equations presented above is necessary to determine the stability behaviour of the array.

Drag force coefficient variations are less complex due to the direct interaction between central

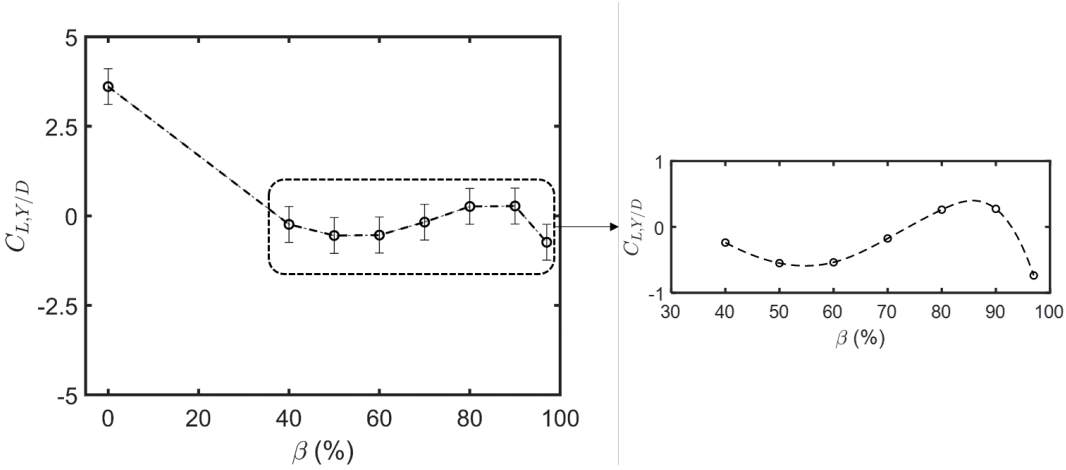


Figure 5.8 Variation of the lift coefficient derivative of tube C with respect to Y/D for void fractions $0 \leq \beta \leq 97\%$, with a close-up view for $40 \leq \beta \leq 97\%$.

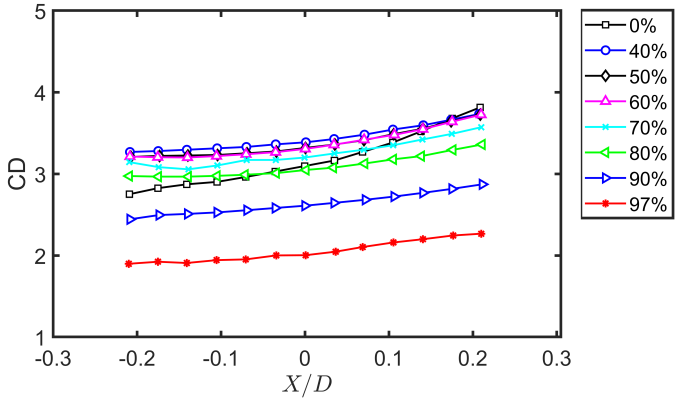


Figure 5.9 Variation of tube C drag coefficient with streamwise displacement (X/D) for void fractions $0 \leq \beta \leq 97\%$.

tube motion and neighbouring tube forces in the flow direction. The variation of the central tube drag force coefficient with respect to its streamwise displacement is presented in Fig. 5.9 for all void fractions. C_D shows a slightly increasing trend with displacement (X/D) in the streamwise direction. The slope of the drag coefficient is found to be positive in this array. This was also the case for the rotated triangle array (see Olala and Mureithi [19] and Shahriary et al. [126]). Figure 5.10 presents the variation of the drag coefficient derivative ($C_{D,X/D}$) with flow void fraction. The highest value of the derivative is in water flow. In two-phase flow it is generally low with an approximately constant value of 1.

Figure 5.11 compares the lift and drag derivatives of the central tube with respect to its displacement, for the present RS array versus those for a rotated triangular array having

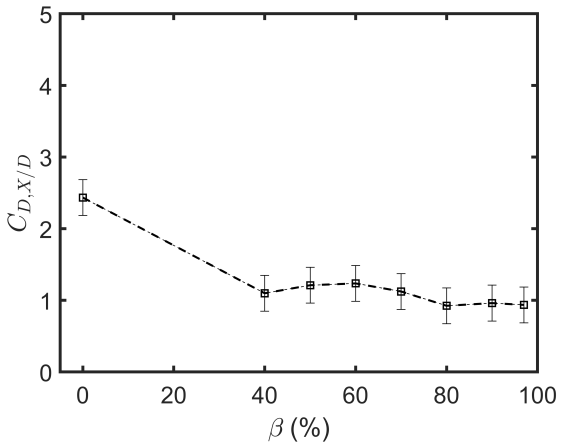


Figure 5.10 Variation of tube C drag coefficient derivative with respect to X/D for void fractions $0 \leq \beta \leq 97\%$.

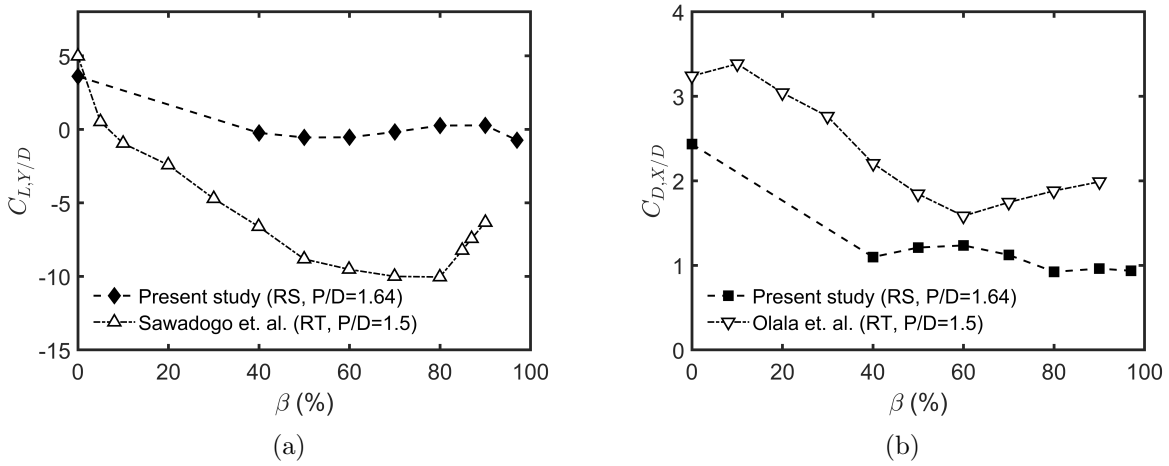


Figure 5.11 Variation of the lift and drag coefficients derivatives for different arrays with flow void fraction in the: (a) transverse and (b) streamwise directions

P/D=1.5. Rotated triangular arrays are known to be strongly fluidelastically unstable in the transverse direction. From a quasi-steady model point of view, this is reflected in the magnitude of the lift force derivative. The derivative magnitude indicates the strength of fluid-structure coupling. The sign indicates whether fluid damping is positive or negative (when the *Re* effects are small). This observation is valid when the damping mechanism drives the stability behaviour. The test results here show that for the present rotated square array with moderately large spacing, the lift force derivatives in two-phase flow vary near zero (Fig. 5.11(a)). By comparison the rotated triangular array (P/D=1.5) has a maximum magnitude of 10. This is a significant reduction in fluid-structure coupling for the rotated

square array. The result suggests higher transverse direction stability for a single flexible tube in the RS array, more specifically a tube in the RS array has weak susceptibility to 1 d.o.f damping controlled instability.

The drag force coefficients have the same trend found for the rotated triangular array. Drag coefficient derivatives have values in water and two-phase flow with an overall reduction near 50% versus the rotated triangular array (Fig. 5.11(b)). This significant reduction suggests that a single tube is likely to be more stable in the flow direction within a rotated square array than in a rotated triangular array due to the weaker fluidelastic excitation forces.

For an array with multiple flexible tubes (multi degrees-of-freedom), cross-coupling forces must be considered. Figure 5.12 presents the variation of the quasi-static lift and drag force coefficients of tubes 2-4 (defined in Fig. 5.1(a)) with respect to the normalized transverse displacement (Y_c/D) of the central tube. The corresponding force coefficients for streamwise tube C displacement are presented in Fig. 5.13. Measurement with respect to tube C displacement is somewhat easier and less complex than displacing all the tubes and measuring the central tube fluid forces as was done in previous tests by Kuran [123]. The lift coefficient derivatives with respect to tube C displacement are plotted together in Fig. 5.14. The results obtained from these measurements provide the fluid stiffness information required in the quasi-steady model. From the symmetry of the array, non-instrumented tube fluid force derivatives can be inferred as shown in Table 5.1.

Figures 5.12 and 5.13 show a clear change in the lift force direction with respect to tube displacement at around 60% void fraction. For the downstream tubes (tubes 1 and 2) lift forces change near 80% void fraction. Tube 3 is the least sensitive to tube C transverse displacement (Fig. 5.12c). The lift coefficient derivative for tube 4 is positive for all void fractions (Fig. 5.12e). The upstream tube (tube 5) shows similar coupling behaviour to that observed for tube 3.

For streamwise tube C displacement (Fig. 5.13), drag force coefficient derivatives are the lowest for the downstream tubes (1-3). Downstream neighbouring tubes drag force derivatives are the least sensitive to tube motion, while the upstream tubes derivatives decreases with the increase of flow void fraction. Tube 3 is also not significantly affected by central tube motion except at high void fractions of 90% and 97%. Upstream tubes, on the other hand, are more significantly affected at the lower void fractions. In comparison with a rotated triangular array with P/D=1.5 [19], Fig. 5.16 shows the variation of the drag force coefficient derivatives for both rotated square array and the rotated triangle. The comparison is addressed between tubes having the same location relative to the central tube is each array. The cross coupling fluid force drags the downstream tube (tube 1) in the rotated square array, while this effect is

reversed in the rotated triangle. The same observation is noticed in the downstream diagonal tube (tube 2) in water flow only. Generally, there is a significant difference between both arrays in the downstream tubes drag force cross coupling, as the rotated square array has lower drag force coefficient derivative. Tube 3 in this array could not be compared to the rotated triangle due to the geometrical differences. Upstream tubes (tubes 4 and 5) do not show clear differences in comparison with the rotated triangle geometry, except tube 4 in two-phase flow in the range $20\%<\beta<70\%$. Apparently, in the rotated square array, the change in the upstream tube location in the flow direction does not significantly affect its downstream neighbour drag coefficient (at least compared to the rotated triangle array). Nevertheless, the opposite occurs with the upstream tubes where downstream tube position clearly affects the fluid drag force.

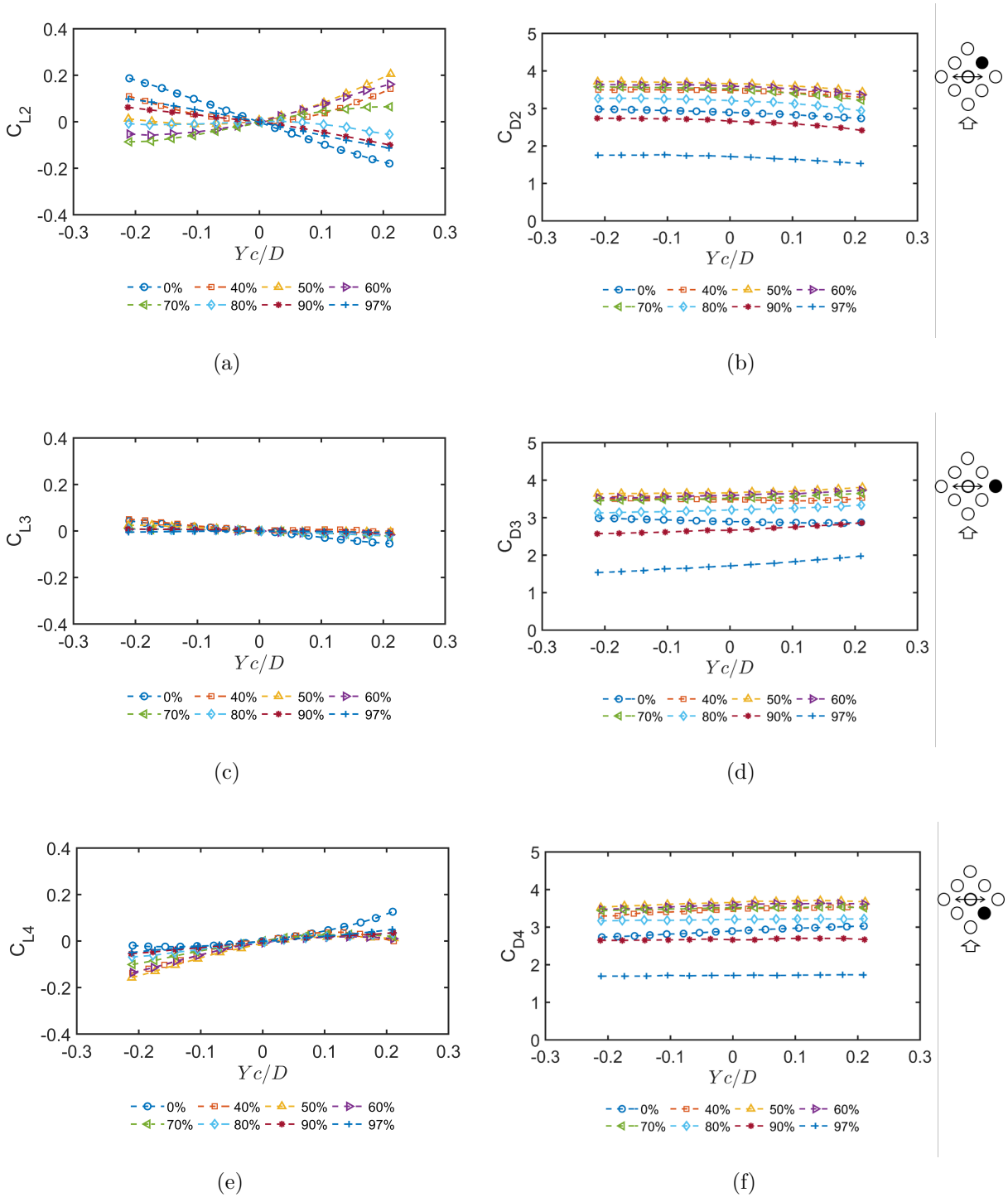


Figure 5.12 Fluid lift and drag coefficients variation with respect to the central tube transverse displacement Y_c/D : (a) & (b) Tube 2, (c) & (d) Tube 3 , (e) & (f) Tube 4

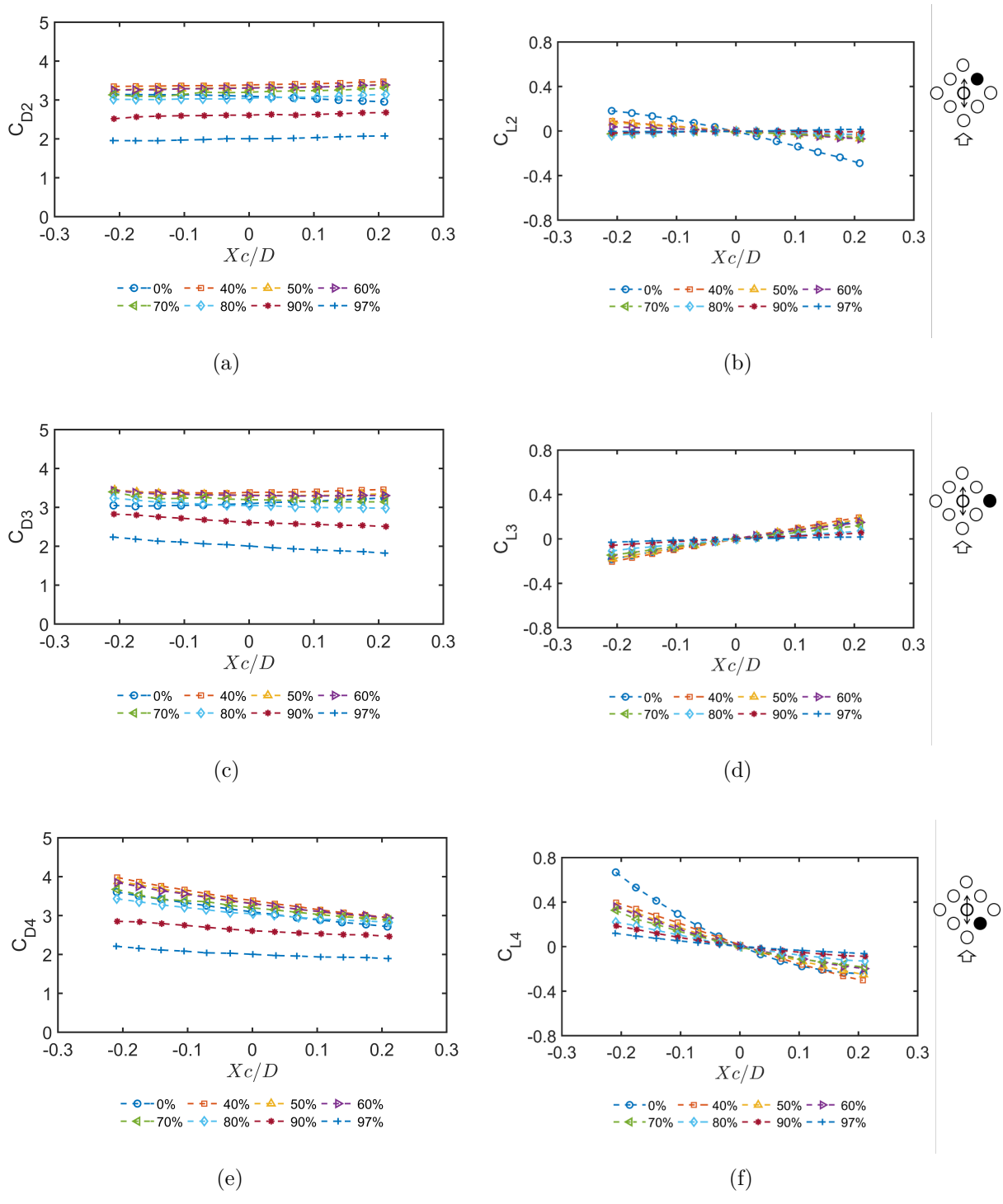


Figure 5.13 Fluid drag and lift coefficients variation with respect to the central tube streamwise displacement X_c/D : (a) & (b) Tube 2, (c) & (d) Tube 3 , (e) & (f) Tube 4

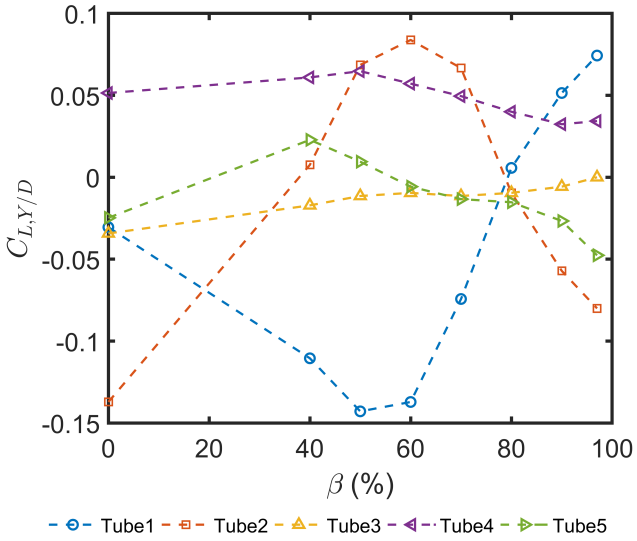


Figure 5.14 Variation of the lift coefficient derivative of the neighbouring tubes for different void fractions.

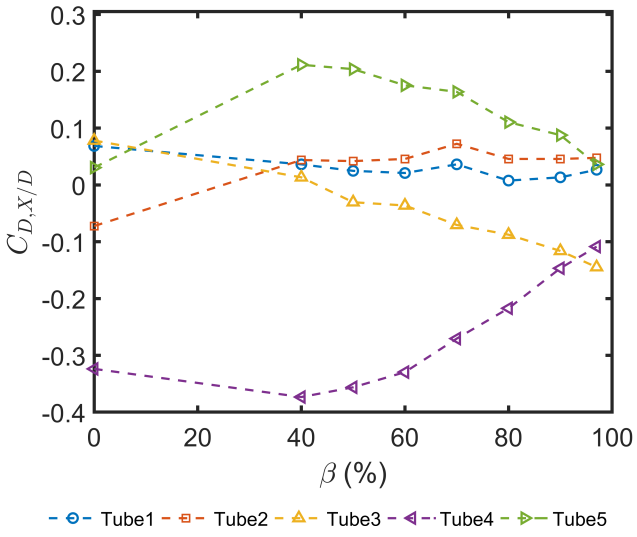


Figure 5.15 Variation of the drag coefficient derivative of the neighbouring tubes for different void fractions.

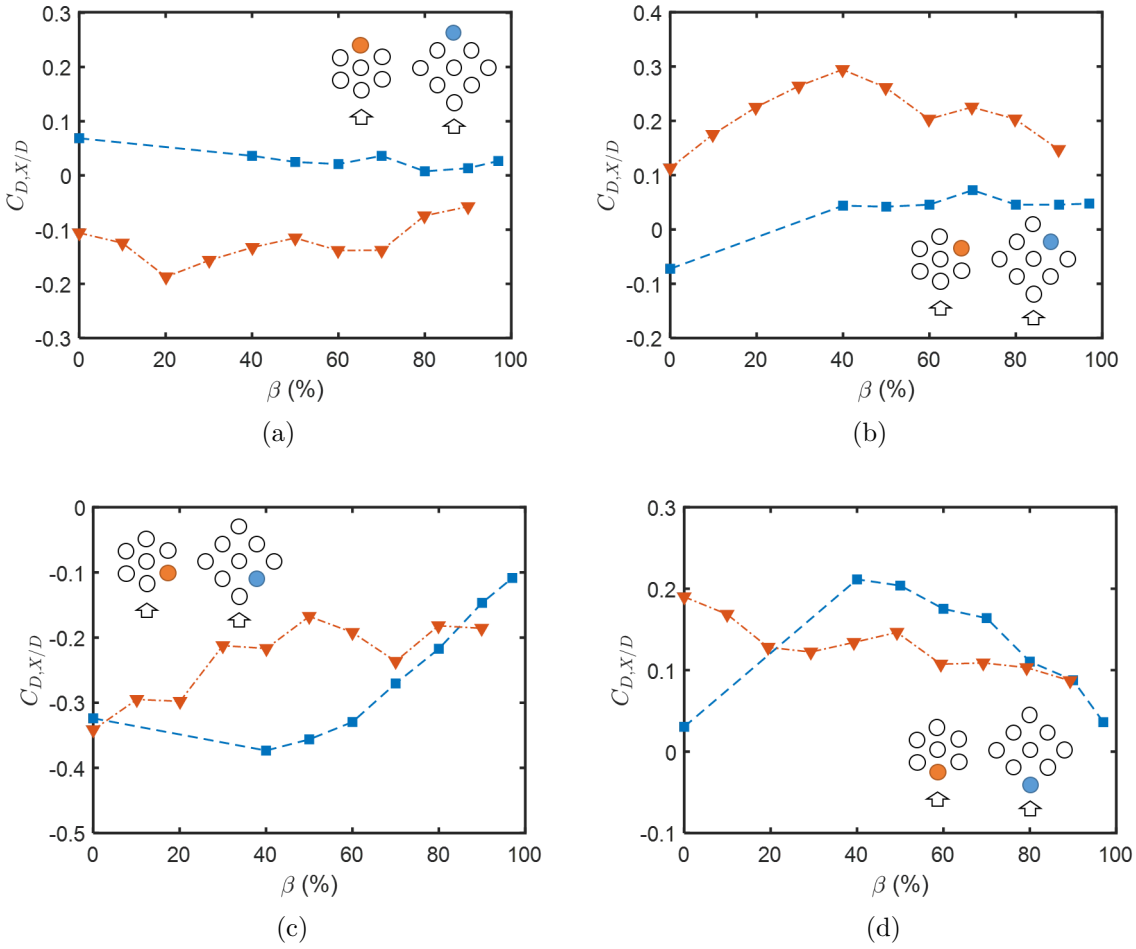


Figure 5.16 Variation of the neighbouring tube drag force coefficient derivatives for the present RS array in comparison with derivatives for a triangular array [19].

5.5 Fluidelastic Stability Analysis

Equations 5.19 and 5.20 can be expressed in the generalized coordinate system, $\tilde{\mathbf{z}}$, as

$$[M]\ddot{\tilde{\mathbf{z}}}(t) + [C]\dot{\tilde{\mathbf{z}}}(t) + [K]\tilde{\mathbf{z}}(t) = 0 \tag{5.30}$$

In equation 5.30, $\mathbf{z(t)} = [x_1(t), x_2(t), ...]^T$ for the streamwise vibration case, while $\mathbf{z(t)} = [y_1(t), y_2(t), ...]^T$ for the transverse vibration case. In the same equation, M is the total mass matrix, C is the total damping matrix, and K is the total stiffness matrix. The matrices are defined as $[M] = [M_s] + [M_f]$, $[C] = [C_s] + [C_f]$, and $[K] = [K_s] + [K_f]$. Consider the case of an array with 3 flexible tubes (e.g. 1-3 in Fig. 5.1(a)) free to vibrate in the transverse (y) direction. The matrices M, C, K in Eq. 5.30 are then 3×3 matrices. For harmonic motions,

$y = y_0 e^{i\omega t}$, this yields

$$
\begin{aligned}
&-\omega^2 \begin{bmatrix} m_s + m_a & 0 & 0 \\ 0 & m_s + m_a & 0 \\ 0 & 0 & m_s + m_a \end{bmatrix} \\
&+i\omega \begin{bmatrix} c_s + \rho_h V_p (\frac{1}{2} D C_{D01} + \frac{1}{2\omega} V_p D \frac{\partial C L_1}{\partial y_1} \sin\omega\tau) & \frac{1}{2\omega}\rho_h V_p^2 D \frac{\partial C L_1}{\partial y_2} \sin\omega\tau & \frac{1}{2\omega}\rho_h V_p^2 D \frac{\partial C L_1}{\partial y_3} \sin\omega\tau \\ \frac{1}{2\omega}\rho_h V_p^2 D \frac{\partial C L_2}{\partial y_1} \sin\omega\tau & c_s + \rho_h V_p (\frac{1}{2} D C_{D02} + \frac{1}{2\omega} V_p D \frac{\partial C L_2}{\partial y_2} \sin\omega\tau) & \frac{1}{2\omega}\rho_h V_p^2 D \frac{\partial C L_2}{\partial y_3} \sin\omega\tau \\ \frac{1}{2\omega}\rho_h V_p^2 D \frac{\partial C L_3}{\partial y_1} \sin\omega\tau & \frac{1}{2\omega}\rho_h V_p^2 D \frac{\partial C L_2}{\partial y_3} \sin\omega\tau & c_s + \rho_h V_p (\frac{1}{2} C_{D03} + \frac{1}{2\omega} V_p D \frac{\partial C L_3}{\partial y_3} \sin\omega\tau) \end{bmatrix} \\
&+ \begin{bmatrix} k_s - \frac{1}{2}\rho_h V_p^2 D \frac{\partial C_{L_1}}{\partial y_1} \cos\omega\tau & -\frac{1}{2}\rho_h V_p^2 D \frac{\partial C_{L_1}}{\partial y_2} \cos\omega\tau & -\frac{1}{2}\rho_h V_p^2 D \frac{\partial C_{L_1}}{\partial y_3} \cos\omega\tau \\ -\frac{1}{2}\rho_h V_p^2 D \frac{\partial C_{L_2}}{\partial y_1} \cos\omega\tau & k_s - \frac{1}{2}\rho_h V_p^2 D \frac{\partial C_{L_2}}{\partial y_2} \cos\omega\tau & -\frac{1}{2}\rho_h V_p^2 D \frac{\partial C_{L_2}}{\partial y_3} \cos\omega\tau \\ -\frac{1}{2}\rho_h V_p^2 D \frac{\partial C_{L_3}}{\partial y_1} \cos\omega\tau & -\frac{1}{2}\rho_h V_p^2 D \frac{\partial C_{L_3}}{\partial y_2} \cos\omega\tau & k_s - \frac{1}{2}\rho_h V_p^2 D \frac{\partial C_{L_3}}{\partial y_3} \cos\omega\tau \end{bmatrix} = \tilde{\mathbf{0}}
\end{aligned}
\tag{5.31}
$$

Equation 5.30 can be reduced to first order by introducing the state vector

$$\vec{\Upsilon} = [\dot{\vec{z}} \;\; \vec{z}], \quad \dot{\vec{\Upsilon}} = [\ddot{\vec{z}} \;\; \dot{\vec{z}}] \tag{5.32}$$

Then equation 5.30 expressed in state space becomes

$$\dot{\vec{\Upsilon}}[I] - \vec{\Upsilon}[A] = 0 \tag{5.33}$$

where the matrix $A_{2N\times 2N}$ is defined as

$$A = \begin{bmatrix} -M^{-1}C & I \\ 0 & -M^{-1}K \end{bmatrix} \tag{5.34}$$

In Eq. 5.34, 0 and I are the $(N \times N)$ zero and identity matrices, respectively. Assuming a solution of Eq. 5.33 of the form $\vec{\Upsilon}(t) = \psi e^{\lambda t}$ leads to the following eigenvalue problem

$$(A - \lambda I)\{\psi\} = \{0\} \tag{5.35}$$

The eigen-solution is the set of eigenvalues and eigenvectors

$$\left.\begin{matrix} \lambda_i, \lambda_i^* \\ \psi_i, \psi_i^* \end{matrix}\right\}, : \text{ i=1,2,...,N} \tag{5.36}$$

where each eigenvector ψ_i is of the form

$$\psi_i = \begin{Bmatrix} \psi_{i,1} \\ \psi_{i,2} \\ \vdots \\ \psi_{i,N} \end{Bmatrix}_{N\times 1} \tag{5.37}$$

For the present fluidelastic system the eigenvalue pair (λ_i, λ_i^*) can be represented in the general form

$$(\lambda_i, \lambda_i^*) = \zeta_i\omega_i \pm i\omega_i\sqrt{1-\zeta_i^2} = -\zeta_i\omega_i \pm j\omega_{d,i} \tag{5.38}$$

where the ζ_i and ω_i are the modal damping ratio and the natural frequency. These can be explicitly obtained from the eigenvalues as

$$\omega_i = |\lambda_i| = \sqrt{\Re(\lambda_i)^2 + \Im(\lambda_i)^2} \tag{5.39}$$

and

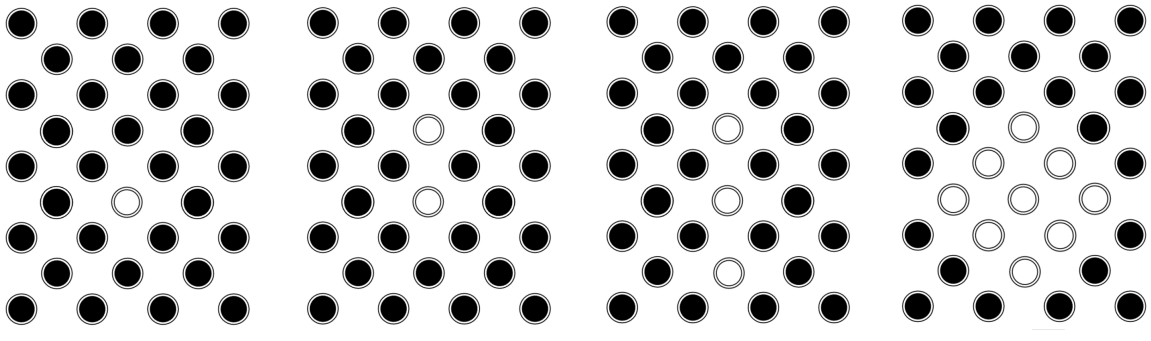
$$\zeta_i = -\frac{\Re(\lambda_i)}{\omega_i} = -\frac{1}{\sqrt{1+\left(\frac{\Im(\lambda_i)}{\Re(\lambda_i)}\right)^2}} \tag{5.40}$$

$$\omega_{d,i} = \omega_i\sqrt{1-\zeta_i^2} \tag{5.41}$$

where $\omega_{d,i}$ is the damped natural frequency.

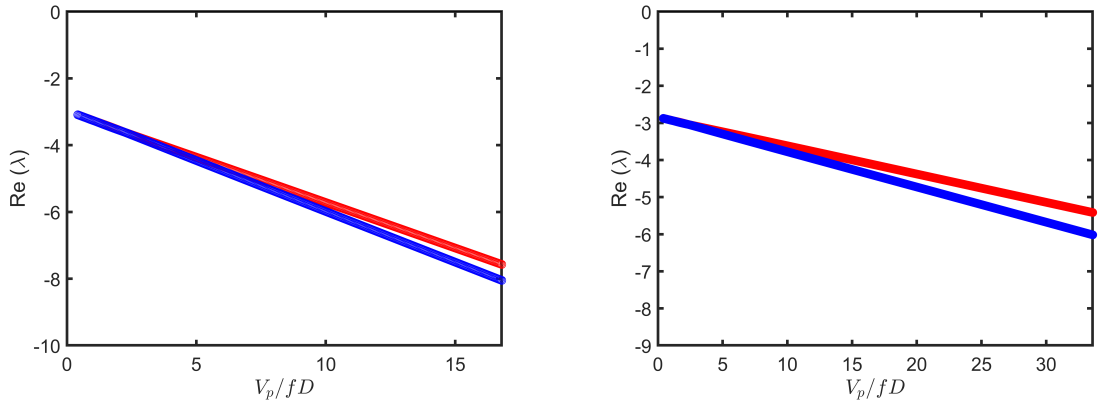
Equation 5.35 is solved as a standard eigenvalue problem to determine the critical flow velocity at which the real part of the eigenvalue, $\Re(\lambda_i)$, vanishes, which corresponds to zero effective tube array modal damping. This velocity defines the onset of fluidelastic instability.

The quasi-steady model is applied over a wide range of mass-damping parameters ($m\delta/\rho D^2$) varying based on the void fraction for the same tubes modal parameters. The results of the theoretical prediction are presented and discussed in two separate parts, for the transverse, and the streamwise vibration results. The Connors equation expresses the relationship between the non-dimensional (or reduced) critical pitch velocity and tube mass-damping parameter. The equation takes the form



(a) (b) (c) (d)

Figure 5.17 Configurations of flexible tubes - stability analysis.



(a) (b)

Figure 5.18 Evolution of the eigenvalues with flow velocity of the single flexible tube in the transverse direction for: (a) β =70%, and (b) β =90%

$$\frac{V_{pc}}{fD} = K\sqrt{\frac{m\delta}{\rho D^2}} \tag{5.42}$$

The equation provides a convenient basis for presentation of the analysis results and for comparison with previous work.

5.5.1 Transverse direction stability behaviour

The quasi-steady model presented above, with the force coefficients presented in Sec. 5.5, was used to perform a stability analysis of the tube array for both single and two-phase flows.

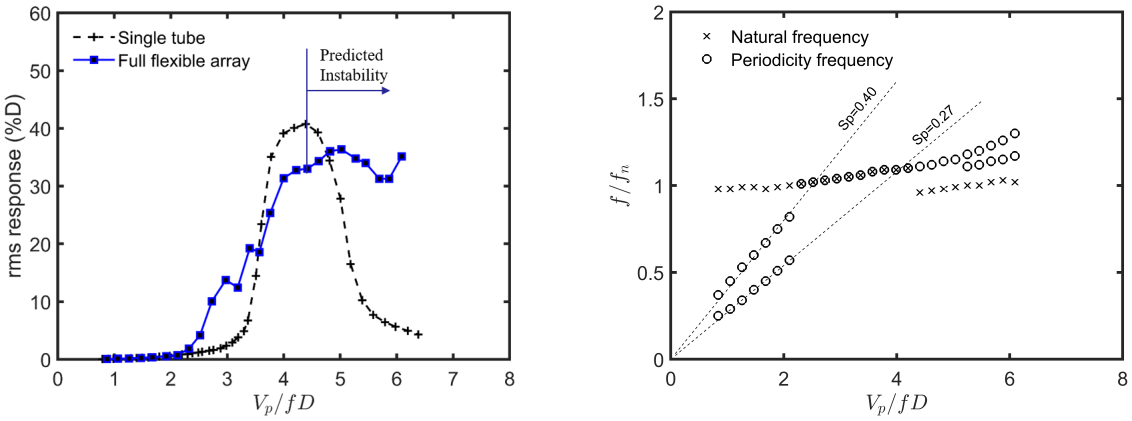


Figure 5.19 Dynamic response in transverse direction in water flow showing: (a) tube vibration amplitude, (b) dominant vibration frequency and periodicity frequencies.

Single flexible tube dynamics in the transverse direction

Figure 5.18 shows the real part, $\Re(\lambda)$, from an eigenvalue analysis for the case of the single flexible tube in two-phase flow for 70% and 90% void fractions. For a single flexible tube, the total damping vanishes at the threshold of instability for a sufficiently large reduced velocity (V_p/fD). The damping is related to $\Re(\lambda)$ by Eq. 5.40. Increasingly negative $\Re(\lambda)$ translates into increasing stability of the single flexible tube with reduced flow velocity. For this array then, no fluidelastic instability of the single flexible tube is predicted in the transverse direction; at least within what could be considered a practical flow velocity range that may be encountered, for instance, in an operating steam generator. The quasi-steady model predicts transverse direction stability for the single flexible tube for both single phase and two-phase flow conditions. This was verified by solving the eigenvalue problem for all void fractions.

Flexible array dynamics in the transverse direction

For the case of multiple flexible tubes, the stiffness-controlled instability mechanism comes into play, in addition to the 1 d.o.f damping controlled mechanism. The stiffness mechanism requires strong fluid cross-coupling between the adjacent tubes. Several cases of multiple flexible tubes are studied as shown in Fig. 5.17 (b-d). The fully flexible array can be represented by a cluster of 9 flexible tubes, Fig. 5.17 (d).

Figure 5.20 presents the eigenvalue evolution with flow reduced velocity for the flexible cluster.

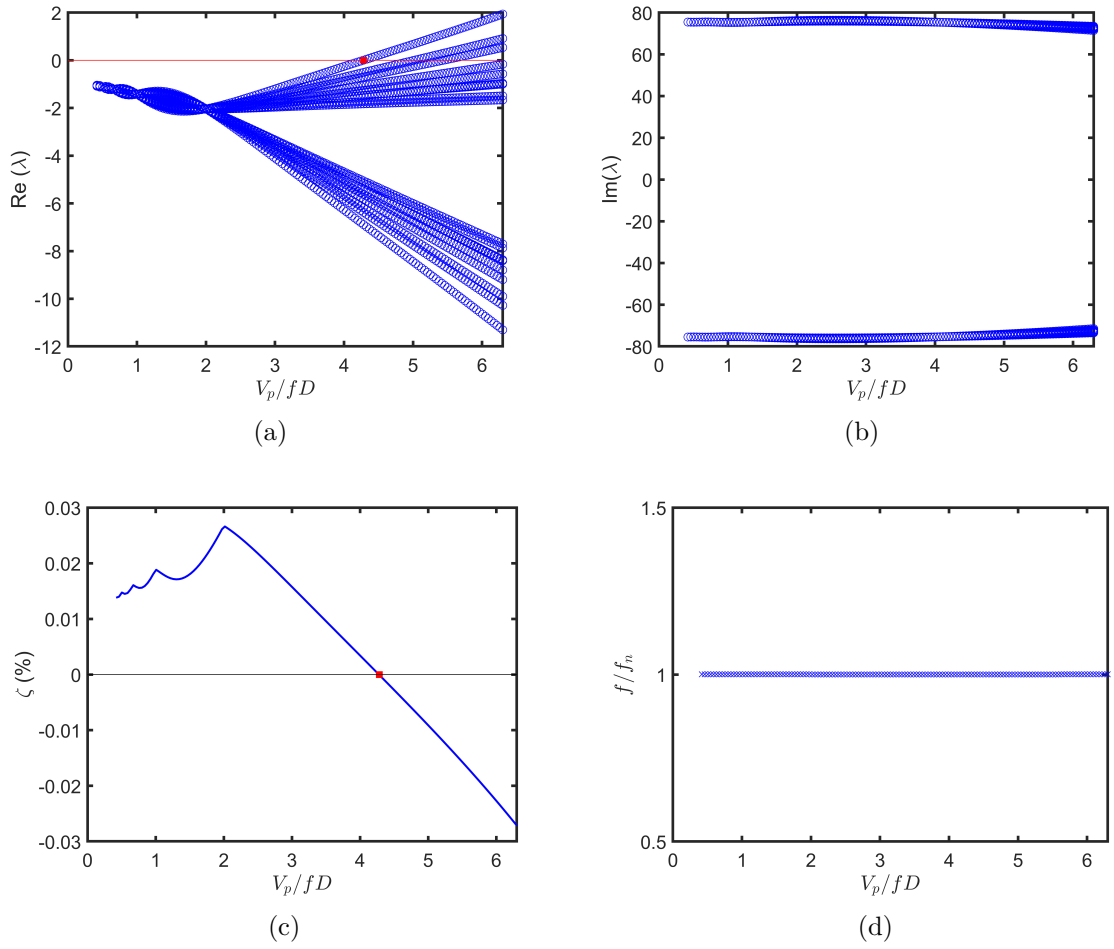


Figure 5.20 Evolution of the eigenvalues with flow velocity of the cluster case (9 flexible tubes) in the transverse direction in water flow

The corresponding (lowest mode) damping and frequency evolution with reduced velocity are also presented in the figure. Results show that one of the eigenvalues (and thus the damping) vanishes at a reduced velocity V_p/fD=4.3, Fig. 5.20 (a,c). This suggests that for this array at least, the cross-coupling forces are significant and effective to cause transverse fluidelastic instability in water flow. A comparison between the different configurations is depicted in Fig. 5.21. As discussed above, a single flexible tube was found to be fluidelastically stable. The presence of multiple flexible tubes therefore renders the tube array fluidelastically unstable in water flow. The case of 2 and 3 flexible tubes show that fluidelastic instability will occur, but at considerably higher reduced flow velocities of 6.4 and 6.2, respectively, compared to the flexible cluster case. As shown in Fig. 5.22, the modal damping ratio is strongly dependent on the level of array flexibility or number of degrees-of-freedom of the array.

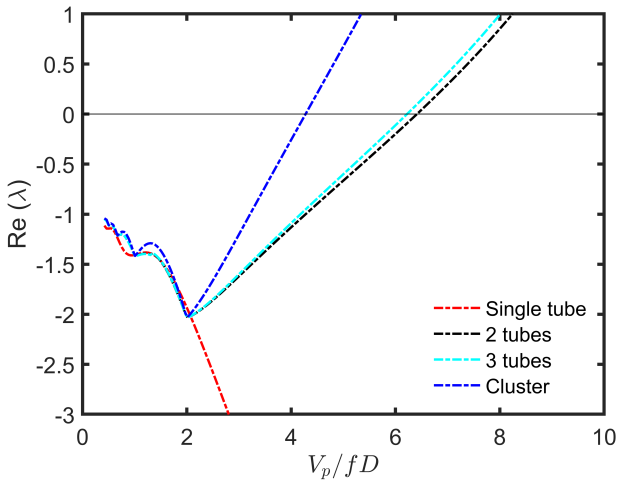


Figure 5.21 Evolution of eigenvalues for multiple cases in water flow. Tubes are free to vibrate in the transverse direction.

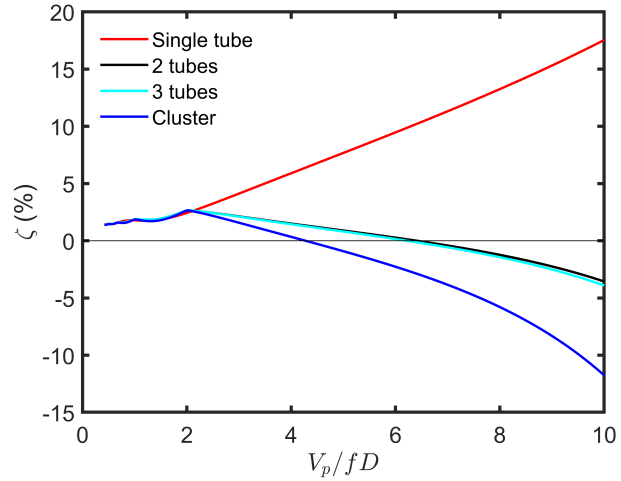


Figure 5.22 Evolution of damping ratio for multiple cases in water flow. Tubes are free to vibrate in the transverse direction.

Experimental results on the stability behavior of the present array in water flow have been reported by the authors in [12]. Figure 5.19a presents the measured vibration response of the tube array for the case of a single flexible tube and a fully flexible array. For both arrays, the tube response is found to rapidly increase to amplitudes as high as 40% of the tube diameter. For the single flexible tube case, high amplitude response subsequently drops to below 10%D for reduced velocities V_p/fD>5. The large amplitude response of the single flexible tube was shown to be vortex-induced vibration (VIV) resulting from lock-in between

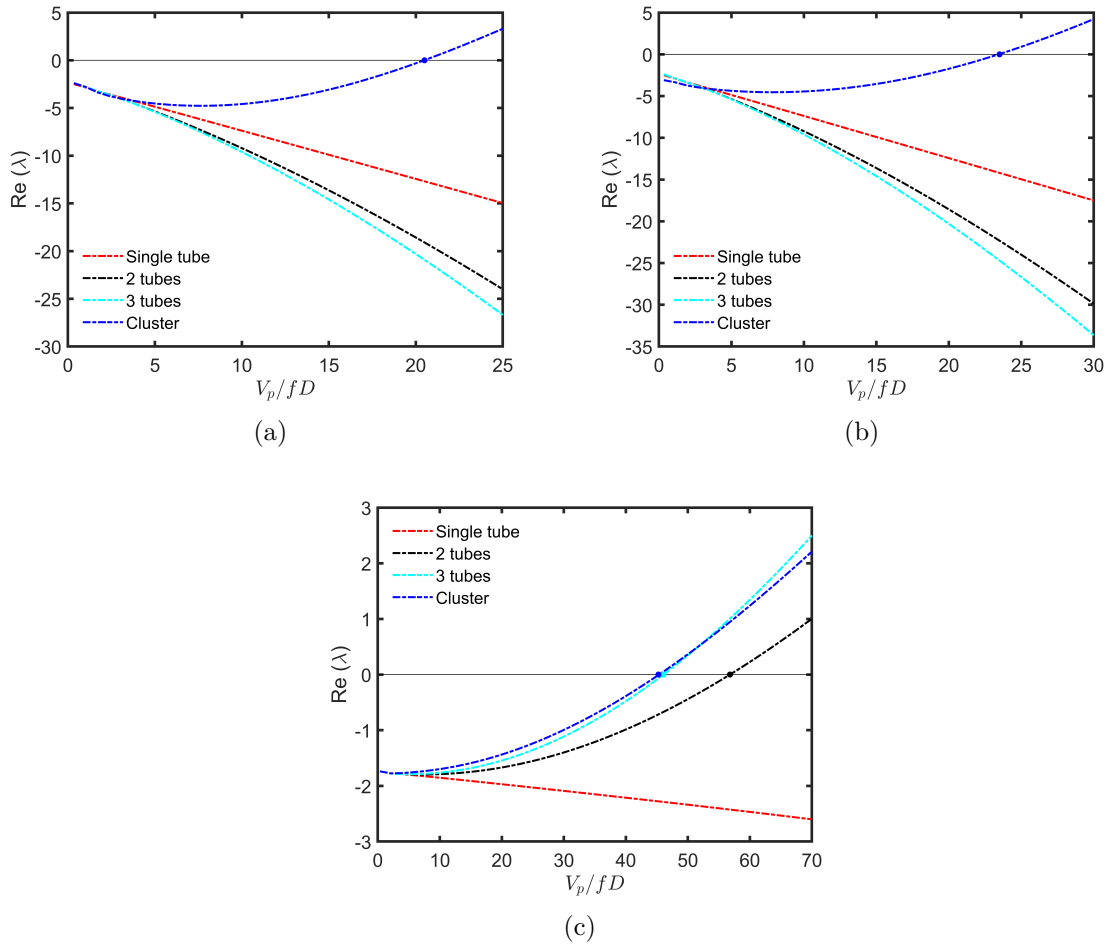


Figure 5.23 Evolution of the eigenvalues with two-phase flow velocity of a single flexible and multiple flexible tubes in the transverse direction for: (a) β =40%, (b) β =70%, and (c) β =97%

vortex shedding frequencies in the tube array and the tube natural frequency. This lock-in behavior is confirmed in Fig. 5.19b where two flow periodicity (vortex shedding) frequencies (having Strouhal numbers 0.40 and 0.27) increase with flow velocity and locks into the natural frequency starting near V_p/fD=2.0. The drop in amplitude for the single flexible tube marks the decoupling between the flow periodicity and tube natural frequencies. Unlike the single flexible tube, the fully flexible array response was found to remain high well beyond the lock-in velocity range. This suggested the possible existence of a second excitation mechanism, perhaps fluidelastic instability. However, the experimental test could not confirm this possibility. The stability analysis results for the flexible cluster (simulating a fully flexible array) predicts a reduced critical velocity V_p/fD=4.3. This reduced velocity just at the end of the lock-in velocity range in Fig. 5.19b. Fluidelastic instability at this reduced velocity

would sustain the high amplitude response for high reduced velocity beyond the VIV lock-in range. The theoretical model provides a plausible explanation for the sustained tube response which is explained by the occurrence of fluidelastic instability at the correct velocity range for sustained tube vibration. The model furthermore predicts the stability of the single flexible tube case thus also demonstrating its predictive capability.

A stability analysis of the tube array when subjected to two-phase flow was also done. Figure 5.23 presents the evolution of $\Re(\lambda)$, with reduced flow velocity for 40%, 70% and 97% void fractions for arrays with multiple flexible tubes, free to vibrate in the transverse direction. The results for the single flexible tube are also included for comparison. The cases with 2 or 3 flexible tubes are predicted to be more stable (with higher damping) than the single flexible tube for lower void fractions in the range 40% - 70% . However, for high void fractions (>90%), the 2 and 3 flexible tube arrays are predicted to undergo fluidelastic instability. The flexible tube cluster is predicted to undergo instability for all void fractions analyzed. The critical instability velocities predicted by the model are, however, very high as discussed below.

Using the quasi-steady model solution, the damping ratio of the tube flexible in the transverse direction was extracted to further investigate the possible tube dynamic behaviour. Figure 5.24 shows the calculated damping ratio for a single flexible tube for 60%, 90%, and 97% void fractions plotted versus reduced flow velocity. The rate of increase (slope) of damping with reduced velocity shows a large drop between the 60% and 90% void fraction cases. As the void fraction reaches 97% the flow appears to add no damping at all despite increasing flow velocity. This void fraction seems to be a limiting case from a damping or stability point of view, according to the model. The predicted stable behavior of the single flexible tube in 60% and 90% void fraction two-phase flow is confirmed experimentally in the work of Darwish et al. [129]. The limiting stability behavior for 97% void fraction is also supported by experiments. The tests results for this void fraction showed a tendency to fluidelastic instability (a slight increase in vibration response above background turbulence excitation) but without growth to large amplitude vibrations for single flexible tube. In practice this means that the damping does become marginally negative in the experiments, in the range of $20<V_p/fD<30$, however, this level of precision is not caught by the present theoretical model. The 9 tube cluster, approximating a fully flexible array is predicted to be strongly unstable compared to the single flexible tube case. This is confirmed by the experimental test where tube vibration amplitudes of up to 40%D were measured for the unstable array.

The instability data is summarized in the stability map in Fig. 5.25, presenting the threshold

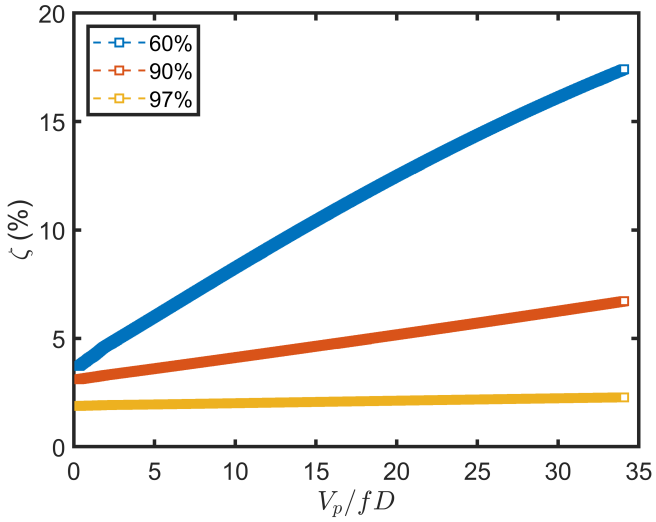


Figure 5.24 Damping ratio variation with flow reduced velocity in the transverse direction for various flow void fractions.

of instability detected by the model for all void fractions. The results show that the reduced critical velocity decreases with increasing the number of flexible tubes. The so-called Connors constant K indicated in the figure appears in the commonly used stability boundary equation (Eq. 5.42). The Connors constant serves as a convenient basis for comparison of stability of tube arrays. For square and triangular array geometries, this constant is typical found to be in the range K=4-5. The Values of K=9 in water flow and above K=18 in two-phase flow indicate that the present rotated square array is highly stable when compared to other array geometries.

5.5.2 Streamwise direction stability behaviour

Array dynamics for 1-3 flexible tubes

A single flexible tube, as well as multiple flexible tubes of 2,3 and a cluster of 9 flexible tubes, are analyzed for the streamwise direction instability. Figure 5.26 presents the eigenvalues evolution for a single flexible tube for 80% and 97% void fractions. The results show that a single flexible tube in the streamwise direction remains stable up to high flow velocities. Fluid damping was found to increase monotonically with flow velocity. Figure 5.27 presents the eigenvalues for the cases of 2 or 3 flexible tubes, compared with the 1 flexible tube case. The same stable behavior found for the single flexible tube is replicated for the cases of 2 or 3 flexible tubes where no instability is predicted.

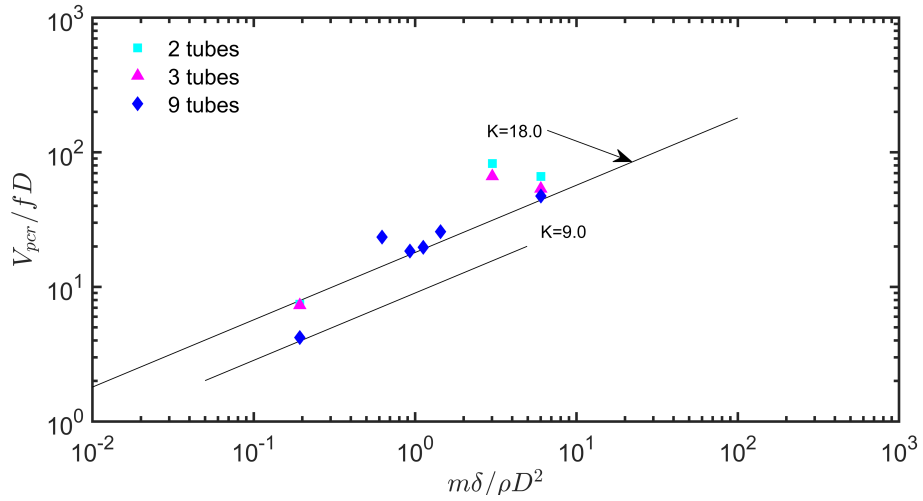


Figure 5.25 Instability map showing the predicted reduced critical velocity for the transverse direction case of a cluster of flexible tubes.

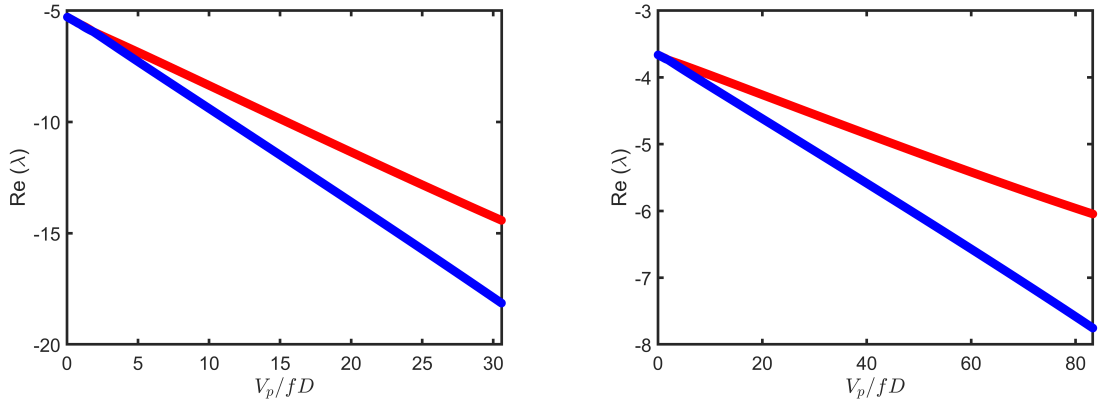


Figure 5.26 Evolution of the eigenvalues with flow velocity of the single flexible tube in the streamwise direction for: (a) β =80%, and (b) β =97%

Flexible array dynamics

When the array is fully flexible, streamwise instability is predicted to occur at very high flow velocities. Figure 5.28 shows the eigenvalue evolution for the 80% void fraction. The predicted critical velocity is well beyond the flow velocities that would be found in practical application (e.g. in a steam generator). However, the threshold of instability detected at very high flow velocity is reported here for completeness.

The stability map showing the threshold of instability predicted by the present model is

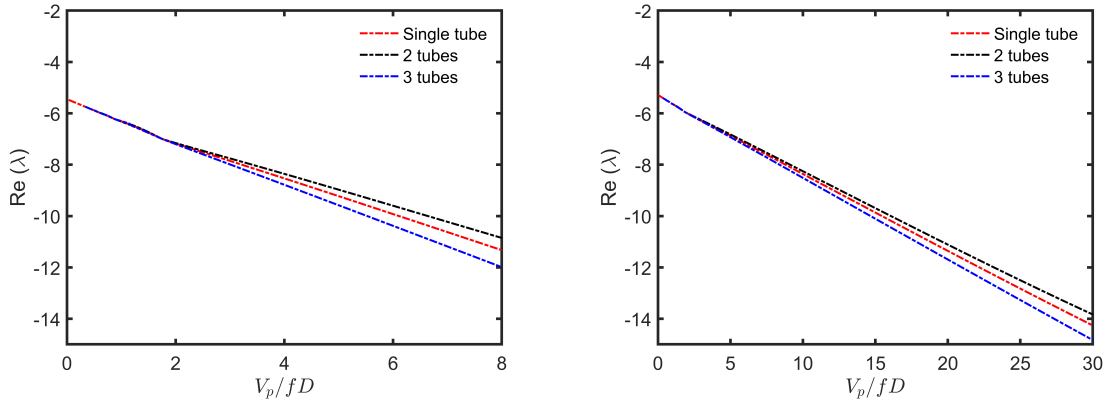


Figure 5.27 Evolution of the eigenvalues with flow velocity of a single flexible and multiple flexible tubes in the streamwise direction for: (a) β =50% and (b) β =80%

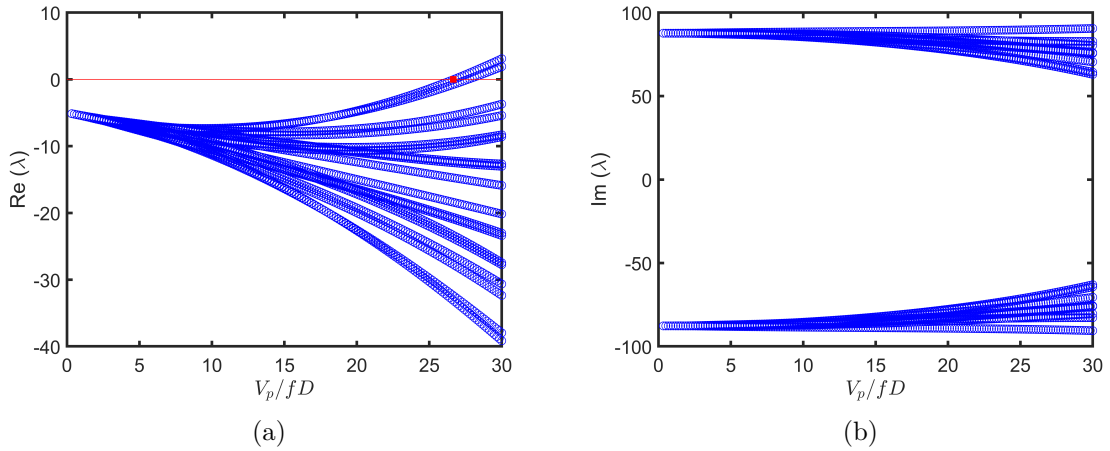


Figure 5.28 Evolution of the eigenvalues with flow velocity of the cluster case (9 flexible tubes) in the streamwise direction for β =80%

presented in Fig. 5.29. For reference, the stability boundary expressed using the Connors equation corresponds to K=15. The time delay parameter, μ, plays a determining role in tube array stability. This parameter was estimated to be equal to one for lack of more precise data. To investigate the sensitivity of the instability threshold to the time delay constant, analysis was also done varying μ by $\pm$20%. The results are included in Fig. 5.29. It is clearly seen that the time delay constant does not have a significant effect on flow critical velocity in two-phase flow. For water flow, the critical velocity varied depending on the value of μ by approximately 9%.

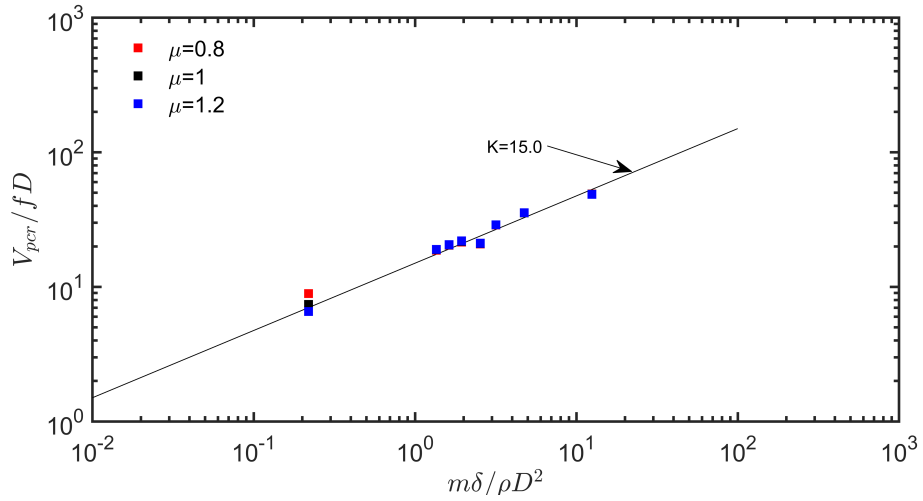


Figure 5.29 Stability map showing the predicted streamwise reduced critical velocity for the cluster of flexible tubes.

Quasi-steady model damping prediction

For the stable cases, the accuracy of the quasi-steady model results can be verified by comparing the predicted damping ratio from the model with the experimental damping results. The experimental damping values were extracted from the available experimental data collected from flow-induced vibration tests in two-phase flow. The data was analyzed to obtain the tube damping values and trends over a wide range of flow velocities. The experimental damping was found to continuously increase with flow velocity as shown in Fig. 5.30 where it is compared with model prediction. While the quasi-steady model estimated damping is slightly higher, the agreement between the experimental data and model estimations is considered very good. This finding is important as it confirms the applicability of the quasi-steady model in its current form in the rotated square array, for the streamwise direction fluidelastic dynamics. The results presented above support the experimental results which showed the rotated square array to be particularly stable when compared to other tube arrays, e.g .the rotated triangle array of similar spacing ratio under the same flow conditions.

5.6 Conclusions

A quasi-steady fluidelastic instability model was employed to study the stability behaviour of a rotated square tube array in single and two-phase flow. To complete the model, a test apparatus was designed to measure the quasi-static fluid forces for both streamwise and transverse direction motion. The simple quasi-steady model form was utilized with a time

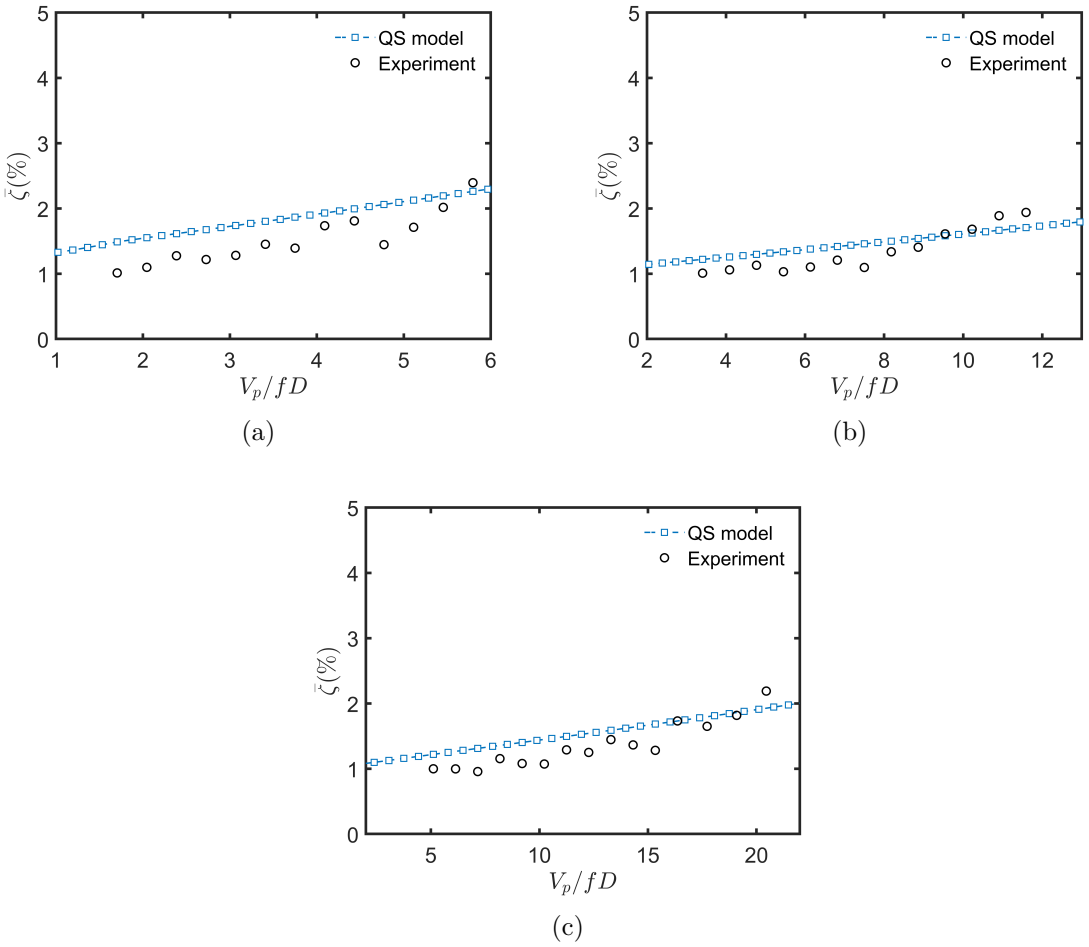


Figure 5.30 Damping in the streamwise direction for: (a) β =40%, (b) β =80%, and (c) β =90%

delay constant μ=1. The occurrence of the stiffness controlled mechanism instability in the rotated square array in both directions was also investigated in this study. This allowed the prediction of the fluidelastic instability onset of single and multiple flexible tubes. The results of the quasi-static force measurements showed significantly small lift force variation with the tube displacement compared to what was previously observed for rotated triangular arrays. The linear change of the lift coefficient over a large tube displacement differs from the rotated triangular array which shows a change in lift coefficient slope for similar tube displacement. The quasi-steady analysis confirmed that a single flexible tube in this array is fluidelastically stable in both the streamwise and transverse directions. The absence of the negative damping instability mechanism in this array is a clear difference from the rotated triangle array. Analysis results showed substantial difference between the fluidelastic behaviour of a single tube and multiple flexible tubes in the rotated square array. A cluster of tubes allowed to

vibrate in the transverse direction was found to be stable in the practical (steam generator operating) range of flow velocities in two-phase flow. However, when the velocity is practically very high, instability is detected. A group of flexible tubes was found to be unstable in water flow. The transverse and streamwise instability in this array is mainly controlled by the fluidelastic stiffness mechanism. For two-phase flow, it was found that single and multiple flexible tubes are fluidelastically stable, and a cluster of flexible tubes are also stable in the reasonable range of practical flow velocities in steam generators. Experimental and analytical results show that the rotated square array is, in general, effectively stable in both streamwise and transverse directions.

CHAPTER 6 UNSTEADY FORCE MEASUREMENTS & PROPOSED IPFEI DESIGN GUIDELINE

The aforementioned findings presented in Chapters 3-5 confirmed that the the rotated square array is fluidelastically stable for all tested void fractions in two-phase flow, except for 97%. The quasi-steady analysis showed a significant reduction in damping for 97% void fraction compared to lower void fractions. The quasi-steady model, however, could not resolve the increase in tube bundle vibrations in the transverse direction for 97% void fraction. Hence, further analysis is required to deeply look into the array using the unsteady theory. The advantage the unsteady theory has is taking into consideration the variation of the fluid force phase with reduced flow velocity. This is not encountered in the quasi-steady theory where the fluid force phase is always assumed to be constant. Unlike the quasi-static force measurements, the unsteady fluid dynamic force component and the vibration modes of the tubes are taken into account in the unsteady theory.

6.1 Unsteady Force Measurements

Very few research work measured experimentally the unsteady forces of tube arrays, and non yet did for the rotated square array. A full set of unsteady measurements was performed using the same test apparatus presented in Chapter 5. The method employed in the analysis of the measured unsteady fluid forces is as outlined below [119].

When a harmonic motion of the form $x(t) = x_o e^{i\omega t}$ is applied to a tube in a rigid tube bundle, the fluid force per unit length on the tube may be expressed as

$$F = [\omega^2(m + 2\rho R^2 c_{ma}) + i\omega\rho U R c_{da} + \frac{\rho U^2}{2} c_s]x(t) \tag{6.1}$$

where, R is the tube radius, U flow velocity, ρ flow density, m is the tube mass per unit length, D is tube diameter, c_{ma}, c_{da} and c_s are are the fluid added mass, damping and stiffness coefficients, respectively.

By defining a force/displacement transfer function

$$H_{Fx} = \frac{F}{x_o e^{i\omega t}} \tag{6.2}$$

By equating the real and imaginary parts of this transfer function to the corresponding

components of the fluid force yields

$$\Re[H_{Fx}] = \omega^2(m + 2\rho R^2 c_{ma}) + \frac{\rho U^2}{2} c_s \tag{6.3}$$

$$\Im[H_{Fx}] = \omega \rho U R c_{da} \tag{6.4}$$

The fluid stiffness together with the added mass component is therefore given by

$$F_{s,ma} = [\omega^2(m + 2\rho R^2 c_{ma}) + \frac{\rho U^2}{2} c_s] x_o - m\omega^2 x_o \tag{6.5}$$

where the last term is related to tube inertia, and determined by performing tests in air. The damping force then will be

$$F_{da} = \Im[H_{Fx}] x_o \tag{6.6}$$

The force coefficient magnitude will be

$$c_f = \frac{(F_{s,ma}^2 + (\Im[H_{Fx}] x_o)^2)^{0.5}}{0.5\rho U^2 x_o} \tag{6.7}$$

The phase angle between the fluid force and displacement then becomes

$$\phi_f = tan^{-1}\left[\frac{\Im[H_{Fx}] x_o}{F_{s,ma}}\right] \tag{6.8}$$

Then the damping coefficient becomes

$$c_f = \frac{-\Im[H_{Fx}]}{\omega} \tag{6.9}$$

and the added mass is calculated as

$$m_a = \frac{\Re[H_{Fx}] - \omega^2 m}{\omega^2} \tag{6.10}$$

while the total damping factor is given by

$$\zeta = \frac{-\Im[H_{Fx}]}{2(m + m_a)\omega^2} \tag{6.11}$$

Results

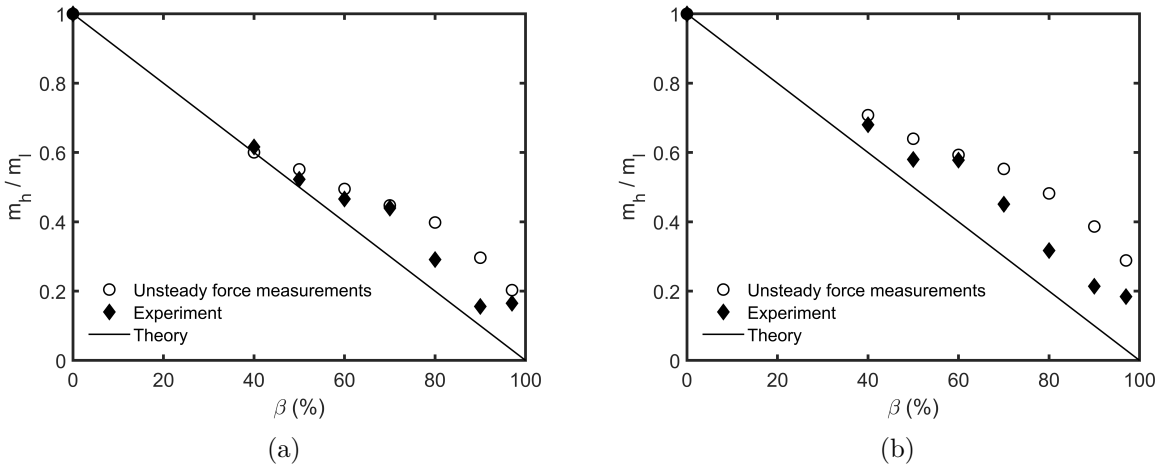


Figure 6.1 Variation of the tube added mass with flow void fraction in the: (a) transverse and (b) streamwise directions

Since the added mass is an important parameter in the FEI analysis, it was estimated from the unsteady fluid forces on the central tube from equation 6.10. Results show fairly good agreement with experiments as shown in figure 6.1. The added mass ratio was over estimated from the unsteady forces in high void fractions (above 60%).

The unsteady fluid force phase and magnitude are presented in figures 6.2 and 6.3 for the transverse direction, and in figures 6.4 and 6.5 for forced oscillations in the streamwise direction, for single phase flow as well as 40% and 70% void fraction two-phase flows. An approximate analytical curve was fitted to the exported data to show the trend of the fluid phase and force coefficient with reduced flow velocity, V_p/fD. The phase angle is seen to decrease with the flow reduced velocity. This is, however, different in the 97% void fraction case in the transverse direction, where the phase is seen to gradually increase, reaching a maximum value near V_p/fD=20, followed by a decrease at high velocities. This is found to clearly occur for 97% void fraction, and only in the transverse direction. The range of the flow velocity where the fluid phase is positive indicates a reduction in fluid damping. Figure 6.6 presents the calculated damping from the unsteady model for 60%, 90%, and 97% void fractions. This is the net (velocity dependent) damping. Compared to the 60% and 90% void fractions, it is clear that the net fluid damping decreases, and becomes negative in the range $7 \leq V_p/fD \leq 30$ for 97% void fraction. This has significant implications for the tube array subjected to two-phase flow of 97% void fraction. The reduction in the total damping of the flexible tube would be expected to lead to an increase in tube vibrations and fluidelastic

instability in this velocity range. Figure 6.7 shows the single flexible tube vibration in the transverse direction for the 97% void fraction. The foregoing effect is precisely observed in the tests. This effect may be amplified for a fully flexible array with multiple flexible tubes.

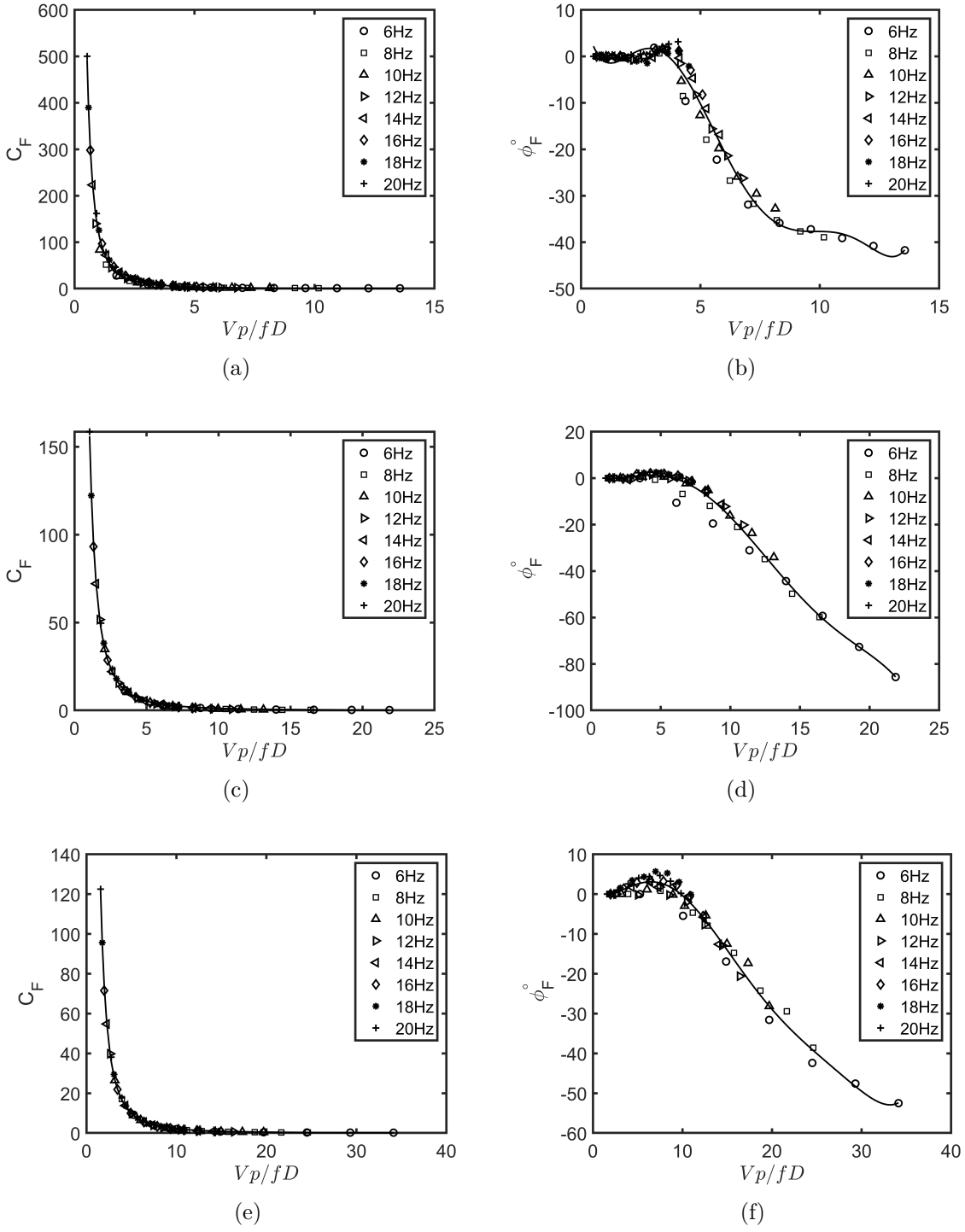


Figure 6.2 Force coefficient and fluid phase in the transverse direction for the central tube for 6-20 Hz excitation frequencies : (a) 0%, (b) 40%, (c) 70%

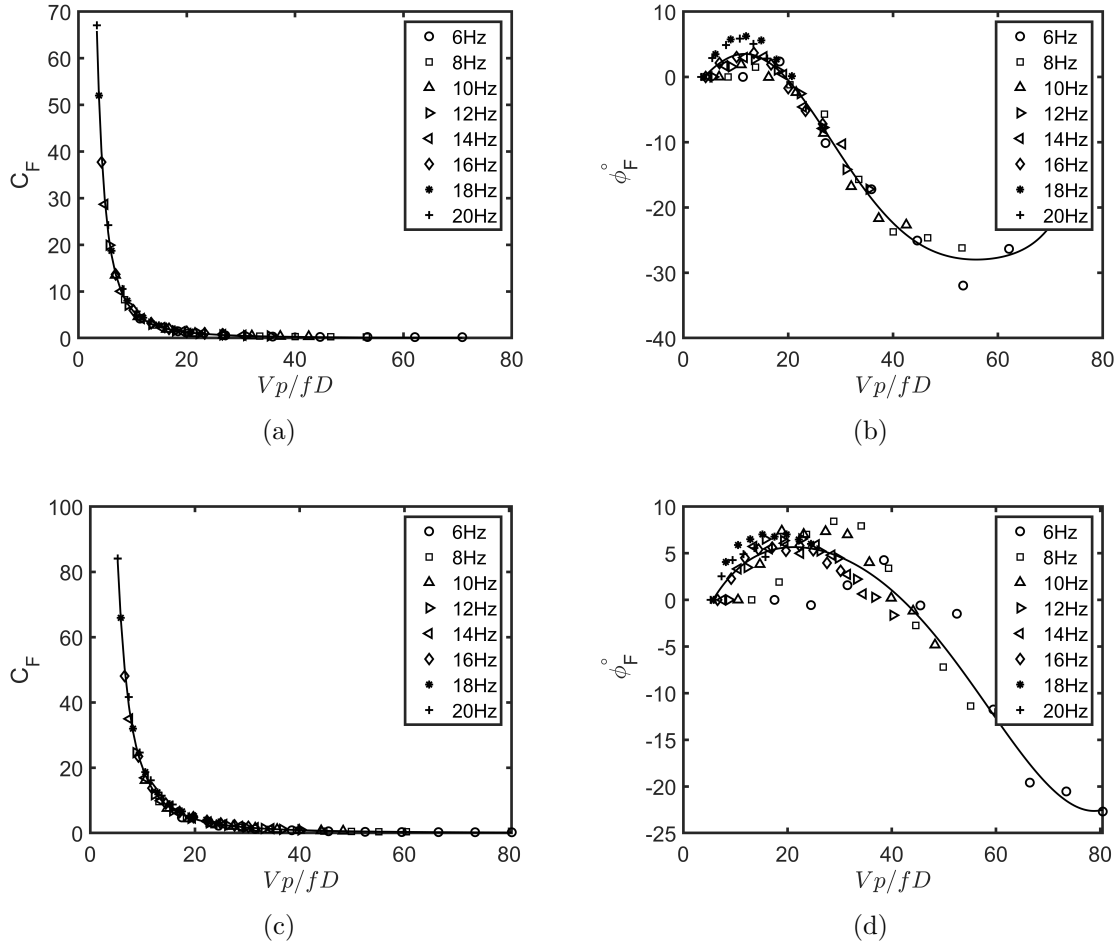


Figure 6.3 Force coefficient and fluid phase in the transverse direction for the central tube for 6-20 Hz excitation frequencies : (a) 90%, (b) 97%

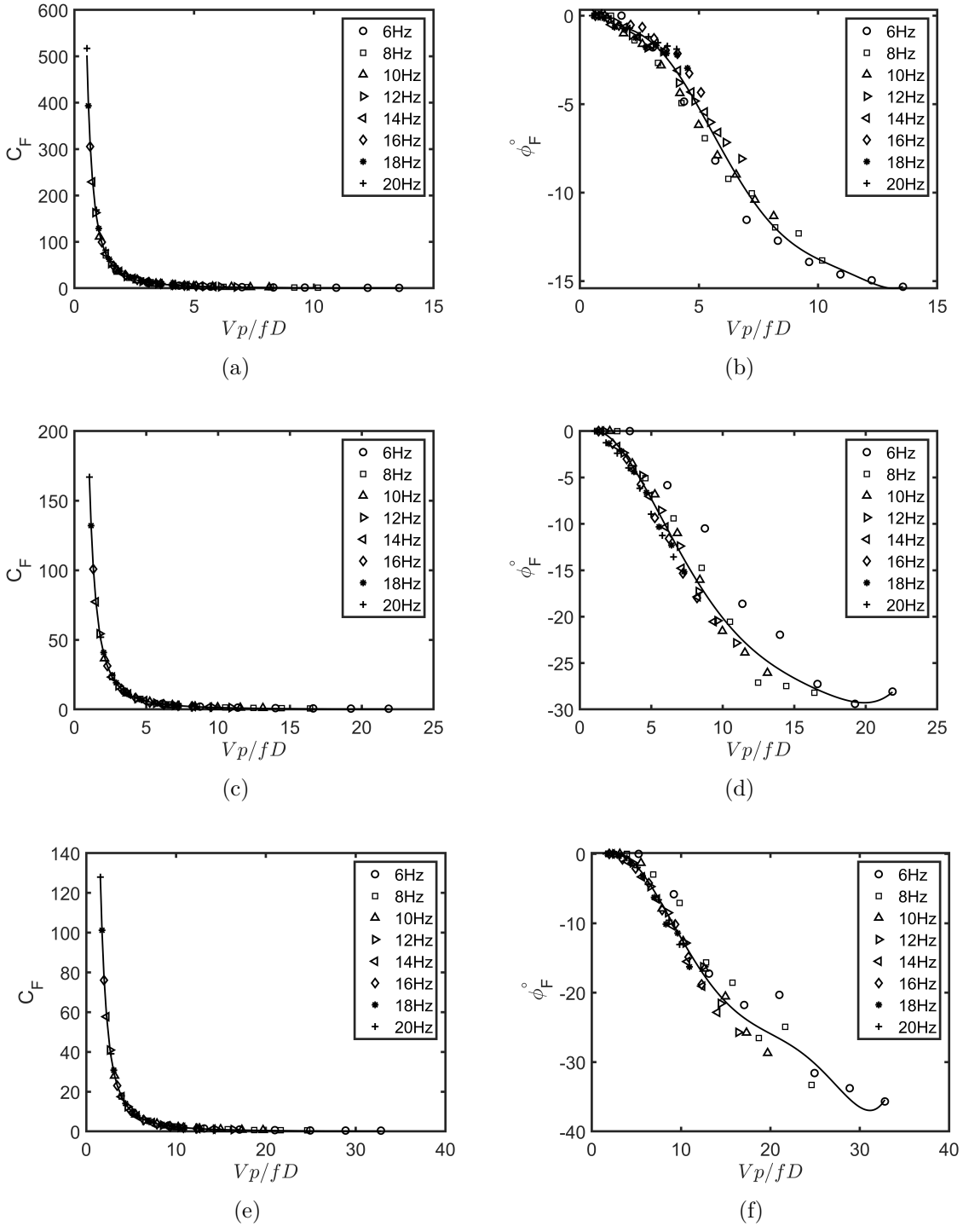


Figure 6.4 Force coefficient and fluid phase in the streamwise direction for the central tube for 6-20 Hz excitation frequencies : (a) 0%, (b) 40%, (c) 70%

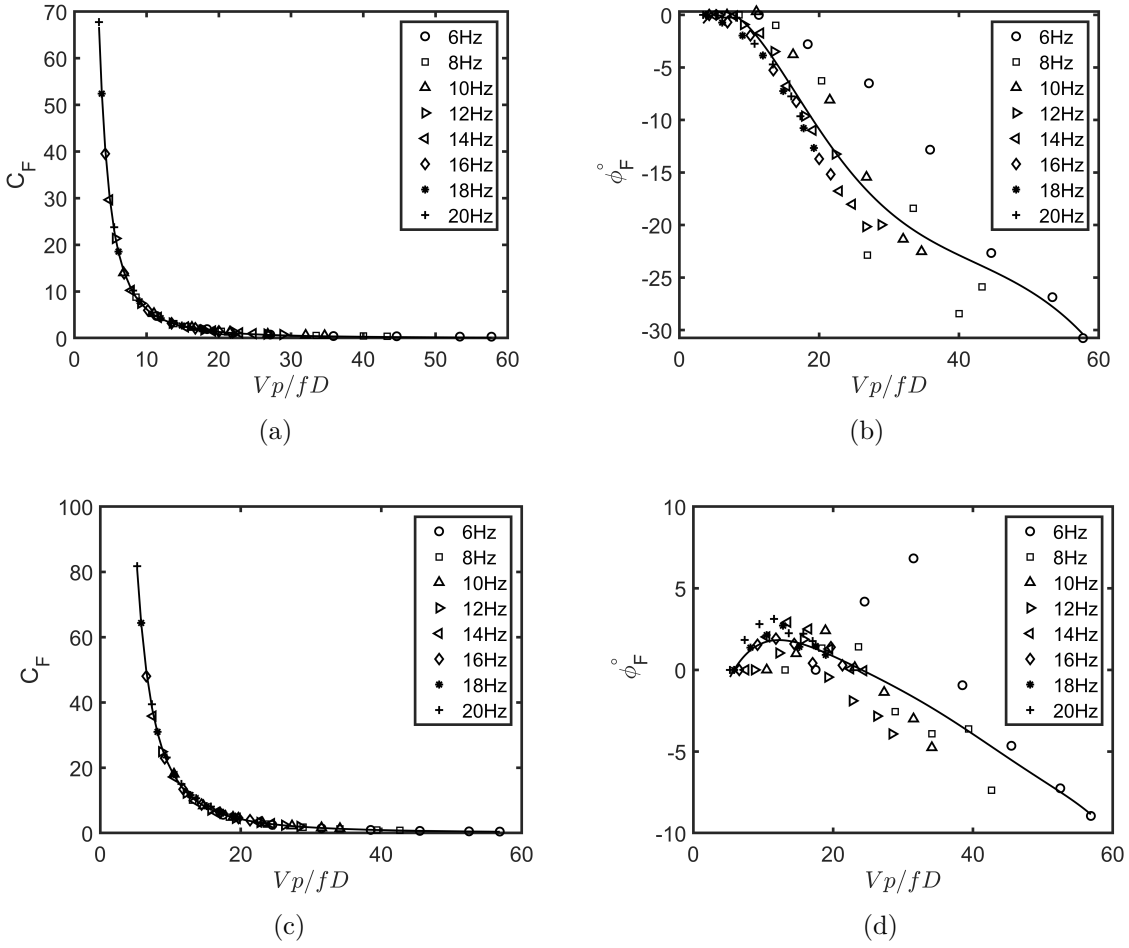


Figure 6.5 Force coefficient and fluid phase in the streamwise direction for the central tube for 6-20 Hz excitation frequencies : (a) 90%, (b) 97%

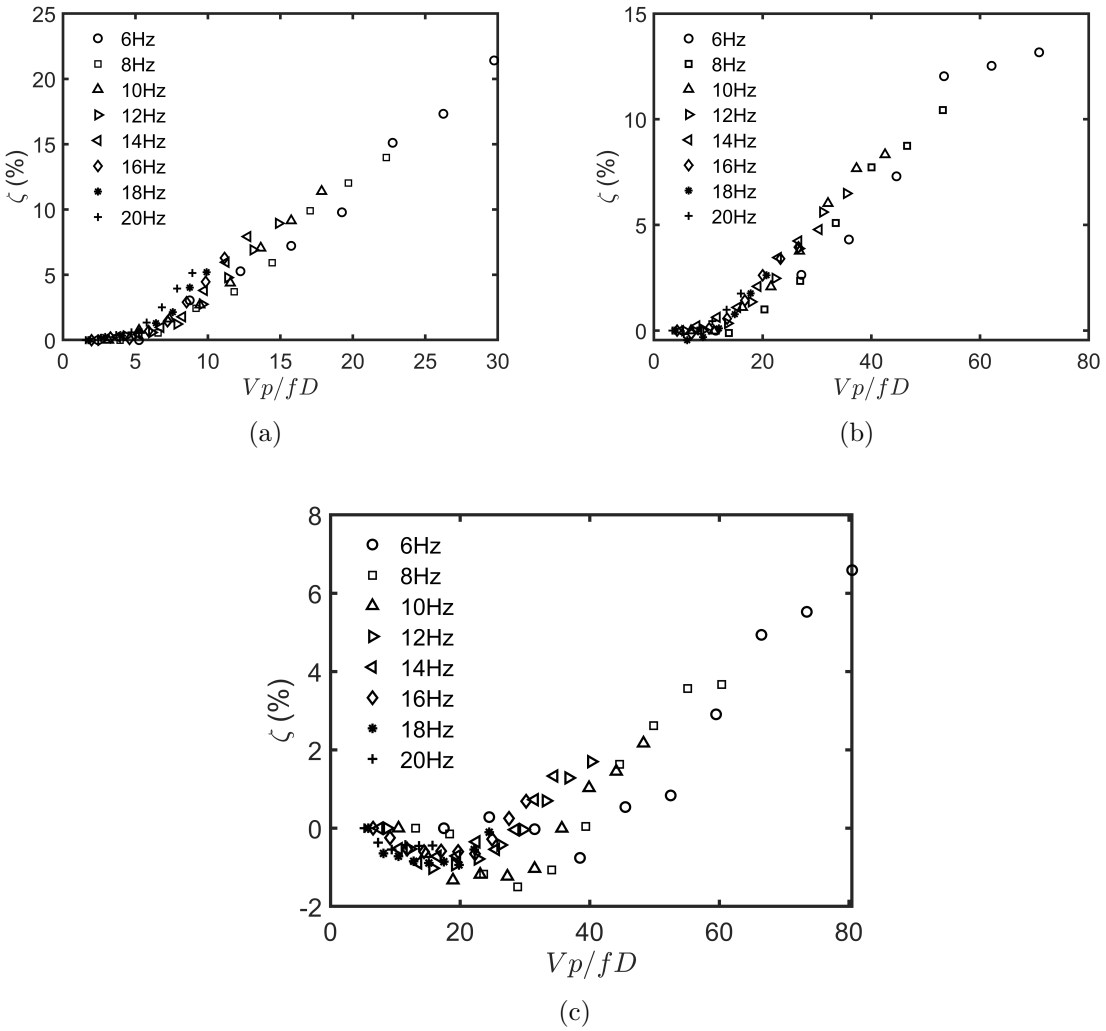


Figure 6.6 Damping variation of central tube in the transverse direction in: (a) 60%, (b) 90% and (c) 97% void fractions

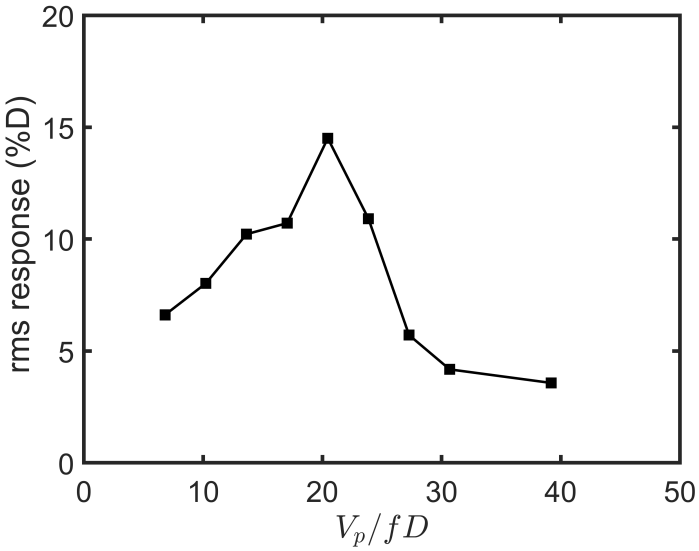


Figure 6.7 Single flexible tube vibrations in the transverse direction for β=97%

CHAPTER 7 GENERAL DISCUSSION

7.1 Flow-induced Dynamics of the Rotated Square Array

There have been numerous investigations into the fluidelastic instability of tube arrays with triangular and in-line geometries. In spite of the fact that the rotated square geometry presents a unique behaviour and characteristics compared to the other geometries, such as strong vortex-induced vibrations (VIV) and dynamic stability, the array is not yet understood and could not be practically recommended for the industrial use. There is an industrial need to study the rotated square geometry in order to provide a deeper understanding of the array. In this thesis, the fluidelastic instability of a rotated square array, with P/D = 1.64, was investigated in depth. An experimental study was performed to investigate the fluidelastic instability and understand the dynamic behaviour of the array in single phase (water) flow and two-phase (air-water) flow for void fractions up to 97%. The complex dynamics for the two-phase flow tests led to an extension of the study to investigate the array dynamics in air cross-flow. The study separately covered both flexibility directions, streamwise and transverse to the flow.

The results of this work are presented in three main research articles. In the first article (Chapter 3), the flow-induced vibration (FIV) of the array was studied through a series of experiments in water cross-flow. A strong lock-in effect was uncovered in this array due to vortex shedding excitation. In comparison to other array geometries, much larger resonance vibration amplitudes were found in this array in water flow. This could, at least in part, be explained by the geometrical pattern of the tubes in the array. In the rotated square geometry, the wake area downstream each tube is 40% larger than in the rotated triangular array geometry, having the same P/D spacing ratio. This allows for strong vortices to form and shed behind the tubes resulting in large periodic pressure fluctuations. Frequency analysis of the response showed that three Strouhal numbers existed in this array, with two only effectively participating in the tube vibrations. The third periodicity is not practically effective in the tested range of flow velocities. The vortex-tube frequency synchronization was confirmed by suppressing the vortex shedding in the tube wake with a vortex suppressor plate which could eliminate VIV. Unsteady numerical simulations were performed to study the flow structure and the periodicities formed in the tube vicinity. The CFD simulations showed the highly coherence vortex formation and confirmed the Strouhal numbers found in the experimental results.

Two-phase flow fluidelastic instability tests were conducted, and results are presented in the

second article (Chapter 4). The results are mainly divided into two main sections: (i) transverse, and (ii) streamwise fluidelastic instability results. A wide range of void fractions was tested up to β=97%. The stability of the single flexible tube was experimentally confirmed in the rotated square array in both directions. The dynamic behaviour in the streamwise direction is also stable when the full bundle is tested. No different conclusion was drawn from the transverse tests, except for the 97% void fraction. This void fraction is the highest that has been tested, and it could be considered more special than the other void fractions due to the low average flow density. For β=97% a single flexible tube tends to be fluidelastically unstable in the transverse direction. However, the tube stabilized with an increase in the flow velocity. The restabilization behaviour is uncommon for tube arrays once fluidelastic instability occurs. The vibration amplitudes were seen to significantly increase with the number of flexible tubes. This observation suggests that the stiffness controlled mechanism could be leading the instability in this case. Flow damping was estimated from the frequency spectra by using the frequency response curve fitting method for an accurate estimation. Results showed that the damping in this array is generally higher than what was observed in all the other array geometries. The aforementioned part of the work leads to the strong conclusion that this rotated square array is generally stable in both the streamwise and transverse directions in two-phase flow. The only exception is the case of very high void fractions where instability is possible in the transverse direction. The fundamental finding from this work is that the flow damping increases in the flow direction, leading to completely stable dynamic behaviour.

The change in stability behaviour for very high void fractions led to the need to extend the study to the limitly case of β=100%, i.e. air flow. In a direct comparison with the research results presented by Kuran [123], this array showed similar behaviour to the array previously studied with P/D=2.12. However, the effect of the first row in the rotated square array in the streamwise direction is still questionable, since the study here showed that fixing the most upstream row in the array has led to a significant delay in the instability onset.

The quasi-steady model was adopted to delve deeper into the array dynamic behaviour in the third article (Chapter 5). It was found that the quasi-steady model successfully predicted total stability of the single flexible tube in this array. This differs from predictions by previous models, including Leaver and Weaver [7], and Granger and Paidoussis [6], that predicted a single flexible tube in this array to be unstable. The stability results from the quasi-steady model were in very good agreement with the experimental results. For void fractions up to β=90%, instability was not possible to occur in this array in the streamwise and transverse directions, even with increasing the number of flexible tubes in the bundle. The only exception to this case is that, as what was interestingly found from the model, a

cluster of tubes, flexible in the transverse direction is unstable in water flow. With a deeper look into the water flow FEI test results, this result is in good agreement with the experiments as the array was not found to be "stabilizing" with the increase in flow velocity, compared to what has been seen in the partially flexible array and single flexible tube. The accuracy of the quasi-steady model was verified by comparing the damping ratio in two-phase flow in the streamwise direction with the experimental results. The model results agreed very well with the damping increasing behavior in the FEI tests.

It should be noted, however, that apparent transverse instability in the 97% void fraction was still questionable and contradicted the prediction of the stable behaviour according to the quasi-steady model. This was a motivation for further investigation of this unique behaviour by turning to the more general unsteady modal concept. Another set of experiments was performed to measure the unsteady fluid forces in both the transverse and streamwise directions. Pertinent results are presented in Chapter 6. The results covered the single phase (water) flow in addition to two-phase flow. The measured fluid force phase showed a substantial difference in the 97% void fraction phase in the transverse direction compared to lower void fractions. The damping calculated from the unsteady force showed a clear reduction in the same range of flow velocities as observed in the FEI experiments confirming the limited velocity range instability. The damping results thus provide a physical explanation of the array behaviour for β=97%. In order to complete the stability analysis of the APR1400, a rotated triangular array was studied in single and two-phase cross-flow (see Appendix A). A key finding addressed the question of SG tube stability. The results show stable streamwise fluidelastic behaviour for flow conditions matching the operating range of flow velocities of the steam generator.

7.2 Practical Implications of Research Findings and Proposed IPFEI Design Guideline

This thesis is a part of a large industrial project related to studying the fluidelastic instability of an operating steam generator. Several industrial reports have been written throughout the project, providing the technical requirements and the results of studying the steam generator tube bundle [130–136].

This study aimed in part to analyse the APR1400 steam generator tube bundle in single and two-phase cross-flow. The steam generator tube geometry is a hybrid geometry, with a rotated triangle layout in the vertical tube legs and rotated square layout at the upper horizontal section of the U-bend. The continuation of the steam generator study is presented in the 4^{th} article presented in Appendix A. In-plane fluidelastic instability has become

a significant concern since the tube failures of the SONGS generating station in 2012. A main conclusion from this work is that the the APR1400 steam generator is unlikely to be susceptible to in-plane fluidelastic instability (IPFEI) due to the stability of both arrays as confirmed in the work presented here.

Research work on the fluidelastic instability has aimed to provide experimental data to produce design information for steam generator tube bundles. Most of the reported data is generated from real geometries used in steam generators. This data pertains fluidelastic instability in several tube array geometries and different array pitch spacings (P/D). The majority of the fluidelastic instability studies showed that instability predominantly occurs in the OOP direction. Consequently, anti-vibration bars were introduced to suppress the OOP vibrations in steam generators. However, since the incident showing the existence of in-plane instability in steam generators, a redirection has been noticed in the research with renewed focus on IPFEI. Thus far, however, there is no design guideline for IPFEI. It was shown by Blevins [137] that the SONGS U-tubes became unstable in the first in-plane vibration mode. Based on the ASME guideline, Blevins suggested that the Connors constant of K=2.4 could be used. This may be considered an overly conservative estimation for a general design guideline specifically when it comes to IPFEI. The current ASME design guideline in essence takes no consideration of the important difference in tube array stability behaviour between the OOP and IP directions. The existing guideline, which is based on data collected for OOP, or combined OOP & IP, instability has "unfortunately" been recently used by engineers, for lack of an alternative. Hence, an effort was made here to collect data resulting only from in-plane instability in two-phase cross-flow. Test results in this thesis are also added to the IP instability data. The data from this study forms nearly 40% of all the data presented in the figure, which currently makes up the (publicly available) world data. Figure 7.1 shows that all currently (published) world data is lower bounded by the line K=6.5. Physically this means that no IPFEI has been measured at reduced velocities below V_p/fD=6.5 $m\delta/\rho D^2$. This is true for all array geometries. The lower bound stability constant of K=6.5 for IPFEI is $\simeq$ 63% higher than the average value of K=4.0 for out-of-plane (dominated) fluidelastic instability, and 171% higher than the value (of K=2.4) recommended for design analysis by the ASME.

Taking a lower bound envelop of all data, including the transverse instability data, would be excessively conservative. When looking for a design guideline for in-plane instability, it is more realistic to have a lower bound based on data exclusively presenting instability onset in the in-plane direction. The use of ASME's proposed stability boundary for IPFEI analysis clearly highly conservative. The present work leads to a proposed design stability

boundary with a Connors constant of K=6.5. This stability boundary includes "built-in" conservativeness since it is based on idealized laboratory tests. However, the steam generator designers would be expected to introduce a factor of safety in their analysis.

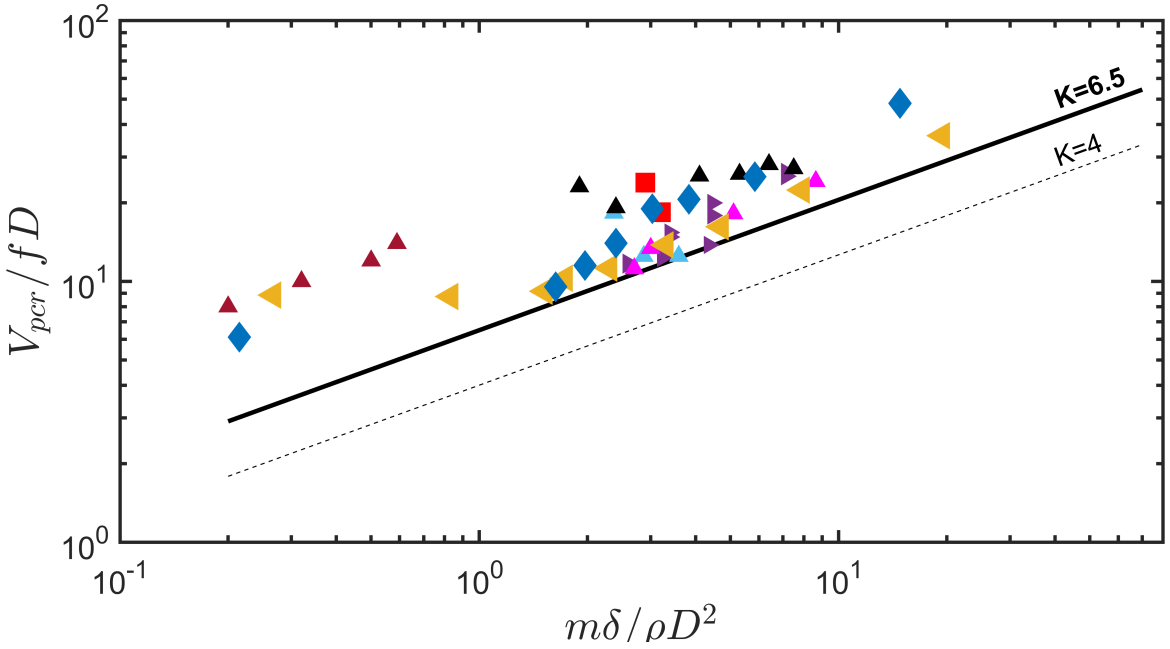


Figure 7.1 Suggested in-plane fluidelastic instability design guideline in the fluidelastic instability map showing two-phase flow test results in the in-plane direction for: (◆) rotated square array stability boundary based on maximum flow velocity attained (present study), (◀) rotated triangle array (present study), and data from the literature: (▲) Tan et al. [20], (■, ▲) Azuma et al. [21], (▲) Mureithi et al. [10], (▲) Joly et al. [22], (▶) Violette et al. [23]

CHAPTER 8 CONCLUSIONS

8.1 Research Contributions and Findings

The research work carried out in this PhD thesis has led to several contributions to the state of knowledge in the field of fluidelastic instability of heat exchangers. These contributions meet the research objectives presented in Sec. 1.1:

- The dynamic behaviour of the rotated square array with moderate pitch spacing (P/D=1.64) in the in-plane and out-of-plane directions in two-phase flow was found to be generally stable. This includes the single flexible tube and fully flexible bundle, operating in a wide range of void fractions.
- The rotated square array damping in two-phase flow was found to be practically higher than what was found in the other array geometries in two-phase flow. This has a significant effect on the array dynamic behaviour and explains the array's susceptibility to fluidelastic instability.
- The work presented is the first attempt to measure the quasi-steady fluid forces in a rotated square array in two-phase flow. The measurements included measuring the cross-coupling forces between the tubes in the array which made it possible to model the multiple flexible tubes fluidelastic instability.
- The rotated square array dynamic behaviour in the transverse direction in the 97% void fraction was found to be unique compared to the lower void fractions. A complex behaviour was found with an increase followed by a decrease in tube vibrations over a wide range of flow velocities.
- Another outcome is the measurement, for the first time, of the unsteady fluid force phase in the two-phase flow, in both for the transverse and streamwise directions. These measurements have led to the finding that for very high void fraction, and only in the transverse direction, the flow damping ratio decreases, leading the array to vibrate with vibration amplitudes increasing with the number of flexible tubes. Uniquely, the restabilization of the array was explained by the damping increase for high flow velocity; an unexpected result based on past research on fluidelastic instability
- An additional fluidelastic instability study was conducted on a confined space array with a rotated triangular geometry (P/D=1.33). The study presented the dynamic behaviour

of the array in both streamwise and transverse directions. The main contribution of this study is the finding that the instability in the streamwise direction occurs at a significantly high Connors constant of K=7.4 (see Appendix A).

- These results provided the valuable input needed to evaluate the stability of the APR1400 steam generator which contains both the rotated square and rotated triangular arrays, both subjected to two-phase flow with different void fractions along the tube span. A main practical contribution that can be drawn here is the confirmation of the stable behaviour of the APR1400 steam generator in the in-plane (IP) direction.
- For the first time, design guideline for in-plane fluidelastic instability is proposed from the results of this study as well as world data in the literature.

8.2 Recommendations for Future Work

- Tube array confinement (i.e., P/D) is considered a key factor in determining the two-phase flow damping. This is true based on the experimental observations were reported in the literature, which do not include inclusively the rotated square geometry dynamic behaviour. Hence, a study of tube arrays with pitch ratios other than 1.6 is recommended. Taking into consideration that much larger spacing may not be practical from the industrial point of view, as in any steam generator tube array, a much larger pitch spacing could result in a significant reduction in the steam generator efficiency.
- It is apparent that rotated square arrays are more stable than other geometries, at least in the practical range of flow velocities. A study of the flow structure within such an array is recommended in order to have a comprehensive understanding of the flow dynamics in the array. This may be done using optical methods of flow visualization such as PIV (Particle Image Velocimetry), or numerically using CFD.
- Rotated square array behaviour in air cross-flow turned out to be complex. A comprehensive study is recommended to include several pitch ratios and flexible tubes frequency detuning.
- The array behaviour for all void fractions is quite clear, except for the very high 97% case in the transverse direction. Hence, it would be valuable to have a separate study for this void fraction investigating the two-phase flow regime transition and the changes in the flow structure with the flow velocity.

8.3 Publications

The research work in this theses has led to four journal articles and two conference papers:

8.3.1 Journal articles

- S. Darwish *et al.* "Flow-Induced Vibrations of a Rotated Square Tube Array Subjected to Single-Phase Cross-Flow". Journal of Pressure Vessel Technology, 144.4 (2022): 041405.
- S. Darwish *et al.* "Experimental Investigation of Fluidelastic Instability of a Rotated Square Array Subjected to Two-phase and Air Cross-flow". Journal of Nuclear Engineering and Design, 2022 (submitted).
- S. Darwish *et al.* "Force Measurement and Modelling of Rotated Square Array in Two-phase Flow". Journal of Nuclear Engineering and Design, 2022 (submitted).
- S. Darwish *et al.* "In-Plane Fluidelastic Instability Study of a Tube Bundle with a Rotated Triangular Layout and Small Pitch Ratio". Journal of Nuclear Engineering and Design, 2022 (submitted).

8.3.2 Conferences

- S. Darwish *et al.* "Flow-Induced Vibration Behaviour of a Rotated Square Tube Array Subjected to Cross-Flow". Pressure Vessels and Piping Conference. Vol. 85338. American Society of Mechanical Engineers, 2021.
- S. Darwish *et al.* "On the stability of the rotated square array in two-phase flow using the quasi-steady model". Flow induced Vibrations Conference.

8.3.3 Technical reports

- N. Mureithi, S. Darwish *et al.* “Rotated Square Array Tests Interim Report I: Commissioning and Preliminary Tests”, Tech. Rep., 2020.
- N. Mureithi, S. Darwish *et al.* “Rotated Square Array Tests Interim Report II: FEI/FIV and Wear Workrate Tests”, Tech. Rep., 2020.
- N. Mureithi, S. Darwish *et al.* “Rotated Square Array Tests Interim Report III: Damping Tests”, Tech. Rep., 2020.

- N. Mureithi, S. Darwish *et al.* "Rotated Triangular Array Tests Interim Report I: Commissioning and Preliminary Tests", Tech. Rep., 2020.
- N. Mureithi, S. Darwish *et al.* "Rotated Triangular Array Tests Interim Report II: FEI/FIV and Wear Workrate Tests", Tech. Rep., 2020.
- N. Mureithi, S. Darwish *et al.* "Rotated Triangular Array Tests Interim Report III: Damping Tests", Tech. Rep., 2020.
- N. Mureithi, S. Darwish *et al.* "Normal Triangular Array Tests Interim Report II: FEI/FIV and Wear Workrate Tests", Tech. Rep., 2020.

REFERENCES

[1] K. Karwoski, "Circumferential cracking of steam generator tubes," Nuclear Regulatory Commission, Washington, DC (United States). Div. of ..., Tech. Rep., 1997.

[2] G. Assi, P. Bearman, and J. Meneghini, "On the wake-induced vibration of tandem circular cylinders: the vortex interaction excitation mechanism," *Journal of Fluid Mechanics*, vol. 661, pp. 365–401, 2010.

[3] M. Pettigrew *et al.*, "Vibration of tube bundles in two-phase cross-flow: part 2—fluid-elastic instability," 1989.

[4] D. Weaver *et al.*, "Flow-induced vibrations in power and process plant components—progress and prospects," *J. Pressure Vessel Technol.*, vol. 122, no. 3, pp. 339–348, 2000.

[5] B. W. Roberts, "Low frequency, self-excited vibration in a row of circular cylinders mounted in an airstream," Ph.D. dissertation, University of Cambridge, Eng., 1962.

[6] S. Granger and M. Paidoussis, "An improvement to the quasi-steady model with application to cross-flow-induced vibration of tube arrays," *Journal of Fluid Mechanics*, vol. 320, pp. 163–184, 1996.

[7] J. Lever and D. Weaver, "A theoretical model for fluid-elastic instability in heat exchanger tube bundles," 1982.

[8] D. Weaver, H. Lian, and X. Huang, "Vortex shedding in rotated square arrays," *Journal of Fluids and Structures*, vol. 7, no. 2, pp. 107–121, 1993.

[9] P. M. Scott, "Flow visualization of cross-flow-induced vibrations in tube arrays," Ph.D. dissertation, McMaster University, 1987.

[10] N. Mureithi *et al.*, "Fluidelastic instability tests on an array of tubes preferentially flexible in the flow direction," *Journal of fluids and structures*, vol. 21, no. 1, pp. 75–87, 2005.

[11] T. R. Sahu *et al.*, "Flow-induced vibration of a circular cylinder with rigid splitter plate," *Journal of Fluids and Structures*, vol. 89, pp. 244–256, 2019.

[12] S. Darwish *et al.*, "Flow-induced vibrations of a rotated square tube array subjected to single-phase cross-flow," *Journal of Pressure Vessel Technology*, vol. 144, no. 4, p. 041405, 2022.

[13] S. Price and S. Kuran, "Fluidelastic stability of a rotatedsquare array with multiple flexible cylinders, subject to cross-flow," *Journal of fluids and structures*, vol. 5, no. 5, pp. 551–572, 1991.

[14] M. Paidoussis *et al.*, "Flow-induced vibrations and instabilities in a rotated-square cylinder array in cross-flow," *Journal of Fluids and Structures*, vol. 3, no. 3, pp. 229–254, 1989.

[15] T. Nakamura and T. Tsujita, "Study on the stream-wise fluidelastic instability of rotated square arrays of circular cylinders subjected on cross-flow," in *Pressure Vessels and Piping Conference*, vol. 57977. American Society of Mechanical Engineers, 2017, p. V004T04A025.

[16] R. Hartlen, *Wind-tunnel Determination of Fluid-elastic-vibration Thresholds for Typical Het-exchanger Tube Pattens*. Ontario Hydro Research Division, 1974.

[17] B. Soper, "The effect of tube layout on the fluid-elastic instability of tube bundles in crossflow," 1983.

[18] E. M. M. ElKashlan, "Array geometry effects on vortex shedding and instability in heat exchanger tube bundles," Ph.D. dissertation, 1984.

[19] S. Olala and N. W. Mureithi, "Prediction of streamwise fluidelastic instability of a tube array in two-phase flow and effect of frequency detuning," *Journal of Pressure Vessel Technology*, vol. 139, no. 3, 2017.

[20] W. Tan, H. Wu, and G. Zhu, "Investigation of the vibration behavior of fluidelastic instability in closely packed square tube arrays," *Transactions of Tianjin University*, vol. 25, no. 2, pp. 124–142, 2019.

[21] S. Azuma *et al.*, "Investigation of in-plane fluid elastic instability for a triangular tube bundle subjected to two-phase flow," *Journal of Pressure Vessel Technology*, vol. 142, no. 2, 2020.

[22] T. Joly, N. Mureithi, and M. Pettigrew, "The effect of angle of attack on the fluidelastic instability of tube bundle subjected to two-phase cross-flow," in *ASME Pressure Vessels and Piping Conference*, vol. 43673, 2009, pp. 115–126.

[23] R. Violette, M. Pettigrew, and N. Mureithi, "Fluidelastic instability of an array of tubes preferentially flexible in the flow direction subjected to two-phase cross flow," 2006.

[24] M. Pettigrew, C. Taylor, and B. Kim, "The effects of bundle geometry on heat exchanger tube vibration in two-phase cross flow," *J. Pressure Vessel Technol.*, vol. 123, no. 4, pp. 414–420, 2001.

[25] T. Sawadogo and N. Mureithi, "Fluidelastic instability study on a rotated triangular tube array subject to two-phase cross-flow. part ii: Experimental tests and comparison with theoretical results," *Journal of Fluids and Structures*, vol. 49, pp. 16–28, 2014.

[26] H. Connors Jr, "Fluid elastic vibration of tube arrays excited by cross flow," in *ASME Symposium on Flow-Induced Vibration in Heat Exchanger, Winter Annual Meeting*, 1970, pp. 42–47.

[27] M. Paidoussis, "A review of flow-induced vibrations in reactors and reactor components," *Nuclear Engineering and Design*, vol. 74, no. 1, pp. 31–60, 1983.

[28] M. Rottmann and K. Popp, "Influence of upstream turbulence on the fluidelastic instability of a parallel triangular tube bundle," *Journal of fluids and structures*, vol. 18, no. 5, pp. 595–612, 2003.

[29] G. Rzentkowski and J. Lever, "An effect of turbulence on fluidelastic instability in tube bundles: a nonlinear analysis," *Journal of fluids and structures*, vol. 12, no. 5, pp. 561–590, 1998.

[30] R. E. D. Bishop and A. Hassan, "The lift and drag forces on a circular cylinder oscillating in a flowing fluid," *Proceedings of the Royal Society of London. Series A. Mathematical and Physical Sciences*, vol. 277, no. 1368, pp. 51–75, 1964.

[31] R. D. Blevins, "Flow-induced vibration," *New York*, 1977.

[32] J. Vandiver and J. Jong, "The relationship between in-line and cross-flow vortex-induced vibration of cylinders," *Journal of Fluids and Structures*, vol. 1, no. 4, pp. 381–399, 1987.

[33] J. Cheung and W. Melbourne, "Turbulence effects on some aerodynamic parameters of a circular cylinder at supercritical numbers," *Journal of Wind Engineering and Industrial Aerodynamics*, vol. 14, no. 1-3, pp. 399–410, 1983.

[34] M. Pettigrew and C. Taylor, "Vibration analysis of shell-and-tube heat exchangers: an overview—part 2: vibration response, fretting-wear, guidelines," *Journal of Fluids and Structures*, vol. 18, no. 5, pp. 485–500, 2003.

[35] R. D. Blevins, "Models for vortex-induced vibration of cylinders based on measured forces," *Journal of fluids engineering*, vol. 131, no. 10, 2009.

[36] G. Birkhoff, "Formation of vortex streets," *Journal of Applied Physics*, vol. 24, no. 1, pp. 98–103, 1953.

[37] R. T. Hartlen and I. G. Currie, "Lift-oscillator model of vortex-induced vibration," *Journal of the Engineering Mechanics Division*, vol. 96, no. 5, pp. 577–591, 1970.

[38] H. Benaroya and T. Wei, "Hamilton's principle for external viscous fluid–structure interaction," *Journal of Sound and Vibration*, vol. 238, no. 1, pp. 113–145, 2000.

[39] R. Ogink and A. Metrikine, "A wake oscillator with frequency dependent coupling for the modeling of vortex-induced vibration," *Journal of Sound and Vibration*, vol. 329, no. 26, pp. 5452–5473, 2010.

[40] S. Chen, S. Zhu, and Y. Cai, "An unsteady flow theory for vortex-induced vibration," *Journal of Sound and Vibration*, vol. 184, no. 1, pp. 73–92, 1995.

[41] T. Sarpkaya, "Fluid forces on oscillating cylinders," *Journal of the Waterway, Port, Coastal and Ocean Division*, vol. 104, no. 3, pp. 275–290, 1978.

[42] O. Griffin, "Vortex-excited cross-flow vibrations of a single cylindrical tube," 1980.

[43] O. Griffin and G. Koopmann, "The vortex-excited lift and reaction forces on resonantly vibrating cylinders," *Journal of Sound and Vibration*, vol. 54, no. 3, pp. 435–448, 1977.

[44] X. Wang, R. So, and K. Chan, "A non-linear fluid force model for vortex-induced vibration of an elastic cylinder," *Journal of Sound and Vibration*, vol. 260, no. 2, pp. 287–305, 2003.

[45] C. Taylor *et al.*, "Vibration of tube bundles in two-phase cross-flow: Part 3—turbulence-induced excitation," 1989.

[46] P. Feenstra, D. Weaver, and R. Judd, "An improved void fraction model for two-phase cross-flow in horizontal tube bundles," *International Journal of Multiphase Flow*, vol. 26, no. 11, pp. 1851–1873, 2000.

[47] S. Chen and J. Jendrzejczyk, "Flow velocity dependence of damping in tube arrays subjected to liquid cross-flow," 1981.

[48] R. Rogers, C. Taylor, and M. Pettigrew, "Fluid effects on multi-span heat exchanger tube vibration," *ASME Journal of Pressure Vessel and Piping, ASME Publication H*, vol. 316, pp. 17–26, 1984.

[49] H. Tanaka and S. Takahara, "Unsteady fluid dynamic force on tube bundle and its dynamic effect on vibration," in *ASME century 2 emerging technology conference*, 1980.

[50] ——, "Fluid elastic vibration of tube array in cross flow," *Journal of sound and vibration*, vol. 77, no. 1, pp. 19–37, 1981.

[51] H. Tanaka, S. Takahara, and K. Ohta, "Flow-induced vibration of tube arrays with various pitch-to-diameter ratios," 1982.

[52] S. Chen, "Instability mechanisms and stability criteria of a group of circular cylinders subjected to cross-flow. part i: theory," 1983.

[53] ——, "Instability mechanisms and stability criteria of a group of circular cylinders subjected to cross-flow—part ii: Numerical results and discussions," 1983.

[54] B. W. Roberts, "Low frequency, aeroelastic vibrations in a cascade of circular cylinders," *Mechanical Science Monograph*, no. 4, 1966.

[55] S. Price and M. Paidoussis, "A theoretical investigation of the parameters affecting the fluidelastic instability of a double row of cylinders subject to a cross-flow," in *Vibration in nuclear plant. Vol. 1. Proceedings of the 3rd international conference on'vibration in nuclear plant'held on 11-14 May 1982, Keswick (GB)*, 1983.

[56] S. Price, "A review of theoretical models for fluidelastic instability of cylinder arrays in cross-flow," *Journal of fluids and structures*, vol. 9, no. 5, pp. 463–518, 1995.

[57] S. Price and M. Paidoussis, "An improved mathematical model for the stability of cylinder rows subject to cross-flow," *Journal of Sound and Vibration*, vol. 97, no. 4, pp. 615–640, 1984.

[58] ——, "Fluidelastic instability of a full array of flexible cylinders subject to cross-flow," in *Proceedings of the ASME Tenth Biennial Conference on Mechanical Vibration and Noise: Fluid-Structure Interaction and Aerodynamic Damping. Cincinnati, OH*, 1985, pp. 171–192.

[59] ——, "A constrained-mode analysis of the fluidelastic instability of a double row of flexible circular cylinders subject to cross-flow: A theoretical investigation of system parameters," *Journal of sound and Vibration*, vol. 105, no. 1, pp. 121–142, 1986.

[60] S. Price, M. Paidoussis, and N. Giannias, "A generalized constrained-mode analysis for cylinder arrays in cross-flow," *Journal of fluids and structures*, vol. 4, no. 2, pp. 171–202, 1990.

[61] T. Sawadogo, "Modélisation de l'instabilité fluide Élastique d'un faisceau de tubes soumis à un Écoulement diphasique transverse," Ph.D. dissertation, École Polytechnique de Montréal, 2012.

[62] S. O. Olala, *Streamwise fluidelastic instability of tube arrays subjected to two-phase flow*. Ecole Polytechnique, Montreal (Canada), 2016.

[63] M. P. Paidoussis, D. Mavriplis, and S. Price, "A potential-flow theory for the dynamics of cylinder arrays in cross-flow," *Journal of Fluid Mechanics*, vol. 146, pp. 227–252, 1984.

[64] M. Paidoussis, S. Price, and D. Mavriplis, "A semipotential flow theory for the dynamics of cylinder arrays in cross flow," 1985.

[65] J. Lever and D. Weaver, "On the stability of heat exchanger tube bundles, part i: Modified theoretical model," *Journal of Sound and vibration*, vol. 107, no. 3, pp. 375–392, 1986.

[66] M. Hassan and D. S. Weaver, "Modeling of streamwise and transverse fluidelastic instability in tube arrays," *Journal of Pressure Vessel Technology*, vol. 138, no. 5, 2016.

[67] M. Hassan and D. Weaver, "Pitch and pattern effects on streamwise fluidelastic instability in tube arrays," *Journal of Pressure Vessel Technology*, vol. 144, no. 4, 2022.

[68] S. Price and N. Valerio, "A non-linear investigation of single-degree-of-freedom instability in cylinder arrays subject to cross-flow," *Journal of Sound and Vibration*, vol. 137, no. 3, pp. 419–432, 1990.

[69] J. Lever and G. Rzentkowski, "An investigation into the post-stable behavior of a tube array in cross-flow," 1989.

[70] C. Meskell and J. Fitzpatrick, "Investigation of the nonlinear behaviour of damping controlled fluidelastic instability in a normal triangular tube array," *Journal of Fluids and Structures*, vol. 18, no. 5, pp. 573–593, 2003.

[71] F. Axisa, J. Antunes, and B. Villard, "Overview of numerical methods for predicting flow-induced vibration," 1988.

[72] E. De Langre *et al.*, "Chaotic and periodic motion of a nonlinear oscillator in relation with flow-induced vibrations of loosely supported tubes," in *Proceedings of the ASME Conference on Pressure Vessels and Piping, New York, NY*, vol. 189, 1990, pp. 119–125.

[73] A. Fricker, "Numerical analysis of the fluidelastic vibration of a steam generator tube with loose supports," *Journal of Fluids and Structures*, vol. 6, no. 1, pp. 85–107, 1992.

[74] S. Price *et al.*, "The flow-induced vibration of a single flexible cylinder in a rotated square array of rigid cylinders with pitch-to-diameter ratio of $2 \cdot 12$," *Journal of Fluids and Structures*, vol. 1, no. 3, pp. 359–378, 1987.

[75] S. Price, B. Mark, and M. Paidoussis, "An experimental stability analysis of a single flexible cylinder positioned in an array of rigid cylinders and subject to cross-flow," 1986.

[76] S. Price, M. Paıdoussis, and B. Mark, "Flow visualization of the interstitial cross-flow through parallel triangular and rotated square arrays of cylinders," *Journal of Sound and Vibration*, vol. 181, no. 1, pp. 85–98, 1995.

[77] H. J. Chung and I. Chu, "Fluid-elastic instability of rotated square tube array in air-water two-phase cross-flow," *Nuclear Engineering and Technology*, vol. 38, no. 1, p. 69, 2006.

[78] S. Kuran, "Fluidelastic stability of a rotated square array with multiple flexible cylinders subject to cross-flow." 1994.

[79] S. Olala and N. Mureithi, "Prediction of streamwise fluidelastic instability of a tube array in two-phase flow and effect of frequency detuning," *Journal of Pressure Vessel Technology*, vol. 139, p. 031301, 10 2016.

[80] D. Weaver and M. El-Kashlan, "The effect of damping and mass ratio on the stability of a tube bank," *Journal of Sound and Vibration*, vol. 76, no. 2, pp. 283–294, 1981.

[81] R. Austermann and K. Popp, "Stability behaviour of a single flexible cylinder in rigid tube arrays of different geometry subjected to cross-flow," *Journal of Fluids and Structures*, vol. 9, no. 3, pp. 303–322, 1995.

[82] A. Khalifa, "Fluidelastic instability in heat exchanger tube arrays," Ph.D. dissertation, 2012.

[83] D. Polak and D. Weaver, "Vortex shedding in normal triangular tube arrays," *Journal of Fluids and Structures*, vol. 9, no. 1, pp. 1–17, 1995.

[84] P. Feenstra, D. Weaver, and T. Nakamura, "Vortex shedding and fluidelastic instability in a normal square tube array excited by two-phase cross-flow," *Journal of Fluids and Structures*, vol. 17, no. 6, pp. 793–811, 2003.

[85] D. Weaver and A. Abd-Rabbo, "A flow visualization study of a square array of tubes in water crossflow," 1985.

[86] D. Weaver and H. Yeung, "Approach flow direction effects on the cross-flow induced vibrations of a square array of tubes," *Journal of Sound and vibration*, vol. 87, no. 3, pp. 469–482, 1983.

[87] S. Price and M. Paidoussis, "The flow-induced response of a single flexible cylinder in an in-line array of rigid cylinders," *Journal of fluids and structures*, vol. 3, no. 1, pp. 61–82, 1989.

[88] V. Shinde, E. Longatte, and F. Baj, "Large eddy simulation of fluid-elastic instability in square normal cylinder array," *Journal of Pressure Vessel Technology*, vol. 140, no. 4, p. 041301, 2018.

[89] V. Shinde *et al.*, "Numerical simulation of the fluid–structure interaction in a tube array under cross flow at moderate and high reynolds number," *Journal of Fluids and Structures*, vol. 47, pp. 99–113, 2014.

[90] M. Hassan, A. Gerber, and H. Omar, "Numerical estimation of fluidelastic instability in tube arrays," *Journal of Pressure Vessel Technology*, vol. 132, no. 4, 2010.

[91] H. H. Jafari and B. G. Dehkordi, "Numerical prediction of fluid-elastic instability in normal triangular tube bundles with multiple flexible circular cylinders," *Journal of Fluids Engineering*, vol. 135, no. 3, p. 031102, 2013.

[92] E. Longatte, Z. Bendjeddou, and M. Souli, "Methods for numerical study of tube bundle vibrations in cross-flows," *Journal of Fluids and Structures*, vol. 18, no. 5, pp. 513–528, 2003.

[93] S. Granger, R. Campistron, and J. Lebret, "Motion-dependent excitation mechanisms in a square in-line tube bundle subject to water cross-flow: an experimental modal analysis," *Journal of fluids and structures*, vol. 7, no. 5, pp. 521–550, 1993.

[94] S.C.E, "San onofre nuclear generating station unit 2 return to service report," Arlington, Texas, Tech. Rep., 2012.

[95] E. De Langre, "Frequency lock-in is caused by coupled-mode flutter," *Journal of fluids and structures*, vol. 22, no. 6-7, pp. 783–791, 2006.

[96] C. Cossu and L. Morino, "On the instability of a spring-mounted circular cylinder in a viscous flow at low reynolds numbers," *Journal of Fluids and Structures*, vol. 14, no. 2, pp. 183–196, 2000.

[97] S. Price *et al.*, "The flow-induced vibration of a single flexible cylinder in a rotated square array of rigid cylinders with pitch-to-diameter ratio of $2 \cdot 12$," *Journal of Fluids and Structures*, vol. 1, no. 3, pp. 359–378, 1987.

[98] S. Price, B. Mark, and M. Paidoussis, "An experimental stability analysis of a single flexible cylinder positioned in an array of rigid cylinders and subject to cross-flow," 1986.

[99] S. Price, M. Paıdoussis, and B. Mark, "Flow visualization of the interstitial cross-flow through parallel triangular and rotated square arrays of cylinders," *Journal of Sound and Vibration*, vol. 181, no. 1, pp. 85–98, 1995.

[100] S. Price and M. Paidoussis, "A single-flexible-cylinder analysis for the fluidelastic instability of an array of flexible cylinders in cross-flow," 1986.

[101] A. Abd-Rabbo and D. Weaver, "A flow visualization study of flow development in a staggered tube array," *Journal of Sound and Vibration*, vol. 106, no. 2, pp. 241–256, 1986.

[102] A. Khalifa, D. Weaver, and S. Ziada, "Modeling of the phase lag causing fluidelastic instability in a parallel triangular tube array," *Journal of Fluids and Structures*, vol. 43, pp. 371–384, 2013.

[103] C. V. Alonzo and E. O. Macagno, "Numerical integration of the time-dependent equations of motion for taylor vortex flow," *Computers & Fluids*, vol. 1, no. 3, pp. 301–315, 1973.

[104] F. R. Menter, "Two-equation eddy-viscosity turbulence models for engineering applications," *AIAA journal*, vol. 32, no. 8, pp. 1598–1605, 1994.

[105] D. Weaver and W. Schneider, "The effect of flat bar supports on the crossflow induced response of heat exchanger u-tubes," 1983.

[106] K. Haslinger and D. Steininger, "Vibration response of a u-tube bundle with anti-vibration bar supports due to turbulence and fluidelastic excitations," *Journal of fluids and structures*, vol. 9, no. 8, pp. 805–834, 1995.

[107] D. Weaver and H. Yeung, "The effect of tube mass on the flow induced response of various tube arrays in water," *Journal of Sound and Vibration*, vol. 93, no. 3, pp. 409–425, 1984.

[108] S. Price and M. Paidoussis, "A single-flexible-cylinder analysis for the fluidelastic instability of an array of flexible cylinders in cross-flow," 1986.

[109] M. J. Pettigrew *et al.*, "Detailed flow and force measurements in a rotated triangular tube bundle subjected to two-phase cross-flow," *Journal of Fluids and structures*, vol. 20, no. 4, pp. 567–575, 2005.

[110] C. Zhang, M. Pettigrew, and N. Mureithi, "Vibration excitation force measurements in a rotated triangular tube bundle subjected to two-phase cross flow," 2007.

[111] ——, "Correlation between vibration excitation forces and the dynamic characteristics of two-phase cross flow in a rotated-triangular tube bundle," *Journal of pressure vessel technology*, vol. 130, no. 1, 2008.

[112] G. Noghrehkar, M. Kawaji, and A. Chan, "Investigation of two-phase flow regimes in tube bundles under cross-flow conditions," *International Journal of Multiphase Flow*, vol. 25, no. 5, pp. 857–874, 1999.

[113] R. Ulbrich and D. Mewes, "Vertical, upward gas-liquid two-phase flow across a tube bundle," *International journal of multiphase flow*, vol. 20, no. 2, pp. 249–272, 1994.

[114] R. Blevins, "Fluid elastic whirling of a tube row," 1974.

[115] S. Price and M. Paidoussis, "Fluidelastic instability of an infinite double row of circular cylinders subject to a uniform cross-flow," 1983.

[116] C. Meskell, "A new model for damping controlled fluidelastic instability in heat exchanger tube arrays," 2009.

[117] S. Chen, "A general theory for dynamic instability of tube arrays in crossflow," *Journal of Fluids and Structures*, vol. 1, pp. 35–53, 1987.

[118] T. Nakamura *et al.*, "Dynamics of an in-line tube array subjected to steam-water cross-flow. part i: two-phase damping and added mass," *Journal of fluids and structures*, vol. 16, no. 2, pp. 123–136, 2002.

[119] N. Mureithi *et al.*, "Dynamics of an in-line tube array subjected to steam–water cross-flow. part ii: Unsteady fluid forces," *Journal of fluids and structures*, vol. 16, no. 2, pp. 137–152, 2002.

[120] K. Hirota *et al.*, "Dynamics of an in-line tube array subjected to steam-water cross-flow. part iii: fluidelastic instability tests and comparison with theory," *Journal of fluids and structures*, vol. 16, no. 2, pp. 153–173, 2002.

[121] T. Sawadogo and N. Mureithi, "Fluidelastic instability study in a rotated triangular tube array subject to two-phase cross-flow. part i: Fluid force measurements and time delay extraction," *Journal of Fluids and Structures*, vol. 49, pp. 1–15, 2014.

[122] M. Hassan and D. Weaver, "Transverse and streamwise fluidelastic instability in rotated square tube arrays," in *FIV2018 Conference*, 2018.

[123] S. Kuran, "Fluidelastic stability of a rotated square array with multiple flexible cylinders subject to cross-flow," Ph.D. dissertation, 1992.

[124] M. P. Paidoussis and S. Price, "The mechanisms underlying flow-induced instabilities of cylinder arrays in cross-flow," in *Design & Analysis*. Elsevier, 1989, pp. 147–163.

[125] A. Roshko, "Experiments on the flow past a circular cylinder at very high reynolds number," *Journal of fluid mechanics*, vol. 10, no. 3, pp. 345–356, 1961.

[126] S. Shahriary, N. W. Mureithi, and M. J. Pettigrew, "Quasi-static forces and stability analysis in a triangular tube bundle subjected to two-phase cross-flow," in *ASME Pressure Vessels and Piping Conference*, vol. 42827, 2007, pp. 245–252.

[127] T. Sawadogo and N. Mureithi, "Time domain simulation of the vibration of a steam generator tube subjected to fluidelastic forces induced by two-phase cross-flow," *Journal of Pressure Vessel Technology*, vol. 135, no. 3, 2013.

[128] H. Li and N. Mureithi, "Development of a time delay formulation for fluidelastic instability model," *Journal of Fluids and Structures*, vol. 70, pp. 346–359, 2017.

[129] S. Darwish, N. Mureithi, and M. Cho, "Experimental investigation of fluidelastic instability of a rotated square array subjected to two-phase and air cross-flow," *Journal of Nuclear Engineering and Design*, vol. (submitted), 2022.

[130] N. Mureithi and S. Darwish *et al.*, "Rotated Square Array Tests Interim Report I: Commissioning and Preliminary Tests," Tech. Rep., 2020.

[131] ——, "Rotated Square Array Tests Interim Report II: FEI/FIV and Wear Workrate Tests," Tech. Rep., 2020.

[132] ——, "Rotated Square Array Tests Interim Report III: Damping Tests," Tech. Rep., 2020.

[133] ——, "Rotated Triangular Array Tests Interim Report I: Commissioning and Preliminary Tests," Tech. Rep., 2020.

[134] ——, "Rotated Triangular Array Tests Interim Report II: FEI/FIV and Wear Workrate Tests," Tech. Rep., 2020.

[135] ——, "Rotated Triangular Array Tests Interim Report III: Damping Tests," Tech. Rep., 2020.

[136] ——, "Normal Triangular Array Tests Interim Report II: FEI/FIV and Wear Workrate Tests," Tech. Rep., 2020.

[137] R. Blevins, "Nonproprietary flow-induced vibration analysis of san onofre nuclear generating station replacement steam generators to asme code section iii appendix n," *Journal of Pressure Vessel Technology*, vol. 140, no. 3, 2018.

[138] U. S. N. R. Commission *et al.*, "San onofre nuclear generating station unit 2—confirmatory action letter—actions to address steam generator tube degradation," *United States Nuclear Regulatory Commission, Rockville, MD*, 2012.

[139] S. Darwish *et al.*, "Flow-induced vibrations of a rotated square tube array subjected to single-phase cross-flow," *Journal of Pressure Vessel Technology*, vol. 144, no. 4, p. 041405, 2022.

[140] M. Pettigrew and C. Taylor, "Fluidelastic instability of heat exchanger tube bundles: review and design recommendations," 1991.

[141] T. Nakamura, Y. Fujita, and T. Sumitani, "Study on in-flow fluidelastic instability of triangular tube arrays subjected to air cross flow," *Journal of Pressure Vessel Technology*, vol. 136, no. 5, 2014.

[142] S. Nishida *et al.*, "In-plane fluidelastic instability evaluation of triangular array tube bundle using fluid force measured under steam–water two-phase flow condition," *Journal of Pressure Vessel Technology*, vol. 143, no. 1, 2021.

[143] M. Pettigrew *et al.*, "Vibration of a tube bundle in two-phase freon cross-flow," 1995.

[144] D. Weaver and L. Grover, "Cross-flow induced vibrations in a tube bank—turbulent buffeting and fluid elastic instability," *Journal of Sound and Vibration*, vol. 59, no. 2, pp. 277–294, 1978.

[145] I.-C. Chu, H. J. Chung, and Y. J. Yun, "Fluid-elastic instability in tube bundles and effect of flow regime transition," in *International Conference on Nuclear Engineering*, vol. 42444, 2006, pp. 247–253.

[146] S. Ziada, "Vorticity shedding and acoustic resonance in tube bundles," *Journal of the Brazilian Society of Mechanical Sciences and Engineering*, vol. 28, no. 2, pp. 186–189, 2006.

[147] L. Carlucci and J. Brown, "Experimental studies of damping and hydrodynamic mass of a cylinder in confined two-phase flow," 1983.

[148] R. Violette, N. Mureithi, and M. Pettigrew, "Two-phase flow induced vibration of an array of tubes preferentially flexible in the flow direction," in *ASME Pressure Vessels and Piping Conference*, vol. 41898, 2005, pp. 331–338.

[149] S. Olala *et al.*, "Streamwise fluidelastic forces in tube arrays subjected to two-phase flows," in *Pressure Vessels and Piping Conference*, vol. 46018. American Society of Mechanical Engineers, 2014, p. V004T04A014.

[150] S. J. Kline, "Describing uncertainty in single sample experiments," *Mech. Engineering*, vol. 75, pp. 3–8, 1953.

APPENDIX A ARTICLE 4: IN-PLANE FLUIDELASTIC INSTABILITY STUDY OF A TUBE BUNDLE WITH A ROTATED TRIANGULAR LAYOUT AND SMALL PITCH RATIO

Sameh Darwish, Njuki Mureithi, Minki Cho

This article has been submitted to the "Journal of Nuclear Engineering and Design" on October 26, 2022.

In this chapter, the stability analysis of the rotated triangle array is performed in single phase (water) and two-phase (air-water) cross-flow. This is to meet the specific objectives to:

- Study the fluidelastic instability of the array and determine the instability onset, with a focus on the instability in the streamwise direction.
- Investigate the stability of the APR1400 steam generator tube bundle (along with the rotated square stability analysis results).

The paper presents the in-plane fluidelastic instability of a rotated triangular array with P/D=1.33. Single and multiple flexible tubes configurations were used to investigate the array behaviour in single phase (water) and two-phase flow. The findings from this paper show that the array does not undergo in-plane fluidelastic instability for the case of the single flexible tube and partially flexible array. However, when the fully flexible array was tested, in-plane instability occurred at high flow velocity. On the other hand, transverse instability existed in all the cases tested. This does not raise any concern in the practical applications as tube bundles are supported with anti-vibration bars that support the tubes in the transverse direction.

Abstract

Since the shutdown of the San Onofre Nuclear Generating Station (SONGS), the question of the possibility of in-plane fluidelastic instability in the steam generators was raised. In a step to analyze the stability of the APR1400 steam generator, this paper reports on an experimental fluidelastic instability study in single phase (water) and two-phase (air-water) cross flow of the vertical tube bank in the steam generator. The study concerns the vibration behaviour of single flexible tube with an otherwise rigid array as well as fully flexible array. The tube pattern analyzed is the rotated triangular array (60^o) having a pitch spacing (P/D) of 1.33. This spacing is generally more confined than what is usually seen in the literature. Adjustable tube mounts allow the tubes to vibrate only in one direction, whether in the streamwise or transverse to the flow. The stability threshold in the transverse direction of such a tightly spaced rotated triangular array is somewhat lower than the other layouts. Damping of this rotated triangle array reaches its maximum value at a void fraction near 80%. Fluidelastic instability critical velocity in the streamwise direction was found to be much higher than the range of velocities implied by the ASME design guideline, which implies relatively high Connors constants. This was observed in the case of fully flexible array only, where cross-coupling between the tubes is significant. However, A single flexible tube did not undergo instability, which indicates that the streamwise instability is governed by the fluid stiffness mechanism.

A.1 Introduction

For a long time, the design of nuclear steam generator tube supports was directed to avoid tube vibrations in the direction transverse to the flow (or the out-of-plane direction). This was thought to be sufficient until the in-plane (IP) instability caused tube failures in the San Onofre Nuclear Generating Station (SONGS) in California [138]. The vast majority of the reported research work is oriented towards studying the out-of-plane instability (transverse to the flow direction). Tube failures are now, however, known to be clearly possible as a result of the in-plane fluidelastic instability (IPFEI). There is now, therefore, a concerted effort to investigate IPFEI for the range of the tube array geometries found in nuclear steam generators. This work is needed to provide the data necessary for verification or extension of current FIV design guidelines to account for IPFEI.

A typical steam generator tube bundle, has a semi-circular U-bend region and vertical straight legs. In this case the cross-section tube pattern in the steam generator has a fixed geometry. If the tube bundle has a rectangular U-bend, the tube pattern then transitions from one

arrangement to another in the upper U-bend region if tube spacing also changes. In the APR1400 steam generator for instance, there is a transition from a triangular geometry in the vertical legs, to a rotated square geometry in the upper horizontal section of the U-bend region. Figure A.1 shows the design of the APR1400 steam generator with the U-bend region of the tube bundle. The rotated square geometry was studied in previous studies in detail [129, 139]. In this article, the rotated triangular array is studied. This provides complementary information on the second array geometry found in the APR1400.

The rotated (or parallel) triangular array, was shown to be susceptible to fluidelastic instability in the transverse direction. Recent studies showed that rotated triangular (RT) arrays with small pitch spacing ratios and high mass damping parameters are also susceptible to FEI in the streamwise direction. The array pitch spacing has been found to be a significant parameter with regards to the instability boundary. Its effect was found to be considerable in the normal triangle and rotated square arrays , while it is less significant for the rotated triangle and normal square arrays [140]. In a study by Nakamura et al. [141], multiple arrays with pitch spacings in the range 1.2-1.5 were studied in air flow. The Connors constant (which is a measure of array stability) was seen to increase with the increase of array pitch spacing ratio when the array vibration is limited to the direction transverse to the flow. This was even more clear in the streamwise direction. Interestingly, streamwise instability was found to occur at an earlier onset than in the transverse direction in the most compact array having spacing ratio P/D=1.2. The array pitch ratio may also affect the significance of the tubes cross-coupling as was observed by Scott [9] in water flow experiments. Two rotated triangular arrays of 1.375 and 1.73 pitch ratios were tested. The results showed that in the transverse direction, the single flexible tube had the same stability threshold as the fully flexible array. However, for the larger spacing array, the stability threshold of the fully flexible array was 30% lower than that of the single flexible tube array. This suggests that the significance of the fluid damping instability mechanism may vary depending on the array compactness or pitch spacing.

Theoretical analysis by Shahriary et al. [126] suggested that a single flexible tube in a RT array (P/D=1.5) cannot become unstable in the flow direction. This result was not experimentally confirmed (for water flow) until later by Mureithi et al. [10] who showed that no streamwise fluidelastic instability occurs in air flow or in two-phase flow for a single flexible tube. Furthermore, Nakamura et al. [141] showed an agreement with the model results in air flow vibration experiments. However, a single flexible tube in an otherwise rigid tube array with low mass damping parameter could be susceptible to FEI in the streamwise direction. This was reported by Tan et al. [20] for a rotated triangular array with pitch ratio of 1.48. This is unlikely to happen in RT arrays that have tubes with high mass damping parameter.

The majority of the reported test results confirm the necessity of the stiffness controlled mechanism to induce streamwise fluidelastic instability. An early study considering the partial flexibility in the streamwise direction was conducted by Violette et al. [23] on a rotated triangular array with pitch ratio of 1.5. Other test results were published presenting the rotated triangular array dynamic behaviour in single and in two-phase flow [21, 22, 142–145].

The aforementioned industrial experience and recent findings have redirected the research work to investigate further the possibility of the streamwise fluidelastic instability. The effect of array pitch spacing needs particular attention to understand its effect on the bundle stability behaviour. We here present an experimental study of a rotated triangular array tested in the low mass damping parameter range. This array is compact, having a pitch spacing ratio of 1.33. The study presents the streamwise and transverse dynamics, investigated separately for single (water) and two-phase (air-water) flow. The study provides key information on the streamwise (in-plane) dynamics of the second tube array geometry found in the APR1400 steam generator.

A.2 Tube Bundle Test Apparatus

A test loop is designed and built to perform a wide range of two-phase flow experiments. Water is circulated by a 1.56 m^3/min centrifugal pump from a large reservoir with a 1.5 m^3 capacity. As shown in Fig. A.2, compressed air is injected into the test loop upstream of the test section. The air and water streams are mixed using a two-layer honeycomb mixer. The efficiency of the mixer was verified ahead of performing the FEI tests by measuring the uniformity of the two-phase flow void fraction across the test section. Water flow velocity uniformity was also verified. This is to ensure the quality of the two-phase flow mixing and the uniform distribution of the flow upstream of the tube bundle.

Water flow rate is measured using a magnetic water flow meter (MAG500), and water temperature is monitored in the tank by a thermocouple. The flow rate of the injected air is measured using two distinct orifice plates and a differential pressure transducer, along with air flow temperature and pressure. The pressure at the inlet of the test section, and upstream of tube bundle is measured using another differential pressure transducer to correct the air flow rate for pressure variation.

The experimental test section is designed to suit several test setups. The rotated triangular array is composed of 9 rows and 7 columns of either rigid or flexible tubes, based on the desired experimental setup. Two more columns of half tubes are mounted on the side

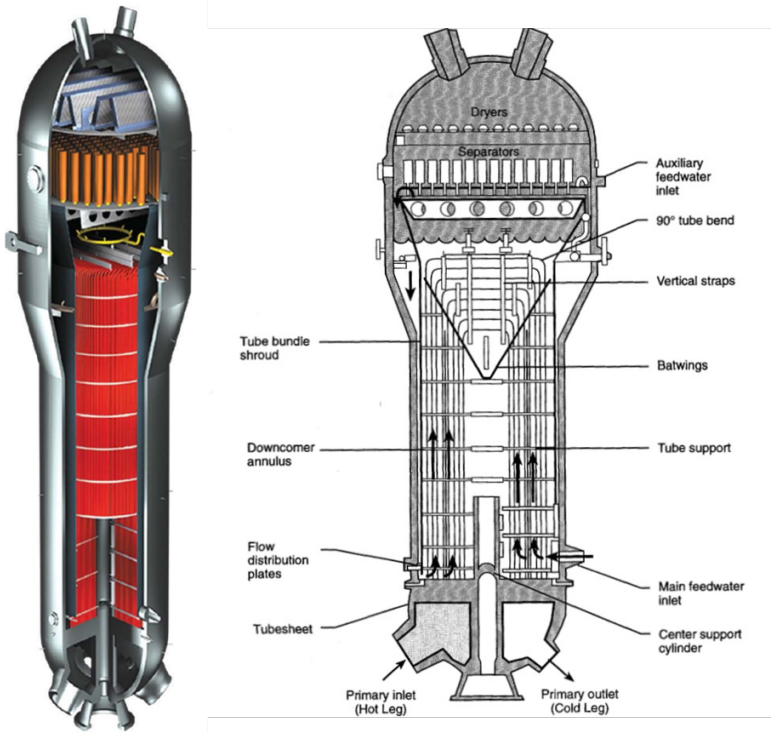


Figure A.1 Schematic drawing showing internal details of the APR1400 steam generator [1]

walls to reduce the wall effect. The clearance between the flexible tube and the wall is approximately 1 mm, thus negligible effect on the flow. Flexible tubes are cantilevered using flexible plates made of Aluminum, having a rectangular cross section. This design allows the tubes to be preferentially flexible in one direction only, either streamwise or transverse to the flow direction. All tubes are designed with the same modal parameters (damping ratio and natural frequency), and a detailed geometrical and experimental verification was carried out to ensure that all tubes are well tuned. Tuning the tube modal parameters provides array behaviour symmetry and experiment repeatability. The dimensions of the rectangular support were carefully chosen to ensure approximate rigidity in the normal direction, with a natural frequency five times higher than the flexible direction. The tube mass damping parameter (in air) is $m\delta/\rho D^2$=20.6.

Flexible tube vibration is measured using strain gauges. The gauges are fixed at the cantilevered tube root where the strain signal is maximum. A full bridge type II tee rosette is utilized. This bridge type has 4 active elements with many advantages such as reducing the signal noise, rejecting the axial strain, compensating for temperature change, aggregate material and lead resistance. Tube tip-to-strain relation was determined using an STI CMCP610 bench-top calibrator. All signals are acquired using a calibrated National Instruments data

acquisition system. A high sampling frequency f_s=2 kHz was used in all the measurements. For the two-phase flow tests, the flow conditions are specified using the homogeneous two-phase flow model. The homogeneous air-water flow void fraction is calculated as a ratio between air flow rate to flow mixture total flow rate

$$\beta = \frac{Q_g}{Q_g + Q_l} \tag{A.1}$$

where, Q_g and Q_l are the gas (air) and liquid (water) flow rates, respectively. The variation of the void fraction is controlled by the air flow and water flow, based on the pre-determined flow velocity. The flow pitch velocity, V_p, is related to the upstream homogeneous flow velocity, V_u, by

$$V_p = V_u \frac{P/D}{P/D - 1} \tag{A.2}$$

V_u is calculated by dividing the total flow rate by the test section area. The homogeneous density, ρ_h, is defined using flow homogeneous void fraction

$$\rho_h = \beta\rho_g + \beta(1 - \rho_l) \tag{A.3}$$

where, subscripts g and l denote gas and liquid, respectively.

A.3 Vibration Test Results

To determine the dynamic behaviour of the array, a series of experiments were conducted in water flow, and in two-phase flow for void fractions in the range β=20-60%. Three different flexible tube configurations were chosen, a single flexible tube located in the 4th row and central column, a column of four flexible tubes, and a fully flexible array (flexible bundle). For brevity, the single flexible tube and fully flexible array test results will be presented in detail. In each case, tubes were tested once in the streamwise direction, and in another test in the direction transverse to the flow. Figure A.3a shows the test section operating in two-phase flow, while Fig. A.3b shows the tube array with instrumented tubes numbers. The results obtained in water flow will be presented first, followed by the two-phase flow test results. In all the following sections, vibration test results are presented in the form of the root-mean-square (rms) of the tube vibration non-dimensional amplitude normalized using the tube outer diameter, D. The vibration test results are presented as a function of the non-dimensional flow velocity, V_p/fD.

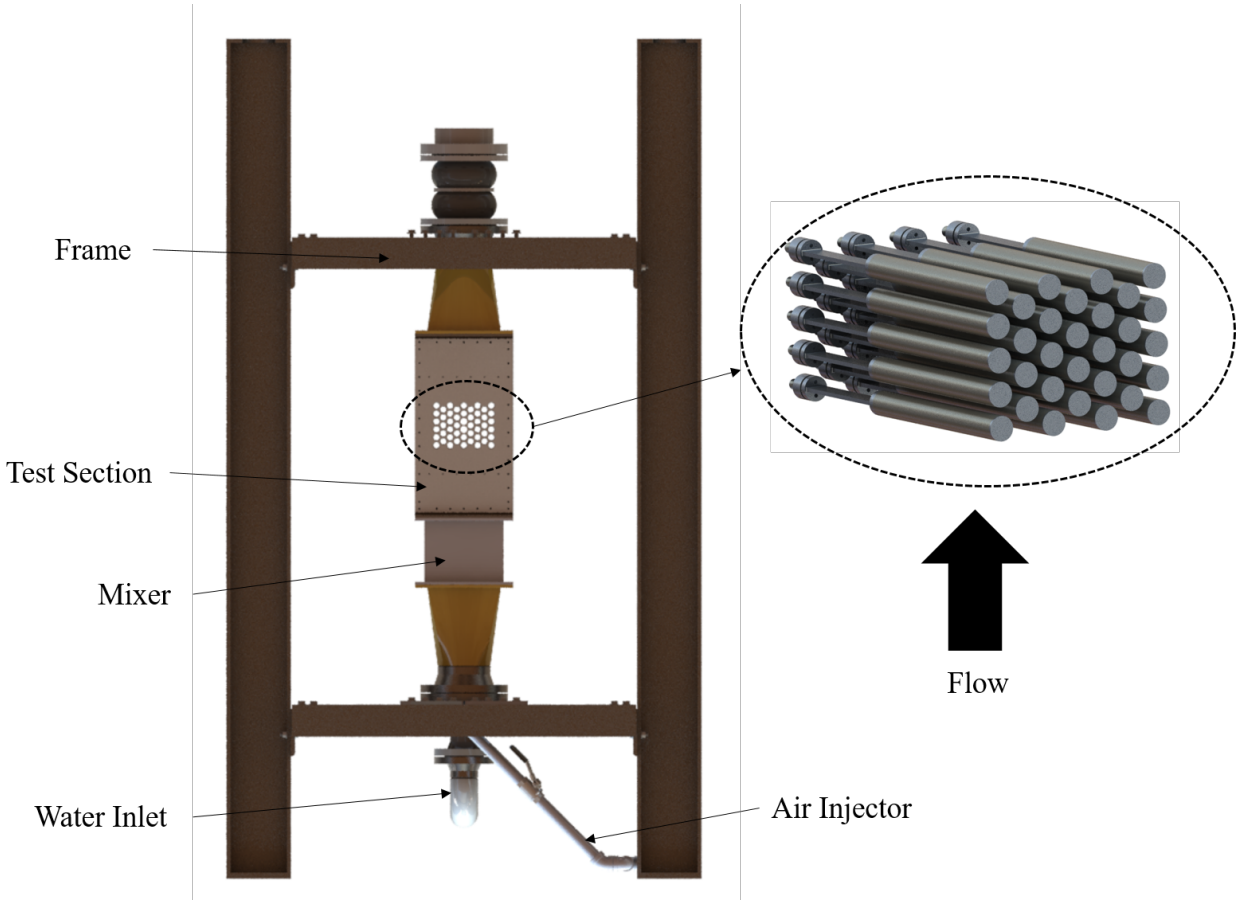
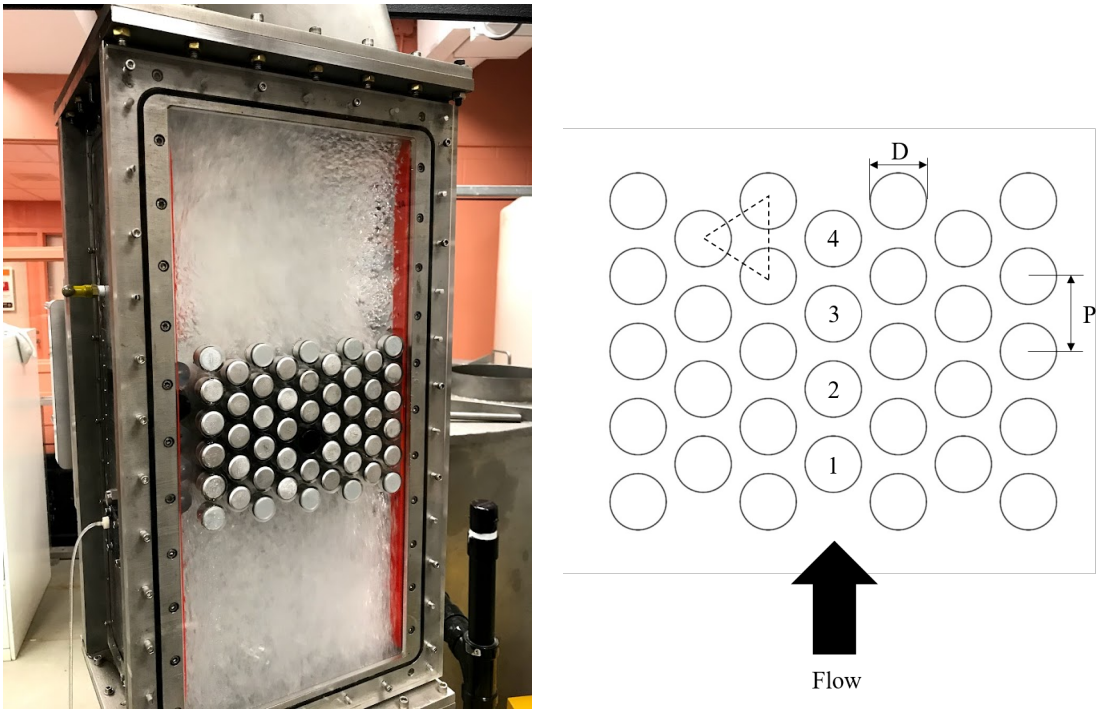


Figure A.2 Test loop showing the tube bundle

A.3.1 Single phase (water) flow results

Transverse direction dynamics

Figure A.4 presents the vibration test results of a single flexible tube subjected to water flow. The tube is oriented to vibrate purely in the direction transverse to the flow. As seen in the figure, low amplitude vibrations were observed at a low reduced velocity near V_p/fD=1.2, followed by a reduction in tube vibration amplitude near V_p/fD= 1.5. The vibration reduction at the reduced velocity of 1.5 suggests that this behaviour is a resonance like behaviour due to flow periodicity generated by the flow through the array. Based on the vibration frequency and flow velocity, a Strouhal number of 0.8 is determined. This agrees well with the experimental results published by Ziada [146], for such a tight spaced array with P/D=1.33. According to Ziada [146], three periodicity frequencies may exist in this array. Practically, however, not all these periodicities may be detected by the tube vibration frequency spectra. Here, the periodicity frequencies could not be easily detected from the



(a) (b)

Figure A.3 Test section

frequency spectra. This could be due to the small pitch spacing and array confinement that leads to formation of weak vortex shedding thus low periodic excitation forces. In Fig. A.4, the tube non-dimensional vibration frequency variation is presented with flow reduced velocity. The dispersion of the frequencies could be due to a high Strouhal number vortex shedding that is around S_p=0.96. Fig. A.5 presents the frequency spectra of the flexible tube for all flow pitch velocities. It was difficult to judge the vortex shedding frequencies in this test. However, a clear Strouhal number of S_p=0.79 could be detected at one frequency spectrum. Clearly this vortex shedding excites the tube for a short range of flow velocity. The abrupt frequency change near the reduced velocity of V_p/fD=1.5 also confirms the vorticity excitation observation, followed by well synchronized frequencies. Parallel triangular arrays generally may show three distinct Strouhal number depending on the array spacing [146]. In this array, in the transverse direction, only the periodicity that corresponds to the mid Strouhal number (S_p=0.79) was observed.

An instability of the single flexible tube is observed near a reduced velocity of V_p/fD= 1.65. For such a tight spacing, it is expected that strong hydrodynamic coupling between the flexible tubes will occur. A reduction in the critical velocity for fluidelastic instability may be observed. In the fully flexible array test, tubes went unstable at a reduced velocity

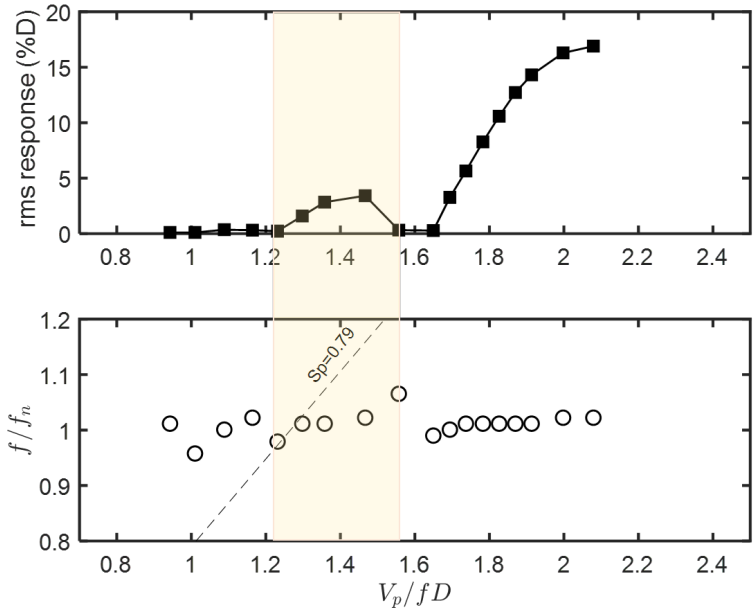


Figure A.4 Frequency spectra of single flexible tube in water flow in the transverse direction

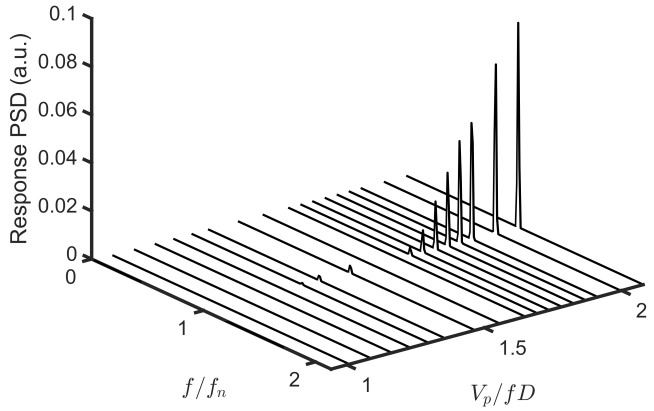


Figure A.5 Single flexible tube vibrations in water flow in the transverse direction

of V_p/fD=1.6 as shown in Fig. A.6. This is only 3% lower than the critical velocity of the single flexible tube. The instability that arises in the case of the single flexible tube indicates that the instability here is due to the negative damping mechanism. Despite the fact that strong cross-coupling between the tubes may exist here, the critical flow velocity did not noticeably decrease in the flexible bundle compared to the single flexible tube. The violent vibrations were found to occur in the bundle. A complex amplitude grow due to the cross-

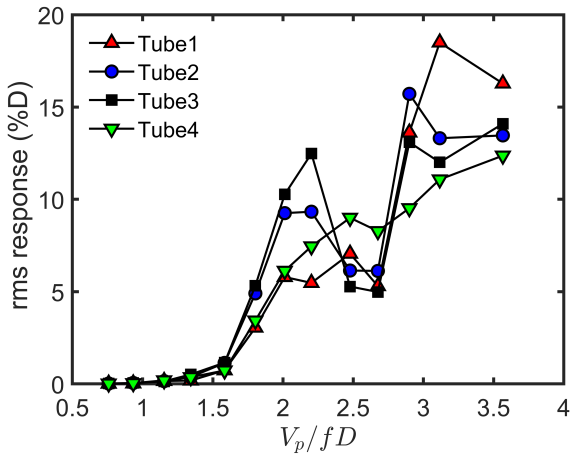


Figure A.6 Fully flexible array vibrations in water flow in the transverse direction

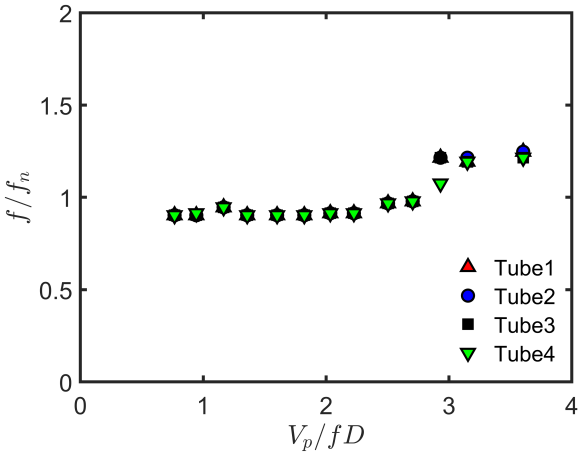


Figure A.7 Fully flexible array frequency variation in water flow in the transverse direction

coupling between the tubes is observed. This may also be a result of interaction between vortex shedding excitation forces and fluidelastic forces. The frequency of the four tubes increases by 20% at reduced velocity V_p/fD=3 as shown in Fig. A.7 which may support this hypothesis. Strong impacts between the tubes were observed when the array went unstable, however, high enough flow velocities were attained to confirm the instability observation and that vibrations are not only vortex-induced.

Streamwise direction dynamics

Figure A.8 presents the tube vibration test results in water flow when the tube is free to vibrate in the flow direction. In the streamwise direction, a similar vibration response to

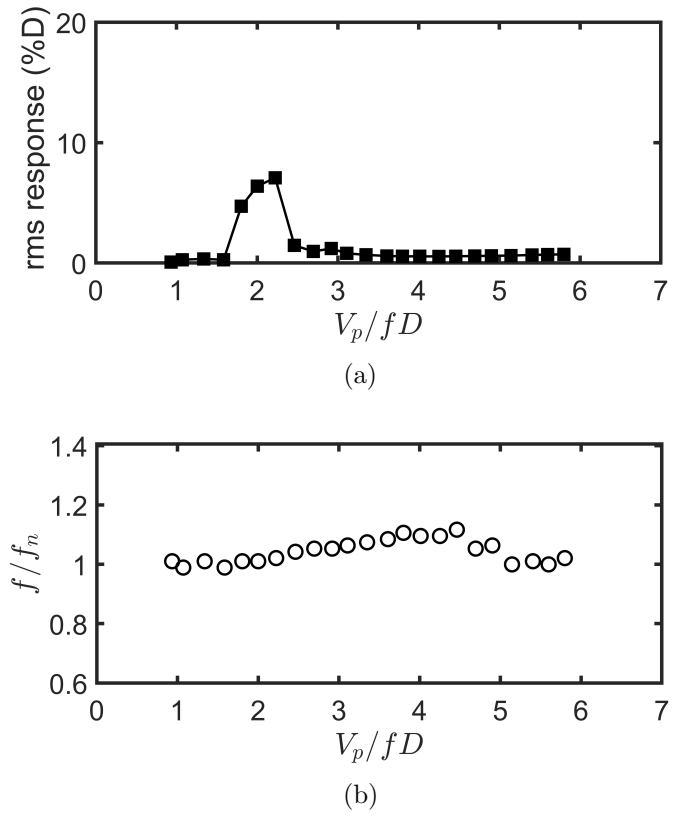


Figure A.8 Single flexible tube water test in the streamwise direction

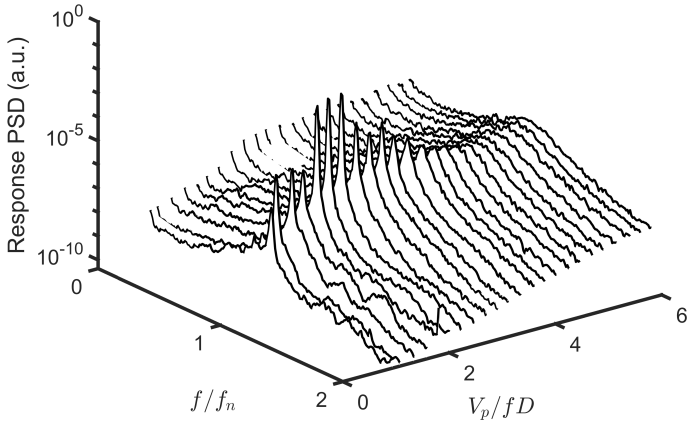


Figure A.9 Frequency spectra of single flexible tube in the streamwise direction in water flow

the transverse direction case is observed here for low flow velocity. A mild increase in tube vibration amplitude is observed in the reduced velocity range of $1.6<V_p/fD<2.5$. This is

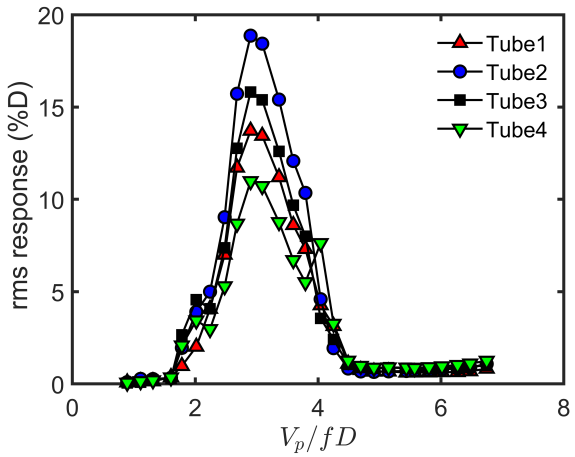


Figure A.10 Fully flexible array vibrations in water flow in the streamwise direction

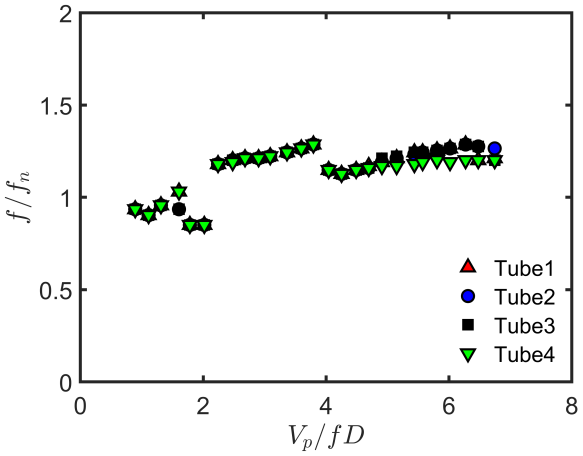


Figure A.11 Frequency variation of the fully flexible array vibrations in water flow in the streamwise direction

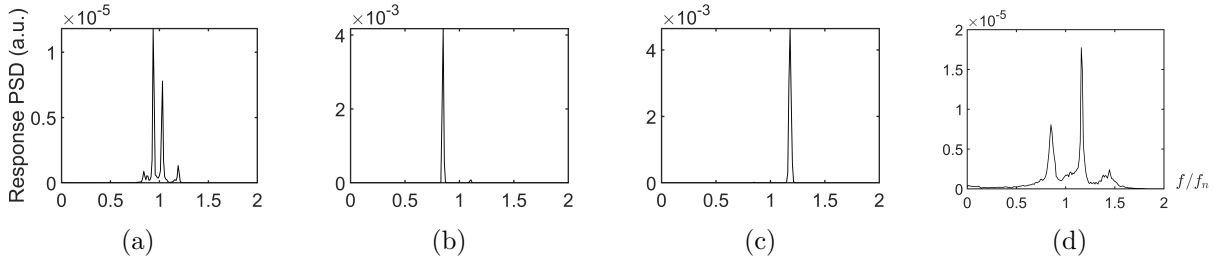
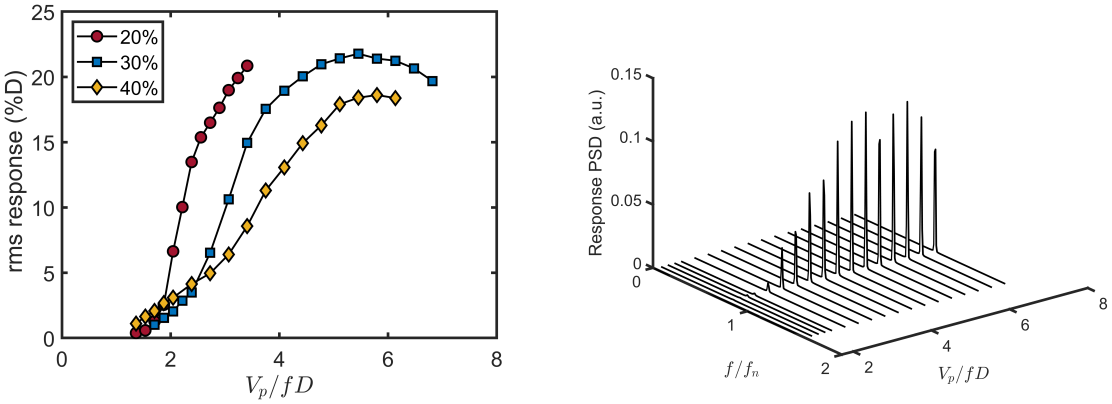


Figure A.12 Frequency spectra at various flow reduced velocities showing the change in tube vibration frequency at reduced velocity of: (a) 0.35, (b) 0.45, (c) 0.55, and (d) 1.05

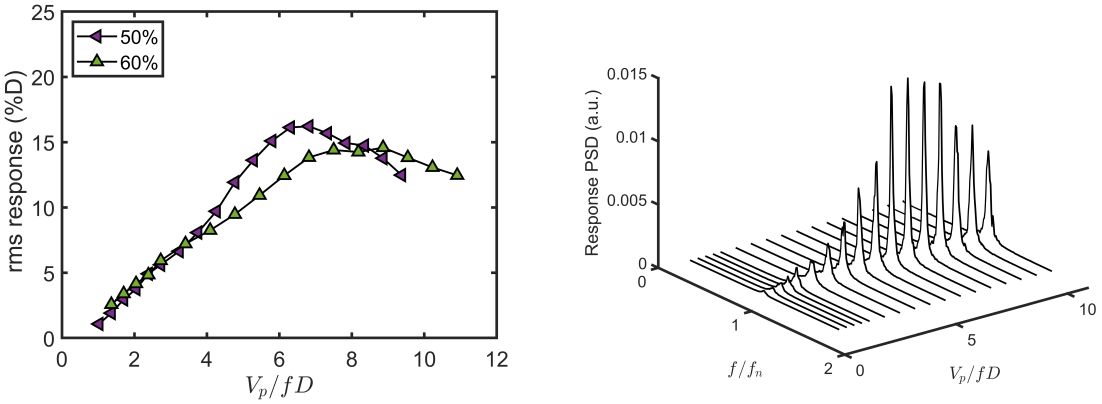
again attributed to vorticity shedding that excites the tube vibrations near a reduced velocity of V_p/fD=1.6. This corresponds to S_p=0.63, which is slightly lower than the Strouhal number observed in the transverse vibrations. When single isolated tube is limited to vibrate in the flow direction, oscillations occur at twice the shedding frequency, as a consequence of the vortex street geometry. This does not necessarily hold for tube arrays. Tubes flexible in the flow direction, within the array, are seen to vibrate due to vortex shedding at the same frequency that induces vibrations in the transverse direction. This was also observed in a previously tested rotated square array in water flow [139]. Figure A.8b presents the tube frequency variation with flow reduced velocity. Despite the observed vortex-induced vibrations, no lock-in like frequency change was observed. However, the tube apparent frequency gradually increases with flow velocity in the range $1.5<V_p/fD<4.5$ well beyond the vibration amplitude reduction at $V_p/fD \simeq 2.5$. It seems that the flow periodicity drags upwards the tube vibration frequency (via frequency synchronization) without amplifying the vibration amplitudes. This could again be due to the weak formation of the vortex shedding in such a small spacing coupled with the streamwise flexibility. The frequency spectra are presented in Fig. A.9. As seen at low flow velocities, the tube does not capture the vortex shedding frequency until it synchronizes with the tube natural frequency. Note also that in the streamwise direction no fluidelastic instability was observed in water flow with one flexible tube.

When the fully flexible bundle was tested, strong vibrations were observed starting at reduced velocity near V_p/fD=1.8 with all tubes synchronized as shown in Fig. A.10. Vibrations reached a maximum amplitude near the reduced velocity V_p/fD=3. Above the maximum vibration amplitude velocity, the tube bundle vibration response fell to significantly low levels and stable behaviour was maintained up to high flow velocities. Compared to the single flexible tube case, the synchronization here is much stronger and effective over a wider range of flow velocities. The response frequency of the four tubes is shown in Fig. A.11. It is more clear here that the tube vibration frequency is locked in the vortex frequency at a reduced velocity V_p/fD=2. This is followed by a gradual frequency increase up to the reduced velocity V_p/fD=4, where an abrupt frequency reduction occurs. A more detailed look is presented in Fig. A.12, where frequency spectra for several flow velocities is shown, depicting the frequency variation and the post lock-in frequency behaviour. Also here, there is not fluidelastic instability observed.



(a) (b)

Figure A.13 (a) Single flexible tube response in the transverse direction for β=20%-40%, and (b) frequency spectra for β=30%

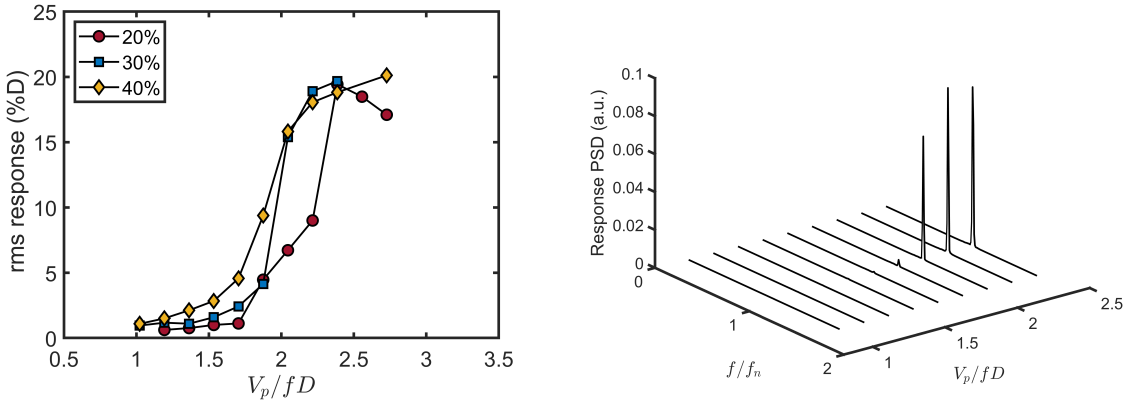


(a) (b)

Figure A.14 (a) Single flexible tube response in the transverse direction for β=50%-60%, and (b) frequency spectra for β=60%

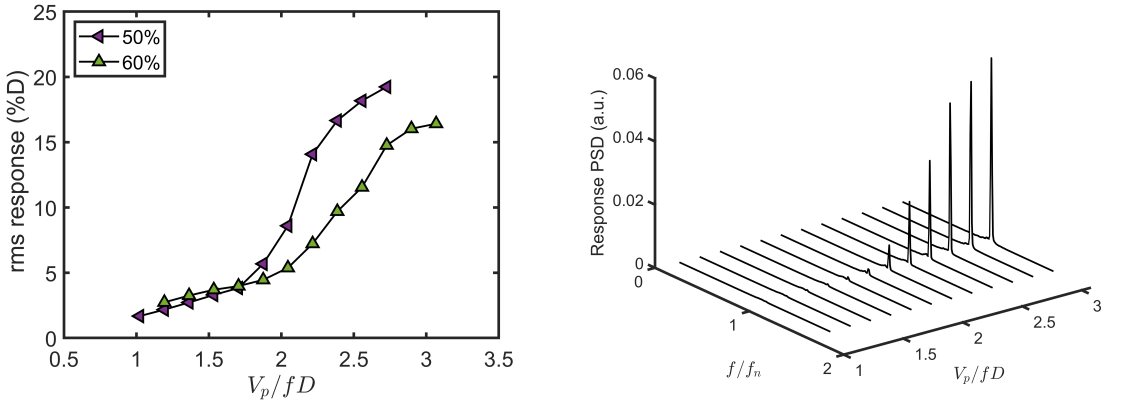
A.3.2 Two-phase flow test results

A range of two-phase flow void fractions is tested from 20%-60% for the main tests. For some specific cases, e.g. the single flexible tube case, a wider range of void fractions up to 97% was tested. Testing at high void fraction provided valuable information on damping behaviour of the array. For the fully flexible array in the streamwise direction, testing also covered high void fractions up to 97%.



(a) (b)

Figure A.15 (a) Fully flexible array response in the transverse direction for β=20%-40%, and (b) frequency spectra for β=30%

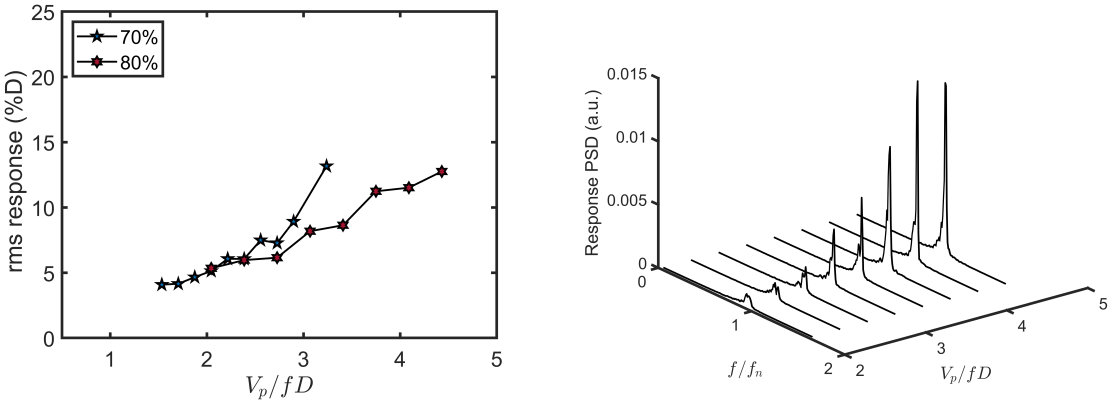


(a) (b)

Figure A.16 (a) Fully flexible array response in the transverse direction for β=50%-60%, and (b) frequency spectra for β=60%

Transverse direction array dynamics

Following the instability observed in the transverse direction in water flow, a single flexible tube in the array is tested in two-phase flow. Figure A.13 presents the vibration test results for 20%, 30% and 40% void fractions. Fluidelastic instability arises at an early velocity. For these low void fractions, instability onset is well defined compared to the higher 50% and 60% void fraction cases shown in Fig. A.14. For 50% and 60% void fractions, a gradual increase in tube amplitude vibrations is noticed and instability cannot be easily judged. This could be due to flow turbulence, or the high two-phase flow damping as will be shown in section



(a) (b)

Figure A.17 (a) Fully flexible array response in the transverse direction for β=70%-80%, and (b) frequency spectra for β=80%

A.4.1. However, high flow velocity was attained here again to investigate the tube behaviour over a wide range of flow velocities. Figures A.13b and A.14b show the frequency spectra of the tube in the two void fraction ranges. The spectrum bandwidth is larger in the high void fractions of 50% and 60% compared to the lower void fraction cases.

When the fully flexible tube bundle was tested for the same void fractions, flow critical velocity is much more clearly defined for void fractions in the range of 20%-40%. Fig. A.15 shows clear fluidelastic instability occurrence between reduced velocities of 1.5-2 for different void fractions. At the post-instability velocities, strong impacts between the tubes were observed due to the small spacing in the array. A similar observation is made for 50% and 60% void fractions, where critical reduced velocities are near 2. Testing higher void fractions was also done to investigate the evolution of the dynamic behaviour of the array with void fraction. For 70% and 80% void fractions, random turbulence excitation was found to overcome the fluidelastic forces, causing the vibration amplitudes to gradually increase, see Fig. A.17.

Streamwise direction array dynamics

Figure A.18a shows the single tube vibrations in the streamwise direction for 20%-60% void fractions. Stability analysis is performed on the obtained experimental results. Because the tubes are flexible in the flow direction, the bundle is subjected to two-phase flow quasi-periodic forces. These forces excite the bundle at low frequency around 4-5 Hz. To study the fluidelastic vibration behaviour, tube rms vibrations are calculated at the tube natural

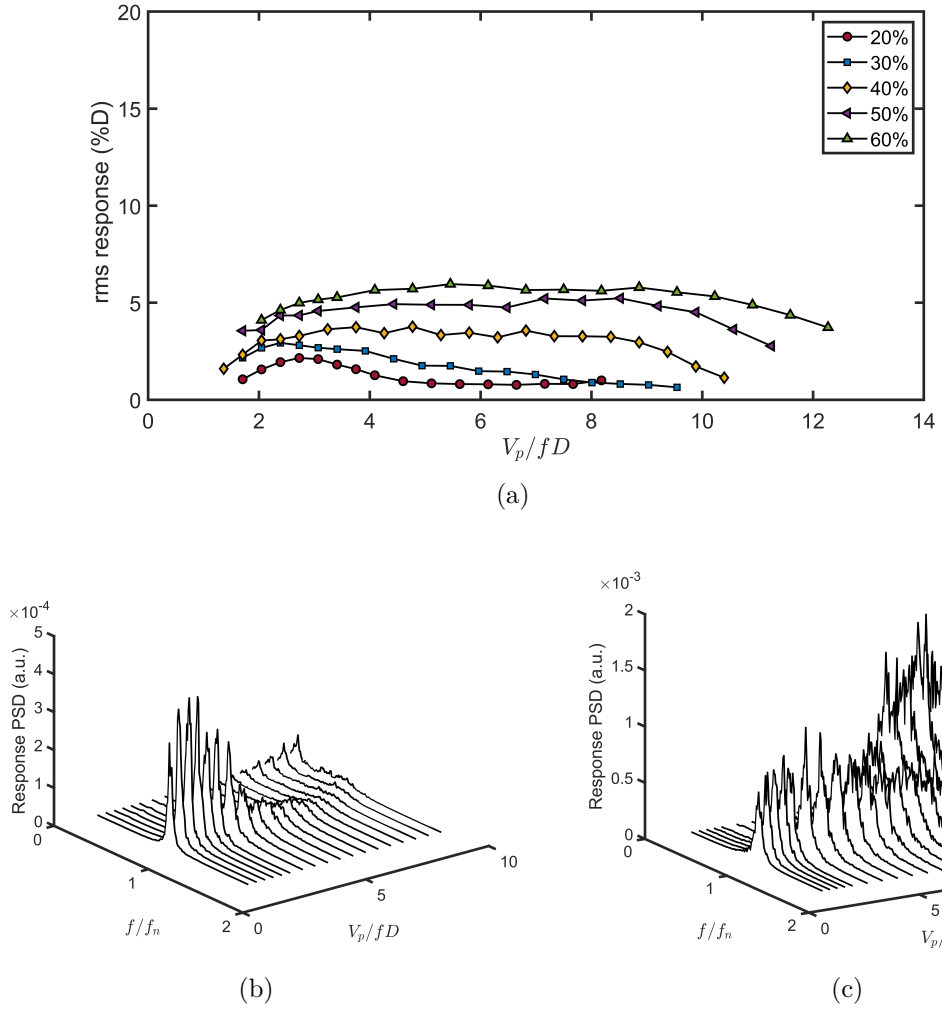
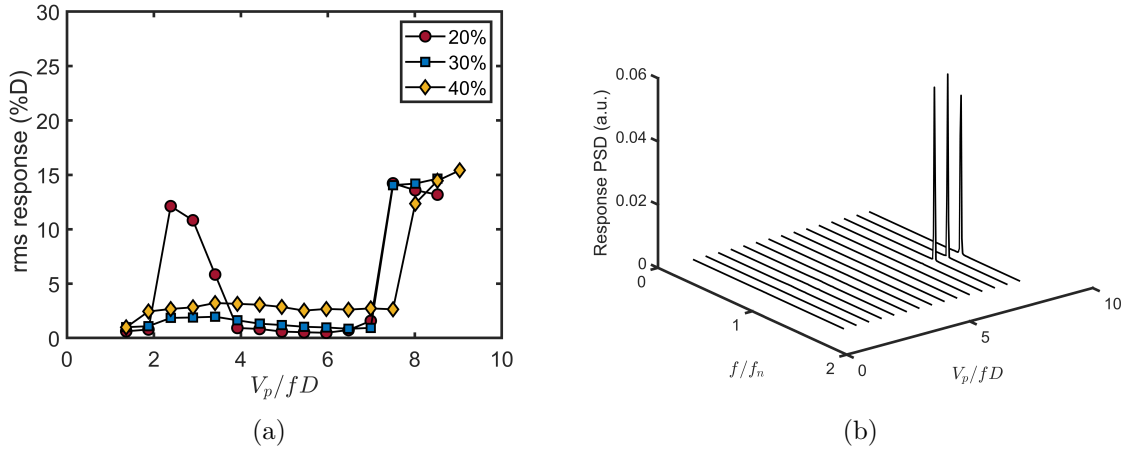


Figure A.18 (a) Single flexible tube response in the streamwise direction at β=20%-60%, and frequency spectra for β=: (b) 30%, and (c) 60%

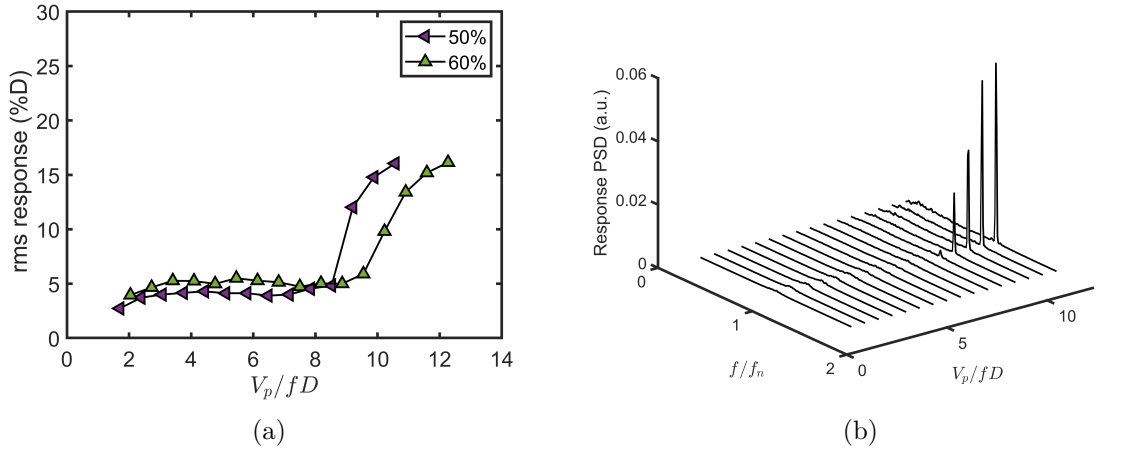
frequency. Due to the two-phase flow density variation with void fraction, tube natural frequency varies based on the flow density. Generally, calculations of the tube rms vibration response in the streamwise direction are done at a band width covering the tube dynamics at its response natural frequency. More details about the quasi-periodic excitation phenomenon is addressed by Pettigrew et al. [109]. Figures A.18b and A.18c present the frequency spectra showing small vibrations at the low reduced velocities due to flow turbulence. As clearly seen, the tube is stable in two-phase flow up to high flow velocity. The stable behaviour in this case indicates that the negative damping instability mechanism cannot produce fluidelastic instability up to the maximum tested velocity.

When the fully flexible bundle is tested, observations become completely different from what



(a) (b)

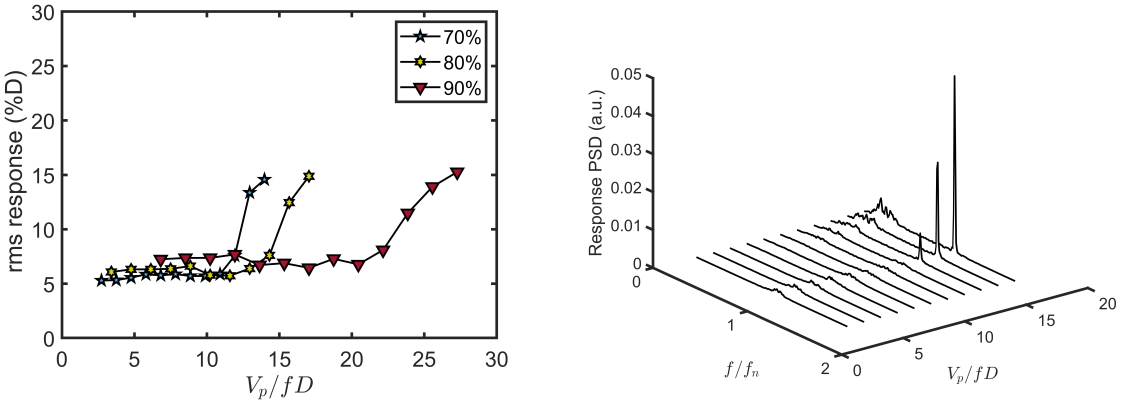
Figure A.19 (a) Fully flexible array response in the streamwise direction for β= 20%-40%, and (b) frequency spectra for β=30%



(a) (b)

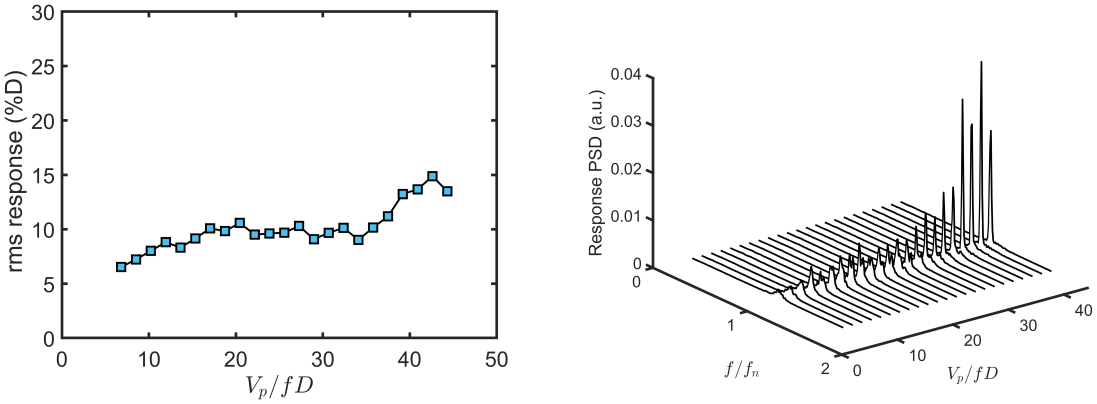
Figure A.20 (a) Fully flexible array response in the streamwise direction for β= 50%-60%, and (b) frequency spectra for β=60%

was found in the single flexible tube test results. The test results for the void fractions 20%-40% are presented in Fig. A.19. Delayed fluidelastic instability is observed for all the void fractions. For 20% and 30% void fractions, instability arises at a reduced velocity V_p/fD=7, while for 40% void fraction, the critical velocity is near 7.5. Stability onset is well defined for the lower void fractions. When the array is tested for 50% and 60% void fractions, the critical velocities increase to 8.5 and 9.6, respectively, as seen in Fig. A.20. For the 20% void fraction, an increase in tube vibration is noticed at a reduced velocity V_p/fD=2. This is a remnant of flow periodicity excitation in water. The continuation of testing at higher void



(a) (b)

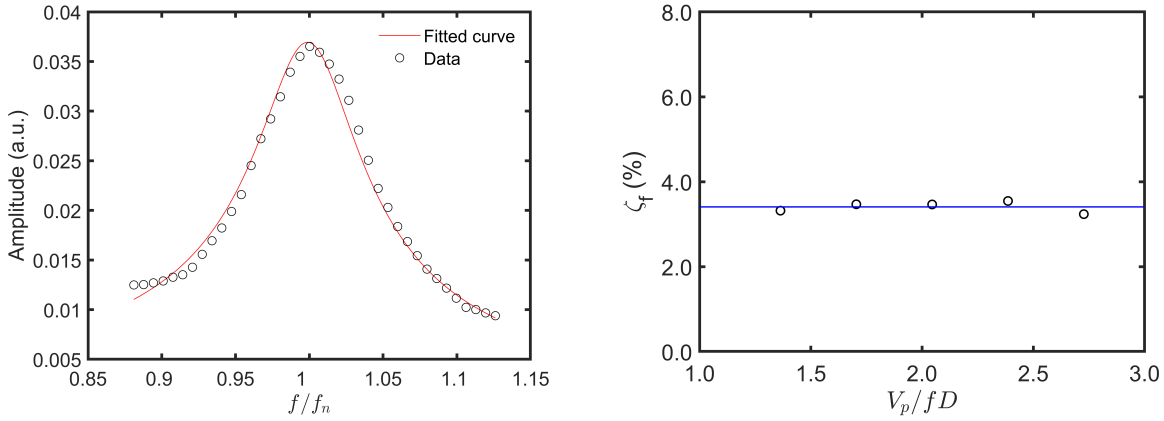
Figure A.21 (a) Fully flexible array response in the streamwise direction for β= 70%-90%, and (b) frequency spectra for β=80%



(a) (b)

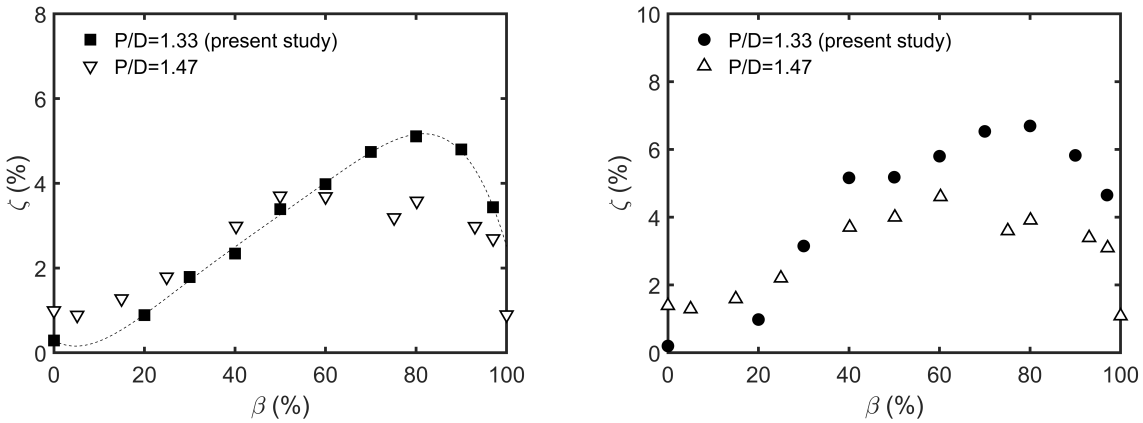
Figure A.22 (a) Fully flexible array response in the streamwise direction and frequency spectra for β= 97%, and (b) frequency spectra

fractions was necessary here to validate the instability at high flow velocities (hence Connors constant as will be shown in a later section). Figure A.21 shows that instability occurs at high flow velocity even at high void fraction of 70%, 80% and 90%. A special case of a very high void fraction of 97% was also tested. Instability was found to occur at a reduced velocity V_p/fD=36 as shown in Fig. A.22.



(a) (b)

Figure A.23 Tube damping ratio estimation showing: (a) curve fitting for low flow velocity for β=50%, (b) fluid damping averaged over multiple velocity points



(a) (b)

Figure A.24 Tube damping ratio in comparison with Pettigrew et al. [3]

A.4 Discussion

A.4.1 Damping measurements

Damping is a key parameter characterizing the array behaviour in two-phase flow. The damping ratio was estimated at low flow velocities where the fluidelastic forces are negligible. Theoretically, damping ratio should be measured in still fluid, but this is not attainable for two-phase mixtures. In the present work, the two-phase flow damping ratio is calculated using a direct curve fit of the tube frequency response spectrum. This approach leads to the

best estimate of the tube damping under conditions of turbulence excitation. The curve fit is done based on the following one degree-of-freedom FRF:

$$|H(j\omega)| = \frac{1}{k\sqrt{(1-r^2)^2 + (2\zeta r)^2}} \tag{A.4}$$

where, ζ is tubes damping ratio, $r = \omega/\omega_n$, $\omega = 2\pi f$. The general form of this equation is also valid for the tube response spectrum, under the assumption of a flat turbulence force spectrum in the frequency band centred on the tube natural frequency. This is also equivalent to the assumption of uniform turbulence in this frequency band in the tube arrays.

This methodology is used to estimate tube natural frequencies and damping values from frequency data in water flow and in the two-phase flow tests. Figure A.23 presents samples of the curve fitting in two-phase flow (β=50%), and averaged fluid damping over different low reduced flow velocity points. The frequency results are in turn used to determine the tube added mass. Figure A.24 presents the calculated damping ratio for all void fractions tested. A comparison is made in the figure with another rotated triangle array with a pitch ratio of 1.45 [3].

Generally, the damping ratio diminishes at low void fractions where the flow is more likely to be liquid, and at high void fractions where the flow have a tendency to damping in air. Damping ratio is seen to gradually increase with flow void fraction, reaching a maximum value near β=80%. Previous damping results presented by Pettigrew et al. [3] and Sawadogo and Mureithi [25] for rotated triangular arrays of 1.45 and 1.5 pitch ratios showed a similar trend with the array presented in this work. However, the maximum two-phase flow damping was attained near 60% void fraction for the large spacing arrays, while for the small spacing array presented in this work the maximum damping ratio was attained near 80% void fraction. For low void fractions ($< 50\%$), the two-phase flow damping ratio was seen to be lower in this array compared to the lager spaced array. From a practical point of view, the effect of the array confinement is not considered to be strong, except for void fractions between 70% and 90%. In the streamwise direction, the trend is similar to the transverse direction, although the damping ratio is relatively higher.

A.4.2 Hydrodynamic mass

The hydrodynamic mass is also measured at low flow velocities. It is determined based on tube natural frequency variation with flow density, hence flow void fraction. The ratio of the hydrodynamic mass at a given void fraction to that in liquid, (m_h/m_l) is given by the following equation [3, 147]

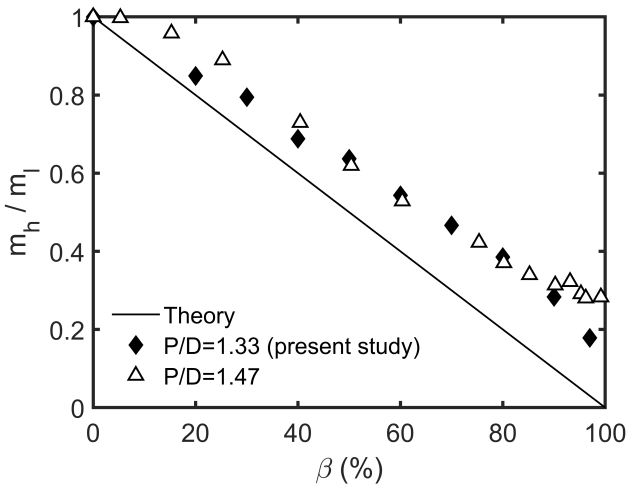


Figure A.25 Hydrodynamic mass ratio for the flexible tube in the streamwise direction in comparison with Pettigrew et al. [3]

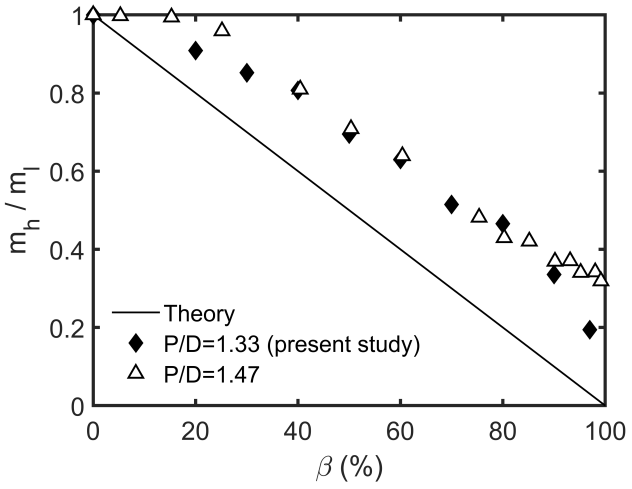


Figure A.26 Hydrodynamic mass ratio for the flexible tube in the transverse direction in comparison with Pettigrew et al. [3]

$$m_h/m_l = \frac{(f_s/f)^2 - 1}{(f_s/f_l)^2 - 1} \tag{A.5}$$

where, and f_s, f_l, and f are the tube structural frequency (in air), tube natural frequency in water, and tube natural frequency in the two-phase flow mixture, respectively. Theoretically, the tube added mass is modelled in liquid flow as follows [48]

$$m_h = (\frac{\rho_h \pi D^2}{4})\frac{(D_e/D)^2+1}{(D_e/D)^2-1}; \quad D_e/D = (0.96 + 0.50P/D)P/D \tag{A.6}$$

where, ρ_h is the two-phase flow homogeneous density, D is tube outer diameter, and D_e is the equivalent diameter.

The hydrodynamic mass ratio versus void fraction relationship for this array is shown in Fig. A.25 and Fig. A.26 for the streamwise and transverse directions, respectively. Theoretically, the added mass ratio should vary linearly with flow density, from unity in water, to approximately zero in air. In this array, the measured added mass is generally higher than that predicted by the simple linear model approximation in both directions. As shown in Fig. A.26, the two-phase flow added mass does not follow this theoretical model developed by Rogers et al. [48] shown in equation A.6. Pettigrew et al. [3] related this, for a larger spaced rotated triangular array, to the slip between gas and liquid phases that results in liquid hold-up around the tubes, thus a larger hydrodynamic mass. In a later study by Pettigrew et al. [109], it was found that the gas flow tends to deviate from the tube surface and flow in the middle of the inter-column area. This explains why the added mass is closer to the liquid added mass for low void fractions for the rotated triangular array with 1.47 pitch spacing (See Fig. A.26). However, the confinement in the array presented in this work results in less spatial distribution and the gas phase seems to remain close to the tube surface. From what is seen in the figures, the wider spacing array added mass ratio deviates from that for this array with P/D=1.33 at high and low void fractions. This is the case for both streamwise and transverse directions. Similarly, at high void fractions, the flow void fraction would be more uniform across the interspacing tube area, which results in a added mass closer to the homogeneous model.

A.4.3 Stability map

The Connors equation commonly used in industry to express the relationship between the non-dimensional (or reduced) critical pitch velocity and the tube mass damping parameter. The equation takes the form

$$\frac{V_{pc}}{fD} = K\left(\frac{m\delta}{\rho D^2}\right)^n \tag{A.7}$$

where, V_p is the two-phase flow velocity, f is tube natural frequency in the two-phase mixture, D is the tube outer diameter, m is the tube mass per unit length including tube hydrodynamic mass, δ is tube logarithmic decrement of damping, ρ is the two-phase flow density, and (K, n) are empirical constants. The critical reduced flow velocities are summarized in Table A.1

Table A.1 Summary of FEI test results with instability constants

Direction	β	$m\delta/\rho D^2$	Flexible tubes	V_{pc}/fD^2	K
Streamwise	0%	0.08	Single	-	-
			Fully flexible	-	-
	20%	0.27	Single	-	-
			Fully flexible	8.86	17.2
	30%	0.83	Single	-	-
			Fully flexible	8.75	9.6
	40%	1.52	Single	-	-
			Fully flexible	9.16	7.4
	50%	1.73	Single	-	-
			Fully flexible	10.28	7.8
	60%	2.3	Single	-	-
			Fully flexible	11.25	7.4
	70%	3.3	Fully flexible	13.8	7.6
	80%	4.7	Fully flexible	16.2	7.5
	90%	7.9	Fully flexible	22.4	8.0
	97%	19.4	Fully flexible	36.2	8.2
Transverse	0%	0.10	Single	1.58	5.0
			Fully flexible	1.58	5.0
	20%	0.26	Single	2.44	4.8
			Fully flexible	2.2	4.3
	30%	0.52	Single	3.06	4.2
			Fully flexible	2.4	3.3
	40%	0.76	Single	-	-
			Fully flexible	2.2	2.5
	50%	1.21	Single	-	-
			Fully flexible	2.3	2.1
	60%	1.71	Single	-	-
			Fully flexible	2.7	2.0

along with the mass damping parameter for each void fraction. The Connors constant, K, is calculated for the single flexible tube and fully flexible array test results.

Using the Connors equation, the stability limit for the various test cases can be conveniently summarized in a stability map. This map also allows comparison between stability results from different researchers. Figure A.27 presents the stability map for the tests presented here. It was found in previous studies that a single flexible tube in a rotated triangle array does not become unstable in the flow direction [140,141,148,149]. An important confirmation that can be made from the results addressed above is that this is also true for small spacing rotated triangular array. This means that the damping controlled instability mechanism is

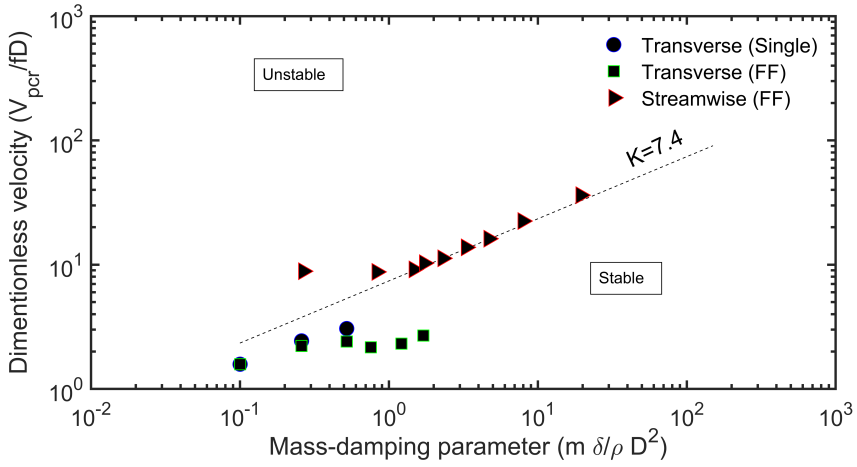


Figure A.27 Fluidelastic instability map showing test results of the present study

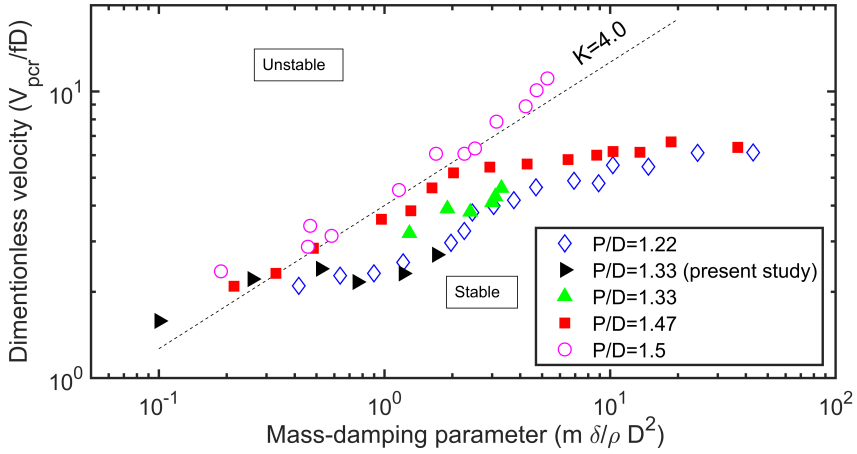


Figure A.28 Fluidelastic instability map showing rotated triangular array test results in the transverse direction in comparison with data from the literature: (◊, ■) Pettigrew et al. [24], ◯ Sawadogo and Mureithi [25], ▲ Azuma et al. [21].

absent in the rotated triangular layout in the flow direction even for confined arrays. It is evident that the critical velocity for the fully flexible array is lower than that found for the single flexible tube in the transverse direction. This would be of less concern compared to the instability in the flow direction in the steam generators since anti-vibration bars (AVBs) impede vibrations in the out-of-plane direction.

Figure A.28 presents the rotated triangular array the transverse direction test results for different pitch ratios. All the data represent FEI test results for flexible tube bundles in

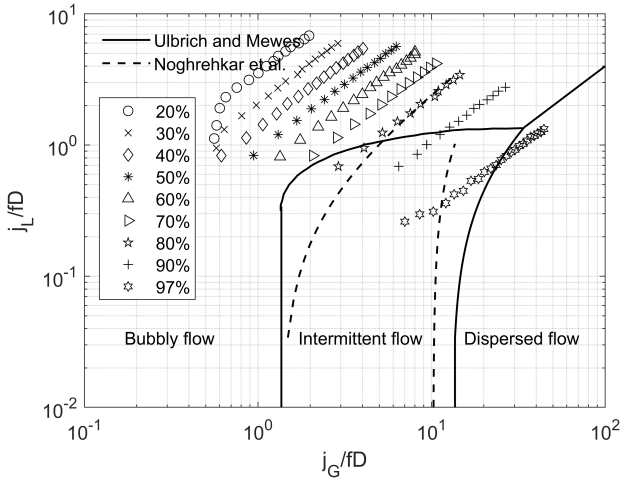


Figure A.29 Flow regime map for the tube bundle. Symbols show the flow velocity at different void fractions in the streamwise direction

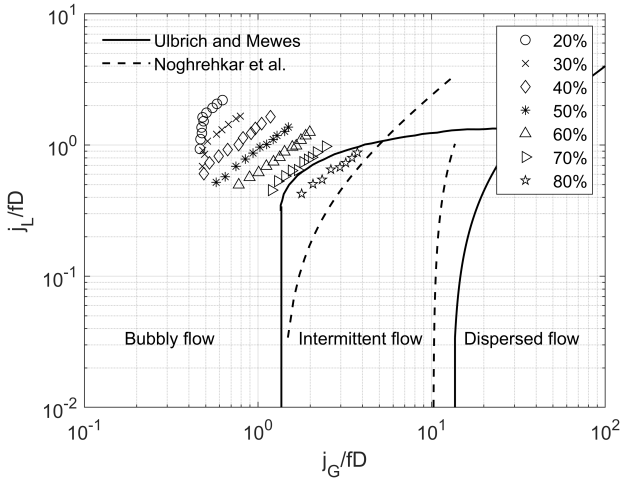


Figure A.30 Flow regime map for the tube bundle. Symbols show the flow velocity at different void fractions in the transverse direction

two-phase flow. Results show the FEI occurrence at low flow velocities for small pitch ratios. Generally, the instability constant (K) decreases with the decrease of array pitch spacing. For lower pitch ratios, two regions are found. One region is where the exponent n is approximately 0.5, and at higher mass damping parameters it becomes significantly lower. This behaviour was explained by Pettigrew et al. [24] to be the result of flow regime change between continuous and intermittent flow for the arrays with small pitch spacing. However, for the large spacing array with P/D=1.5, the decrease in the exponent was not observed and n=0.5 is reasonable for all test results data, even at high void fractions. Another region

is found where the mass damping parameter is very low (< 0.8). The instability constant changes with the same slope that has an exponent of 0.5.

One significant factor that should be considered for two-phase flow is the flow regime. For a tube bundle subjected to two-phase flow, the flow regime may affect the dynamic behaviour, hence, fluidelastic nature, and damping mechanism for different flow conditions. Here, Ulbrich and Mewes [113] flow map as well as Noghrehkar et al. [112] flow map have been used. Figures A.29 and A.30 show the flow regime for all the tested velocities of the fully flexible array in the streamwise and transverse directions, respectively. It is seen that flow in the transverse vibration tests is continuous for void fractions below 70%. Intermittent flow prevails for 80% void fraction. Streamwise flow map shows a similar observation except that in the 97% void fraction the flow becomes dispersed at high flow velocities.

The foregoing results report on part of the stability analysis of the APR1400 steam generator. The instability found in the transverse direction does not pose a practical concern since in nuclear steam generators the anti-vibration bars (AVBs) are used to suppress the vibrations in the transverse direction. However, they are not effective to restrain tube motion in the streamwise direction. The instabilities reported here in the streamwise direction, however, occur at a significantly high Connors constant (K =7.4), indicating highly stable behaviour.

The overall in-plane stability of the steam generator is governed by the dynamics of the triangular array geometry reported here as well as the rotated square geometry at the upper horizontal section of the U-bends. Previous work by the authors (Darwish et al. [129]) on the rotated square array geometry found the geometry to be even more stable than the triangular array studied here. Put together, the findings on these two arrays strongly suggest that the U-bend tube bundle composed of these two arrays is highly stable in the in-plane direction. The steam generator is therefore expected to have minimal susceptibility to IPFEI. To unequivocally confirm the in-plane stability behavior of the steam generator, experimental tests on full U-bend tubes are needed in order to also account for the dynamical effect of the array geometry transition from triangular to rotated square at the U-bends. The tube spacing in the transition region is larger than that in the vertical and horizontal U-bend sections suggesting that transition region effects should be less significant and unlikely to be destabilizing.

A.5 Conclusion

In a step to study the APR1400 steam generator tube bundle, a fundamental experimental program was carried out to test a rotated triangle array with P/D=1.33 in air and air-water

two-phase flows. Based on the results presented in this paper, a number of significant conclusions are drawn. Fluidelastic instability occurs in the transverse direction and is governed by the negative damping mechanism. This was seen also for wider spaced arrays, which confirms that this conclusion remains valid even in more confined rotated triangular arrays. Array confinement due to the proximity of the tubes did not show significant effect for low void fractions, while for 70%-90% void fraction damping increased in this array. This is a general observation in the flow direction and transverse direction. Streamwise fluidelastic instability was not observed in this array at the practical flow velocities that may exists in the APR1400 steam generator. The fact of having very high Connors constant confirms the stable behaviour of this array in the streamwise direction. The late occurrence of fluidelastic instability in the streamwise direction only in the fully flexible array also confirms the fact that the stiffness mechanism is necessary to induce instability in the rotated triangular arrays. However, this is not the case for the transverse direction where the negative damping mechanism is dominant. Generally, this rotated triangular array is stable from a practical point of view in the streamwise direction. Pitch spacing clearly influences the exponent in Connors equation and the trend of the FEI critical velocity. The smaller the array spacing, the lower the exponent is at high mass damping parameters.

APPENDIX B UNCERTAINTY ANALYSIS

This appendix presents the uncertainty analysis of the experimental parameters in all the experimental results. The purpose of this analysis is to predict the uncertainty interval of a calculated parameter based on the uncertainty of the raw data used in calculating the result.

The parameter Y is a dependent variable and given as a function of independent variables such that:

$$Y = Y(X_1, X_2, X_3, ..., X_n) \tag{B.1}$$

Let ∂Y be the uncertainty of the dependent variable, and ∂X_1, ∂X_2,...., ∂X_n be the uncertainties of the independent variables. Following Kline and McClintok approach [150], the uncertainty of the dependent variable Y can be expressed as

$$\delta Y = \left[\sum_{i=1}^{n}\left(\frac{\partial Y}{\partial X_i}\delta X_i\right)^2\right]^{1/2} \tag{B.2}$$

The Strouhal number is expressed as

$$S_p = \frac{f_v D}{V_p} \tag{B.3}$$

Then the uncertainty of the Strouhal number calculation is

$$\delta S_p = \sqrt{(\frac{D}{V_p}\delta f_v)^2 + (\frac{f_v}{V_p}\delta D)^2 + (\frac{-f_v D}{V_p^2}\delta V_p)^2} \tag{B.4}$$

from equations B.4 and B.3, the relative uncertainty of the Strouhal number is

$$\frac{\delta S_p}{S_p} = \sqrt{(\frac{\delta f_v}{f_v})^2 + (\frac{\delta D}{D})^2 + (\frac{\delta V_p}{V_p})^2} \tag{B.5}$$

Since all the equipment and sensors used in the experiments are calibrated, the uncertainty of all the readings are provided in the calibration certificates. The flow velocity is calculated using the water flow rate measure by a magnetic water flow meter. The uncertainty of the water flow velocity is 0.5%. The uncertainty of the frequency is very small due to the data

acquisition system high accuracy. However, it can be estimated from the frequency resolution used in the frequency analysis, which is 0.01 Hz. Since the lowest frequency measured is around 2 Hz, the relative uncertainty of the frequency is 0.5%. The tubes are fabricated with an accuracy around 0.005". This yields a relative uncertainty in tube's diameter and length of 0.67% and 0.067%. From equation B.5, the relative uncertainty of the Strouhal numbers calculated is ± 0.97%.

Following the same calculation procedure of the Strouhal number, the uncertainty of the lift and drag force coefficients can be calculated. The lift coefficient is given as

$$C_L = \frac{F_L}{\frac{1}{2}\rho V_p^2 D l} \tag{B.6}$$

This yields that the lift coefficient relative uncertainty is

$$\frac{\partial C_L}{C_L} = \sqrt{(\frac{\partial F_L}{F_L})^2 + (\frac{2\partial V_p}{V_p})^2 + (\frac{\partial D}{D})^2 + (\frac{\partial l}{l})^2} \tag{B.7}$$

The relative uncertainty of the drag force coefficient can also be calculated using equation B.7 by using drag force F_D. The resolution of the force sensor in the lift and drag directions is around 0.0208 N. The lowest measured force is around 1 N. So the uncertainty of the force values is 2.08%. Using equation B.7, the relative uncertainty of the lift and drag force coefficients is 2.43%.

The added mass is calculated from tube stiffness and vibration frequency in water

$$m = \frac{k}{(2\pi f)^2} \tag{B.8}$$

Hence, the uncertainty of the tube added mass is

$$\frac{\partial m}{m} = \frac{2\partial f}{f} \tag{B.9}$$

This results in mass relative uncertainty of 1%.

The Connors constant can be expressed in a simple form as

$$K = \frac{V_p}{f} / \sqrt{\frac{m\delta}{\rho}} \tag{B.10}$$

Following the same approach, the uncertainty of the Connors constant can be calculated as

$$\frac{\partial K}{K} = \sqrt{(\frac{\partial V_p}{V_p})^2 + (\frac{\partial f}{f})^2 + (\frac{\partial m}{2m})^2 + (\frac{\partial \delta}{2\delta})^2} \tag{B.11}$$

The logarithmic decrement of the tube is calculated directly from the tub damping, where the tube damping is directly dependent on the frequency. For simplicity, the uncertainty of the logarithmic decrement is taken to be the same as the frequency uncertainty. From equation B.11, the uncertainty of the Connors constant is around 0.9%.